UNIVERSITY OF SOUTHAMPTON

FACULTY OF MEDICINE

Cancer Sciences

Targeting OX40 with monoclonal antibodies as a form of cancer immunotherapy

by

Jordana Griffiths

Thesis for the degree of Doctor of Philosophy

September 2018

UNIVERSITY OF SOUTHAMPTON

ABSTRACT

FACULTY OF MEDICINE

Cancer Sciences

Thesis for the degree of Doctor of Philosophy

Targeting OX40 with monoclonal antibodies as a form of cancer immunotherapy

Jordana Griffiths

It has been well established that for an effective and controlled immune response multiple inputs are integrated. For example, the interaction of the T cell receptor (TCR) with an MHC-peptide complex alone is insufficient to cause complete T cell activation and concomitant interaction of co-stimulatory T cell receptors with their ligands is required. OX40 (CD134) and its ligand, OX40L (CD252), are members of the tumour necrosis factor receptor/tumour necrosis factor (TNFR/TNF) superfamily. Investigation into targeting such receptors with monoclonal antibodies (mAb) for use in cancer immunotherapy is ongoing, and in recent years OX40 has been shown to be a promising therapeutic target. This thesis explores the development, characterisation and therapeutic potential of a panel of novel anti-hOX40 mAb in a unique hOX40 knock-in (KI) mouse model.

The Antibody and Vaccine Group at the University of Southampton developed a number of anti-hOX40 mAb within the Southampton Antibody Programme (SAP) using hybridoma technology. These mAb were characterised in terms of binding domain and affinity using techniques such as flow cytometry and surface plasmon resonance (SPR) It was found that the panel of mAb all possessed a high affinity for the hOX40 receptor and binding spanned over all four extracellular domains (ECD). Their activity was then determined *in vitro* using proliferation assays and *in vivo* using a novel hOX40 KI mouse expressing human ECD and mouse intracellular domains. The immunostimulatory potential of these reagents was first assessed in an CD8+ OT-I transfer model. Subsequently, the therapeutic efficacy

of these mAb were assessed using a number of mouse tumour models. Collectively the data highlighted both the importance of mAb isotype but also specific domain binding in relation to the type and strength of the anti-hOX40 mAb effector function; with mAb binding to the membrane proximal region delivering stronger agonism (T cell expansion) as mIgG1 mAb and stronger regulatory T cell (Treg) depletion as mIgG2a. Intriguingly, mAb of both isotypes were seen to eradicate established tumours, albeit through different mechanisms. Together the work in this thesis demonstrates the desired characteristics, functional effects and mechanisms of action of anti-hOX40 mAb and provides encouragement for their translation towards the clinic as potential cancer therapeutics.

Contents

List of Tables

List of Figures

Academic Thesis: Declaration Of Authorship

I, Jordana Griffiths

declare that this thesis and the work presented in it are my own and has been generated by me as the result of my own original research.

Targetting OX40 with monoclonal antibodies as a form of cancer immunotherapy .

I confirm that:

1. This work was done wholly or mainly while in candidature for a research degree at this University;
2. Where any part of this thesis has previously been submitted for a degree or any other qualification at this University or any other institution, this has been clearly stated;
3. Where I have consulted the published work of others, this is always clearly attributed;
4. Where I have quoted from the work of others, the source is always given. With the exception of such quotations, this thesis is entirely my own work;
5. I have acknowledged all main sources of help;
6. Where the thesis is based on work done by myself jointly with others, I have made clear exactly what was done by others and what I have contributed myself;
7. Parts of this work have been published as:
   Willoughby, J., et al., OX40: Structure and function - What questions remain? Mol Immunol, 2017. 83: p. 13-22.

Signed: .....

Date: .....

Acknowledgements

I would firstly like to thank my supervisor Professor Mark Cragg, his continuous support, guidance and relatable personality and humour throughout this research has made my PhD experience so enjoyable. Secondly I would like to thank Dr Jane Willioughby, what would I have done without you?! You have been there every step of they way, teaching me, supporting me and encouraging me, I can't thank you enough for making my experience the fond memory that it is. Thanks also to Dr Ivo Tews for his supervision and knowledge in the structural aspects of this thesis.

To the many members of the Antibody and Vaccine group, thank you for the wealth of knowledge, the continuous guidance and the endless fun, I have truly had such a wonderful time working with you all. In particular, I would like to thank Dr Ruth French and Dr Kam Hussain for their involvement in my project, you have both taught me a lot. I would also like to thank Chris Penfold, Jinny Kim, Dr Claude Chan and Ian Mockaridge for supplying me constantly with the finest antibodies, without you my project would not have gotten very far! A special thanks also to Alison Tutt, you run a fine ship!

Eternal thanks also goes out to all the staff in the PCU, in particular Vikki Field and Lisa Dunning. Thank you for the endless laughs, the secret crying locations and all the guidance and support when it came to my mice, my experience wouldn't have been half of what it was without you crazy lot!

A special thank you also to all the friends that made being in Southampton bearable and maintaining my (in)sanity, in particular the old and current Ranelagh residents.

And lastly I would like to give a big thank you to my family (Mum, Ed, Bethany, Jacob and Dad), you are my biggest cheerleaders and I will forever be thankful for that. Mum and Ed, your never ending support (emotional and financial), constant love and words of wisdom have made this journey possible for me. Bethany and Jacob, thanks for being the best siblings a person could wish for, our weekends together full of laughter and shenanigans has kept me sane. And to Dad, thank

you for always answering my late night phone calls of panic and always having the right words to say.

Definitions and Abbreviations

Ab	Antibody
ADCC	Antibody Dependent Cellular Cytotoxicity
ADCP	Antibody Dependent Cellular Phagocytosis
Ag	Antigen
AID	Activation-Induced Cytidine Deaminase
APC	Antigen Presenting Cell
AS	Ammonium Sulphate
BCR	B-Cell Receptor
BSA	Bovine Serum Albumin
CD	Cluster of Differentiation
CDR	Complementary Determining Region
CFA	Complete Freunds Adjuvant
CFSE	Carboxyfluorescein Succinimidyl Ester
C_H	Constant region of an antibody heavy chain
CHO-S	Chinese Hamster Ovary Suspension cells
C_L	Constant region of an antibody light chain
CLP	Common Lymphoid Progenitor
CMP	Common Myeloid Progenitor
CNS	Central Nervous System
CRD	Cysteine Rich Domain
CRUK	Cancer Research UK
CSR	Class Switch Recombination
CTLA-4	Cytotoxic T-lymphocyte Associated protein-4
CTL	Cytotoxic T-lymphocyte
DC	Dendritic Cell
dH_2O	Distilled Water
DMEM	Dulbecco’s Modified Eagle Medium

DN	Double Negativel
DNA	Deoxyribose Nucleic Acid
DP	Double Positive
ECD	Extracellular Domain
EDTA	Ethylene-diamine-tetra-acetic acid
ELISA	Enzyme-Linked Immunosorbant Assay
EOMES	Eomesodermin
F(ab)	Fragment, Antigen Binding
FACS	Fluorescent Activated Cell Sorting
FADD	Fas Activating Death Domain
Fc	Fragment, Crystallisable
FcR	Fc Receptor
FCS	Foetal Calf Serum
FcγR	Fc Gamma Receptor
FDA	Food and Drug Administration
Foxp3	Forkhead box p3
GC	Germinal Centre
GMEM	Glasgow Minimal Essential Medium
HEK	Human Embryonic Kidney
hOX40	Human OX40 Receptor
HPV	Human Papilloma Virus
HSC	Haematopoietic Stem Cell
IFN	Interferon
Ig	Immunoglobulin
IgSF	Immunoglobulin Superfamily
IL	Interleukin
IMAC	Immobilised Metal Affinity Chromatography
ITAM	Immunoreceptor Tyrosine Activation Motif
ITIM	Immunopreceptor Tyrosine Inhibitory Motif
iTreg	Induced Regulatory T-cell

KI	Knock-In
KIR	Killer-cell Immunoglobulin-like Receptor
KO	Knock-Out
LAT	Linker for Activation of T-cells
LB	Lysogeny Broth
mAb	Monoclonal Antibody
MAPK	Mitogen Activated Protein Kinase
MFI	Mean Fluorescence Intensity
MHC	Major Histocompatibility Complex
mOX40	Mouse OX40 receptor
NETs	Neutrophil Extracellular Traps
NFAT	Nuclear Factor of Activated T-cells
NHL	Non-Hodgkin's Lymphoma
NIK	NK-κB Inducing Kinase
NK	Natural Killer
NKT	Natural Killer T-cell
nTreg	Natural Regulatory T-cell
PBMC	Peripheral Blood Mononuclear Cells
PBS	Phosphate Buffered Saline
PCR	Polymerase Chain Reaction
PD-1	Programmed cell Death protein-1
PDB	Protein Data Bank
pIgR	Polymeric Immunoglobulin Receptor
PKC	Protein Kinase C
ROS	Reactive Oxygen Species
RPMI	Roswell Park Memorial Institute (Media)
RT	Room Temperature
SAP	Southampton Antibody Programme
SC	Secretory Component
SDS-Page	Sodium Dodecyl-Sulphate – Polyacrylamide Gel Electrophoresis

SEC	Size Exclusion Chromatography
SHM	Somatic Hyper Mutation
SNP	Single Nucleotide Polymorphisms
SPR	Surface Plasmon Resonance
TCR	T-Cell Receptor
T_{CM}	Central Memory T-cell
T_{EM}	Effector Memory T-cell
TF	Transcription Factor
TFH	Follicular T-Helper cell
TGF	Transforming Growth Factor
TLR	Toll-Like Receptor
TNF	Tumour Necrosis Factor
TNFR	Tumour Necrosis Factor Receptor
TNFRSF	Tumour Necrosis Factor Receptor Super Family
TRAF	TNF Receptor Associated Factors
Treg	Regulatory T-cell
T_{RM}	Tissue Resident Memory T-cell
TSLP	Thymic Stromal Lymphopoietin
V(D)J	Variable, Diversity, Joining
V_H	Variable region of an antibody heavy chain
V_L	Variable region of an antibody light chain
WB	Western Blot
WBC	White Blood Cell
WT	Wild type
ZAP-70	Zeta-chain Associated Protein kinase 70

Chapter 1 Introduction

1.1 Cancer

The incidence rate of cancer within the UK has risen dramatically since the late 1970's, and currently 1 in every 2 people born after 1960 will be diagnosed with some form of the disease [1]. The development of cancer is a multi-step process underpinned by genomic instability, which typically presents as an uncontrolled proliferation of cells [2]. The complexity surrounding cancer and the dramatic differences that can be observed in genotype, phenotype and morphology of the same type of cancer in two individuals has made it difficult to understand the disease as a single condition. In an attempt to rationalise the diversity seen within the disease, Hanahan and Weinberg described six biological capabilities that normal cells acquire during the transition to becoming a tumour. They named them the hallmarks of cancer and are listed as follows; evading apoptosis, autonomy in growth signal production, insensitivity to anti-growth signals, replicative immortality, inducing angiogenesis and activating tissue invasion and metastasis [3]. In 2011, two additional hallmarks were added to the list as a result of research over the intervening decade highlighting the importance of contributions from the tumour microenvironment to tumourigenesis. The two added hallmarks were, reprogramming of energy metabolism and evasion of immune destruction [2].

Normal cells acquire these hallmarks through the accumulation of mutations within the cell and there are certain risk factors associated with a higher frequency of these lesions occurring. Numerous lifestyle choices are risk factors for cancer such as smoking (largely linked to the development of lung cancer) [4], obesity [5] and UV exposure (principally linked to the development of melanoma) [6]. Viral infections have also been shown to increase the risk of developing certain types of cancers. Most notable is the human papilloma virus (HPV) and its strong link to the development of cervical cancer [7]. Some of these risks can therefore be reduced by lifestyle changes however some cancers arise in patients, not as a result of personal lifestyle choices, but as a result of an inherited gene mutation. Two of the best recognised are the *BRCA1* and *BRCA2* tumour suppressor genes. Germline mutations in one or both of these genes accounts for 5-10% of all breast cancers [8] and 15% of all ovarian cancers [9].

Another inherent factor which impacts the host in the fight against cancer is the immune system. The immune system has critical interactions with tumour cells from the initiation and development stages through to metastasis [10] and immune deficiency within cancer patients has been well documented [11], highlighting how tumour cells have developed a variety of cellular and molecular mechanisms to avoid the anti-tumour immune response. This is discussed in more detail in Introduction; Section 1.3.

1.2 Types of cancer therapy

Due to the complexity and diversity seen within cancer patients a 'one-treatment-fits-all' approach has not yet been established and is unlikely to become a reality. Conventionally there have been three main approaches through which cancer patients have been treated dependent on a number of factors including the severity of the disease and the accessibility of the tumour; these are surgical removal, radiotherapy and chemotherapy [12]. Each method of treatment comes with its advantages and disadvantages, and typically a combination of these techniques are used to provide a better prognosis for the patient.

Surgery is most effective for the treatment of patients with solid tumours that are contained within one area. Limitations of this approach arise when patients present with haematological malignancies or tumours which are not readily accessible, or have disseminated. Further limitations include the damage to surrounding tissues that may occur in surgery as well as the lack of efficacy if malignant cells remain after re-section either through an inability to remove all of the tumour or through metastases [13].

Radiotherapy involves the use of ionising energy to cause DNA damage in cancerous cells which interrupts their ability to divide and leads to their death via apoptosis. It is often used in conjunction with surgery (to shrink the tumour beforehand or remove any residual cancer cells post surgery) or chemotherapy (sensitising the cancerous cells towards radiation damage). In particular, radiotherapy targets highly proliferating cells and whilst this includes cancer cells, it will also affect highly proliferating healthy cells such as those of the immune system, liver, bone marrow, gut and hair follicles, hence this form of treatment can induce significant side effects [14]. It is also less likely than surgery to eradicate all

the cancerous cells and it does not kill metastases or blood borne cells [15] as the treatment is targeted to a specific site.

Chemotherapy is the use of chemical agents to induce cell death via interference with DNA production and disruption to the cell cycle. Over 100 different agents are used for chemotherapy treatment [16] and are grouped based on factors such as how they work and their chemical compositions. One example of a group of chemotherapy drugs are alkylating agents. These agents were one of the earliest classes of drugs used to treat cancer and they function by adding an alky group directly to DNA, causing DNA breaks and ultimately cell death, preferentially in rapidly proliferating cells [16]. As they are typically given systemically they have the potential to remove cancers from throughout the body however this brings about toxicity to proliferating healthy tissues such as those mentioned above for radiotherapy.

In addition to these three stalwarts of oncological treatments, the idea of harnessing the power of the immune system to treat cancer has been established over the last few decades. Activation and manipulation of the immune system as a form of treatment is referred to as immunotherapy. The use of immunotherapy dates back as far as the 1800's with the most well recognised early work coming from American surgeon William B. Coley, who used a bacterial preparation derived from infected bandages to cure 10% of inoperable sarcomas [17]. Whilst it has taken some time, it is now well established that various components of the immune system play pivotal roles in protecting us from cancer.

As described briefly in Introduction; Section 1.1, there is a complex interplay between the immune system and tumour cells which is able to either promote or suppress cancerous cell growth. Furthermore, tumour persistence in the presence of a competent immune system is not uncommon [18]. This is due to tumour cells evolving a number of mechanisms to avoid the host immune system; 'hiding' from the cells of the immune system, commonly known as immunoediting, or disabling/eliminating them by induction of a suppressive tumour microenvironment [18].

Cancer is proposed to evolve through three phases of interaction with the immune system; Elimination, Equilibrium and Escape. Elimination describes the ability of the immune system to recognise and destroy the most immunogenic cancer cells

[18]. However, due to the genetic variation within the cancer coupled with the environmental changes that the cancer cell can enforce, malignant cells with reduced immunogenicity develop that have increased ability to avoid the immune attack, this is described as the equilibrium phase, whereby the tumour is held in check but not eliminated [18]. The most common abnormality observed with the capacity to reduce immunogenicity is the loss of antigen processing and presentation. Changes in the expression of major histocompatibility complex (MHC) class 1 molecules [19, 20], linked with down-regulation of co-stimulatory molecules, render tumour cells poor antigen presenting cells (APCs) [21]. Furthermore, tumours are also known to induce an immunosuppressive tumour environment by directly interfering with the host immune system. They either produce and release factors that modulate functions of immune cells such as inhibitory cytokines IL-10 and TGF-β, or they induce apoptosis of effector immune cells using mechanisms such as Fas-FasL mediated killing [22]. Lastly, the escape phase is the process in which these immunologically sculpted tumours finally expand in an uncontrolled manner due to their ability to evade the host immune system due to reasons discussed above. A central principle of cancer immunoediting is the ability of T cells to recognise tumour antigens and drive either the immunological elimination or sculpting of the developing cancer. It is therefore unsurprising that the development of monoclonal antibodies (mAb) targeting T cells as a form of cancer immunotherapy has become one of the major areas of interest over the last decade. However, to be able to target the immune system we first need to understand it.

1.3 The Immune system

As mentioned above, the immune system plays a pivotal role in the control and clearance of cancerous cells. The immune system is classically divided into two aspects, mediated through the innate and the adaptive immune responses [23]. The innate immune system is classified as the first line of defence; it acts quickly, responding to evolutionary-hard-wired pathogen-derived molecules, and produces no immune memory. This initial response limits damage to the host and allows the adaptive immune response time to specialise and generate a bespoke response to the antigen. Conversely, the adaptive immune system is slower in its initial

response to antigen, however, has an ability to recognise virtually all foreign antigens with exquisite specificity and is capable of generating memory, allowing the host to exert a more rapid and robust response upon secondary infection [23].

The immune system is composed of many different cell types with specialised functions in order to mediate the two different arms of the immune response. All types of immune cells initially arise from hematopoietic stem cells (HSC) produced in the bone marrow. Lineage decisions are under the control of transcription factors (TF) resulting in the production of two distinct progenitor cells, the common myeloid progenitor (CMP) and the common lymphoid progenitor (CLP) [23]. Commitment to a myeloid lineage (i.e. via CMP) results in the production of granulocytes and monocytes [24] which are activated to elicit functions such as phagocytosis and the release of inflammatory cytokine such as TNF-α, IL-6 and IL-12 [23]. This can result in the clearance of infected cells and the recruitment of other immune cells involved in the adaptive immune response. Cells derived from the CMP are the first to respond to invasion of the host and therefore orchestrate the innate immune response. On the other hand, commitment to a lymphoid lineage (i.e. via CLP) produces natural killer (NK) cells and B- and T- lymphocytes. These cells are the principal players in the adaptive immune response and will be discussed in further detail in later sections. One cell type which is not clearly grouped into either a myeloid or lymphoid lineage is the dendritic cells (DC) as they can arise from both CMPs and CLPs [25]; furthermore DC serve as an important bridge between the innate and adaptive immune response.

1.3.1 Cells of the myeloid lineage

As described above, cells arising from the myeloid lineage are major players in the innate immune response due to their ability to phagocytose infected cells and secrete inflammatory cytokines and chemokines. A number of cells arise from the CMP and are described in more detail below.

Monocytes are a heterogeneous group of cells which possess unique functions as mononuclear phagocytic cells and are also the precursors for professional APC); macrophages and DCs [26]. Upon tissue damage or infection, monocytes are rapidly recruited to the tissue where they differentiate into tissue resident

macrophages. In addition to their role in an immune response, these cells can also play an important role in development, for example osteoclasts which develop from monocytes are involved in regulating bone formation and skeletal homeostasis [27].

Macrophages are prominent and active phagocytes in the immune system and remove apoptotic cells, pathogens and cellular debris [26]. They are defined in mice as F4/80^{hi} cells [28], although multiple markers are typically used to delineate them from other myeloid cells.

DCs are classed as professional APCs as they can efficiently capture and process antigen, subsequently presenting it on their surface as immune peptides to activate T cell responses. DCs are also a heterogeneous population e.g. conventional and plasmacytoid DC's (cDCs and pDCs, respectively); although they are both capable of antigen processing and presentation the subtypes have distinct markers and differ in location and immunological function [29]. cDCs are typically recognised in mice by the markers CD8 alpha+ or CD11b+ [30] and collectively are capable of activating both CD8+ and CD4+ T cells as well as secreting inflammatory cytokines such as IL-12 and IFN-γ [30]. In addition to lymphoid tissue-resident cDCs, three subsets of migratory/non-lymphoid tissue cDCs have been identified in mice using markers CD103 and CD11b [30]. These migratory cDCs are functionally similar to the lymphoid tissue-resident cDCs described above. A second type of DC are the pDCs, a rare subset that are unique from cDCs. Upon activation pDCs initially function in an innate capacity and secrete pro-inflammatory cytokines such as type I interferons, TNF-alpha and IL-12 [30]. In addition to this they up-regulate T cell co-stimulatory molecules, increase MHC-class II expression and develop a more cDC-like morphology enabling them to function as APCs. pDCs are recognised in mice using the markers CD11c and Ly-6C [30].

Another cell type originating from the CMP are granulocytes which are characterised by the presence of granules in their cytoplasm. Three types of granulocytes emerge from the CMP; neutrophils, basophils and eosinophils. Neutrophils are a major player in acute inflammation and are the first cell type to be recruited to sites of inflammation where their full activation leads to phagocytosis and killing of pathogens through the production of reactive oxygen

species (ROS), degranulation of cytoplasmic granules containing anti-microbial components, and generation of neutrophil extracellular traps (NETs) [31]. These cells are identified in mice using the markers CD11b and Ly-6G [32].

Basophils are mainly involved in hypersensitivity responses and anaphylaxis and are recognised in mice using markers CD200R3 and FCεRIα [33]. Likewise, eosinophils are involved in various inflammatory processes, especially allergic reactions, and play a role in the clearance of parasitic infections [34]. These cells are identified in mice using the markers CD11b, CD193 and F4/80 [32].

The cell types described above predominantly control the innate immune response but also play an essential role in helping to activate the adaptive immune response. This arm of the immune response is essential for prolonged immunity and memory production and is orchestrated by B cells, T cells and NK cells all of which are discussed below.

1.3.2 B cells

The primary function of B cells is to recognise foreign antigens, differentiate into plasma cells and then produce antibodies which protect the host against foreign particles or infection. B cells develop in the bone marrow and are released into the periphery as naïve B cells. The cells are classed as mature once they have encountered antigen after leaving the bone marrow [35]. B cell development is tightly controlled to prevent auto-reactive B cells entering the periphery. Self-reacting B cells undergo clonal deletion in the bone marrow; a process known as central tolerance [36]. B cells recognise their targets through the expression of a critical cell surface receptor, the B cell receptor (BCR). The BCR is composed of a membrane immunoglobulin and a signalling subunit containing ITAM motifs, which is encoded by a disulphide-linked heterodimer of the Ig-α (CD79a) and Ig-β (CD79b) proteins [37]. The generation of the BCR is essential for the maturation of B cells, with each successful stage in its production leading to the next stage in B cell differentiation. Variable-Diversity-Joining (V(D)J) recombination of the multiple germline variable regions of both light (V an J) and heavy chain (V, D and J) immunoglobulin (Ig) genes allows for the generation of a large and diverse repertoire of BCR's, with each B cell carrying a unique receptor [23]. The process

of V(D)J recombination assembles the different segments described above to produce variable domain Ig and is analogous with the TCR genes. This process is directed by highly conserved recombination signal sequences (RSS), consisting of a heptamer sequence followed by either a 12 or 23 nucleotide spacer followed by a conserved nonamer sequence [38]. Only a RSS with a 12 nucleotide spacer can join that of a 23 spacer thereby minimising the potential for two of the same segments to join. For example, at the heavy chain locus, the V and J segments are flanked by RSS with a 23 nucleotide spacer, preventing them from joining directly to each other, whilst the D segment contains a 12 nucleotide spaced RSS [38]. The process of segment joining is facilitated by enzymes RAG1 and RAG2, they recognise and bind to the RSS, bringing together the two segments to be joined with any DNA inbetween forming a hairpin structure [39]. The heptamer is then cleaved by associated endonucleases, thereby releasing the hairpin which is degraded and lost from the genome from that individual cell – leaving the two segments in close association where they are ligated together. For the heavy chain variable gene this recombination event occurs in a defined order; D binds to J to form DJ, then a second recombination event attaches the V to the DJ (Figure 1.1). The recombination events discussed above produce imprecise junctions providing the opportunity for additional modifications to the gene to occur therefore resulting in a larger number of possible unique combinations than encoded for within the genome [40]. Types of additional modifications include the insertion (by terminal deoxynucleotidyl transferse, TdT) or deletion (by exonuclease activity) of nucleotides at numerous stages of the reaction such as the initial single strand break of the hairpin and the ligation stage [38]. Collectively these processes result in a hyper-variable CDR3, which allows much greater diversity than the recombination of encoded gene segments could provide.

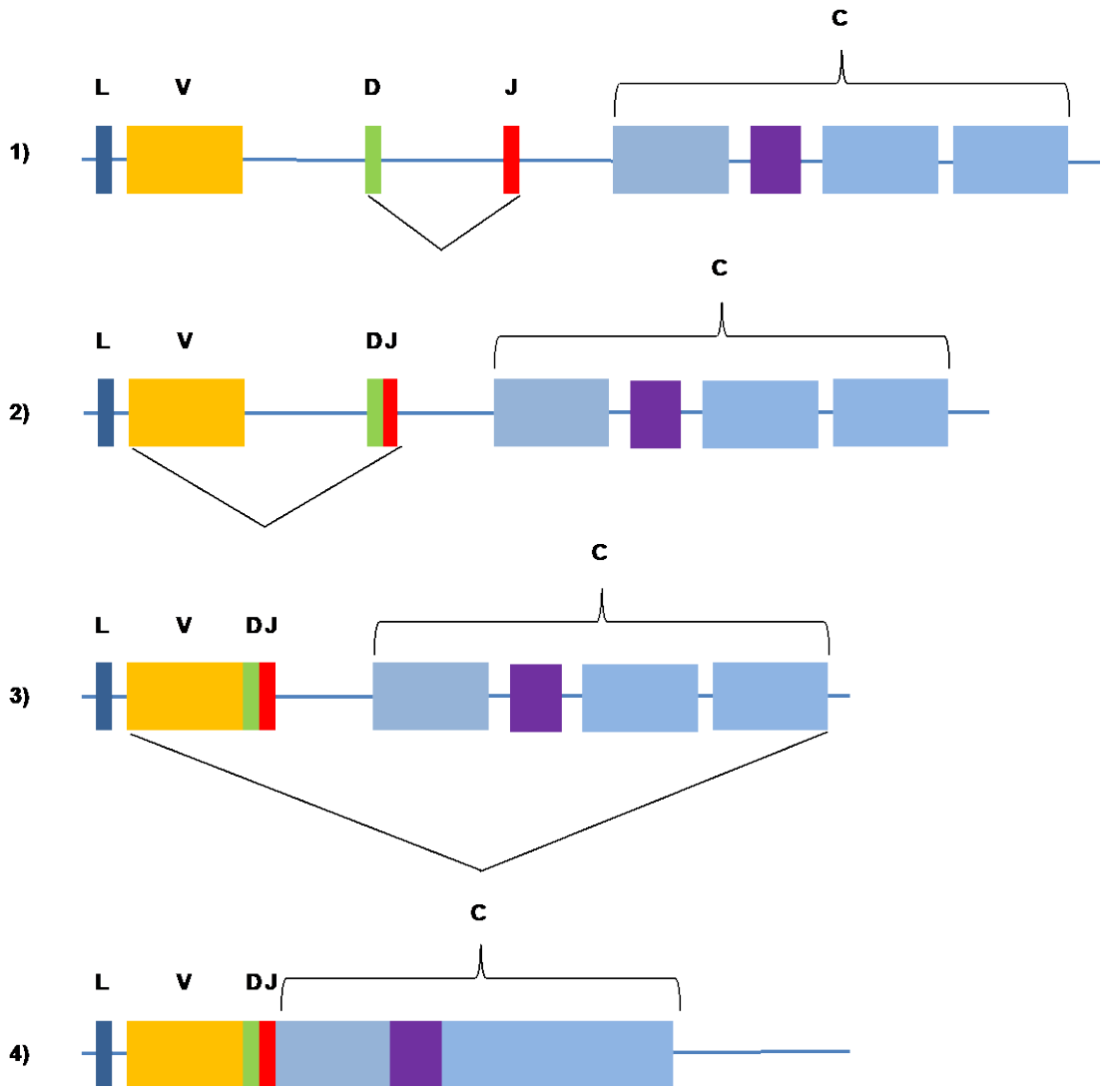

Figure 1.1 V(D)J recombination for the formation of complete Ig heavy chain

Heavy-chain V regions are constructed from three gene segments (V, D and J). 1) First, the D and J gene segments join, 2) then the V gene segment joins to the combined DJ sequence, forming a complete V_H exon. 3) A heavy-chain C-region gene is encoded by several exons which are spliced to the V-domain sequence during processing of the heavy-chain RNA transcript. 4) A complete Ig heavy chain transcript allowing for the translation of a complete Ig heavy chain.

V(D)J recombination events happen early in B cell development after which these B cells move to the secondary lymphoid organs, such as the spleen and lymph nodes, where they can recognise foreign antigen and undergo a second round of diversification. Further diversification and specificity of the BCR is achieved when T cell activated B cells enter germinal centres (GCs). Here, the variable region of the BCR undergoes somatic hyper mutation (SHM) [41]. Ig gene class switch recombination (CSR) can also occur in this location, leading to the production of different isotypes [42].

SHM involves single base substitutions in the variable gene region catalysed by the enzyme activation-induced deaminase (AID) [43]. AID enzymatically converts cytosine to uracil at specific ‘hotspots’ within the Ig locus resulting in a mutagenic U-G base pair which undergoes error prone DNA repair [44]. SHM drives the selection of high affinity B cells within the GC while B cells expressing low affinity BCR are removed via a process known as affinity maturation [45]. Affinity maturation describes the process in which B cell clones which are able to bind antigen with high affinity but also process and present antigen to T cells most efficiently will be selected for over those which are weaker [23]. Subsequently, these B cells go on to become plasma cells and produce antibodies which serve to mediate the important immunological effector functions of humoral immunity.

Conversely, in CSR, to diversify the effector function of specific antibodies, recombination occurs within the downstream portion of the Ig locus; the Cμ region is replaced by Cγ, Cϵ, or Cα segments downstream of the Cμ to switch the isotype from IgM to IgG, IgE, and IgA antibodies, respectively. The process involves a recombination/deletion mechanism that causes the prevailing isotype to be switched out and deleted from the genome [46]. This switching is important for maximal efficacy of the immune response as each of the different isotypes have varying functions, as described later in Introduction; Section 1.3.3. CSR requires CD40-CD40L interaction, between B cells and CD4+ helper cells respectively, and specific cytokine presence adds further selectivity to the antibody isotype synthesised by the B cell; for example, B cells cultured in IL-4 produce IgE antibodies while in the presence of IL-10 IgG, IgA and IgM are produced [47]. The AID enzyme has also been implicated in this process [45] and deficiencies in this enzyme as well as other molecular defects in CSR, such as between the CD40-CD40L interaction or within DNA repair systems, result in immunoglobulin class-switch recombination deficiencies (Ig-CSR-Ds) [48]. These are rare primary immunodeficiencies characterised by normal or elevated IgM levels and either the partial or full absence of the other antibody isotypes (IgG, IgA and IgE). This imbalance in antibody isotypes can result in opportunistic infections, autoimmunity such as haemolytic anaemia, hepatitis and thrombocytopenia as well as an increased occurrence of cancer such as lymphomas [48]. The severity of disease associated with defects in CSR highlight the importance of class switching and hence the presence of all antibody isotypes for normal immune homeostasis.

The selection process of high-affinity B cells described above is essential for a successful immune response to antigen. The events described above occur within GCs and is critically dependent on sequential antigen presentation processes in the GC microenvironment. Thus, follicular dendritic cells (FDCs) first present antigen to B cells, and these B cells then present antigen in the form of antigenic peptides to antigen-specific T-follicular helper (TFH) cells, which, in turn, deliver survival and proliferation signals to the cognate B cells [49]. The selected high-affinity GC B cells then differentiate into either plasma cells or memory B cells. Plasma cells produce large amounts of antibody (each plasma cell producing a unique specificity) and provide the primary response. Subsequent antibody responses upon secondary infection are produced by memory B cells, which are capable of producing a more rapid and robust response upon antigen re-exposure in comparison to naïve B cells as a result of affinity maturation occurring during the primary response [50].

1.3.3 Antibody Isotypes

In humans and mice, B cells produce two different classes of antibody light chain, κ and λ alongside the five different classes of antibody heavy chain μ, δ, γ, α and ε already mentioned above which determine the isotype of the antibody. The IgG and IgA isotypes also have further sub-groups attributed to minor differences in the amino acid sequence of their heavy chains. The five different Ig isotypes within humans and mice have all evolved to possess certain functions that are required for the host immune response to foreign antigen [23]

IgM accounts for 5-10% of the Ig pool in humans and predominates in the innate immune response. It is also expressed as a monomer on the surface of B cells as the BCR [51]. IgM is the most efficient complement-fixing Ig and functions in agglutination and cytolytic reactions resulting in the elimination of target cells. In its soluble form IgM forms a multimer of 5-6 individual antibody molecules with a molecular weight of ~970kDa, linked by an associated J chain. The association of the J chain provides these antibodies with several features. Firstly, a high valency of antigen-binding sites, which makes them suitable for agglutinating bacteria and viruses; and secondly, only J-chain-containing polymers show high affinity for the polymeric Ig receptor (pIgR), also known as transmembrane secretory component

(SC) [52]. This receptor mediates active transfer of pentameric IgM to exocrine secretions such as saliva and tears as a first line of defence at these sites.

IgD antibodies form 1% of the Ig pool. In its soluble form it's function still remains unclear [53]. However, this isotype of antibody, like IgM, is capable of being expressed on the surface of B-cells as a second isotype of BCR, for example of naïve B cells where in fact IgD forms the predominant isotype [53, 54].

IgA antibodies make up 5-15% of the soluble Ig pool and can exist as a monomer or a dimer linked via the J chain. It is the predominant antibody in secretions such as saliva and tears and is found in mucosal areas such as the gut, respiratory and urinary tract preventing their colonisation by pathogens [55].

IgE antibodies are scarce in serum but are found associated with basophils and mast cells and are the primary antibody associated with type 1 hypersensitivity reactions [56].

IgG is the most abundant antibody in both human and mouse serum and has four isotypes in both humans (IgG1, IgG2, IgG3 and IgG4) and mice (IgG1, IgG2a (or the highly related IgG2c), IgG2b and IgG3). IgG antibodies have a molecular weight of ~150kDa and the longest half-life amongst the five main sub-classes (human = ~21 days and mouse = 6-8 days) [57]. IgG antibodies are involved in complement activation as well as inducing effector functions due to their interaction with Fc gamma receptors (FcγR) which is discussed in more detail in Introduction; Section 1.4.2.

1.3.4 IgG structure

IgG antibodies exist as an assembly of four polypeptide chains (150kDa), consisting of two identical light chains (25kDa) and two identical heavy chains (50kDa). Each light chain is made up of a variable domain (VL) and a constant domain (CL) and each heavy chain, one variable domain (VH) and several constant domains (e.g. CH1,2 and 3) [58]. Figure 1.3 shows a schematic of antibody structure. The fragment antigen binding (Fab) fragments of an antibody are responsible for antigen binding, in particular the hyper-variable regions in the V domains, termed complementary determining regions (CDRs). These portions of

the antibody (paratopes) interact with the antigen (epitope) and therefore encode the affinity and specificity of an antibody [58]. The fragment crystallisable (Fc) portion of the antibody is responsible for interaction with the immune system which in turn delivers the biological activity. Most Fc portions of an antibody are glycosylated to maintain the antibody conformation and in some cases contribute towards its therapeutic activity [59]. For example, IgG antibodies have a conserved amino acid, N297 in the CH2 domain, which is glycosylated and stabilises the Fc structure allowing stable interactions with FcγR expressed on immune cells [60]. The Fc portion of a mAb is also responsible for antibody half-life via interactions with the neonatal Fc receptor (FcRn) in a pH dependent manner [61].

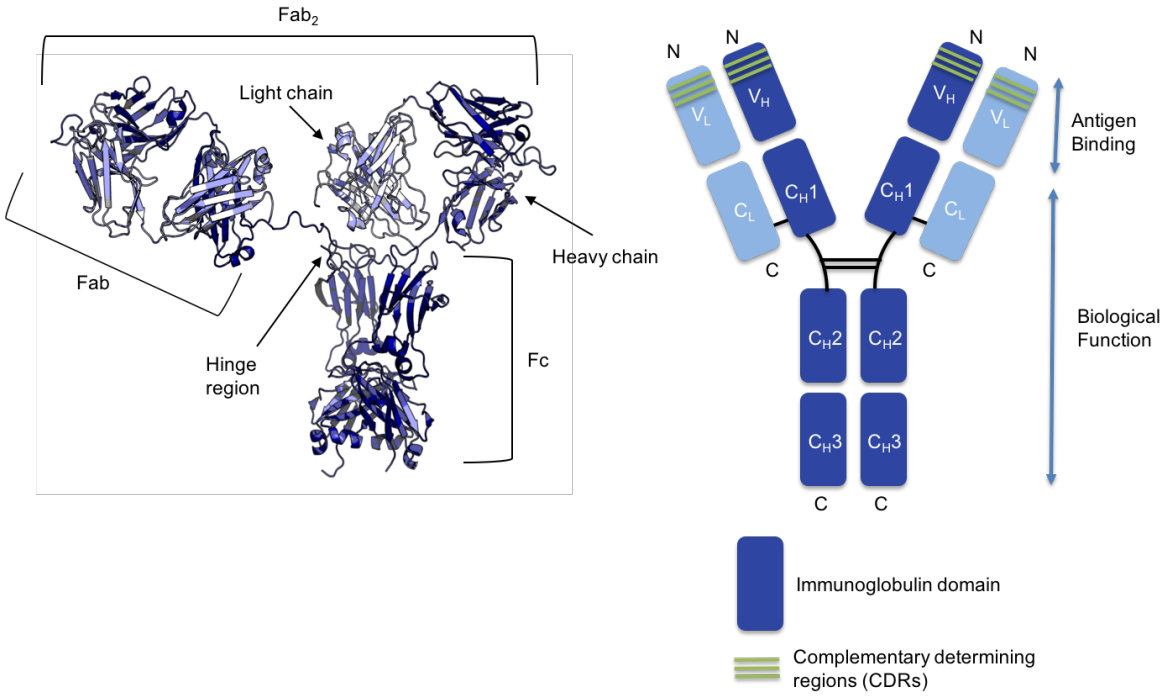

Figure 1.2 Crystal structure and schematic of an antibody

The crystal structure of the antibody was taken from PDB file:1HZH and adapted using Pymol. The antibody schematic shows individual immunoglobulin domains in the light and heavy chains with the CDRs highlighted in green.

Generally the global structures of the IgG subclasses are very similar but they do contain important differences, mainly within the hinge region and the C_H2 domain, which affect their binding to FcγR and C1q, ultimately affecting their functionality (Discussed in detail in Introduction; Section 1.4.2). The main variation seen between these IgG subclasses is the length and flexibility of their hinge regions.

Differences in disulphide binding and length of the hinge region (Table 1.1) affect FcγR binding, antigen binding due to Fab arm flexibility and immune complex formation, all of which impact on effector function [60]. The flexibility of the Fab arms in relation to the Fc share this relationship with effector efficacy as tested by the ability to form immune complexes IgG3 > IgG1 > IgG4 > IgG2 in humans [62], which is also relative to their C1q and FcγR binding (Table 1.2). These types of effector functions elicited by IgG are capable of modulating cells of the immune system such as T cells.

Antibody Isotype	Hinge region
IgG1	2 inter-chain s-s 15 a.a
IgG2	4 inter-chain s-s 12 a.a
IgG3	11 inter-chain s-s ~62 a.a
IgG4	2 inter-chain s-s 12 a.a

Table 1.1 Length and disulphide connectivity within human IgG antibodies

The length and number of disulphide bonds in the hinge regions of human IgG antibodies [60]

1.3.5 T cells

T cells are another population of immune cells derived from the CLP which mature in the thymus and influence all aspects of immunity from direct killing of target cells to immune regulation. Multiple T cell subsets are present within the immune system and distinguished based on the composition of their TCR. The majority of TCRs are of the αβ subtype and react to antigen presented by MHC-I or MHC-II molecules, however approximately 5% of T cells bear γδ TCRs which are

generally not MHC-restricted and seem to be involved in the surveillance of both microbial and non-microbial tissue stress [63]. The work in this thesis focusses on αβ T cells and the modulation of their function therefore they will be discussed solely from now on.

T cells within the thymus can be sub-divided into differing stages of maturity based on the expression of the co-receptors CD4 and CD8. The first of these stages is the double negative (DN) population which does not express CD4 or CD8. The DN population is further sub-divided by the expression of CD44 (adhesion molecule) and CD25 (IL-2R α chain) [64]. Figure 1.3 demonstrates the changes in expression of these markers. DN3 cells, which lack CD44 but express CD25, undergo beta-selection which involves recombination of V, D and J segments of the TCRβ gene via recombination-activating genes RAG1 and RAG2 [64]. This is the first checkpoint during thymocyte development which selects for cells which have successfully rearranged their TCRβ chain locus. This allows the TCRβ chain to be presented at the cell surface where it pairs with the surrogate TCRα chain, Pre-Tα, and produces a pre-TCR that is capable of signalling [64]. Cells which do not undergo successful beta-selection die via apoptosis. This complex leads to the arrest in further β chain loci rearrangement as a result of RAG downregulation and further differentiation of the cell as TCRβ provides signals required for CD4 and CD8 co-receptor expression as well as TCRα gene rearrangement of V and J segments. These cells upregulate both CD4 and CD8 co-receptors and are termed double positive (DP). DP cells rearrange their TCRα chain loci, to produce a functional αβ-TCR. These cells then undergo positive selection via interaction with self-antigens in the context of MHC class I or class II molecules [65]. Those cells that engage antigen/MHC with an appropriate affinity signal through the TCR and are positively selected, whereas those cells that interact with a weaker affinity or not at all die by apoptosis. At this point thymocytes undergo lineage commitment to either CD8+ or CD4+ T cells. They undergo a further selection process with the aim of preventing cells with too high an affinity for self-antigens i.e. autoreactive cells, from entering the periphery. This selection process is termed negative selection. Thymocytes that have too strong an affinity for self-antigen undergo apoptosis whereas those which survive negative selection can enter the periphery [65]. Despite the multiple checkpoint stages in T cell development some autoreactive T cells will escape thymic censorship and be released into the

periphery. One mechanism to deal with this is the development of natural regulatory T cells (nTregs). These cells have the capacity to suppress conventional T cells (see later). Whilst the direct evidence is limited, it is thought that these cells have a higher affinity for self than conventional CD4+ and CD8+ T cells through a process termed agonistic selection [66]. Additional mechanisms known collectively as peripheral tolerance also exist to prevent autoreactive T cells causing autoimmunity. These mechanisms include induction of anergy, deletion and the differentiation of conventional CD4+ T cells into inducible Tregs (iTreg) [67].

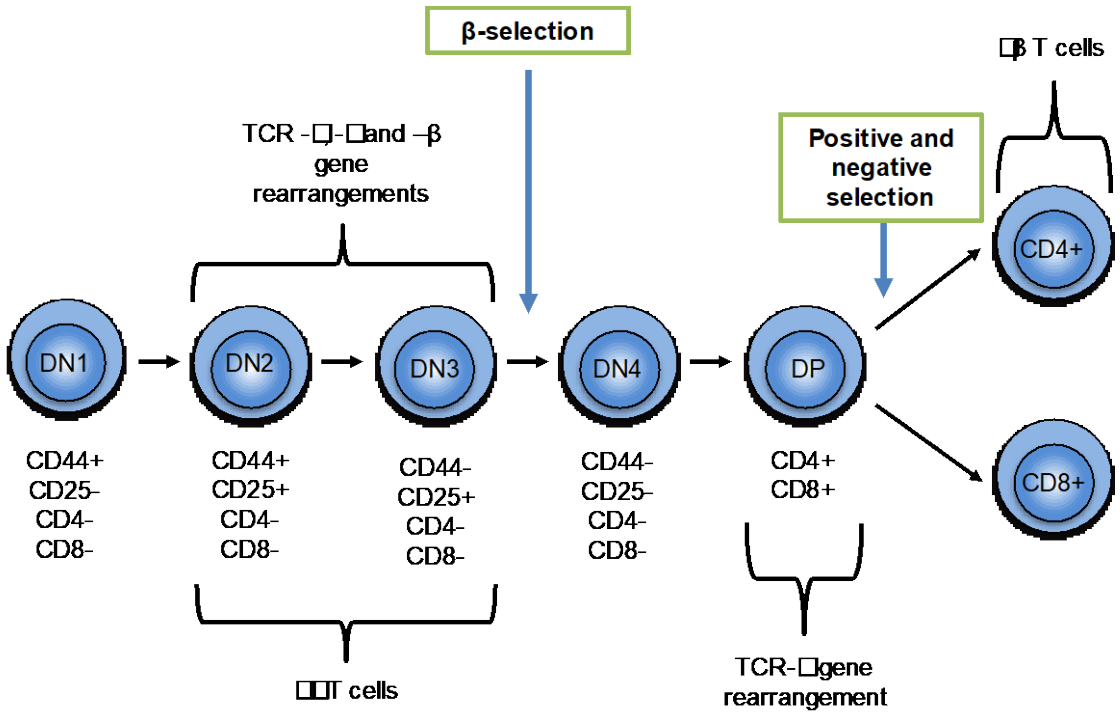

Figure 1.3 Stages of T cell development

T cells mature in the thymus through a series of maturation steps that can be identified based on the expression of different cell surface markers; CD44, CD25, CD4 and CD8. Cells lacking CD4 or CD8 expression are termed double negative (DN), at the DN3 stage cells undergo β-selection. Cells which successfully rearrange their TCR-β chain locus and are able to form a pre-TCR up-regualte CD4 and CD8 expression becoming double positive cells (DP). These cells undergo TCR-α gene rearrangement producing an αβ-TCR. Following this positive and negative selection occur resulting in naïve CD4+ and CD8+ single positive (SP) T cells.

After this multi-step developmental process T cells express functional and unique TCRs composed of α and β polypeptide chains, each of which folds into 2 immunoglobulin domains. TCRs consist of a membrane distal variable region containing 3 CDRs, which recognise peptide bound to self-MHC molecules on APCs, and a membrane proximal constant region [23]. Interaction of MHC-peptide complexes with the TCR induces a cascade of events that propagate through the cell via a multi-layered signal transduction pathway. The evolutionary advantage in having a large number of unique TCRs is that each T cell is capable of recognizing a different peptide, providing a defence against rapidly evolving pathogens [68].

The cells of the adaptive immune response are all highly interlinked and the key to many immune responses are the activation of T cells. This thesis focusses on the immunomodulation of T cells, therefore signalling, activation and cell subtypes are discussed in more detail below.

1.3.6 T cell activation

For T cells to become fully active and fully functional, they must be presented with a minimum of two distinct activation signals and in some cases a third signal is also required [69]. The first signal is from the MHC/peptide interaction with TCR, followed by co-stimulatory receptor interactions and lastly the presence of cytokines. The TCR itself does not contain any intracellular signalling motifs therefore relies upon its association with CD3 subunits which contain ITAMs [70]. CD4 and CD8 co-receptors assist the TCR in the recognition of peptide bound to MHC class II and MHC class I, respectively, and their cytoplasmic tail is associated with the receptor tyrosine kinase, Lck [71]. Lck is responsible for the phosphorylation of the ITAMs on the CD3 subunits which in turn recruits the cytosolic ζ chain associated tyrosine kinase, ZAP70. Activation of ZAP70 is crucial in T cell activation as it phosphorylates adaptor proteins such as linker for activation of T cells (LAT) [72]. As a result of LAT phosphorylation a multiprotein complex called the 'LAT signalosome' is assembled that involves the adaptor protein SLP-76 (LCP2) [73]. This series of phosphorylation events results in the activation of a number of signalling pathways including the Ras/ERK MAPK cascade, the Ca^{2+}/calcineurin/NFAT pathway, and the PKC/NFκB pathway [74] (Figure 1.4). The formation of this signalling complex and activation of the TCR

can result in cellular proliferation, differentiation and the expression of cytokine genes [75].

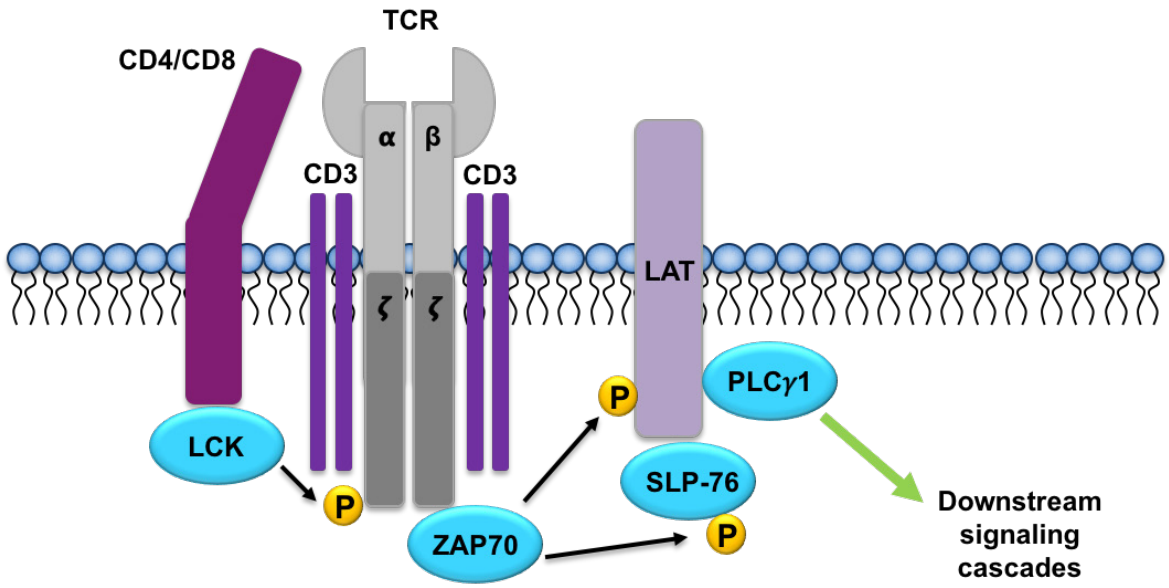

Figure 1.4 Schematic of TCR signalling after MHC:peptide interaction.

After MHC:peptide interaction with the TCR, tyrosine kinase, LCK, phosphorylates the ITAMs within CD3 causing the recruitment of ζ chain associated tyrosine kinase ZAP70. This in turn phosphorylates SLP-76 and LAT and results in the formation of the LAT 'signalosome'. Downstream pathways such as MAPK, NFAT and NFκB are all activated.

Although T cells can be activated via signalling through the TCR it is known that these signals alone are not sufficient for full activation and if sustained for too long can cause apoptosis or anergy in the cells [76, 77]. For optimal proliferation and differentiation T cells require co-stimulation, denoted 'signal 2'. Most co-stimulatory molecules are members of either the immunoglobulin superfamily (IgSF) or the tumour necrosis factor receptor superfamily (TNFRSF). The most well described members of the IgSF are CD28/CTLA-4 and their ligands, the family of B7 proteins (CD80 and CD86). B7 proteins are expressed on the surface of professional APCs and interact with CD28 on the surface of T cells (Figure 1.5). In conjunction with TCR signalling, this interaction has been shown to be co-stimulatory causing up-regulation of cell proliferation [78, 79], cytokine production [80], expression of the IL-2 receptor (IL-2R) [81], and increased survival due to the up-regulation of the anti-apoptotic factor Bcl-xL [82]. Conversely, interaction of CD80/CD86 with the negative regulator and CD28 homolog, CTLA-4, causes inhibitory signals to be sent to the T cells preventing up-regulation of activation markers, entry into the cell

cycle and IL-2 production [83], all of which promote anergy and tolerance. Some examples of co-stimulatory members of the TNFRSF include 4-1BB, OX40 and GITR, all of which are capable of producing co-stimulatory signals to T cells (Figure 1.5). OX40 is the focus of this thesis and is therefore discussed in more detail in Introduction; Section 1.6.

Furthermore, there is evidence that a third signal is required for optimal T cell proliferation and survival and that signal is provided by inflammatory cytokines [69], in particular IL-12 and type I interferons (IFN α/β) for CD8+ T cells and although less well studied IL-1 has been implemented in generating productive CD4+ T cell responses [84]. These cytokines promote transcription of numerous genes involved in T cell differentiation and effector function. The outcome as a result of the integration of these signals will differ according to the subtype of T cell in which they occur.

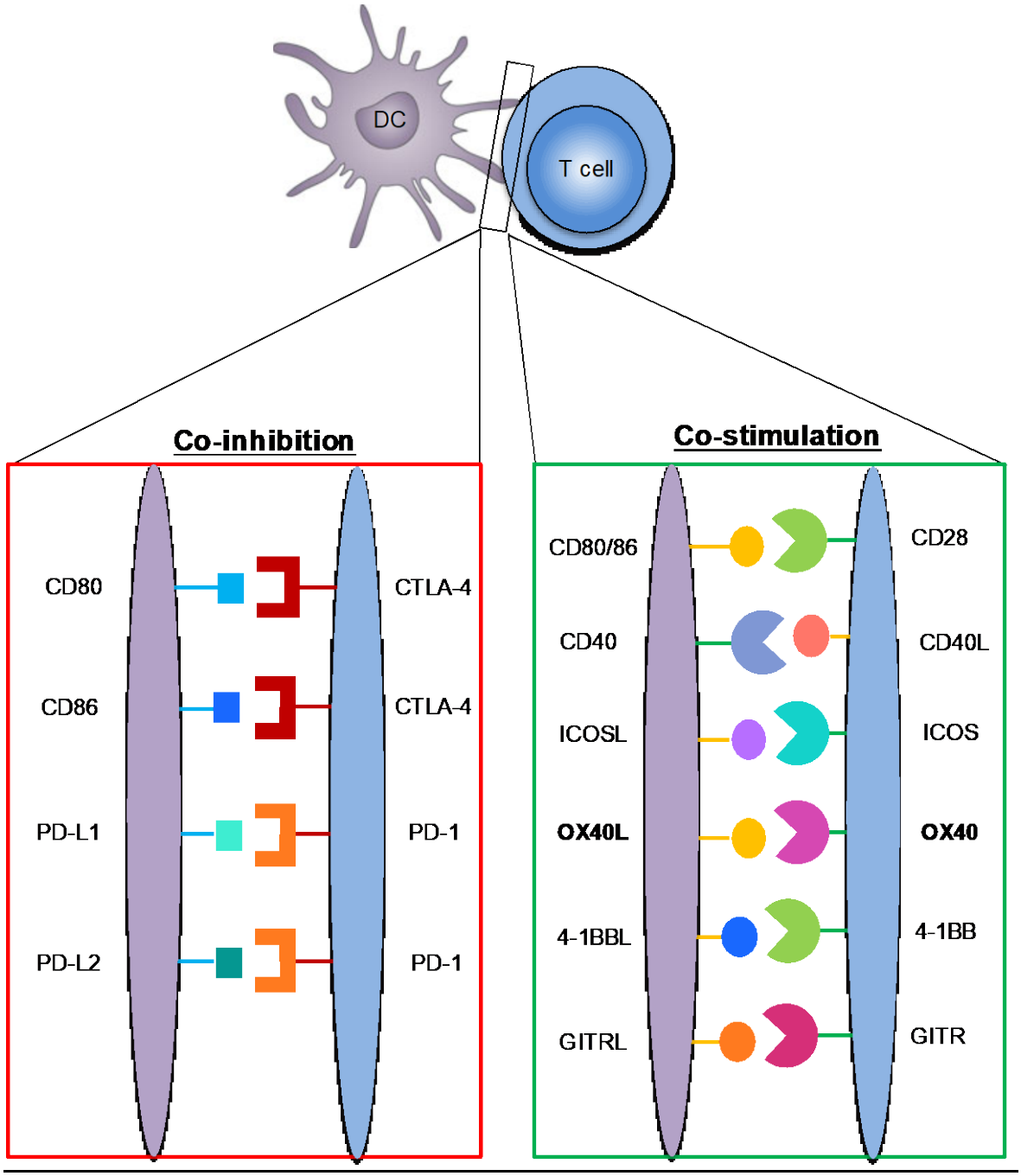

Figure 1.5 Schematic showing T cell co-inhibitory and co-stimulatory receptors

Members of the TNFR and Ig superfamilies and their respective liagnds involved in T cell 'signal 2'; co-stimualtion and co-inhibition.

1.3.7 Mature T cell Subtypes

T cells are classified by expression of CD3 and then split into three main subgroups; CD8+ cytotoxic T cells, CD4+ T helper cells, and CD4+FoxP3+ T regulatory cells.

CD8+ T cells, often termed cytotoxic T lymphocytes (CTLs), recognise antigen presented specifically by MHC-class I molecules [85] which are present on virtually all nucleated cells. The interaction with antigen causes clonal expansion and the development of effector and memory CD8+ T cells [86]. Inflammatory cytokines produced in the innate immune response such as IL-12 and the type I IFN's have been seen to promote CD8+ T cell expansion (signal 3) [87]. Further understanding of the requirements for CD8+ T cells expansion and functional ability has identified T-box transcription factors T-bet and eomesodermin (Eomes) as playing a major role in regulating CD8+ T cell differentiation and function [88]. High levels of T-bet expression promotes short-lived effector CD8 T cells, whereas T-bet expression levels decrease as cells become more memory-like [89, 90]. On the other hand, Eomes expression increases as cells become more memory-like [91] and Eomes knockout mice are deficient in long-term memory formation highlighting its critical role in this process [92]. Both transcription factors cooperate to promote both cytotoxic lymphocyte formation, which correlates with the up regulation of perforin and granzyme B in antigen specific cells [89, 92] as well as sustaining a memory phenotype [92].

Effector CD8+ T cells are capable of killing target cells via two mechanisms; perforin mediated killing and FasL mediated killing [93]. CD8+ T cells can kill directly using granzyme and perforin which are contained within secretory granules within the cell. Although probably too simplistic, it is thought that perforin oligomerises at the membrane of the target cell in a Ca^{2+} dependent manner forming a pore which allows the entry of the serine protease granzyme into the cell resulting in apoptosis [94]. The slower acting, Ca^{2+} independent process, involves the interaction of FASL (CD95L), which is up-regulated on the surface of CD8+ T cells after TCR engagement, and its receptor FAS (CD95) which is expressed on the surface of target cells, in this case infected/cancerous cells, in a more constitutive manner in comparison to the ligand [95]. FAS-FASL interaction results in receptor oligomerisation which engages the intracellular death domain FAS-

associated death domain (FADD) [96]. FADD binds procaspase-8 and allows activation of caspase-8 through self-cleavage, caspase-8 then activates the effector caspases, such as caspase-3, which assign the cell to the controlled process of apoptosis [97].

CD8+ T cells also have the capacity to produce inflammatory cytokines such as IFN-γ and TNF-α which promote certain functions to aid the clearance of infected/cancerous cells such as, macrophage activation, enhanced antigen presentation (IFN-γ) [98] and apoptosis of the cell (TNF-α) [99] . After completion of the primary response and removal of the pathogen most effector cells will die by Bim-mediated apoptosis [100] (Bim is a pro-apoptotic member of the Bcl-2 family), however a proportion of these cells (5-10%) will survive the contraction process and become CD8+ memory cells [101] (Discussed in more detail in Introduction; Section 1.3.8).

CD4+ T cells play a pivotal role in mediating the adaptive immune response and respond to antigen presented by MHC-class II molecules [102] on the surface of APCs (DCs, B cells and activated macrophages). They function to help B cells produce antibody, sustain and enhance the CD8+ T cell response as well as regulate the persistence and strength of the immune response to prevent autoimmunity. Dependant on the cytokine milieu, strength of antigen (i.e. affinity for the TCR), type of APC and co-stimulatory molecules present, naïve CD4+ T cells may differentiate into one of several lineages; T_H1, T_H2, T_H9, T_H17, T_H22 and T follicular helper (Tfh). Transcription factors T-bet and Eomes also play a role in lineage decision. T-bet drives a T_H1 response and represses the alternate T_H2, T_H17 and Treg fates [103]. Furthermore, Eomes expression in CD4+ T cells has been reported to restrict FoxP3 induction and skews towards a T_H1 phenotype [103]. The different subsets of CD4 helper cells are defined by their cytokine production and function. The two subpopulations that have been clearly defined in the mouse are T_H1 and T_H2 cells, each differ in their cytokine profiles and therefore the effector response they generate. The signature cytokine produced by T_H1 cells is IFN-γ, this is a pro-inflammatory cytokine which functions to activate CD8+ T cells and macrophages. In contrast, T_H2 cells fail to make IFN-γ and instead produce IL-4, 5 and 13 as their signature cytokines which promote a humoral immune response.

The third main subtype of T cells are Treg; frequently defined by the expression of CD4 and FoxP3. Tregs function as regulators of the adaptive immune response as they are able to supress the effector functions of a number of immune cells such as other CD4+ and CD8+ T cells, NK and NKT cells, B cells and APCs [104]. These cells are critical in self-tolerance and their dysfunction causes fatal autoimmune diseases, immunopathology and severe allergy [104]. Tregs are broadly classified into natural or induced Tregs; natural Tregs (nTreg) are CD4+CD25+FoxP3+ T cells which are created in the thymus as a result of high avidity MHC-class II interactions [105]. They play a key role in immune homeostasis and self-tolerance as described above. Induced Tregs (iTreg) are derived from naïve conventional CD4+ T cells and are typically induced by inflammation and disease processes such as autoimmunity and cancer. They rely on TCR stimulation and the cytokines TGF-β and IL-2 for both *in vitro* and *in vivo* generation [106]. Several mechanisms of immune suppression have been identified for Treg cells. These include both contact dependent and contact independent mechanisms. Examples of contact independent mechanisms include the production of suppressive cytokines IL-10 (which also maintains expression of FoxP3 [107]) and TGF-β, (which also provides a positive feedback loop for Treg cells), consumption of IL-2 through high density surface expression of CD25 which results in Bim-mediated apoptosis of effector cells and release of granzyme B. Examples of contact dependant mechanisms of suppression include the expression of inhibitory receptors on the cell surface such as PD-1, LAG3 and CTLA-4, preventing DC maturation and effective priming of effector cells as well as metabolic dysregulation in effector cells via the delivery of cyclic adenosine [108-111].

The immunosuppressive role of Tregs has been described as a “double-edged sword” as it has been seen that although beneficial in protecting the host against autoimmune disease and allergies, the inhibitory activity of Tregs can antagonise protective immunity in cancer settings promoting tumour progression [112]. This is discussed in more detail in the context of OX40 signalling in Introduction; Section 1.6.1.

1.3.8 T cell memory

Both CD8+ and CD4+ T cells undergo a contraction phase towards the end of the immune response where most cells (90-95%) undergo apoptosis, however a small percentage survive and convert to memory cells [113]. Memory T cells have classically been subdivided into three distinct subsets on the basis of effector function, proliferative capacity and migration; these are, central memory (T_{CM}), effector memory (T_{EM}) and tissue resident memory (T_{RM}) cells [101].

T_{CM} cells ($CD127^{hi}CD62L^{hi}CCR7^{hi}KLRG\text{-}1^{lo}$) express receptors which preferentially localises them to secondary lymphoid organs such as the spleen and lymph nodes (which express CCR7 ligands CCL19 and CCL21) [114]. In this location they are well situated to protect from systemic infection and seed the peripheral tissues with new effector cells after antigen re-encounter. Furthermore, these cells are functionally delineated from the other two subsets by their increased ability to proliferate [113]. T_{EM} cell expression of receptors involved in localisation ($CD127^{lo}CD62L^{lo}CCR7^{lo}KLRG\text{-}1^{hi}$) contrasts that of T_{CM} cells and facilitates their ability to migrate between non-lymphoid tissue and the secondary lymphoid organs [113]. This ability to traffic between the two tissue types enables them to act quickly at peripheral sites upon re-encounter with antigen. Likewise, their ability to display rapid effector functions such as granzyme B and IFN-γ production but obtain only limited proliferative potential makes them distinct from the T_{CM} population [113]. T_{RM} cells constitute a more recently identified subgroup that resides within a single tissue without the ability to enter recirculation [115]. The cells possess a phenotype ($CD69^{hi}CD103^{hi}CD49a^{hi}CD44^{hi}$) which highlights their ability to reside in tissues, in particular at mucosal sites such as the intestines, lungs and reproductive tract (CD103) [116] however they have also been found at non-mucosal sites including lymphoid and peripheral tissues, for example the thymus, spleen, heart and skin [116, 117]. These cells display effector functions as described above for T_{EM} cells and also the ability to proliferate rapidly like the T_{CM} cells [118]. Collectively the heterogeneity seen in localisation, recall ability and effector function amongst the different memory cell subsets provides rapid, overlapping layers of protection upon secondary infection of the host.

More recently, Hikono et al. [119] described three distinct memory CD8+ T cell populations using the markers CXCR3, CD43 and CD27. The group used these

markers to further divide the more commonly known T_{EM} and T_{CM} arms of memory T cells into subsets that differed in homeostatic proliferation, persistence, granzyme B expression, IL-2 production and recall responses. $CXCR3^{hi}CD43^{lo}CD27^{hi}$ memory CD8+ T cells were able to produce the strongest recall response and persist longer than $CXCR3^{lo}CD43^{lo}CD27^{lo}$ expressing cells which produced the weakest recall response, however provided the most efficient protective immunity against the infection model tested (vaccinia virus) [119].

1.3.9 NK cells

NK cells are another immune cell population that originate from the CLP and play roles in both the innate and adaptive immune response. Despite their lack of a specific antigen receptor, as seen in B- and T cells, these cells are capable of inducing death in infected, stressed and tumour cells via the release of perforin and granzymes from granules in their cytoplasm [120]. NK activity is stimulated by the presence of innate immune cytokines such as IFN-α, IFN-β and IL-12 produced by cell types such as macrophages and DCs [120]. Upon activation they can then release cytokines such as IFN-γ which influences both the innate and adaptive immune response [121]. The activity of NK cells is regulated by functional categories of receptors expressed on their surface; inhibitory receptors that bind MHC-I and block the NK cells from killing, and activating receptors that trigger NK cell activity if an inhibitory receptor is not occupied. The inhibitory receptors are members of the immunoglobulin-like family known as killer-cell immunoglobulin-like receptors (KIR) [122]. The activatory receptors are typically C-lectin like receptors which contain calcium-dependent carbohydrate recognition domains [122]. NKG2D has been recognised as an important activating receptor on NK cells and it recognises non-polymorphic MHC class I molecules that do not associate with β2-microglobulin [123]. These MHC-I molecules are often induced on cells undergoing stress i.e. DNA damage or infection therefore focusing NK cells cytolytic activity to where it would be most useful. Furthermore, NK cells also express the activatory FcγR, FcγRIII, which is responsible for antibody dependent cellular cytotoxicity (ADCC) which will be discussed in Introduction; Section 1.4.1 [124].

1.3.10 NKT cells

NKT cells are a distinct population of T cells which express an invariant αβ TCR and a number of cell surface molecules related to NK cells; CD56 in humans and NK1.1 in mice [125, 126]. Unlike conventional T cells, which mostly recognise peptide antigen presented by MHC molecules, NKT cells recognise glycolipid molecules bound to the MHC-like molecule CD1d which can be expressed on the surface of APCs such as DCs, macrophages and B cells [127]. Functionally, NKT cells are different to conventional T cells in that they can be autoreactive and produce cytokines such as IFN-γ, IL-4 and IL-10 [128]. NKT cells are divided by their TCR repertories into two groups; Type I/invariant and Type II/diverse NKT cells. The invariant NKT cells express an invariant TCR-α chain and a limited number of non-invariant TCR-β chains which recognise the glycolipid α-GalCer [129]. Three defined populations have been described in mice and humans; CD4+, CD8+ and CD4-CD8- (DN) [130] . CD4+ NKT produce all of the cytokines mentioned above and therefore have an immunoregulatory role whereas CD8+ and DN NKT cells appear to have a stronger cytolytic ability as defined by IFN-γ secretion. Diverse NKT cells express a diverse TCR-α and TCR-β chain which do not recognise α-GalCer but react with a range of molecules including self antigens such as sulfatide [129]. The cytokines produced by these cells can modulate several other immune populations including NK cells, conventional CD4+ and CD8+ T cells, macrophages, B cells and DCs.

1.4 Monoclonal antibodies as immunomodulatory agents

Over the last 20 years the use of mAb to manipulate the cells of the immune system and their effector functions has been established. The development of the hybridoma technology by Köhler and Milstein [131] led to the generation of murine antibody against antigens. These mAb possessed relatively little clinical utility when administered to humans due to their inability to efficiently activate human effector functions [132] and their immunogenicity [133], leading to short half-life [134]. Advances in techniques such as DNA recombination, protein engineering [135], phage display [136] and transgenic mice [137] have allowed the development of chimeric, humanised and fully humanised mAb which have

overcome the limitations listed above and resulted in a multitude of mAb being FDA approved [138]. One of the modes of action of mAb are their interactions with cognate Fc receptors which are discussed in detail below, specifically in relation to IgG.

1.4.1 IgG and FcγR interaction

Fc receptors are a family of proteins expressed predominantly on the surface of immune cells which bind the Fc portion of antibodies. These receptors exist for every antibody isotype and are grouped dependent upon which heavy chain class of antibody they interact with i.e. IgA antibodies interact with FcαR and IgG with FcγR. The most utilised isotype of therapeutic mAb is IgG, therefore understanding its interactions with cognate FcγR and the subsequent effector mechanisms produced has proven to be important when developing this isotype for use in the clinic.

Humans possess six different FcγR which differ in their expression patterns and specificity and affinity for IgG (Table 1.2). There is one high-affinity receptor hFcγRI, and five low-affinity IgG receptors, hFcγRIIa, IIb, and IIc and hFcγRIIIa and IIIb. hFcγRI and hFcγRIIIa are associated with an adaptor protein, the common gamma chain, for expression at the cell surface and intracellular signalling [139]. Activating receptors, hFcγRIIa and hFcγRIIc are single-chain activating receptors that contain an ITAM motif, and the inhibitory receptor, hFcγRIIb, contains an immunoreceptor tyrosine-based inhibitory motif (ITIM). hFcγRIIIb is unique as it has no intracellular domain but instead is anchored to the membrane via a GPI anchor; its signalling function is still uncertain [139].

The multiplicity and complexity of FcγR is further expanded by a series of single nucleotide polymorphisms (SNPs) that occur in these receptors. Two variants are present in hFcγRIIa; (H131 and R131) [140], likewise two variants are present in hFcγRIIIa; (V158 and F158) [141]. hFcγRIIIb also contains two variants which differ at four amino acid positions; NA1 (R36 N65 D82 V106) and NA2 (S36 S65 N82 I106), furthermore, a point mutation (A78D) of the NA2 allele generates another hFcγRIIIb variant named SH. These polymorphisms can affect the affinity and

specificity of the receptor to certain IgG isotypes (Table 1.2). For example, a number of studies looking into the affect of the anti-CD20 IgG1 mAb rituximab in lymphoma patients revealed that patients had a better response to the antibody and prolonged progression-free survival if they carried the V158 version of hFcγRIIIa over the F158 [142, 143]. This effect seems to be associated with the affinity of the V variant being 3-fold higher than the F variant (Table 1.2)

	hIgG1	**hIgG2**	**hIgG3**	**hIgG4**
hFcγRI	650	0	610	340
hFcγRIIa H131	52	4.5	8.9	1.7
hFcγRIIa R131	35	1	9.1	2.1
hFcγRIIb	1.2	0.2	1.7	2
hFcγRIIIaV158	11.7	0.3	77	2
hFcγRIIIaF158	20	0.7	98	2.5
hFcγRIIIb*	2	0	11.1	0

Table 1.2 Relative binding affinities of human IgG subclasses to human FcγRs

Affinities constants ($K_a = 10^5\ M^{-1}$) of the Fc domain of different human IgG isotypes to human FcγRs as determined by SPR. * all 3 CD16b variants had the same specificity pattern. Adapted from Bruhns et al. [144].

The expression profile of these receptors is dependent on the type of immune cell present and the microenvironment and stimulation that it receives. hFcγRI is restricted to monocytes/macrophages and DCs although its expression can also be induced on neutrophils [141]. B cells predominantly only express the inhibitory receptor, hFcγRIIb [145], and NK cells the activatory receptor hFcγRIIIa, with a proportion also expressing hFcγRIIc [146]. hFcγRIIa is expressed on all myeloid cells and hFcγRIIIb on neutrophils [147].

Mice also have a homologous family of FcγR, with three activatory FcγR and a single inhibitory receptor (Table 1.3). The three activatory receptors expressed in mouse are mFcγRI, mFcγRIII and mFcγRIV. They all require association with the common γ chain for expression at the cell surface and signalling via an ITAM motif [148]. In contrast the inhibitory receptor, mFcγRII contains an ITIM motif for intracellular signalling and does not require the γ chain for expression or function. mFcγRI is expressed on macrophages and DCs [149], whilst the rest of the myeloid population express a combination of mFcγRIII, mFcγRIV and mFcγRII [141]. Similar to humans, mouse B-cells only express mFcγRII, and NK cells only express mFcγRIII [150].

	mIgG1	**mIgG2a**	**mIgG2b**	**mIgG3**
mFcγRI	0	750	ND	ND
mFcγRII	52	4	22	0
mFcγRIII	35	38.5	6	0
mFcγRIV	1.2	650	200	0

Table 1.3 Mouse FcγR specificity towards mouse IgG isotypes

Affinities constants (K_a = 10^5 M^{-1}) of the Fc domain of different mouse IgG isotypes to mouse FcγRs as determined by SPR.. Adapted from Bruhns et al.[144].

There are no direct comparisons in terms of FcγR and antibody isotype biology between mouse and humans as evidenced above, therefore interpretation of results between the two requires care.

1.4.2 IgG isotype and effector function

The type/strength of effector function elicited by a mAb is clearly influenced by isotype mainly due to differences in FcγR affinities. The outcome of interactions between the antibody and FcγR depends on the balance between activatory and inhibitory receptor expression which has been described as the

activatory:inhibitory ratio (A:I), and also on which cell types they are expressed [151]. There are a number of effector mechanisms that IgGs may engage dependent upon their affinities for certain FcγRs. mAb which have a higher affinity for the activatory FcγR induce mechanisms such as antibody dependent cellular cytotoxicity (ADCC), which refers to the killing of a target cell, typically through release of cytotoxic granules such as granzyme and perforin, usually from NK cells [152], and antibody dependent cellular phagocytosis (ADCP) which describes the engulfment of a target cell by either macrophages or monocytes [153]. Certain isotypes with a high A:I FcγR ratio such as the murine IgG2a and human IgG1 are optimal for engaging activatory FcγR and eliciting target mediated deletion [154-158] e.g. for NK-mediated ADCC using mouse antibodies IgG2a>IgG2b>IgG1 [159-161]. On the other hand, mAb with a low A:I ratio such as murine IgG1 and human IgG2 are sub-optimal and more effective at precipitating the receptor clustering required to drive TNFR signalling (anti-CD40 for example). For human IgG2 mAb this appears to be largely due to the IgG2B isoform, independent of FcγR and relates to the special properties of the IgG2 hinge [157, 162]. These isotype dependent rules of agonistic activity have been shown for a number of mAb targeting TNFR family members [160, 163, 164].

The concept of having a beneficial A:I FcγR ratio has been highlighted in a number of mouse tumour studies. It has been demonstrated that intra-tumoural depletion of Tregs via mAb which engage activatory FcγRs with high affinity, provided the most efficient therapy in comparison to mAb isotypes with lower affinities for the activatory receptors [165-167]. Furthermore, it has been shown in clinically relevant mAb rituximab (anti-CD20) and trastuzumab (anti-HER2), both hIgG1 isotypes, that they both require activatory FcγRs for effective therapy, which was reduced in the presence of the inhibitory FcγR [168]. These studies highlight that selective use of particular isotypes in cancer therapeutics can dramatically alter the outcome, and is therefore an aspect of mAb design and development that needs to be considered carefully. For example, deletion of Tregs would be favoured by hIgG1 which would be beneficial in the tumour to raise the CD8:Treg ratio, whereas hIgG2 may favour agonistic responses generating expansion of effector cells. It remains to be seen whether a single antibody format can deliver both of these activities.

However, this is not the only variable which affects the final effector function of a mAb; epitope/domain binding as well as ligand interaction in the presence of the mAb also need to be considered. Furthermore, these effector functions can typically only be carried out if the required FcγR are present on the required cell type. With respect to oncology, different tumours have different microenvironments and infiltrates which will influence the FcγR availability. The route of administration will also influence the FcγR an antibody may encounter and hence the overall outcome, for example, it has been shown with a number of mAb reporting Treg depletion that administration of the mAb intratumourally results in local immunomodulation which proved to be more therapeutically beneficial and less toxic than systemic administration [169, 170].

1.5 Immunotherapy

The idea of exploiting the host immune system to combat cancer dates back centuries but it is only within recent years that the use of immunotherapy has gained significant clinical use. Broadly cancer immunotherapy is split into two categories; active and passive. The difference between the two hinges on how it influences the patient's immune system. Active cancer immunotherapy describes activating the hosts own immune response to generate effector populations capable of mounting a long-term response and memory, examples of this include cancer vaccines [171], and oncolytic virus-based therapy [172]. Alternatively, passive cancer immunotherapy doesn't necessitate an immune response but delivers the response via immune components generated outside the host, such as direct targeting mAb [173] and cell-based therapies [174]. In this thesis the use of immunomodulatory mAb was studied as a form of cancer immunotherapy.

As described above the use of monoclonal antibodies as a form of cancer immunotherapy has been established over the past few decades (Table 1.4). Following numerous disappointing efforts and clinical failures, the field has more recently received a significant boost with successful mAb becoming part of first line treatments used in the clinic to treat patients. Immunotherapeutic mAb can come in various forms but are typically described as either direct targeting or immunomodulatory antibodies. Direct targeting antibodies recognise a specific antigen expressed on the tumour (or other target) cell surface, and upon administration to patients will delete that target [175]. An example of a direct

targeting antibody is rituximab which targets the CD20 surface marker found on normal and malignant B-cells. This mAb was approved for treatment of Non-Hodgkin's lymphoma (NHL) in 1997 and since then the field of cancer immunotherapeutics has continued to expand [176] (Table 1.4). Despite the success of direct targeting anti-tumour antibodies, other types of immunotherapy such as immunomodulatory mAb hadn't shown success until more recently [177]. The pioneering mAb of this field were the checkpoint inhibitors anti-CTLA-4 and anti-PD-1.

mAb name	Brand name	Format	Target	Indication	FDA approval	Eu approval
Rituximab	MabThera/Rituxan	Chimeric IgG1	CD20	NHL	1998	1997
Trastuzumab	Herceptin	Humanised IgG1	HER2	Breast Cancer	1998	2000
Ibritumomab tiuxetan	Zevalin	Murine IgG1	CD20	NHL	2002	2004
Cetuzimab	Erbitux	Chimeric IgG1	EGRF	Colorectal Cancer	2004	2004
Panitumumab	Vectibix	Human IgG2	EGRF	Colorectal Cancer	2006	2007
Ofatumumab	Arzerra	Human IgG1	CD20	CLL	2009	2009
Pertuzumab	Perjeta	Humanised IgG1	HER2	Breast Cancer	2012	2013
Obinutuzumab	Gazvya	Humanised IgG1; glycoenginered	CD20	CLL	2013	2014
Dintuximab	Unituxin	Chimeric IgG1	GD2	Neurolastoma	2015	2015
Nectimumab	Portrazza	Human IgG1	EGRF	NSCLC	2015	2015
Dararumumab	Darzalex	Human IgG1	CD38	Multiple Myeloma	2015	2016
Bevacizumab	Avastin	Humanised IgG1	VEGFR2	Colorectal Cancer	2004	2005
Ipilimumab	Yervoy	Human IgG1	CTLA-4	Metastatic melanoma	2011	2011
Ramucirumab	Cyramza	Human IgG1	VEGFR2	Gastric Cancer	2014	2014
Pembrolizumab	Keytruda	Humanised IgG4	PD-1	Melanoma	2014	2015
Blinatumomab	Blincyto	Murine bispecfic tandem scFv	CD19,CD3	Acute lymphoblastic leukaemia	2014	2015
Nivolumab	Opdivo	Human IgG4	PD-1	Melanoma, non-small cell lung cancer	2014	2015
Elotuzumab	Empliciti	Humanised IgG1	SLAMF	Multiple Myeloma	2015	2015
Olaratumab	Lartruvo	Human IgG1	PDGFRα	Soft tissue sarcoma	2016	2016
Atezolizumab	Tencentriq	Humanised IgG1	PD-L1	Bladder Cancer	2016	2017
Avelumab	Bavencio	Humanised IgG1	PD-L1	Merkel cell carcinoma	2017	2017
Durvalumab	IMFINZI	Human IgG1	PD-L1	Bladder Cancer	2017	In review

Table 1.4 Current approved mAb for use in cancer therapy

Table modified from 'Approved antibodies' produced by JM Reichert; The Antibody Society, *Last Updated: 20Aug18.* Blue shaded section indicated direct targeting mAb and green shaded section immunomodulatory mAb.NHL= Non-hodgkin lymphoma, CLL = Chronic lymphocytic leukemia, NSCLC = Non-small cell lung cancer.

1.5.1 Checkpoint Inhibitors

As discussed in Introduction; Section 1.3.5, it is essential for T cells to have intrinsic regulatory mechanisms in order for them to not become inappropriately activated and to maintain self-tolerance. Tumour cells, however, have exploited these mechanisms in order to prevent immune surveillance and avoid T cell destruction [2]. Therefore, it is important to understand immune checkpoints within the cancer setting so that they can be targeted therapeutically.

The first immune checkpoint to be clinically targeted was the receptor cytotoxic T lymphocyte-associated protein 4 (CTLA-4) which is stored in intracellular vesicles and expressed on the surface of T cells after they have been activated [178]. CTLA-4 functions by competing with receptor homolog CD28 for interaction with their ligands CD80/CD86 which are expressed on APCs [179]. CTLA-4 has a higher affinity for these molecules and hence inhibits T cell responses by blocking CD28 co-stimulation of the cell. The importance of CTLA-4 in maintaining self-tolerance is demonstrated in CTLA-4 knock out mice which develop a lethal immune hyper-activation [180]. Furthermore, CTLA-4 is expressed constitutively on Treg cells and the receptor has an important role in maintaining Treg suppressive abilities [178].

Another targeted checkpoint molecule found on T cells is programmed cell death protein 1 (PD-1) which upon interaction with its ligands PD-L1/PD-L2 negatively regulates T cell mediated immune responses [181]. As with CTLA-4, signalling through this receptor contributes to T cell tolerance and immune homeostasis, the importance of which is highlighted by *Pdcdi* (encodes PD-1) deficient mice which develop accelerated autoimmunity [182, 183] Similarly to CTLA-4, PD-1 is also highly expressed on Treg cells, however, rather than inhibiting their function, PD-1 receptor ligation may increase their ability to proliferate [184].

High and sustained expression of these negative checkpoint receptors and their ligands described above are commonly seen in tumours [185]. Pre-clinical studies showed that blocking the receptor ligand interactions could improve T cell functions and reduce tumour burden [186]. In 2011 approval of the first anti-CTLA-4 mAb, ipilimumab (IgG1) was granted for use in human patients followed by the approval of the anti-PD-1 mAb, Nivolumab (IgG4) in 2014 [187], initially for the

treatment of melanoma. These mAb have now been shown to result in increased patient survival in a number of studies including those of renal cell carcinoma, squamous cell carcinoma and non-small cell lung cancer when compared to conventional chemotherapies [188]. Although both are effective forms of treatment they are thought to function differently and at different time points in the T cell immune response.

CTLA-4 blockade is thought to work by a number of different mechanisms most likely impacting T cell activation in the lymph nodes: Firstly, via release of CD4+ helper T cell suppression allowing them to provide help to cytotoxic CD8+ T cells, increasing the endogenous tumour response [189]; Secondly, anti-CTLA-4 treatment is capable of blocking and suppressing Treg populations as the receptor on these cells functions to increase their activity [190], and in some cases may even cause depletion when high CTLA-4 expression is observed [167]. All of these mechanisms lead to high levels of inflammation [191] and may be the reason why this form of treatment is associated with autoimmune side effects as seen in pre-clinical models of CTLA-4 knock-out mice as well as patients (see below).

The mechanism of action of PD-1 blockade is thought to act within the tumour microenvironment. It has been observed that tumour infiltrating lymphocytes (TILs) have an increased expression of PD-1 on their surface due to chronic antigen stimulation leading to exhausted T cells [192]. As tumour cells also highly express the PD-1 ligands, PD-1 expressing TILs can be inhibited by PD-L1/2 on the surface of tumour cells [193]. The blocking mAb therapy is therefore thought to reverse the exhaustion of TILs, as shown in chronic viral models [194], and also allow them to remain fully functional in the tumour environment.

Inhibition of CTLA-4 and PD-1 through therapeutic antibodies in the treatment of cancer have been associated with a range of autoimmune side effects due to the receptors roles in maintaining self-tolerance and immune homeostasis as described above. The rates of immune side effects documented vary between trials but almost all patients treated with immune checkpoint inhibitors experience mild side effects such as fatigue, diarrhoea, rash and nausea [188]. More severe adverse effects include colitis, dermatitis and hepatitis. Interestingly, certain treatment related autoimmune reactions such as rash have been shown to correlate with better disease prognosis [195].

In addition to the side effects listed above, PD-1 and CTLA-4 blocking agents are not effective in all patients and even those patients that respond initially have the potential to relapse [188]. Bearing this in mind, the need for improved or alternative treatments is clear. One possible option is to target the co-stimulatory receptors, such as members from the TNFR superfamily, to see whether agonising the immune system might provide an option for those patients not responding to checkpoint blockade.

1.5.2 Targeting TNFR family members

The TNFRSF and cognate TNF ligands constitute a family with diverse roles in the immune response. They are involved in biological processes ranging from selective induction of cell death via death inducing ligands binding to their respective death receptors e.g. FasL-Fas, as well as providing co-stimulatory signals to cells within an immune response [196]. While at an earlier stage in development compared to checkpoint inhibitors, various co-stimulatory TNFR ligand/TNFR pairs have been trialled as therapeutic targets; CD40L/CD40 [197], 4-1BBL/4-1BB [198] and OX40L/OX40 [199], and revealed potent anti-tumour activity in pre-clinical models [200, 201] gaining prominence as possible targets for cancer immunotherapy.

CD40 is one such TNFR that is expressed on the surface of B cells, monocytes, DCs and activated CD8+ T cells [202]. One of the main functions of the interaction of this receptor with its cognate ligand, CD40L, found on the surface of activated CD4+ and CD8+ T cells, is to license DCs to prime effective cytotoxic CD8+ T cell responses [203]. Thus, the main aim of therapeutically targeting CD40 with agonistic mAb is the induction of this efficient DC-mediated T cell priming allowing for an effective anti-tumour immune response to be established. Therapeutic benefit when using agonistic anti-CD40 mAb has been demonstrated in both mice [204] and humans [197] however not without side effects. Systemic and dose-limiting toxicity towards normal cells due to agonistic anti-CD40 mAb causing inflammatory side effects has been witnessed in both mice and humans [197, 205] highlighting the need to selectively stimulate CD40.

4-1BB is another member of the TNFRSF expressed on the surface of activated T cells and constitutively expressed on Tregs [206] that has been targeted using agonistic mAb. The interaction of this receptor with its ligand, 4-1BBL, results in enhanced proliferation and survival of T cells [207], as well as resulting in enhanced cytokine secretion from these T cell subtypes. Agonistic 4-1BB mAb trigger effective anti-tumour immune responses in a variety of mouse models [198, 208] as well as showing promise in human patients [209]. However, like anti-CD40 mAb, anti-4-1BB mAb have shown toxicity in both murine models [210] and clinical trials i.e. inflammatory liver toxicity [209], again highlighting the need for more selective targeting of the receptor.

Another candidate for activation of anti-tumour T cell immunity is OX40. Targeting this receptor forms the basis of this research therefore it is discussed in more detail below.

1.6 OX40/OX40L

OX40 (CD134), and its interacting ligand OX40L (CD252) are members of the TNFRSF involved in potentiating T cell responses triggered through the TCR [211]. OX40 was initially described as a T cell activation marker on rat CD4+ cells [212]. It is now known, however, that both mouse and human OX40 are expressed primarily on activated T cells, including CD4, CD8, T helper cell subtypes; T_H1, T_H2, and T_H17 as well as CD4+ FoxP3+ Tregs [211, 213, 214]. OX40 is also expressed to a lesser extent on neutrophils, NK and NKT cells [215-217]. Unlike other co-stimulatory receptors, such as CD28 and CD27, OX40 is not expressed on most naïve T cell subsets; however antigen (Ag) stimulation and subsequent signalling through the TCR results in OX40 expression that peaks between 12 hours and 5-6 days post Ag stimulation [218-221]. The kinetics of receptor expression are determined by a number of factors including; T cell subset, persistence of antigen as well as immunogenicity, inflammatory environment i.e cytokine milieu, as well as the presence of other co-stimulation [220]. CD28-B7.1/2 interactions sustain the expression of OX40 on the surface of T cells [219, 220], allowing increased survival and proliferation due to prolonged OX40 signalling.

However, CD28 stimulation is not involved in the re-expression of OX40 on effector cells [219, 222, 223].

Like OX40, human and mouse OX40L is only induced after stimulation – in this case through signals such as CD40-CD40L interactions, Toll-like receptors (TLRs) and inflammatory cytokines such as thymic stromal lyphoprotein (TSLP) [224, 225]. OX40L has been detected on the surface of APCs 1-3 days after antigen encounter [226]. It was thought previously that OX40L expression was limited to professional APCs such as activated B cells, DC and macrophages, however its expression has also been observed on NK cells and mast cells [227-231], as well as structural cells such as smooth muscle cells and vascular endothelial cells in the presence of inflammatory cytokines [223, 232, 233].

1.6.1 Signalling through OX40:

A number of signalling pathways have been identified downstream of OX40-OX40L interactions including those mediated by PI3K/PKB, NF-κB and NFAT that account for the reported functional consequences of T cell division, survival and cytokine production [234, 235]. Nonetheless, delineation of signalling directly downstream of OX40 is limited as the majority of studies have been done in conjunction with TCR signalling (because naive T cells do not express OX40 until they have been activated through the TCR) and have thus showed how OX40 can augment signalling downstream of TCR – MHC/peptide interactions. [223]

The cytoplasmic tail of OX40 contains a QEE motif characteristic of many TNFRSF members that allows binding to TNFR-associated factors (TRAFs) [235, 236]. Formation of trimeric receptor:ligand complexes clusters the cytoplasmic domain of OX40, creating docking sites for TRAF adaptor proteins linking receptor activation to various signalling pathways. The QEE motif in the cytoplasmic domain of h/mOX40 is able to recruit TRAF 2, 3 and 5 [236]. The GGSFRTPI sequence immediately upstream of the QEE motif in humans is required for association of TRAFs 1,2,3 and 5 [237]. TRAF 2 and 5 have been shown to activate the NF-κB signalling pathway whereas TRAF 3 has an inhibitory effect [237]. TRAF 2, 3 and 5 are also able to directly interact with the inhibitor of NF-κB α-subunit (Iκ-Bα), IκB kinase complex catalytic subunit IKKβ and NF-κB inducing

kinase (NIK) demonstrating that OX40 can regulate both the canonical (NF-κB1) and non-canonical (NF-κB2) signalling pathways [211, 237, 238]. Through its regulation of the NF-κB pathways, OX40 activation has been shown to increase the expression of a number of anti-apoptotic proteins including Bcl-2, Bcl-xL and Bfl-1 (A1) causing suppression of apoptosis and enhanced cell survival [220, 223]

As mentioned above, OX40 activation and its consequent downstream signalling has also been shown to augment the signalling downstream of the TCR, mainly through effects on the PI3-K/PKB pathway. In the absence of OX40 activation of PKB is not sustained within T cells resulting in these cells undergoing extensive cell death suggesting that OX40 is central to T cell longevity through combined effects on PKB from the TCR and OX40 after antigen encounter [239]. Furthermore, synergy between TCR and OX40 signalling increases the expression of survivin and Aurora B kinase through sustained PKB activation [240, 241]. These two proteins function together to promote the activity of cyclin dependent kinases allowing for G1 to S phase progression in the cell cycle and maintenance of mitosis in T cells [240, 241]. Additionally, OX40 ligation in conjunction with TCR signalling can increase calcium influx and enhance NFAT activation. This pathway is involved in the production of cytokines such as IL-2, IL-4, IL-5 and IFN-γ [194]. Thus, signalling downstream of OX40 has the potential to augment proliferation, suppress apoptosis and induce greater cytokine responses from T cells; all effects that agonist OX40 antibodies have the capacity to elicit for immunotherapy [223].

1.6.2 Functional effects of OX40:

The most recognised function of OX40 is to enhance proliferation and survival of CD4 and CD8 T cells through the pathways described above. These activities were first shown *in vitro* whereby addition of OX40L or agonistic anti-OX40 mAb resulted in proliferation of CD4 T cells [212, 242, 243]. The development of more sophisticated *in vitro* systems alongside the generation of OX40 and OX40L knock-out (KO) animals, plus the use of agonist and blocking antibodies *in vivo* revealed the full spectrum of effects induced by engaging OX40. For example, it is now well established that OX40 interaction with ligand enhances sustained proliferation and optimal clonal expansion of CD4 T cells in primary and secondary

response to antigen; as well as promoting effective memory generation [218, 219, 225, 244-246]. OX40 has also been shown to have effects on cytokine production, which depending on context can lead to differentiation of CD4 T cells into either T_H1 or T_H2 subsets whilst also demonstrating a role in IL-17 production and T_H17-mediated diseases [211, 224, 247, 248]. The engagement of OX40L with OX40 on naïve CD4 T cells (after its TCR-mediated upregulation) preferentially leads to the differentiation of T_H2 cells as a result of autocrine IL-4 production [224, 249, 250]. However, the presence of IL-12 or Type I interferons can override this divergence and lead to T_H1 differentiation [224, 251, 252]. It has also been demonstrated in a mouse model of asthma that the absence of OX40 results in an impaired T_H1 response but the T_H2 response remains normal [253, 254] suggesting T_H1 development is more reliant on OX40 and its signals. Conversely, others have shown that there is no primary role in OX40 signalling in directing T_H1 or T_H2 differentiation [255]. The role of OX40 on T_H17 cells is less clear. It has been shown to be involved in IL-17 and IL-23 cytokine production in both *in vitro* and *in vivo* models leading to the differentiation and expansion of T_H17 helper cells [247, 256]. However, data also suggest that OX40 engagement antagonises T_H17 development by inhibiting IL-17 production [223, 248, 257].

The understanding of the role of OX40 on CD8 T cells has lagged behind that of CD4 T cells mainly because initial studies using OX40 KO mice challenged with virus suggested that OX40 had minimal impact on the CTL response [246, 258]. However, subsequent studies using TCR transgenic mice revealed that CD8 T cells are also affected by OX40-OX40L interactions [221, 259]. The results observed were similar to that seen in the CD4 response i.e. in the absence of OX40, TCR transgenic CD8 T cells showed defective expansion, decreased survival and poor memory generation [221, 223, 234, 259, 260]

Overall, the signalling and functional data described above indicate that OX40 signalling promotes robust immune responses and therefore agonistic antibodies are a potential therapeutic target for cancer. One potential caveat to this simplistic approach is the complexity relating to how OX40 is regulated on different T cell subsets; in particular, the role of OX40 in Treg development and function [223].

1.6.3 Role of OX40 in Treg Development and Function:

OX40 is expressed constitutively on murine Tregs unlike human T cells. It has also been reported that OX40 is more highly expressed on Tregs, particularly on those isolated from tumour sites [165, 169, 223, 261].

A lot of controversy has surrounded the affect of OX40 on Treg development and their suppressive function. Initially it was thought that OX40 was essential for Treg development [262, 263], however, later studies revealed little to no defect in the development and homeostasis of Tregs in the absence of OX40 [264, 265]. Similar controversy surrounds the effects of OX40 signalling on FoxP3 expression. Some groups report that signalling through OX40 is capable of down-regulating FoxP3 expression [264, 266], however others have shown no changes in the expression of the transcription factor [262, 264]. These OX40 signalling effects seem to play more of a central role in iTreg development compared to nTregs yet still maintain the controversy. *In vitro* studies using OX40L showed that OX40 signalling was detrimental to the development of iTregs [267-269]. On the other hand, a study using an OX40 agonistic antibody revealed that OX40 signalling enhanced the development of iTregs [270]. As with the majority of murine studies, whilst a clear role for OX40 in the development of human nTregs has not been established, OX40 signalling has been shown to be detrimental to the induction of human iTregs and their function [271]. Controversy surrounds OX40's affect on Treg function as well as their development. OX40 KO Tregs display a mild defect in suppressive capability *in vitro* and reduced capacity to suppress mast cell degranulation [235, 263, 272]. Likewise, *in vivo*, Tregs are shown to require OX40 in order to maintain their suppressive function [265]. As with the initial controversy over a role in Treg development, OX40 KO Tregs have subsequently been shown to be fully functional [223, 264].

In relation to cancer immunotherapy, studies where signalling was provided by either an agonistic anti-OX40 mAb or OX40L overexpressing APCs have consistently shown inhibition of Treg function [261, 264, 273]. Whilst some of these tumour studies report clear Treg depletion, the majority do not [165, 169, 261, 263, 274]. [223]

1.6.4 OX40 as a therapeutic target:

OX40 as a therapeutic agent has been investigated in a number of preclinical tumour models; using both anti-OX40 mAbs and OX40L-Fc fusion proteins. OX40 therapy has been shown to cause tumour regression and delayed tumour growth mainly in immunogenic models [213, 214, 261, 275-280], with the anti-tumour immunity relying upon expansion of CD8 and CD4 T cells, with a proportion of mice showing evidence of strong memory responses sufficient to provide resistance upon tumour re-challenge [276, 281]. In addition to promoting effector T cell expansion recent studies have also shown that in certain models depletion of tumour infiltrating Tregs that constitutively express OX40 [165, 169] could also be an important component of OX40 therapy . Bulliard et al demonstrated that the OX40 antibody OX86 (a rat IgG1) required the activatory FcγR for depletion of Tregs and therapeutic benefit [165]. This deleterious effect was influenced by isotype as the use of a mIgG2a mAb showed greater depleting capacity, resulting in an increased CD8:Treg ratio compared with the rat IgG1. Furthermore, the preferential depletion of Tregs over effector T cells was due to differential OX40 expression on the T cell subsets. [223]

In the first-in-human clinical trial with an anti-human OX40 agonist antibody promising results were seen, where 12 out of 30 patients showed evidence of tumour regression after just one cycle of treatment in a number of solid tumour types [199]. Nevertheless, despite its promising results anti-OX40 monotherapy, like the checkpoint blockers, was insufficient to treat all cancer types or patients. However, further mouse model studies using anti-OX40 in combination with other monoclonal antibodies (anti-CTLA-4 [282] and anti-PD-1 [283]), chemotherapy [274] and cytokines [284] have all shown increased therapeutic effects in comparison to monotherapies. This provides an encouraging direction for clinical development [278], as being shown by the currently recruiting anti-OX40 trials which are all combination studies (Further discussion in Chapter 3; Introduction). Targeting OX40 with an OX40L-Fc fusion protein has also been tested in clinical trials (NCT02221960), however the majority of focus is on targeting the receptor with mAb, which is the focus of the research presented in this thesis.

1.7 Summary

The use of immunomodulating mAb to generate anti-tumour responses offers an exciting new approach to cancer immunotherapy. It has been shown that antibodies targeting T cell co-stimulatory receptors, such as OX40, can be used to enhance the effector T cell response, inhibit the suppressive Treg population and provide immune memory in a number of murine models. However, translating these mAb into effective clinical therapeutics carries many challenges as described in the sections above; isotype choice, expression of FcγR and on which cell types, expression of target and on which cell types, tumour immune infiltrate, route of administration etc. Initial clinical studies have shown the potential of anti-OX40 mAb to be beneficial in human patients, it is therefore imperative that we understand more clearly the effects of these antibodies on specific cell subtypes as well as the effect of isotype choice for these specific mAb.

1.8 Hypothesis and project aims

Anti-OX40 mAb have shown therapeutic promise in preclinical tumour models but have yet to show the same level of success in human patients. We hypothesise that anti-hOX40 mAb isotype and binding domain will influence functional outcome and ultimately therapeutic ability. The aims below will be used to test this hypothesis.

Aims:

1. To characterise a panel of anti-hOX40 mAb in terms of binding affinities, binding domains and ability to bind in the presence of the ligand.
2. To validate a novel hOX40 KI mouse model for its use in the pre-clinical evaluation of the anti-hOX40 mAb.
3. To investigate the effects of the anti-hOX40 mAb, specifically on T cell subsets, using *in vitro* assays and *in vivo* mouse models.
4. To assess pre-clinically the anti-tumour immunity produced by the mAb using a number of mouse tumour models.
5. To determine the structure of the hOX40 ECD in complex with anti-hOX40 Fab fragments to define exact binding epitopes.

Chapter 2 Materials and Methods

2.1 Reagents

2.1.1 Media and supplements for mammalian cell culture

A number of mammalian cell lines were used throughout this research and listed in the table are the supplements and media used for their culture. Components were purchased from ThermoFisher unless otherwise stated.

Table 2.1 Mammalian cell culture media

Media	Components	Cells
Complete RPMI	RPMI media, 10% FCS (Sigma-Aldrich), L-glutamine (2mM), sodium pyruvate (1mM), Penicillin-Streptomycin (50U/ml)	Human PBMC's Jurkat cells
Complete RPMI + 2ME	RPMI media, 10% FCS (Sigma-Aldrich), L-glutamine (2mM), sodium pyruvate (1mM), Penicillin-Streptomycin (50U/ml), 2-Mercaptoethanol (50µM) (Sigma-Aldrich)	Primary mouse cells and tumour cell lines E.G7 and MC38
Complete DMEM + 2ME	DMEM media, 10% FCS (Sigma-Aldrich), L-glutamine (2mM), sodium pyruvate (1mM), Penicillin-Streptomycin (50U/ml), 2 Mercaptoethanol (50µM) (Sigma-Aldrich)	MCA-205 tumour cell line
FortiCHO growth media	FortiCHO growth media, L-glutamine (2mM), sodium pyruvate (1mM)	CHO cells
CHO selection media	GMEM, 5% FCS (Sigma-Aldrich), L-glutamine (2mM), sodium pyruvate (1mM), Geneticin (1mg/ml)	CHO cells
293F expression media	Freestyle 293F expression media	293F cells
OptiPRO media	OptiPRO expression media	ExpiCHO-s cells
Hybridoma nutrition media	DMEM, L-glutamine (2mM), sodium pyruvate (1mM)	NS-1/B-cell hybridoma

Hybridoma growth media	DMEM, 5% FCS (Sigma-Aldrich), L-glutamine (2mM), sodium pyruvate (1mM)	NS-1/B-cell hybridoma

2.1.2 Media and supplements for bacterial cell culture

Table 2.2 Bacterial cell culture media

Media	Components	Company	Cells
Lysogeny broth (LB)	Tryptone (1%), Yeast Extract (0.5%), Sodium Chloride (1%)	Melford	E. coli

Table 2.3 Cell culture selection agents

Selection Agent	Working Concentration	Company
Ampicilin	100μg/ml	Sigma-Aldrich
Kanamycin	50μg/ml	Sigma-Aldrich
Puromycin	1μg/ml	Sigma-Aldrich
Geneticin (G418)	0.4mg/ml	Thermo-Fisher Scientific

2.1.3 Buffers

All buffers were prepared in double distilled water, or PBS where stated, and corrected to a certain pH when needed. All buffer components were purchased from Sigma-Aldrich unless otherwise stated.

Table 2.4 Buffer components

Buffer	Components	Application
0.2M TE8	Tris (0.2M), HCl (100mM), EDTA (12.7mM), pH 8	Chromatography buffer
HEPES	HEPES (50mM), KCl (150mM), pH 7.5	Chromatography buffer
Bicarbonate Buffer	$NaHCO_3$ (440mM), $Na2CO_3$ (100mM), pH 9.5	FITC labelling

1:5 Tris:NaCl	Tris (40mM), NaCl 200mM) HCl (20mM), EDTA (2.5mM), pH 8.0	Chromatography buffer
0.2M Citrate	Citric acid (0.2M), NaOH (0.58M)	Antibody coupling to sepharose
Saturated $(NH_4)_2SO_4$	$(NH_4)_2SO_4$ (5.8M), 0.2M TE8	Ammonium sulphate precipitation
Equilibration buffer	PO_4 (20mM), NaCl (500mM)	Ni^{2+} column
Glycine	Glycine (100mM), HCl (22.5mM), EDTA (1.2mM), pH 3.0	Elution buffer for affinity chromatography
PBS-Tween	PBS, Tween (0.6mM)	ELISA
Coating buffer	Na_2CO_3 (15mM), $NaHCO_3$ (34.8mM)	ELISA
Substrate buffer	*o*-Phenylenediamine dihydrochloride (44.1mM) (Thermo Fisher Scientific), Citric acid (2.5mM), Na_2HPO_4 (5mM), H_2O_2 (1.4mM)	ELISA
Running buffer	Tris (23.9mM), Glycine (192mM), SDS (3.46mM)	SDS-PAGE
Transfer buffer	Tris (11.5mM), Glycine (96mM), 20% Ethanol (v/v)	Western blot
Blocking buffer	PBS, 10% Tween (v/v), 5% Milk powder (w/v) (Marvel)	Western blot
Wash buffer	PBS, 10% Tween (v/v)	Western blot
FACS wash	PBS, NaN_3 (10mM), 1% BSA (w/v)	FACS
TE	Tris (10mM), EDTA (1mM), pH 8.0	DNA extraction
TAE	Tris acetate (40mM), EDTA (1mM), pH 8.2	Agarose gel electrophoresis

Gentle red cell lysis buffer	NH_4Cl (15.5mM), $KHCO_3$ (1mM), EDTA (0.01mM)	Red cell lysis
Red cell lysis buffer (Serotec)	-	Red cell lysis
PBS-EDTA	PBS, EDTA (2mM)	PBMC isolation
Buffer H (Promega)	Tris-HCl (90mM), $MgCl_2$ (10mM), NaCl (50mM)	Restriction digest

2.1.4 Western Blot antibodies

Table 2.5 Western blot antibodies

Primary Ab Specificity	Species	Concentration used	Supplier	Secondary Ab	Dilution for WB	Supplier
Human OX40	Mouse mAb	1.375ug/ml	In-house	Rabbit anti-goat	1:80,000	Sigma-Aldrich
6x His-tag	Rabbit polyclonal Ab	1ug/ml	Abcam (ab18184)	Goat anti-mouse	1:10,000	Dako

2.1.5 Flow cytometry antibodies

All antibodies used for flow cytometry were purchased from affymetrix eBioscience unless otherwise stated.

Table 2.6 List of fluorescently labelled antibodies used for flow cytometry

Target	Clone	Isotype	Host	Reference
Isotype control	P3.6.2.8.1	IgG1	Mouse	[285]
Isotype control	MOPC-173	IgG2a	Mouse	[286]
Isotype control	eBRG1	IgG1	Rat	[287]
Isotype control	eBR2a	IgG2a	Rat	[288]

Isotype control	-	IgG	Syrian hamster	-
Isotype control	eBio299Arm	IgG	Armenian hamster	[289]
Human CD134 (OX40)	ACT35	IgG1	Mouse	[290]
Mouse CD134 (OX40)	OX-86	IgG1	Rat	[291]
Human CD8	SK1	IgG1	Mouse	[292]
Mouse CD8a	53-6.7	IgG2a	Rat	[293]
Human CD4	RPA-T4	IgG1	Mouse	[294]
Mouse CD4	GK1.5	IgG2b	Rat	[295]
Human CD3	SK7	IgG1	Mouse	[296]
Mouse CD3	145-2C11	IgG	Armenian Hamster	[297]
Human Granzyme B	GB11	IgG1	Mouse	[298]
Human kappa light chain	In House (Cp4/3)	-	Mouse	
Mouse CD161	PK136	IgG2a	Mouse	[299]
Mouse FoxP3	FJK-16s	IgG2a	Rat	[300]
Mouse IgG, Fcγ specific	115-116-071	F(ab)$_2$ fragment	Goat	[301]
Mouse CD44	IM7	IgG2b	Rat	[302]
Mouse CD62L (L-selectin)	MEL-14	IgG2a	Rat	[303]
Mouse KLRG1	2F1	IgG	Syrian hamster	[304]
Mouse CD127 (IL-7Rα)	A7R34	IgG2a	Rat	[305]

Mouse CD183 (CXCR3)	CXCR3-173	IgG	Armenian hamster	[306]
Mouse T-Bet	eBio4B10	IgG1	Mouse	[307]
Mouse EOMES	Dan11mag	IgG2a	Rat	[308]
Mouse CD45.2	104	IgG2a	Mouse	[309]
Mouse CD43 activation associated glycoform (Biolegend)	1B11	IgG2a	Rat	[310]
OVA specific TCR	In-house	-	-	[311]

2.1.6 Antibodies for *in vitro* assays

All antibodies used in *in vitro* assays were prepared in-house.

Table 2.7 Antibodies used in *in vitro* assays

Antibody specificity	**Clone**	**Isotype**	**Reference**
Anti-human CD3	OKT3	Mouse IgG2a	[312]
Anti-mouse CD3	145-2C11	Hamster IgG	[313]
Anti-mouse CD28	37.51	Hamster IgG	[314]
Anti-mouse CD16/CD32	2.4G2	Rat IgG	[315]

2.2 Animals

C57BL/6 wild type mice, C57BL/6 OT-1 transgenic [316] and hOX40 knock-in mice were bred and maintained in-house. Mice were fed regular chow and had access to freely accessible water. All procedures were carried out in accordance with home office licences PPL P4D9C89EA and PIL I7280D069.

2.3 Molecular Biology

2.3.1 Cloning and Sub-cloning

The Zero Blunt® TOPO® PCR Cloning Kit (Invitrogen) was used to create clones from blunt end PCR products. This type of cloning exploits the ability of the enzyme, Topoisomerase I, to cleave the phosphodiester backbone of DNA and conserve the energy from this break in a covalent bond between the 3' phosphate of the DNA strand and a tyrosol residue in the enzyme. The ability of the 5' hydroxyl group of DNA to break this bond enables the insertion of blunt end PCR products into the vector without the need for ligases or primers.

1µl of Blunt II-TOPO® vector and 1µl of salt solution (1.2 M NaCl, 0.06 M MgCl)

was added to 4µl of DNA and left at room temperature (RT) for 30 minutes. The sample was then used for transformation. To sub-clone from the TOPO® vector to an expression vector, such as pcDNA3, restriction digests using restriction enzymes (Promega) were carried out followed by DNA extraction and ligation of the 2 products using a 1:3 vector:insert ratio.

2.3.2 Restriction Digest

Restriction digests were used to excise the DNA of interest from the cloning vector so that it could be ligated into an expression vector. 5µl of plasmid DNA was added to 7µl of a restriction digest master mix (1µl of buffer H and 1µl enzyme) and incubated at 37°C for 1 hour. The sample was run on a 0.7% agarose gel to check for correct digestion.

2.3.3 Agarose gel electrophoresis

Agarose gel electrophoresis was performed to confirm the size of various DNA fragments and plasmids. Different percentages of agarose were added to gels dependent upon the size of the fragments being separated. The higher the percentage the better resolution of smaller fragments, and vice versa for larger fragments.

0.7% agarose gels were typically used and prepared by dissolving agarose (Sigma) into TAE buffer (Table 2.4) via heating in a microwave on full power for 1

½ minutes. 5µl of gel red stain (Biotium) was added before the gel was poured into a 15x15 cm gel cast and a 1.5mm comb inserted. The gel was left to set at RT. The set gel was submerged in TAE buffer in an electrophoresis tank, DNA samples, reconstituted in loading dye, were loaded into wells and a current of 160V was applied for 20-30 minutes. DNA bands were visualised using UV light from an imager (Gel Doc XR, Bio-Rad) and associated software (Quantity One).

2.3.4 DNA Extraction

DNA bands of interest were excised directly from the agarose gel and the DNA extracted using Qiaex II Gel Extraction Kit (Qiagen). In brief, a dissolving buffer and silica DNA binding beads were added to the gel slice and left to melt for 10 minutes at 50°C. The DNA binding beads were pelleted via centrifugation at 14500g and washed with an ethanol containing buffer to remove any salt. TE buffer (Table 2.4) was added to the beads and incubated at 50°C for 10 minutes to elute the DNA. The beads were then pelleted as before and the supernatant, containing DNA, was transferred to a sterile tube. These DNA samples were then ligated into an expression vector.

2.3.5 Ligation of DNA and plasmid

DNA ligation was carried out to insert the DNA of interest into an expression vector. 3µl of T4 DNA Ligase (Promega) and 3µl of 10x Ligase buffer (Promega) was added to a vector:insert ratio of 1:3 and left overnight at 4°C. The resulting plasmid DNA was used for *E.coli* transformations.

2.3.6 *E.coli* Transformation

Transformation is the genetic alteration of a cell by the direct uptake of exogenous DNA. This process was performed to amplify the plasmid DNA. Two *E.coli* strains were used for transformation experiments; One Shot® TOP10 Chemically Competent *E. coli* (Invitrogen) for use with the TOPO® PCR cloning kit and Bacterial Strain JM109 (Promega) for all other transformations.

Plasmid DNA was incubated on ice for 30 minutes with a 10x volume of *E.coli*. The competent cells were then heat shocked at 42°C for 45 seconds and placed back on ice for 2 minutes. 0.5ml of S.O.C medium (Invitrogen) was added to the cells

and incubated at 37°C for an hour with shaking. The cells were plated onto agar plates containing the correct selection antibiotic (Table 2.3) and incubated at 37°C for at least 16 hours to allow time for bacterial cells which had taken up the plasmid to colonise, and those that hadn't to die. *E.coli* cells were then cultured in 100ml LB broth to produce substantial amounts of DNA.

2.3.7 Plasmid production in *E.coli*

To obtain large amounts of our DNA of interest LB broth containing the correct selection antibiotic (Table 2.2 and 2.3) was used to propagate *E.coli* strains. A single colony was chosen from an agar plate and pipetted into 10ml LB broth + selection antibiotic (Sigma Aldrich). The cultures were incubated at 37°C with shaking overnight. After overnight incubation, cultures were expanded up to 100ml in LB broth plus selection via inoculation, and overnight incubation repeated. After overnight incubation the cultures were used for either Minipreps or Maxipreps.

2.3.8 Plasmid DNA Miniprep and Maxiprep

Plasmids were isolated from *E.coli* cultures using either the QIAprep spin miniprep kit protocol or the Quickstart Qiagen maxi kit protocol (Qiagen). In brief, the bacterial cells were lysed in an alkaline environment followed by neutralisation of the lysate. The lysate was then added to a spin column (miniprep) or filter tip (maxiprep) capable of capturing plasmid DNA. The plasmid DNA was eluted and used in subsequent experiments. The maxiprep protocol has an additional step using isopropanol to reduce the final volume of DNA.

2.4 Cell Culture

2.4.1 Jurkat cells

Jurkat cells were grown in complete RPMI media (Table 2.1) at 37°C and 5% CO_2. 1µg/ml puromycin was added to cell cultures that had been transiently transfected with hOX40EC-CD40tail construct to select for the positively expressing cells. Cells were split roughly every other day so that a concentration of 0.5-1x10^6/ml was kept.

2.4.2 Tumour cell lines

Suspension cell lines (E.G7 and MC38) were grown in complete RPMI+2ME (Table 2.1) and adherent cell lines (MCA-205) in complete DMEM+2ME (Table 2.1) at 37°C and 5% CO_2. Cells were initially thawed into a T25 flask (Corning) and bulked up until there was enough for $5x10^5$ per mouse. All cell lines were split roughly every other day so that the concentration of cells was kept between 0.5-$1x10^6$/ml. Adherent cells were detached by the addition of 5ml 1X trypsin (Thermo-fisher Scientific) to a T125 flask.

2.5 Protein/antibody production

2.5.1 293F transient transfections

HEK293F cells were transfected using a cationic lipid based transfection reagent, 293fectin (Thermo-Fisher Scientific). In brief, 10µg of DNA was added to 20µl of 293fectin and allowed to form DNA-Cationic lipid complexes in Opti-MEM serum free media (Thermo-Fisher Scientific). This was then added drop-wise to $1x10^7$ HEK293F cells cultured in 10ml of Freestyle293 expression media (Thermo-Fisher Scientific) and shaken at 37°C for 24-48 hours. For more efficient production of protein stable transfections were then created.

2.5.2 ExpiCHO-S transient transfections

ExpiCHO-S cells were transfected using a cationic lipid based transfection reagent, ExpiFectamine CHO (Thermo-Fisher Scientific). In brief, 50µg DNA was added to 160µl ExpiFectamine CHO reagent and allowed to form DNA-Cationic lipid complexes in OptiPRO medium (Thermo-Fisher Scientific). This was then added drop-wise to to $3x10^8$ ExpiCHO-s cells cultured in 50ml OptiPRO medium (Thermo-Fisher Scientific). Cells were incubated in a shaking incubator at 37°C for 24 hours before the addition of 300µl ExpiFectamine CHO Enhancer (Thermo-Fisher Scientific) and 12ml ExpiCHO Feed (Thermo-Fisher Scientific). Supernatant was harvested on days 8-10 post transfection.

2.5.3 CHO-S stable transfections

For stable transfections CHO-K1S cells were grown to late-log phase in FortiCHO growth medium (Life Technologies). 2µg of DNA was added to 16µl GenePORTER® (Genlantis) and allowed to form DNA-Cationic lipid complexes in Opti-MEM serum free media (Life Technologies). $1x10^7$ cells were transfected per well of a 6 well plate in 1.2ml. The plates were incubated at 37°C for 72 hours, harvested and re-suspended in selection media (Table 2.1). The cells were then plated in a 96 well plate, using a limiting dilution method to achieve a monoclonal cell population, and incubated for 2-3 weeks at 37°C. Wells containing a single colony were screened for positive secretion using ELISA and positive secretors sub-cloned. After 2-3 weeks' incubation, at 37°C, single colonies were again screened using ELISA and the highest secretors expanded into 24 well plates and then sequentially up to 175ml flasks. Culture supernatant (containing secreted protein), was harvested weekly for 6-8 weeks and kept at -20°C until purification.

2.5.4 Culture supernatant concentration

A VIVAFLOW (Sartorius AG) system was used to concentrate large amounts of supernatant collected from cell culture. Before addition of culture supernatant, 0.5M NaOH was used to remove any endotoxin in the system followed by washing with distilled water. Cell supernatant was spun at 3400g for 20 minutes and the supernatant collected in a sterile container. The supernatant was passed through the concentrator until a final volume suitable for ammonium sulphate precipitation was achieved (~300ml).

2.5.5 Ammonium sulphate precipitation

Ammonium sulphate precipitation was used to 'salt out' the protein of interest and purify it from any contaminants, such as bovine serum, which is used in the cell culture stage.

A volume of $(NH_4)_2SO_4$ equal to that of the supernatant sample was added drop-wise to the supernatant whilst on a stirrer. Supernatant was spun at 1960g for 35 minutes and the cell pellet re-suspended in 0.2M TE8 buffer (Table 2.4). This process was repeated twice before dialysis of sample into 1:5 Tris:NaCl (Table 2.4). Buffer was changed twice daily for 2 days before the sample was harvested

and passed through a 0.2µm filter to remove any large particles which may interfere with the purification process.

2.5.6 Monoclonal antibody production

A derivative of the method of hybridoma technology invented by Cesar Milstein, Georges J.F. Kohler and Niels Kaj Jerne in 1975 [131] was used to produce the monoclonal antibodies (mAb) used in this research. In brief, splenocytes from a mouse immunised with a soluble fusion protein were fused with NS-1 myeloma cells creating an immortal, antibody producing cell line.

Thymocytes were isolated from a young (4-6 weeks old) BALB/c mouse and co-cultured in a flat bottomed 96 well plate with antibody producing hybridoma cells in antibiotic free media (Table 2.1) using a limiting dilution method. After 1-2 weeks the plates were screened using ELISA and single colonies expanded into 24 well plates along with fresh thymocytes. Once cells were 80-90% confluent the plates were screened using ELISA and the highest secretors expanded sequentially into CL1000 flasks (See Table 2.1 for media compositions). Cell supernatant was harvested weekly and stored at -20°C until purification using a protein G affinity column.

2.6 Protein Purification

2.6.1 Size exclusion chromatography (SEC)

A Superdex 200 (S200) 10/300 column (GE Healthcare) along with an ÄKTA Prime pump (GE Healthcare) was used for all SEC experiments. 1 column volume (CV) of water followed by 1 CV of chromatography buffer (HEPES – Table 2.4) was used to remove the storage ethanol and equilibrate the column, respectively. 200-400µl of sample was then injected into the injection loop and pumped onto the column at a flow rate of 0.4ml/min. 0.2ml fractions were collected once the chromatogram showed an increase in UV detection at 280nm (presence of protein). Relevant fractions were pooled and concentrated using a Vivaspin concentrator (GE Healthcare).

2.6.2 Coupling antibody to CNBr activated sepharose

mAb were coupled to CNBr activated sepharose to create an affinity column which was capable of purifying a target molecule (in this case hOX40) from a CHO cell culture supernatant. 1g of CNBr activated sepharose 4B (GE healthcare) gel was suspended in 10mM HCl and poured into a sintered glass funnel followed by 2-3 washes with 0.2M citrate. Antibody was dialysed into 0.2M citrate (Table 2.4) and mixed with the sepharose on a rotator overnight at 4°C. The gel slurry was harvested back into the sintered glass funnel and washed with 0.2M citrate followed by re-suspension in 10ml of 1M ethanolamine. The antibody-sepharose solution was rotated at RT for 1 hour followed by washing with 0.2M citrate and then 1:5 Tris/NaCl. Antibody coupled sepharose was packed into a 10/300 column (Pharmacia Biotech).

2.6.3 Affinity chromatography

Various affinity chromatography approaches were used through the course of this research, as detailed below:

2.6.3.1 Anti-hOX40 mAb

An anti-hOX40 mAb column was used to purify hOX40 extracellular domain from CHO culture supernatant. Here, anti-hOX40 monoclonal antibody, SAP 25-29, was coupled to CnBr activated sepharose beads (as detailed above - see Methods and Materials 2.5.2). 1:5 Tris:NaCl buffer (Table 2.4) was used to equilibrate the column. Supernatant was applied to the column at a flow rate of 1ml/min. to elute bound protein of interest 5ml glycine pH 3 (Table 2.4) was applied to the column at the same flow rate described above. Flow through was collected as soon as UV absorbance at 280nm was detected (LKB Bromma). Eluted protein was dialysed into PBS overnight to adjust the pH followed by HPLC to check the purity of the sample. Lastly the protein sample was concentrated to smaller volumes for use in further experiments.

2.6.3.2 Protein G

Protein G is a 65 kDa surface protein found in group C and G Streptococcal bacteria. It binds to many mammalian IgG's via interaction with the heavy chain in the Fc region of the antibody so was used to purify mAbs from culture supernatant.

The same protocol as stated in 2.5.3.1 was followed, although in this case supernatant from hybridoma cells containing secreted mAbs was applied to the column. Elution was again carried out using glycine pH 3. mAb was collected into a flask containing Tris:NaCl to return the pH back to 8 followed by concentration of mAb sample to between 2-5mg/ml and a number of purity checks.

2.6.3.3 Ni^{2+}

To purify his-tagged hOX40 a Ni^{2+} column was used. Ni^{2+} columns contain a tetradentate chelator, nitrilotriacetic acid (NTA), which is linked to sepharose beads and occupies 4 out of the 6 binding sites in the coordination sphere of a Ni^{2+} ion. Histidine tags are able to displace the H_2O that occupies the remaining 2 coordination sites causing retention of his-tag proteins on the column.

The HisTrap excel 1ml column (GE Healthcare) was attached to the pump (ÄKTA Prime Plus) and the system equilibrated using equilibration buffer (Table 2.4). The sample was applied to the column at a flow rate of 50ml/min. A stepwise gradient of imidazole was applied to the column to elute the his-tagged protein of interest (Table 2.8) and 1ml fractions were collected.

Table 2.8 % of equilibration and elution buffers to reach different imidazole concentrations

% equilibration buffer	% elution buffer	Final imidazole concentration
98%	2%	10mM
96%	4%	20mM
92%	8%	40mM
50%	50%	250mM
0%	100%	500mM

2.6.4 High Performance Liquid Chromatography (HPLC)

As a method of determining purify and the presence of aggregates after chromatography, HPLC experiments were performed using a LKB HPLC pump 2248 (Pharmacia Biotech) and a MAbPac Sec-1 column (Thermo scientific). The column was equilibrated using 0.2M TE8 buffer (Table 2.4) followed by application of 20µl of sample. Protein was detected at 280nm via a Waters 486 tunable absorbance detector and elution profiles were documented.

2.6.5 Sodium dodecyl sulphate polyacrylamide gel electrophoresis (SDS-PAGE)

To determine the size, presence and purity after chromatography, proteins were separated on a polyacrylamide gel mounted on a vertical gel electrophoresis apparatus system (Xcell SureLock Novex Mini-Cell system, Invitrogen Ltd). Pre-made 1.5mm thick, 15% SDS gels were used (Invitrogen). The gels were placed into a tank and the chamber filled with SDS-running buffer (Table 2.4). 10µl of fraction samples were added to 5X NuPage loading buffer (Thermo-Fisher Scientific), boiled for 10 minutes at 95°C and centrifuged at RT for 10 seconds. The gel was run at 150V for 1 ½ hours. Gels were then either stained with coomassie blue stain (Sigma) and imaged under white light (UVP Gel Doc System) to detect protein bands, or used for western blotting.

2.6.6 Immunoblotting

For the purpose of western blotting gels were transferred onto a polyvinylidene fluoride (PVDF) membrane following the manufacturer's instructions (XCell II Blot Module, Invitrogen Ltd.) The transfer was carried out at 24V for 1 hour with the tank cooled by ice and the chamber immersed in transfer buffer (Table 2.4). After transfer the membranes were blocked at RT for 1 hour using 5% (w/v) milk (Table 2.4) on a tilt plate. The membrane was then incubated with the primary antibody diluted in blocking solution at 4°C overnight on a roller. The blot was washed 3 times (10 minutes each) with TBS-T (Table 2.4) before incubation with the secondary HRP conjugated antibody (Dako/Sigma Aldrich) for 1 hour at RT on a roller. The membrane was washed again 3 times with TBS-T (10 minutes each) and the HRP conjugated antibody was detected using ECL (SuperSignal West Femto, Thermoscientific). Images were taken using an automated imager (Chemidoc imager; UVP software).

2.6.7 Enzyme-linked immunosorbent assay (ELISA)

ELISA utilises an enzyme-substrate reaction which results in a change of colour to detect and quantify the presence of captured antigen. The intensity of the signal detected at 490nm is proportional to the amount of antigen captured on the plate.

A flat bottomed 96 well plate (Corning) was coated with 10µg/ml of the appropriate capture antibody followed by blocking with PBS/1%BSA for 2 hours to stop non-specific binding. 50µl of cell supernatant was then added to the plate and incubated at 37°C for 90 minutes to allowing for binding to the capture antibody. The plate was washed five times with PBS-Tween (Table 2.4) followed by the addition of a HRP-conjugated detection antibody at 0.5µl/ml. The plate was incubated for 90 minutes at 37°C followed by addition of 100µl of enzyme substrate (Table 2.4) and incubation in the dark at RT for 20-30 minutes. Once a significant colour change had occurred the reaction was stopped using 2.5M sulphuric acid. The optical density (OD) of the plate was measured at 490nm using an Epoch Machine (Biotech) and associated Gen5 Programme (BioTek).

2.6.8 Surface plasmon resonance

Surface plasmon resonance (SPR) monitors binding events allowing the affinity, kinetics and specificity of an interaction to be measured. These experiments were performed using a Biacore T100.

To measure OX40:mAb interactions 1µg/ml of hOX40-hFc was immobilised onto a CM5 chip (GE Healthcare) and a range of concentrations from 0-500nM of analyte (anti-hOX40 mAb) was prepared. Each mAb was injected over the chip at a flow rate of 30µl/min. The chip was regenerated between each run using 10mM glycine pH 1.5. Sensograms were produced by the evaluation software (GE Healthcare) and fitted to a 1:1 binding model to determine the association (Ka), dissociation (Kd) and equilibrium dissociation (KD) constants.

For ligand blocking experiments 100nM his-tagged OX40L was captured onto an anti-his chip (GE Healthcare). 100nM hOX40 was then injected over the chip at a flow rate of 30µl/min followed by the injection of 100nM anti-hOX40 mAbs at the same flow rate. The chip was regenerated between each mAb as described above.

2.7 OX40:Fab complex formation for crystallographic trials

2.7.1 IgG digest to F(ab')$_2$ fragment

Pepsin is an endopeptidase which is active only at acidic pH's. It digests full length IgG's under the hinge region producing one F(ab')$_2$ fragment and numerous small peptides of the Fc portion.

Acetate (pH 2.0) and Tris buffer (pH 8.0) were used to pH the antibody solution to pH 4.1, pH was measured using a pH meter (3510 pH meter; Jenway). 10mg of pepsin was dissolved in 1ml endotoxin free water and added to the antibody solution at 3% w/v and incubated at 37°C in a water bath. 20µl samples were taken every 30 minutes and run on HPLC to monitor the progress of the digestion. Once fully digested the pH of the antibody solution was increased to 8.0 by the addition of Tris buffer (pH 8.0).

2.7.2 F(ab')$_2$ reduction and alkylation

F(ab')$_2$ reduction and alkylation was performed use dithiothreitol (DTT) and Iodoacetamide (IAA). DTT is a reducing agent used to reduce the disulphide bonds in the hinge region of antibodies and IAA is an alkylating agent that binds to the thiol groups of cysteine residues so that the disulphide bonds cannot reform.

1M solutions of DTT (Sigma) and IAA (Sigma) were prepared in 0.2M TE8 buffer (Table 2.4). 1/10th volume of DTT was added to the F(ab')$_2$ solution and mixed on a rotator at RT for 30 minutes. 1/10th volume of IAA was then added to the solution and mixed on the rotator for 10 minutes at RT. A sample of the antibody solution was run on HPLC to confirm reduction.

2.7.3 OX40:Fab Complex Formation

Initial OX40:Fab complexes were made using the extracellular domain of hOX40 and anti-hOX40 Fab fragments at either 1:1.5 or 1:1.25 molar ratios incubating the constituents for 30 minutes at RT prior to separation on an S200 10/300 gel filtration column (GE Healthcare) at 0.3ml/min in HEPES buffer (Table 2.4). Subsequent complexes were made at a 1:1.25 molar ratio. Relevant fractions were pooled and concentrated using a spin concentrator (Millipore Centrifugal Filter Concentrator; 8kDa) for use in crystallographic trials.

2.7.4 Crystallisation Trials

Purified proteins (i.e. OX40:Fab complexes) were crystallised in 96-well plates using a sitting drop method. Trays were set up using a Gryphon nanodrop dispenser (Art Robbins Instruments) into 3 drop MRC plates (Molecular Dimensions) which allowed for 3 different protein:mother liquor ratios per well condition; 0.1µl protein 0.2µl mother liquor, 0.1µl protein 0.1µl mother liquor, and lastly 0.2µl protein and 0.1µl mother liquor. Mother liquor describes the liquid remaining after a substance has crystallised out of solution. The plates were sealed with cover sheets and incubated at 21°C. Plates were checked regularly for crystal formation using an LED Leica microscope.

2.8 *In vitro* experiments

2.8.1 PBMC isolation from leukocyte cones

PBMC were isolated from leukocyte cones. These cones are a preparation of concentrated leukocytes lacking platelets, produced as a bi-product of healthy donors attending the blood donation centre at the National Blood Service, Southampton for platelet donation.

Blood from a leukocyte cone was added drop-wise to 2ml PBS-EDTA (Table 2.4) followed by the total volume being made up to 30ml. 15ml of blood sample was layered onto 15ml of Lymphoprep™ (Stem Cell Technologies) using a Pasteur pipette and the cell suspension centrifuged at 800g for 20 minutes. The PBMC layer was removed using a Pasteur pipette and added to 5ml PBS-EDTA, the volume was made up to 40ml and the cell suspension centrifuged at 400g for 10 minutes. The supernatant was discarded and the cell pellet re-suspended in 40ml PBS-EDTA followed by centrifugation at 300g for 10 minutes. The supernatant was discarded and the cell pellet re-suspended in 10ml complete RPMI media (Table 2.1).

2.8.2 CFSE Labelling of PBMC

To allow monitoring of PBMC proliferation $1x10^8$ cells in 10ml of sterile PBS (Severn Biotech Ltd) were labelled with 1µm CFSE (Life Technologies). The cells were incubated at RT for 10 minutes followed by addition of 1ml FCS (Lonza), to

quench the reaction, and the total volume made up to 50ml with sterile PBS (Severn Biotech Ltd). The cells were centrifuged at 267g for 5 minutes and the supernatant discarded; this wash step was carried out twice. After the final wash the cells were re-suspended in 10ml complete RPMI media (Table 2.1).

2.8.3 PBMC activation assays

PBMC were cultured at high density (15 million cells/well) for 2 days at 37°C prior to assay preparation. Cells were plated at $1x10^5$/well and stimulated with 0.005µg/ml soluble anti-CD3 (Clone: OKT3) and soluble 15µg/ml anti-hOX40 mAbs (for proliferation studies) or 1µg/ml plate bound anti-CD3 (Clone: OKT3) (for expression analysis). Cells were stained with antibodies to discriminate between CD4+ and CD8+ T-cells (Table 2.6) and assessed for activation using flow cytometry.

2.8.4 *Ex vivo* blood/splenocyte activation (mouse)

Splenocytes were isolated using a 100µm strainer, washed in PBS and red cell lysed using 5ml lysis buffer (Serotec) at RT for 15 minutes (Table 2.4). Cells were re-suspended in RPMI+2ME and $1x10^5$ cells plated in 200µl/well. Splenocytes were stimulated with 0.1µg/ml anti-CD3 (Clone: 145-2C11) and 5µg/ml anti-CD28 (Clone: 37.51). Cells were stained with antibodies against CD4, CD8 and FoxP3 (Table 2.6) and assessed using flow cytometry. Blood samples were obtained by terminally bleeding mice followed by the same preparation as described above.

2.8.5 NF-κB reporter cell line

NF-κB/Jurkat/GFP cells were plated at $1x10^5$/well and stimulated with plate bound anti-CD3 (Clone:OKT3) at a number of different concentrations and soluble 5µg/ml anti-hOX40 mAbs. Cells were harvested and GFP fluorescence monitored using flow cytometry at a number of time points.

2.9 *In vivo* experiments

2.9.1 OT-I transfer

A spleen from a hOX40/OT-I mouse was harvested and splenocytes isolated using a 100µm strainer (Falcon). The single cell suspension was red cell lysed using gentle lysis buffer (Table 2.4) and the activation status of the lymphocytes checked via flow cytometry with the use of markers CD62L and CD44 (Table 2.6). Assuming a lack of prior activation, $1x10^5$ hOX40/OT-I splenocytes were injected intravenously (i.v.) into mice. 24 hours later mice were given 5mg ovalbumin (Ova) and 100µg antibody via intraperitoneal (i.p.) injection. Day 4 post Ova/mAb administration mice were culled using a rising concentration of CO_2 and their spleens harvested. A single cell suspension was obtained using a 100µm strainer followed by red cell lysis and centrifugation at 267g for 5 minutes. Splenocytes were re-suspended in PBS and stained with fluorescently conjugated antibodies (Table 2.6) before assessment via flow cytometry.

2.9.1 Collection of peripheral blood

Lidocane was used to locally anesthetise the mouse's tail. Mice were warmed at 37°C for 10 minutes before the tip of the tail was cut with a scalpel. 20µl of blood was collected and mixed with 5µl heparin (Wockhardt). Samples were red cell lysed (Serotec) and stained with fluorescently conjugated antibodies (Table 2.6) before assessment via flow cytometry.

2.9.2 Tumour models (monotherapy)

$5x10^5$ tumour cells were injected subcutaneously (s.c.) into the flank of mice. Once tumours reached a certain size (E.G7:10x10mm, MCA-205: 5x5mm) mice were treated with 3x100µg shots of anti-hOX40 mAb every other day via i.p. injection. For phenotyping experiments organs were harvested, processed and analysed via flow cytometry on day 4 post final injection. For survival experiments tumour size was monitored 3 times a week and mice culled once they reached a terminal stage of the disease indicated by lump size (E.G7: 20x20mm, MCA-205: 15x15mm). Mice presenting with no tumour after treatment were rechallenged with $5x10^5$ tumour cells s.c. into the flank and again tumour size monitored every other day. Surviving mice were culled around day 100-120.

2.9.3 Tumour model (combination therapy)

$5x10^5$ MC38 tumour cells were injected subcutaneously into the flank of mice. Once tumours reached 5x5mm (D0) mice were treated with a combination of anti-hOX40 and anti-m4-1BB mAb (total 800µg). Tumour size was monitored every other day until mice reached a terminal end point (15x15mm).

2.10 Antibody Fluorescein-Isothiocyanate (FITC) conjugation

To label antibodies with FITC, antibody was dialysed into PBS and concentrated to 2-5mg/ml using a Vivaspin column. 2mg/ml of FITC (Sigma) solution was prepared in bicarbonate buffer (Table 2.4) and added to the antibody at a final concentration of 0.2mg/ml. The antibody-FITC solution was incubated at 25°C for 45 minutes and run down a desalting column (GE Healthcare) to separate the unbound FITC from the antibody-FITC conjugate. Fractions were collected – by eye – when the pale green band started to elute and antibody was dialysed into PBS overnight. The absorbance at 280nm and 495nm was measured (Nanodrop) in order to calculate the fluorescence:protein (F/P) ratio. A ratio between 0.5-1 was deemed necessary for flow cytometry.

$$F{:}P\ Ratio = \frac{Absorbance\ at\ 495nm}{Absorbance\ at\ 280nm}$$

$$Protien\ Concentration = \frac{A280 - (0.26xA495)}{1.45}$$

2.11 Flow Cytometry

2.11.1 Extracellular Staining

Approximately $1x10^6$ cells were labelled with appropriate fluorescently labelled antibodies (Table 2.6) for 20 minutes at RT. The sample was washed with FACS wash (Table 2.4) to remove any unbound antibody followed by centrifugation for 5 minutes at 267g to pool the cells. Samples were analysed by flow cytometry via monitoring cell surface markers that had been fluorescently labelled. For secondary labelling, unlabelled primary antibody was added to the sample at 10µg/ml and incubated at RT for 20 minutes before washing x 2 in FACS wash

and addition of a secondary antibody at the appropriate concentration. The samples were washed and centrifuged as described above before analysis.

2.11.2 Intracellular Staining

Previously surface stained samples were fixed for 30 minutes at 4°C by addition of 500µl of FoxP3 fixation/permeabilisation solution (eBioscience). The samples were then washed with 1ml permeabilisation buffer 1X (eBioscience) followed by the addition 2µl/tube of fluorescently labelled antibody in 100µl of permeabilisation buffer 1X. Cells were incubated at 4°C for 1 hour prior to washing with FACS wash (Table 2.4) and analysis using a flow cytometer.

2.11.3 Data acquisition and analysis

All flow cytometry experiments were performed using either a FACSCalibur or FACSCanto machine (BD Bioscience). Analysis of data collected on the FACSCalibur was performed using Cellquest Pro (BD Bioscience) and data from the FACSCanto was analysed using FACSDiva (V6.1.2) software (BD Bioscience). Histogram overlays were produced using FCS Express (V.3) software (De Novo Software).

2.12 Statistics

GraphPad Prism (v7) software was used to perform statistical analysis on data and produce graphs. Two-tailed Mann-Whitney tests or unpaired student t-tests were used to calculate significance between groups. Where indicated ns = not significant, * P≤ 0.05, ** P≤ 0.01, *** P ≤ 0.001, **** P≤ 0.0001.

Chapter 3 Characterisation of anti-human OX40 monoclonal antibodies

3.1 Introduction

The use of agonistic antibodies targeting co-stimulatory receptors have emerged as targets for clinical development, in particular members of the tumour necrosis family (TNF) of receptors. Antibodies targeting 4-1BB [317], GITR [318], OX40 [319], HVEM [320] and CD27 [321] enhance co-stimulatory functions and have also shown promising results in pre-clinical assessments [200].

This thesis focuses on the TNFR superfamily member OX40 (CD134). Signalling through this receptor promotes the activity of CD4+ and CD8+ T cells as well as abrogating the effects of Tregs [165, 234], making it an attractive target for cancer immunotherapy. Pre-clinical tumour studies utilising agonistic mAb, namely OX86 (rIgG1), have produced promising results demonstrating that OX40 engagement is capable of enhancing T cell proliferation and differentiation whilst prolonging survival of both CD4+ and CD8+ T cells [278, 319, 322]. This effect on the T cell population has been shown to deliver significant survival benefits and delayed tumour progression in mice. Further studies of OX86 revealed its ability to deplete Tregs when isotype switched to a mIgG2a mAb. Bulliard et al. demonstrated the selective depletion of tumour infiltrating Tregs over CD8 effectors, likely due to differential expression of OX40, via FcγR mediated ADCC and ADCP mechanisms [165]. These effects resulted in tumour rejection and a higher local CD8:Treg ratio. Preferential OX40 expression on Tregs over effector CD4+ and CD8+ T cells within the tumour site have been shown in a number of studies of multiple human tumours [323-325]. This suggests that anti-hOX40 mAb with depleting ability may have the potential to be effective in human patients. Likewise, agonistic mAb may be utilised to expand CD8 T cells, bringing into question whether depletion or agonism would be most beneficial in a therapeutic setting, or if both can act equally.

At present there are nine different therapeutic candidates targeting OX40 in clinical trials, one is an OX40L-Fc fusion protein; the others are agonistic anti-OX40 mAb.

Table 3.1 highlights the cancer immunotherapy related trials that are active or complete. There are however, four other agents (Pfizer; PF-04518600, GSK; GSK3174998, Agneus/Incyte; INCAGN01949 and Bristol-Myers Squibb; BMS986178) being used in clinical trials in which they are still recruiting patients. Interestingly, the majority of these trials are combinations of anti-hOX40 mAb with either a checkpoint inhibitor or another agonistic mAb to a different co-stimulatory receptor.

Agent	Company	Clinical trials (clinicaltrials.gov)	Isotype	Results
9B12 (anti-OX40)	Providence Health and Services	**Phase I** • Prior to surgery in patients with head and neck cancer (Active; NCT02274155) **Phase Ib** • In patients with advanced cancers (Complete; NCT01644968) • + radiation and cyclophosphamide in patients with metastatic prostate cancer (Active; NCT01303705)	mIgG1	• Increased proliferation of CD4+ and CD8+ T-cells. • No effect on Treg proliferation. • Increased IFN-γ production.
MEDI0562 (anti-OX40)	MedImmune	**Phase I** • In patients with advanced solid tumours (Complete; NCT02318394)	Humanised	
MEDI6469 (anti-OX40)	MedImmune	**Phase I/Ib** • In patients with metastatic colorectal cancer (Active; NCT02559024) • + radiation in patients with breast cancer with metastatic lesions (Active; NCT01862900)	Murine?	
MOXR0916 (anti-OX40)	Genentech	**Phase I** • In patients with locally advanced or metastatic solid tumours (Active; NCT02219724)	Humanised IgG1	
MEDI6383 (OX40L fusion protein)	MedImmune	**Phase I** • In patients with advnaced solid tumours (Active; NCT02221960)	Human OX40L fusion protein	-

Table 3.1 Current anti-hOX40 therapeutics in active/completed clinical trials

Four anti-hOX40 mAb and an OX40L fusion protein are in current clinical trials for the treatment of a wide range of malignancies. Information was taken from the ClinicalTrials.gov website [131].

The surrounding interest in targeting this receptor together with the struggle to develop a mAb which is suitable for the clinic, highlights the growing need to gain a better understanding of OX40 biology and the optimal properties of an anti-OX40 mAb. Furthermore, to be able to effectively study mAb pre-clinically it is important to have suitable mouse models.

The Antibody Discovery group at the University of Southampton have used established hybridoma technology to produce a panel of anti-human-OX40 mAb with the aim of gaining a better understanding of the relevant parameters. Furthermore, a knock-in hOX40 mouse model was generated to allow pre-clinical testing of the mAb. This chapter documents the generation and characterisation of these anti-hOX40 mAb alongside the validation of the hOX40 KI mouse model.

3.2 Expression profiles of murine and human OX40 in a KI mouse model

A novel hOX40 knock-in (KI) mouse model was generated so that our panel of mAb could be studied in an *in vivo* system. The transcript for OX40 in both mouse and humans contains 7 exons; 1-5 code for the extracellular domain and 6 and 7 the transmembrane and intracellular domain. Figure 3.1a shows the WT C57BL/6 gene construct and highlights exons 1-5 (red arrow) which are to be replaced with the human equivalent to produce a chimeric human/mouse OX40 receptor. Figure 3.1b shows the chimeric construct produced after replacement of mouse exons 1-5 (blue) with human exons 1-5 (red) along with a selection cassette to allow for antibiotic selection of clones at the culture stage. Finally, Figure 3.1c shows the finished construct produced, once the selection cassette has been removed using the FRT-FLP system, containing human exons 1-5 and mouse exons 6-7 under the control of the mouse promoter. The chimeric receptor therefore allows for anti-hOX40 mAb binding to the human extracellular domain whilst still signalling correctly due to the mouse intracellular domain (Figure 3.2). Importantly, as this mouse model is a knock-in, the mouse OX40 gene is removed when it is replaced by the chimeric receptor. As a result, mice expressing both mouse and human OX40 (heterozygotes; $hOX40^{+/-}$ KI) or mice expressing solely the human receptor (homozygotes; $hOX40^{+/+}$ KI) were produced.

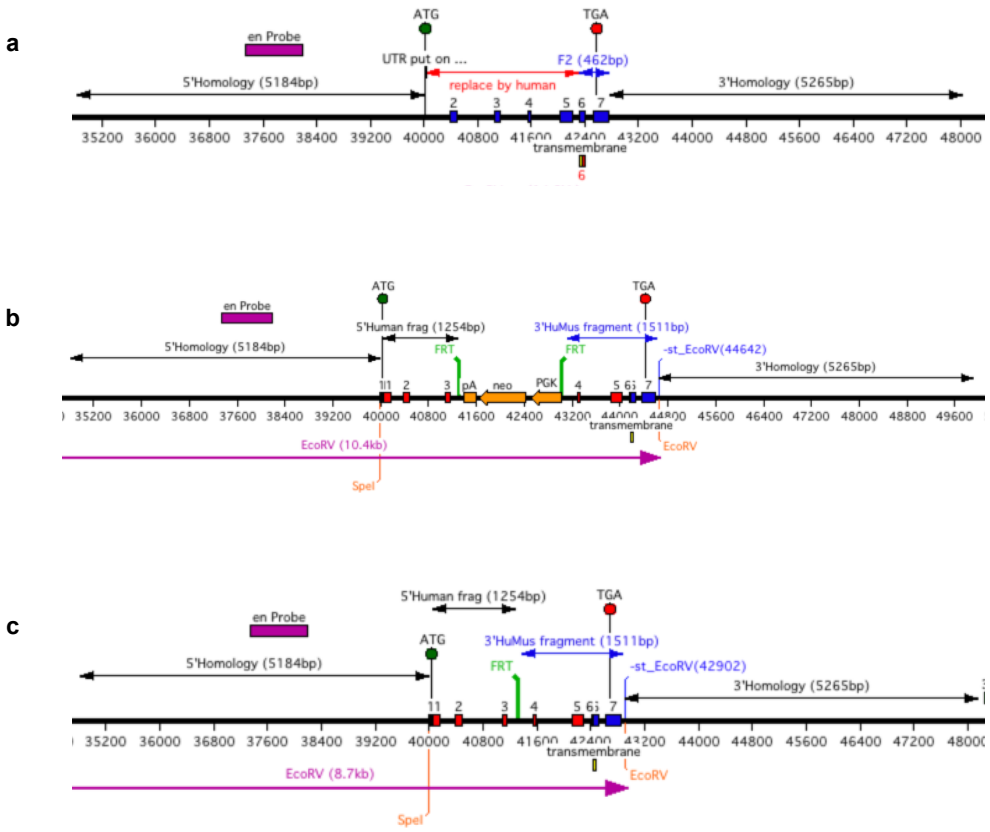

Figure 3.1 Creation of chimeric OX40 receptor and hOX40 KI mice.

a) Construct demonstrating the 7 exons coding for mouse OX40 (blue). Exons 1-5 are highlighted by a red arrow as these are the ones to be replaced by the human equivalent. b) Construct demonstrating the replacement of the targeted sequence, exons 1-5, with the human equivalent (red) along with a selection cassette (orange) for antibiotic selection (neomycin) of embryonic stem cells in culture. c) Complete chimeric construct after the selection cassette has been deleted using FLP mice; Recombinase flippase, which is expressed constitutively in all tissues of FLP mice, causes recombination of DNA between flippase recognition target (FRT) sites.

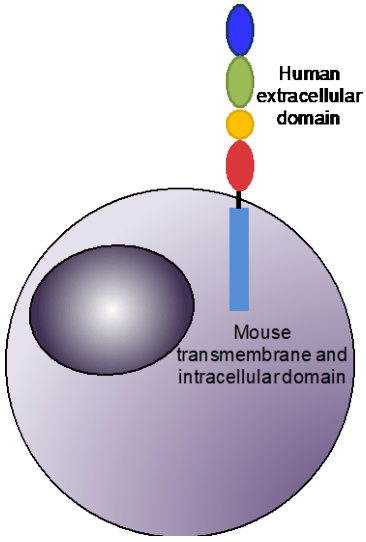

Figure 3.2 Schematic of chimeric OX40 receptor expression on the cell surface

Schematic illustrating how the hOX40KI construct is expressed on the cell curface as a chimeric OX40 receptor

Once generated, the mice were validated for their expression profile of both mouse and human OX40. The majority of studies focused primarily on the T cell subsets, CD8+, CD4+ and CD4+FoxP3+. The gating strategy used for analysing these populations is shown in Figure 3.3.

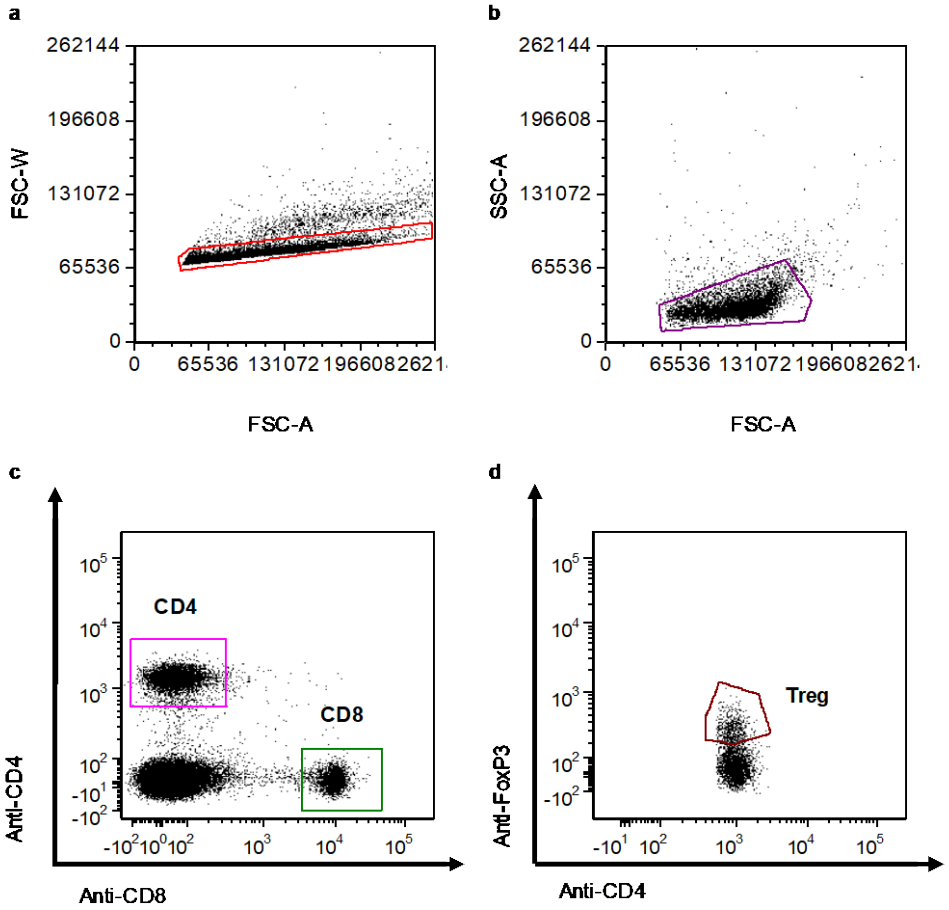

Figure 3.3 Gating strategy used to analyse CD4+, CD8+ and Treg populations by flow cytometry

Processed splenocytes and blood samples (mouse and human) were labelled with an e450-conjugated-anti-CD4+ antibody plus a FITC-conjugated-anti-CD8+ antibody for 20 minutes at 4°C. Cells were then fixed for 1 hour at 4°C, permeabilised and stained with an APC-conjugated-FoxP3 antibody. The cell samples were then assessed using a FACSCanto. Gating was performed in a hierarchal fashion. a) Cells were firstly gated on a FSC-A/FSC-W dot plot to allow gating around singlets. b) Cells were then gated on a FSC/SSC dot plot to remove cellular debris, c) Cells were then gated on a FITC/e450 profile to determine the CD8+ and CD4+ populations of lymphocytes. d) Finally, to allow detection of the Treg population an e450/APC dot plot was created to detect FoxP3+ cells in the CD4+ population.

To determine whether the knock-in of the human OX40 gene was altering immune cell populations within the mice, splenocytes were harvested from WT C57BL/6 mice, hOX40$^{+/-}$ KI mice and hOX40$^{+/+}$ KI mice (N=4 per group) and immune cell populations numerated (Dr J.Willoughby). Figure 3.4 demonstrates that expression of the chimeric receptor generally did not affect normal immune cell development. The major lymphocyte populations (CD4+ and CD8+ T cells and B cells) were unaffected by the introduction of this receptor, however we did witness a small but significant decrease in the number of Tregs within hOX40$^{+/+}$ KI mice and NK cells in both hOX40$^{+/-}$ and hOX40$^{+/+}$ KI mice. Likewise, the myeloid populations also generally seemed to be unaffected by expression of the chimeric receptor. A significant decrease was seen in the monocyte population within both KI genotypes as well as a decrease in the number of pDCs in the hOX40$^{+/+}$ KI (Figure 3.4). Despite this reduction in a number of immune cell populations within the hOX40 KI mice compared to WT mice, hOX40 KI mice developed normally, remained healthy and showed no unexpected effects, with mice having a normal life span. However, it should be noted that the number of mice assessed was relatively low and a greater number should be examined to confirm these differences.

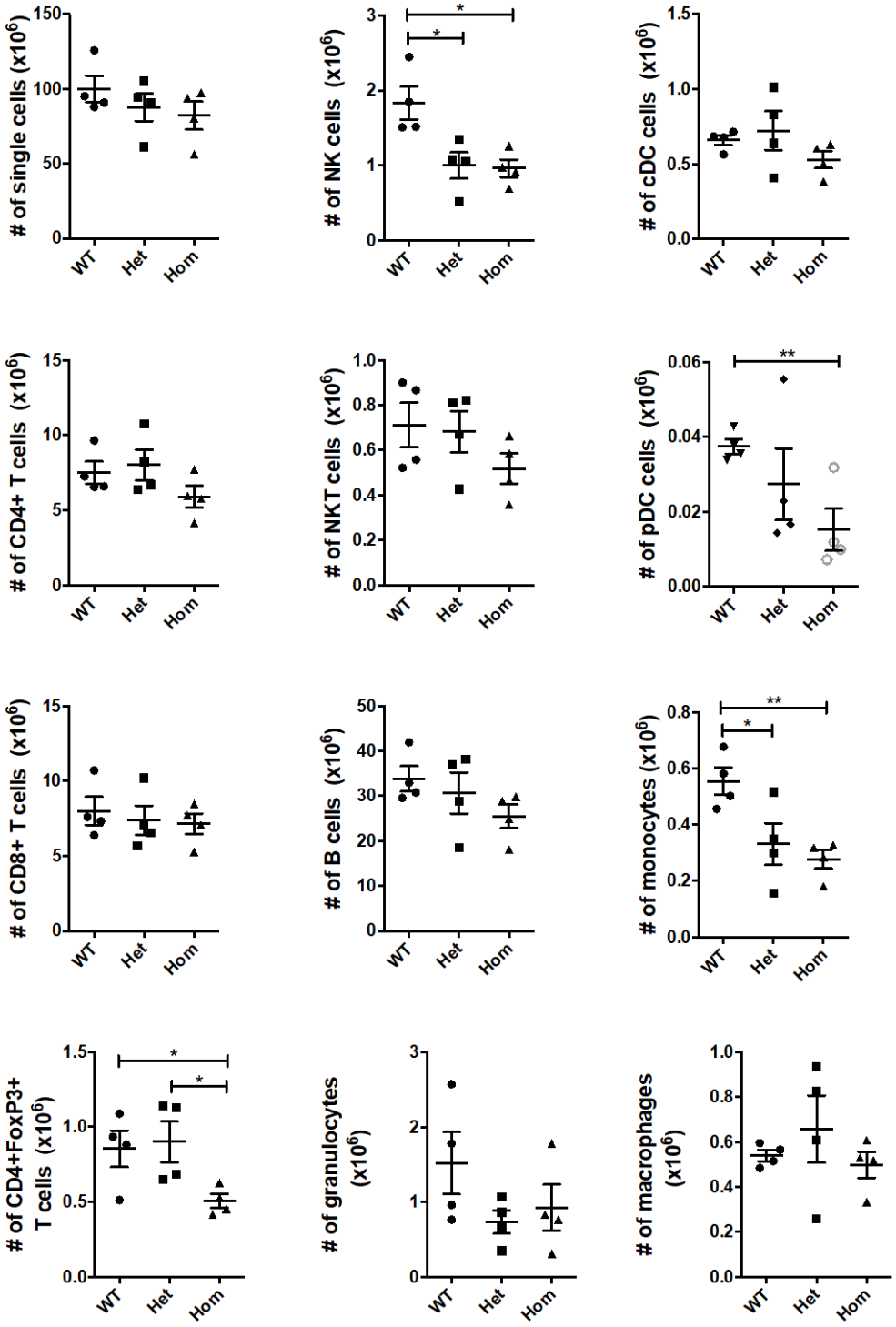

Figure 3.4 Numeration of immune cell populations in WT C57BL/6, hOX40$^{+/-}$ KI and hOX40$^{+/+}$ KI mice

Spleens were harvested from WT C57BL/6 mice, hOX40$^{+/-}$ KI and hOX40$^{+/+}$ KI mice. The number of immune cell subtypes was analysed using flow cytometry. Data is from one experiment with N=4 mice per group. Each data point represents an individual mouse. Error bars represent mean±SEM. Statistical significance was evaluated using an unpaired students t-test; * P≤ 0.05, ** P≤ 0.01, *** P ≤ 0.001.

Prior to testing the antibodies within these mice it was important to determine the expression profile of the receptor on a number of important cell types in resting and activated states. It is well known that OX40 expression is only detected on activated T cells, in both mice and humans [212, 326], with the exception of mouse Treg cells which constitutively express the receptor [263, 327]. It was thought for a long time that OX40 expression was restricted to T cells however expression has also been observed on other cell populations such as NK and NKT cells [211]. Therefore, the expression levels of hOX40 on these two populations as well as on the main T cell subsets; CD4+, CD8+ and CD4+FoxP3+ was determined. hPBMCs and murine splenocytes were examined to allow comparison between OX40 expression on human cells, WT mouse cells and the hOX40 KI mouse cells.

To examine OX40 expression at resting state spleens were harvested from WT C57BL/6 mice, hOX40$^{+/-}$ KI and hOX40$^{+/+}$ KI mice (N=4 per group). Spleens were processed followed by staining for CD4+, CD8+ and CD4+FoxP3+ cells before analysis using flow cytometry and the gating strategy shown in Figure 3.3.

Figure 3.5 displays the histograms showing fluorescence in the FL-2 channel (OX40 expression) from an exemplar mouse per group. Clear expression of mOX40 was seen on both WT and hOX40$^{+/-}$ KI Treg cells, with a lower amount of expression seen on CD4+ cells and no expression seen on CD8+ cells. This expression was less in the hOX40$^{+/-}$ KI compared to the WT mice on all T cell subsets due to the hOX40$^{+/-}$ KI mice expressing only one copy of the mouse receptor, with the other replaced by the human receptor. No mOX40 expression was seen in any of the lymphocyte populations in the hOX40$^{+/+}$ KI background as expected, confirming the full replacement of both copies of the mOX40 gene. Conversely hOX40 expression was observed on Tregs, CD4+ and CD8+ populations in the hOX40$^{+/+}$ KI mice in a hierarchal manner; Tregs > CD4+ > CD8+. Expression of hOX40 was also observed in hOX40$^{+/-}$ KI mice in all 3 populations, in the same hierarchal order as in the hOX40$^{+/+}$ KI mice, but with lower levels of overall expression. As expected, no hOX40 expression was detected in the WT C57BL/6 mice, however clear expression of mOX40 in the Treg population was observed as expected [196].

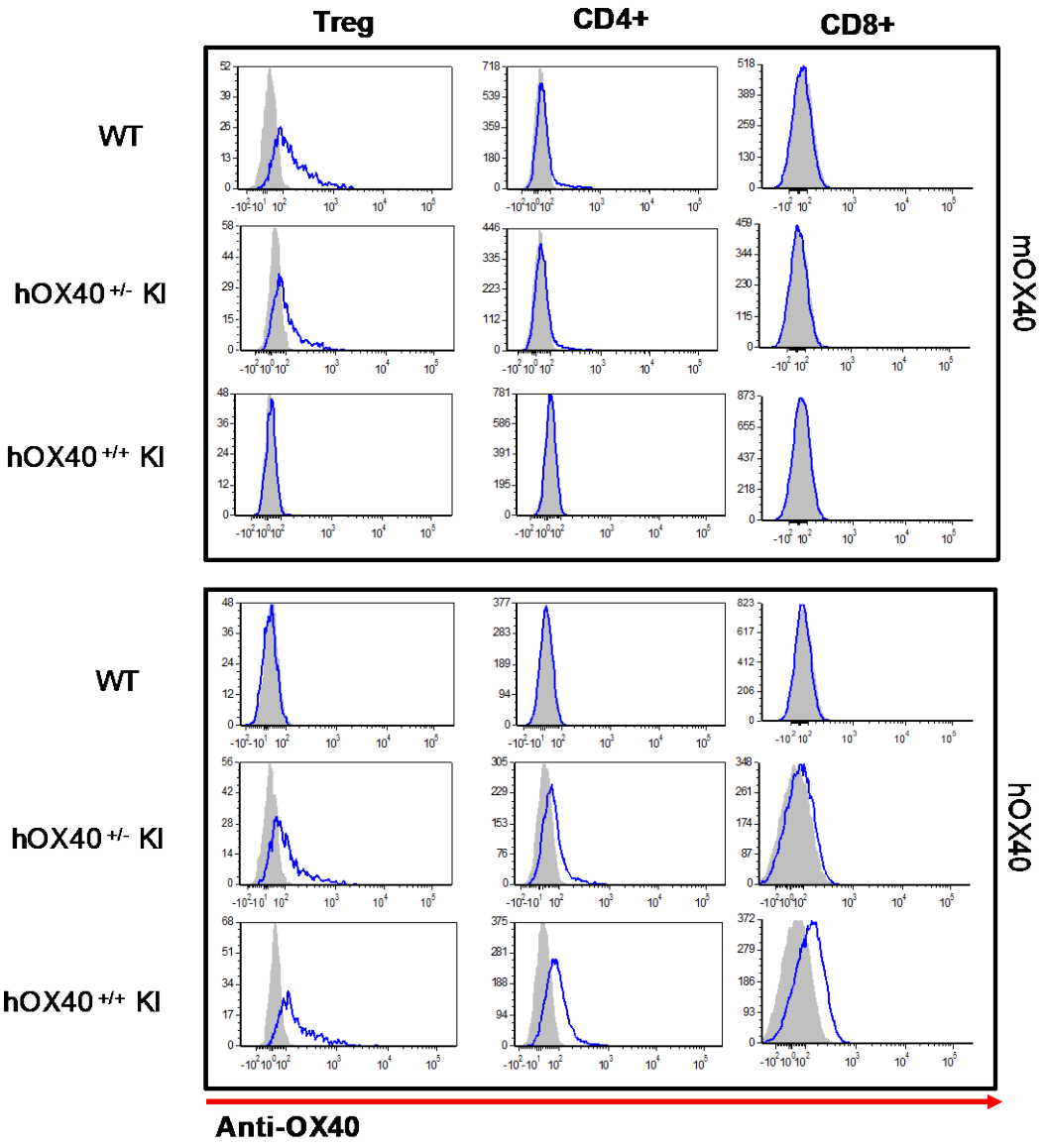

Figure 3.5 Expression of murine and human OX40 on resting mouse splenocytes from WT C57BL/6 mice, hOX40$^{+/-}$ KI mice and hOX40$^{+/+}$ KI mice

Spleens were harvested from WT C57BL/6 mice alongside hOX40$^{+/-}$ KI and hOX40$^{+/+}$KI mice (N=4). Spleens were processed and red cell lysed before analysis of OX40 expression using either a PE-conjugated anti-hOX40 antibody or a PE-conjugated anti-mOX40 antibody. Analysis was carried out via flow cytometry using the gating strategy shown in Figure 3.3. Representative histograms show OX40 expression (blue line) in comparison to an isotype control (grey shaded). The top panel shows mOX40 expression and the bottom panel hOX40 expression. From left to right Treg, CD4+ and CD8+ populations are shown and from top to bottom WT C57BL/6, hOX40$^{+/-}$ KI and hOX40$^{+/+}$ KI mice.

To obtain a more robust understanding of expression levels of OX40 on the various populations, data from the four mice per group was collated and the percentage of cells per sub-population expressing either mouse or human OX40 was plotted and is shown in Figure 3.6. This analysis revealed a gene dosage effect such that the percentage of cells expressing hOX40 in the $hOX40^{+/-}$ KI mice was around half the amount of overall expression in the $hOX40^{+/+}$ KI mice i.e. hOX40 expression on Tregs in Het vs. Hom = 26.5% vs. 43.5%.

In addition to the T cell populations, OX40 expression on NK and NKT cells was monitored at resting state and shown to be measurable but extremely low (<2% of the population were positive) (data not shown).

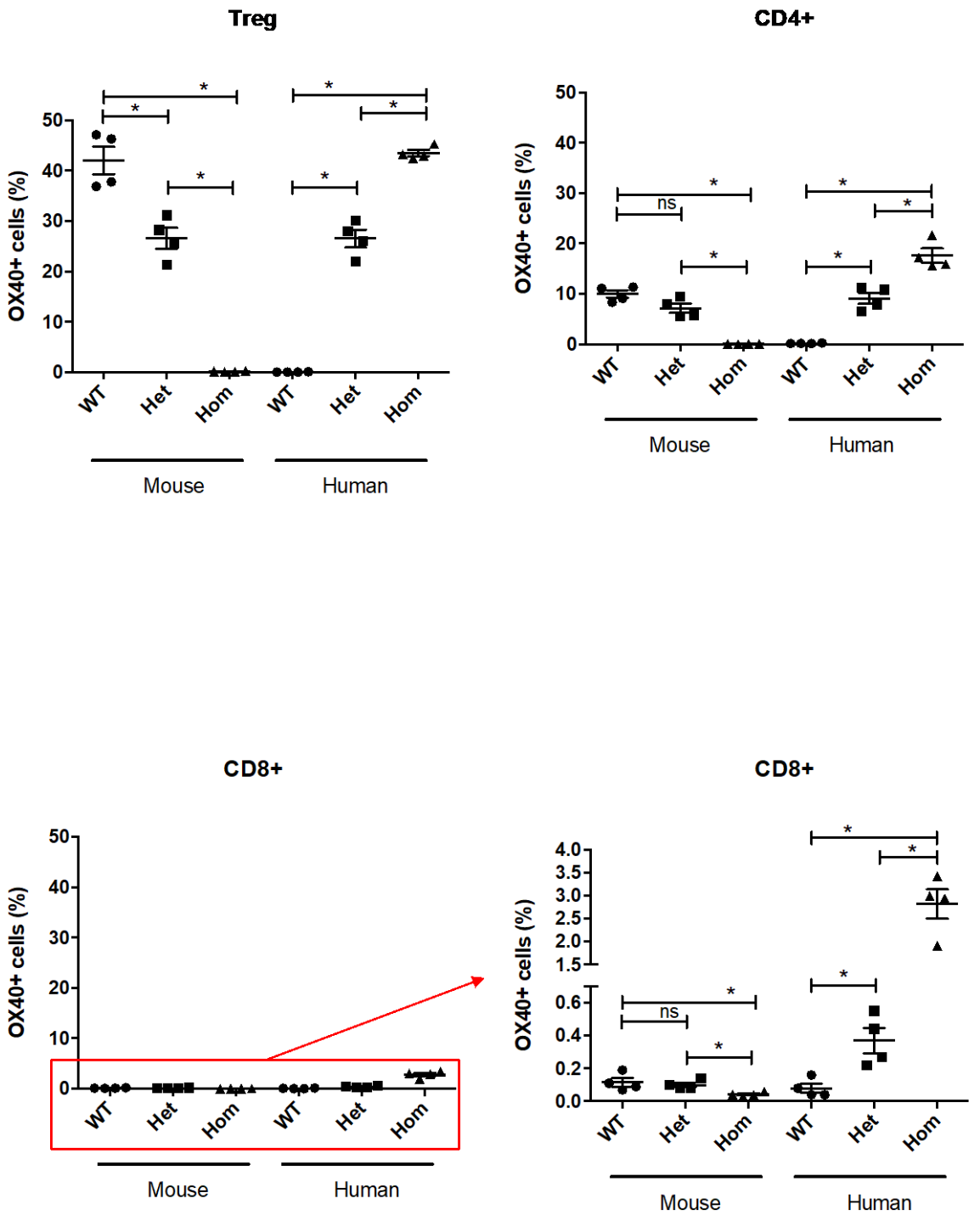

Figure 3.6 Expression of murine and human OX40 on resting mouse splenocytes from WT C57BL/6 mice, hOX40$^{+/-}$ KI and hOX40$^{+/+}$ KI mice

Graphs show the percentage of cells in the Treg, CD4+ and CD8+ T cell populations expressing OX40 (mouse on left hand side of graph and human on the right hand side) in the WT C57BL/6 mice and both the hOX40$^{+/-}$ (Het) and hOX40$^{+/+}$ (Hom) KI mice. Data is from one individual experiment with N=4 mice per group. Each data point represents an individual mouse. Error bars represent mean±SEM. Statistical significance was evaluated using a Mann-Whitney test; ns: non-significant, * P≤ 0.05, ** P≤ 0.01, *** P ≤ 0.001.

On most resting cells OX40 is not expressed and is only up regulated once cells become activated [234]. It was therefore of interest to monitor the expression of the receptor in an activated state, firstly to gain a better understanding of the hOX40 KI mouse model, and secondly so that future experiments could be optimised in terms of treatment timings and optimal read out times.

To assess this, spleens were harvested from WT C57BL/6 mice, hOX40$^{+/-}$ KI and hOX40$^{+/+}$ KI mice, and splenocytes activated *in vitro* using anti-CD28 and anti-CD3 antibodies. Mouse and human OX40 expression was monitored on the surface of naïve cells and cells that had been activated for 24 (day 1), 48 (day 2), 72 (day 3) and 96 (day 4) hours (Figure 3.7). Resting cells showed the same expression profiles as had been seen in the previous experiment described above (Figure 3.5 and Figure 3.6). After 24 hours of activation human OX40 expression increased on CD4+ and CD8+ cells in both the hOX40$^{+/-}$ and hOX40$^{+/+}$ KI backgrounds. Mouse OX40 expression was increased in WT mice and hOX40$^{+/-}$ KI on CD4+ T cells with no expression observed on the CD8+ population. No human OX40 expression was seen in the WT mice after 24 hours activation and likewise no mouse OX40 expression was seen in the hOX40$^{+/+}$ KI mice in either the CD4+ or CD8+ populations. The same patterns of expression described above were also seen after the splenocytes had been activated for 48 hours with the exception of CD8+ cells from a WT mouse, which after 48 hours started to express mouse OX40. Treg cells were also monitored in this experiment using CD4 and FoxP3 as markers, however the population was too small to obtain reliable data. This expression data is represented graphically for all time points measured in Figure 3.8.

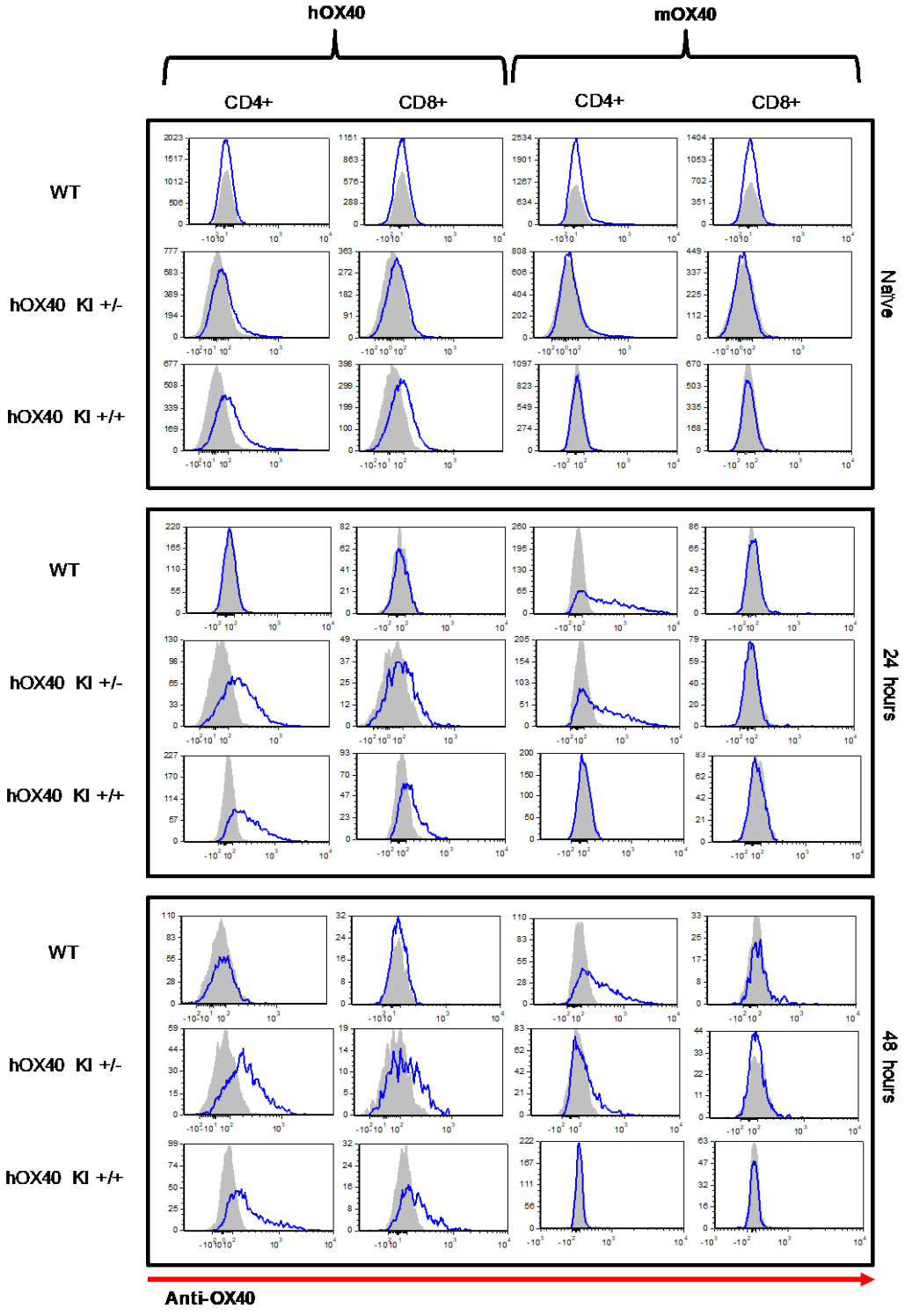

Figure 3.7 Expression of murine and human OX40 on CD3/CD28 activated mouse splenocytes from WT C57BL/6, hOX40$^{+/-}$ KI and hOX40$^{+/+}$ KI mice

Spleens were harvested from a WT C57BL/6 mouse alongside a hOX40$^{+/-}$ KI and hOX40$^{+/+}$ KI mouse (N=1). Splenocytes were processed and stimulated with 0.1μg/ml anti-CD3 and 5μg/ml anti-CD28. 100μl of cells were stained for CD4 and CD8 plus the addition of either a PE-conjugated anti-mOX40 antibody or a PE-conjugated hOX40 antibody every 24 hours post stimulation. Cells were analysed using flow cytometry and the gating strategy used in Figure 3.3 minus the Treg gate.

Mouse OX40 expression on CD4+ T cells peaked on day 1 in both WT and hOX40$^{+/-}$ KI mice (Figure 3.8). The level of expression on CD8+ T cells was much lower and peaked on day 2. A similar pattern of expression was seen with human OX40 expression in the hOX40$^{+/-}$ KI mice; in the CD4+ population expression peaked on day 1 and on day 2 for CD8+ T cells, again at a lower level. In the hOX40$^{+/+}$ KI mice no mouse OX40 expression was seen, and the peak of expression of hOX40 on CD4+ and CD8+ cells was the same as in the hOX40$^{+/-}$ KI mice. Interestingly the expression levels of human OX40, in both hOX40$^{+/-}$ KI and hOX40$^{+/+}$ KI mice, started to increase again from its dip at either day 2 or 3, and by day 4 was reaching expression levels seen at the peak. This experiment is currently being repeated within the lab to increase the N numbers allowing us to draw more reliable conclusions from the data.

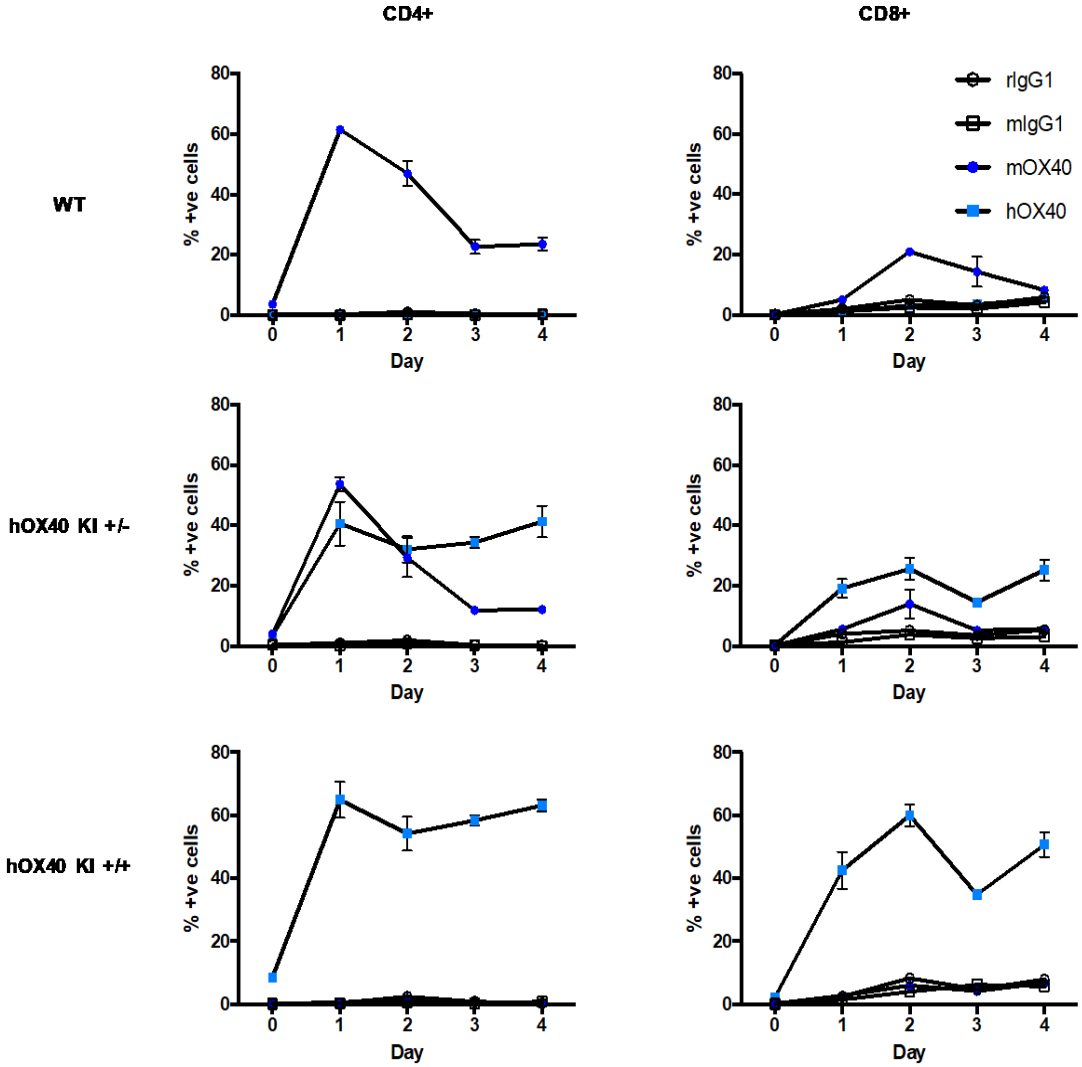

Figure 3.8 Expression of murine and human OX40 on CD3/CD28 activated mouse splenocytes from WT C57BL/6, hOX40$^{+/-}$ KI and hOX40$^{+/+}$ KI mice

Graphs show the kinetics of murine and human OX40 expression over the course of 4 days after cell activation. The left panel shows CD4+ cells and the right panel CD8+ cells. Top to bottom shows WT, hOX40$^{+/-}$ KI and hOX40$^{+/+}$KI mice. Error bars represent mean±SEM of three readings from triplicate wells containing the same sample

Having established the expression pattern of both mouse and human OX40 within the hOX40 KI mouse model, it was important to understand the expression profile of hOX40 in human samples to determine if it was comparable to that in the hOX40 KI mice; and hence represented a viable model for testing mAb efficacy.

Healthy human PBMCs were isolated from two donors and cultured at high density for two days prior to stimulation with plate bound anti-CD3. The staining protocol and gating strategy shown in Figure 3.3 were used for analysis of hOX40 expression on CD4+ effector, CD8+ and Treg cells. hOX40 expression was monitored over 6 days post stimulation using a PE-conjugated anti-hOX40 antibody (Figure 3.9). This expression data is represented graphically in Figure 3.10.

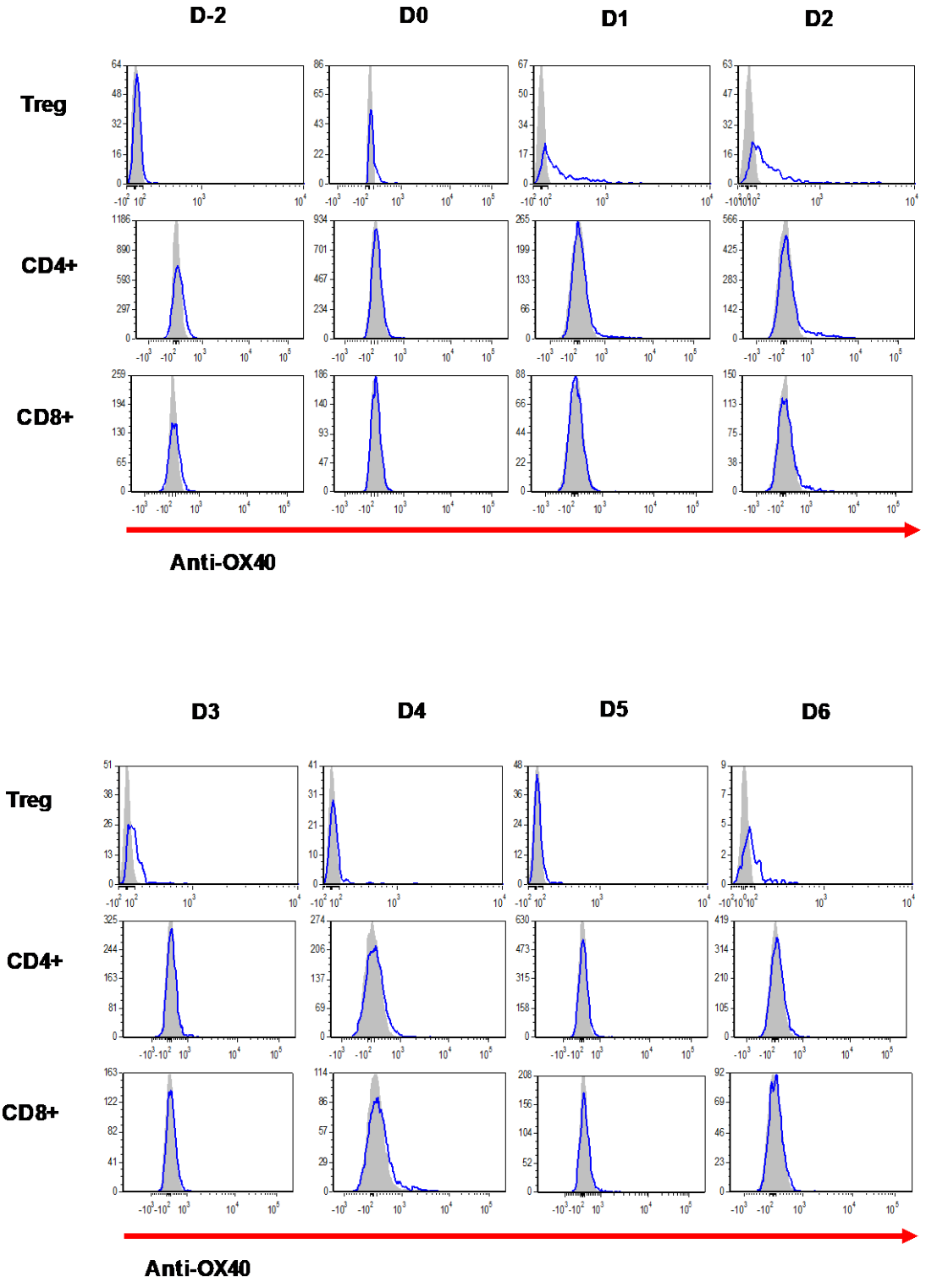

Figure 3.9 Analysis of hOX40 expression on human PBMCs after stimulation with anti-CD3

Human PBMCs were isolated from two healthy donors. Cells were cultured at high density for two days prior to stimulation with 1μg/ml plate bound anti-CD3 (Clone: OKT3). 100μl of cells were harvested per day and stained for CD4+, CD8+ and FoxP3 markers. Human OX40 expression was detected using a PE-conjugated antibody and flow cytometry. Histograms show human OX40 expression from top to bottom on Tregs, CD4+ and CD8+ T cells, and from left to right (top panel) on day -2 (freshly isolated), day 0 (post high density culture), day 1 and day 2 post CD3 stimulation, and from left to right (bottom panel) day 3-6 post CD3 stimulation. Data is representative of two individual donors.

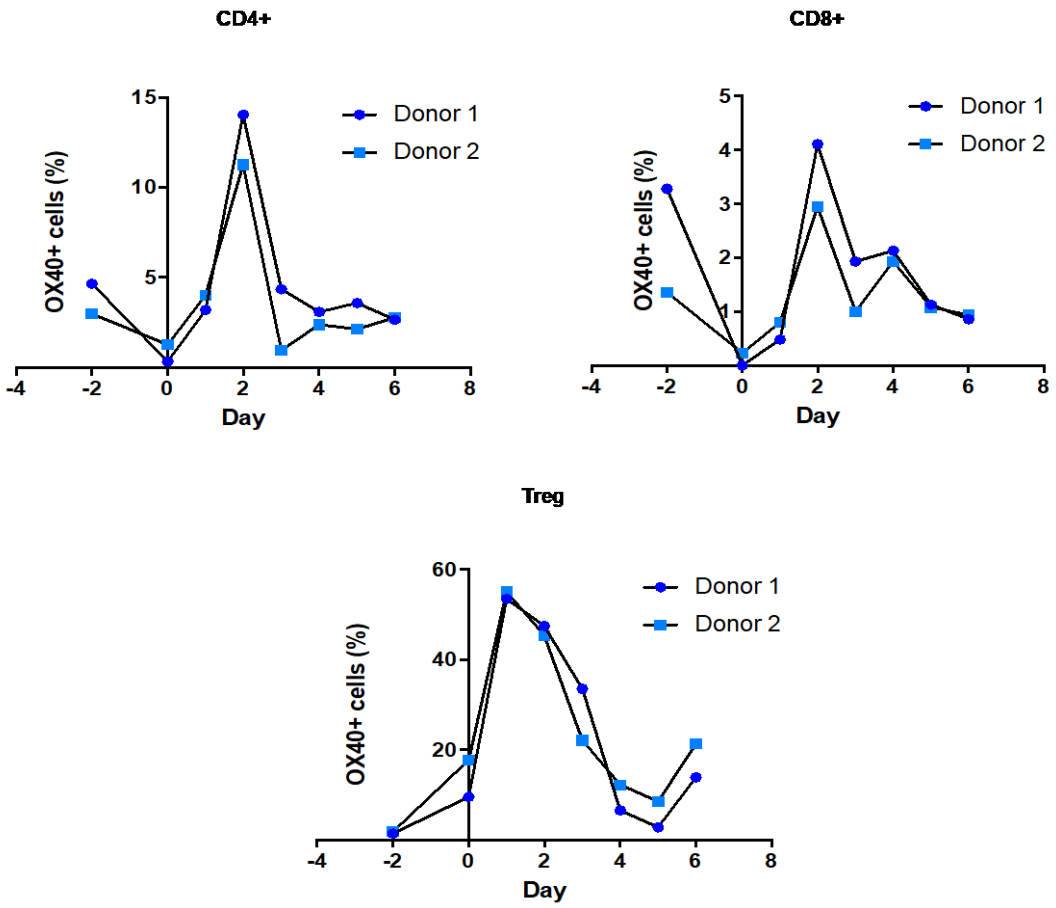

Figure 3.10 Kinetics of hOX40 expression on human PBMCs after stimulation with anti-CD3

The same experimental set up as described in Figure 3.9 was used. Graphs show the percentage of OX40+ cells in Treg, CD4+ and CD8+ populations from two individual donors on day -2 (freshly isolated), day 0 (post high density culture), and days 1-6 post CD3 stimulation.

The same hierarchal expression pattern of hOX40 seen in the hOX40 KI mice was observed in human PBMC samples (Treg>CD4+>CD8+) (Figure 3.9 and Figure 3.10). Likewise, the peak of expression was seen between day 1 and day 2, as with the hOX40 KI mice. We did not, however, witness a second increase in expression at day 4 as had been seen within the mice. One important discovery was that the expression of hOX40 on CD4+ and CD8+ T cells within hPBMCs was lower than that seen in these populations within the hOX40 KI mice. For example, 3-4% of CD8 T cells were hOX40+ in human PBMCs at the peak of expression, whereas 20% of CD8 cells were hOX40+ in the hOX40$^{+/-}$ KI mice and 60% in the hOX40$^{+/+}$ KI mice. This suggests that the mice are an overexpression model in comparison to humans and this will need to be considered when interpreting results from these mice. Ideally this experiment would have been done with four-six donors to obtain more robust data, it is therefore being repeated in the lab currently. It was concluded, however, that our hOX40 KI mouse model was a

suitable starting point to test the therapeutic ability of our panel of anti-hOX40 mAb. However, before *in vivo* testing of the panel of anti-hOX40 mAb, they were characterised *in vitro*.

3.3 Anti-hOX40 mAb production

For the production of anti-hOX40 mAb, mice were immunised with hOX40-hFc fusion and complete freunds adjuvant (CFA). Splenocytes from immunised mice were fused with NS-1 cells using conventional hybridoma technology (By Dr R.French). Plates were screened by ELISA using hOX40-hFc and positive wells tested for binding to hOX40-transfected 293F cells. A panel of seven different mAb were generated (

Table 3.2) and shown to be specific for human OX40 initially via ELISA binding to hOX40-hFc and secondly via binding to hOX40 expressed on the surface of transiently transfected 293F cells.

Antibody	Parental isotype	Isotype switched
SAP 28-2	mIgG1	mIgG2a
SAP 28-3	mIgG1	mIgG2a
SAP 15-3	mIgG1	mIgG2a
SAP 9	mIgG2a	mIgG1
SAP 25-29	mIgG1	mIgG2a
SAP 29-23	mIgG2a	mIgG1
SAP 29-50	mIgG1	mIgG2a

Table 3.2 Anti-hOX40 mAb produced in-house via the hybridoma technology

Seven anti-hOX40 mAb were produced from fusions using conventional hybridoma technology. Five were a mIgG1 isotype and the remaining two mIgG2a isotype. All mAb were isotype switched by subcloning the variable regions into expression vectors containing constant regions of different antibody types (Dr C.Chan). These vectors were transiently transfected into ExpiCHO cells for mAb production.

It is well known that antibody isotype plays a major role in determining the type of effector function elicited. As a general rule, for TNFR mAb, mIgG1 mAb have been shown to be agonistic whereas mIgG2a mAb have not, but can cause depletion of the target cell due to their affinity for activatory FcγR [144]. To enable assessment of not only which mAb, but which isotype of mAb was going to be most effective as a therapeutic, the panel of antibodies were isotype switched (Dr C.Chan) and transiently transfected into ExpiCHO cells allowing production of both mIgG1 and mIgG2a versions of each mAb. Unfortunately, SAP 29-50 mIgG2a did not produce high yields of mAb production despite numerous attempts, we therefore could not include this mAb in future studies.

Following the successful isotype switching of the anti-hOX40 mAb and the demonstration of the mAb binding and specificity to hOX40 (By Dr R.French), the mAb were subsequently assessed by surface plasmon resonance (SPR) using biacore.

3.4 Determining the binding properties of anti-hOX40 mAb

SPR is a technique which allows real time detection of interactions between molecules. The process of SPR is illustrated in Figure 3.11. SPR causes a reduction in the angle of reflected light on the glass side of a sensor chip. As molecules bind to the sensor surface the refractive index close to the surface changes altering the angle of minimum reflected intensity. The change in SPR angle is proportional to the mass on the chips surface.

To examine the panel of anti-hOX40 mAb, a hOX40-hFc fusion protein was bound to the chip and the panel of anti-hOX40 mAb flowed over at a concentration of 100nM and analysed using a 1:1 binding model. Usually a concentration range would be used to determine saturation levels of the mAb as well as any concentration dependant artefacts. This was carried out previously with the parental mAb and produced KD values comparable to those produced in the second run (data not shown) therefore in the interest of time and material it was not repeated

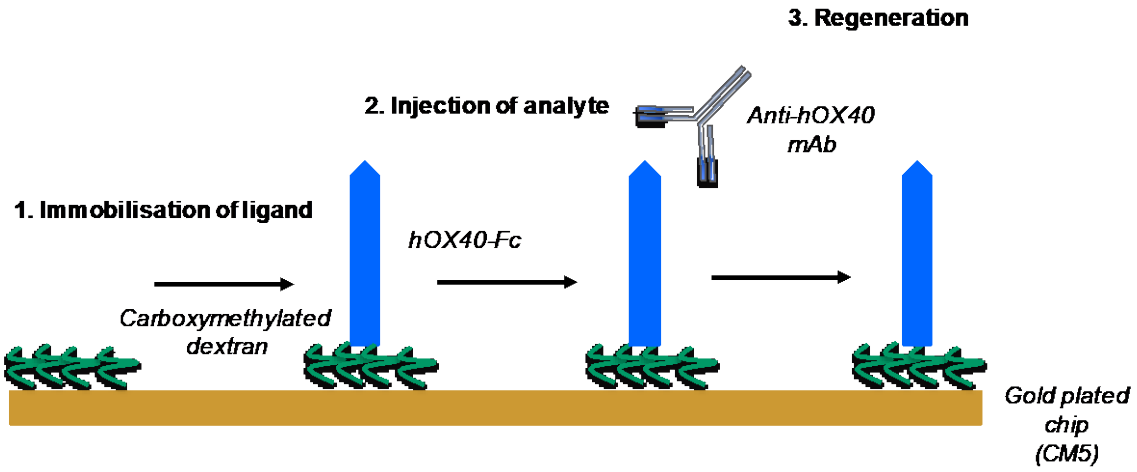

Figure 3.11 Schematic of surface plasmon resonance (SPR)

SPR detection utilises the changes in refractive index (RI) at the surface of a chip; this change in RI is directionally proportional to the mass on the chip. Step 1) The sensor chip; a glass slide plated with a thin layer of gold covered in a dextran matrix, is used to immobilise the ligand. Step 2) Analyte is injected over the chip in solution and allowed a specified amount of contact time with the chip to allow binding to the ligand. Step 3) The chip is then regenerated, removing any analyte without damage to the ligand, in preparation for another run.

Both mIgG1 and mIgG2a isotypes of the anti-hOX40 mAb were tested on the biacore and fitted to a 1:1 binding model to determine kinetics. Sensograms in

Figure 3.12 show the response units recorded for each mAb binding to hOX40 whilst the numerical values from the 1:1 model fitting are presented in

Table 3.3.

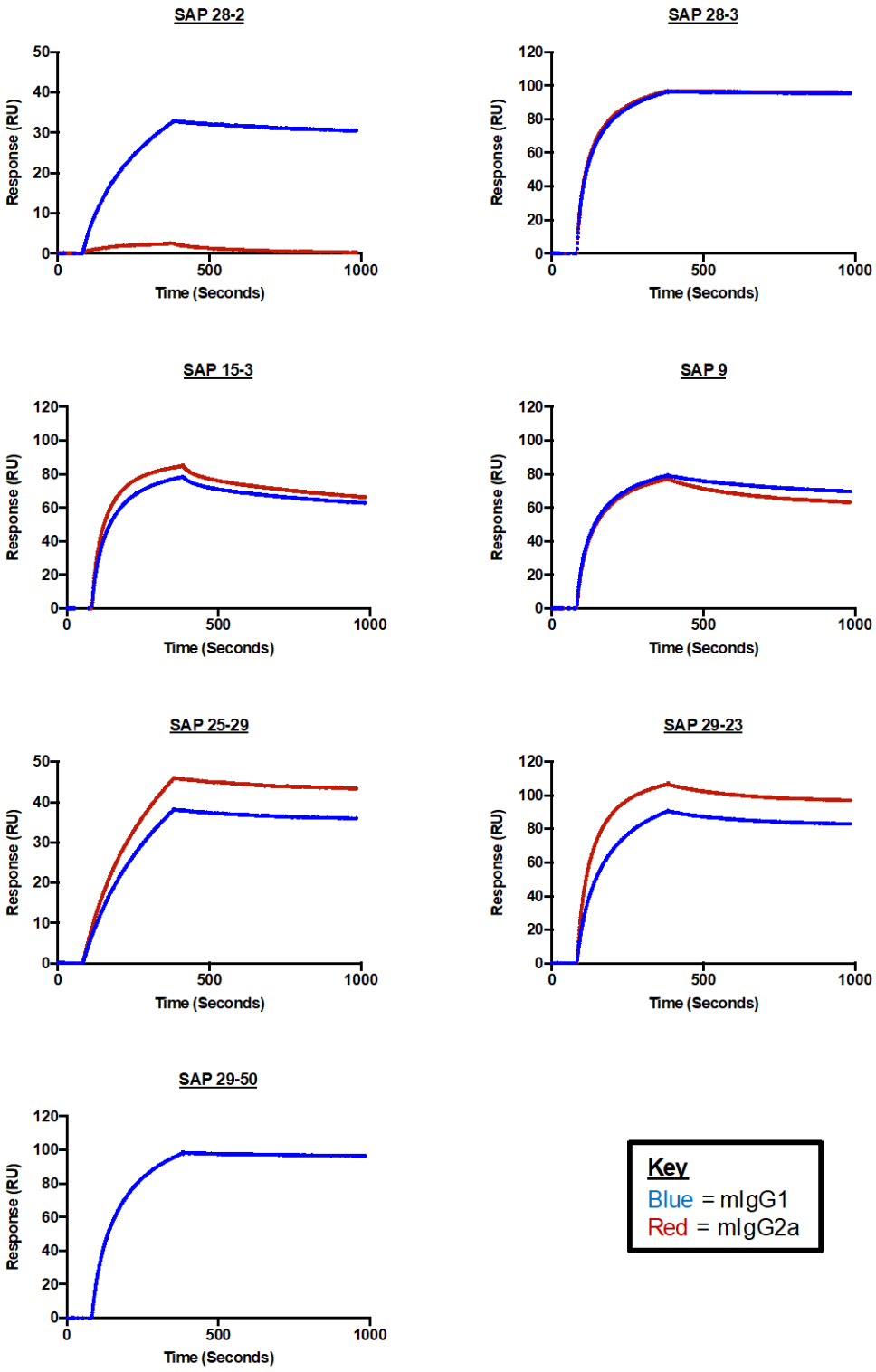

Figure 3.12 SPR analysis of anti-hOX40 mAb

hOX40-hFc fusion protein was immobilised on the CM5 chip at a concentration of 1μg/ml. Anti-hOX40 mAb were injected over the chip at a flow rate of 30μl/minute with contact times of 5 and 10 minutes for on and off, respectively. The chip was regenerated with 10mM glycine pH1.5 for 30 seconds between each run to remove any remaining bound antibody.

Differences between on- (ka) and off- (kd) rates of the antibodies were detected. SAP 28-2 and SAP 25-29 had the slowest on rates in comparison to the remaining anti-hOX40 mAb, whereas SAP 15-3 and SAP 9 had the fastest off rates. However, when calculating the equilibrium dissociation constant (KD = kd/ka), which takes into account both the ka and kd values, all of the mAb examined possessed values of 10^{-9} and above, with the exception of SAP 28-2 mIgG2a (highlighted in red), classing them all as high affinity antibodies. However some (SAP 28-3, SAP 29-50, SAP 29-23 and SAP 9) were higher than others (SAP 28-2, SAP 15-3 and SAP 25-29). Most importantly, again with the exception of SAP 28-2, mIgG1 and mIgG2a isotypes of the same mAb possessed similar KD values. This result indicates that altering the constant regions of the mAb to allow for isotype switching had no significant effects on binding ability.

Table 3.3 summaries this information.

Antibody	Ka (M-1.s-1)	Kd (s-1)	KD (M)
SAP 28-2 mIgG1	5.89×10^{4}	1.02×10^{-4}	1.74×10^{-9}
SAP 28-2 mIgG2a	2.8×10^{4}	6.1×10^{-5}	2.18×10^{-7}
SAP 28-3 mIgG1	2.02×10^{5}	1.35×10^{-6}	6.69×10^{-12}
SAP 28-3 mIgG2a	2.16×10^{5}	5.71×10^{-7}	2.64×10^{-12}
SAP 15-3 mIgG1	1.62×10^{5}	2.86×10^{-4}	1.77×10^{-9}
SAP 15-3 mIgG2a	2×10^{5}	3.21×10^{-4}	1.61×10^{-9}
SAP 9 mIgG1	1.71×10^{5}	1.7×10^{-4}	9.91×10^{-10}
SAP 9 mIgG2a	1.63×10^{5}	2.81×10^{-4}	1.72×10^{-9}
SAP 25-29 mIgG1	4.71×10^{4}	9.04×10^{-5}	2.17×10^{-9}
SAP 25-29 mIgG2a	4.84×10^{4}	8.29×10^{-5}	1.71×10^{-9}
SAP 29-23 mIgG1	1.18×10^{5}	1.1×10^{-4}	9.35×10^{-10}
SAP 29-23 mIgG2a	1.85×10^{5}	1.21×10^{-4}	6.54×10^{-10}
SAP 29-50 mIgG1	1.23×10^{5}	2.78×10^{-6}	2.26×10^{-11}

Table 3.3 Anti-hOX40 mAb kinetic and affinity values

The on (ka), off (kd) and equilibrium dissociation constant (KD) values for the panel of anti-hOX40 mAb are provided in the table. Biacore T100 evaluation software was used to obtain values. Larger ka values equates to a quicker on rate, likewise, smaller kd values indicate a slower off rate. The smaller the KD value the higher the affinity of the antibody.

Due to the stark difference in binding ability demonstrated by the response units on the sensogram as well as the calculated affinities between SAP 28-2 mIgG1 and mIgG2a a number of batches of this mAb were tested. All three mIgG2a batches tested produced the same result, as shown in Figure 3.13. The mAb sequence was checked (By Dr C.Chan) and confirmed the correct mAb and

isotype backbone, therefore it is currently unclear as to why this isotype-dependent difference was observed. It is to be remembered however, that one of the caveats to SPR analysis is that it is an artificial set up, meaning that the results generated won't necessarily depict what happens *in vivo*. This was demonstrated by data showing that the mIgG2a version of the mAb bound to transiently transfected cells to the same level as the mIgG1 isotype (Figure 3.18) and also functioned *in vitro* (Figure 3.24) and *in vivo* (Figure 5.2) indicating its ability to engage the receptor. Therefore, the conclusion was that it reflected an artefact of the SPR.

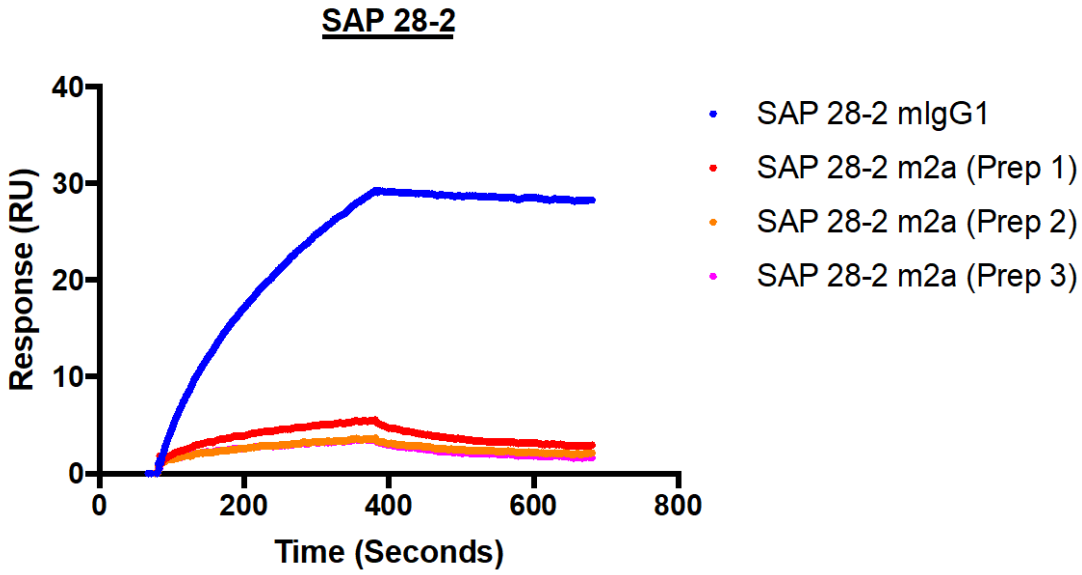

Figure 3.13 SPR analysis of SAP 28-2 mIgG1 and mIgG2a batches

The same experimental set up as described in Figure 3.11 was used. three separate batches of SAP 28-2 mIgG2a (Prep 1 = red line, Prep 2 = orange line and Prep 3 = pink line) were tested alongside the mIgG1 version of the mAb (blue line) for binding to hOX40.

3.5 Anti-human-OX40 mAb binding *in vivo* and cross reactivity

Before we were able to utilise the hOX40 KI mouse model to test the panel of mAb it was imperative that we determined the ability of the mAb to bind to the hOX40 expressed by the hOX40 KI mouse cells as well as establish if the mAb cross-reacted with the mouse OX40 receptor. This was important to know before any *in vivo* work was carried out so that we were able to interpret the data accurately. To study this, splenocytes and blood were taken from WT C57BL/6 mice and

hOX40$^{+/+}$ KI mice. The cells were activated *in vitro* with anti-CD3 and anti-CD28 antibodies for 24 hours before addition of the anti-OX40 mAb (mIgG1 or mIgG2a as indicated in the figure) and a PE-labelled secondary anti-mouse Fc F(ab')$_2$ fragment. The gating strategy and staining as shown in Figure 3.3 was used. Binding of the antibodies was measured via fluorescence in the FL-2 channel.

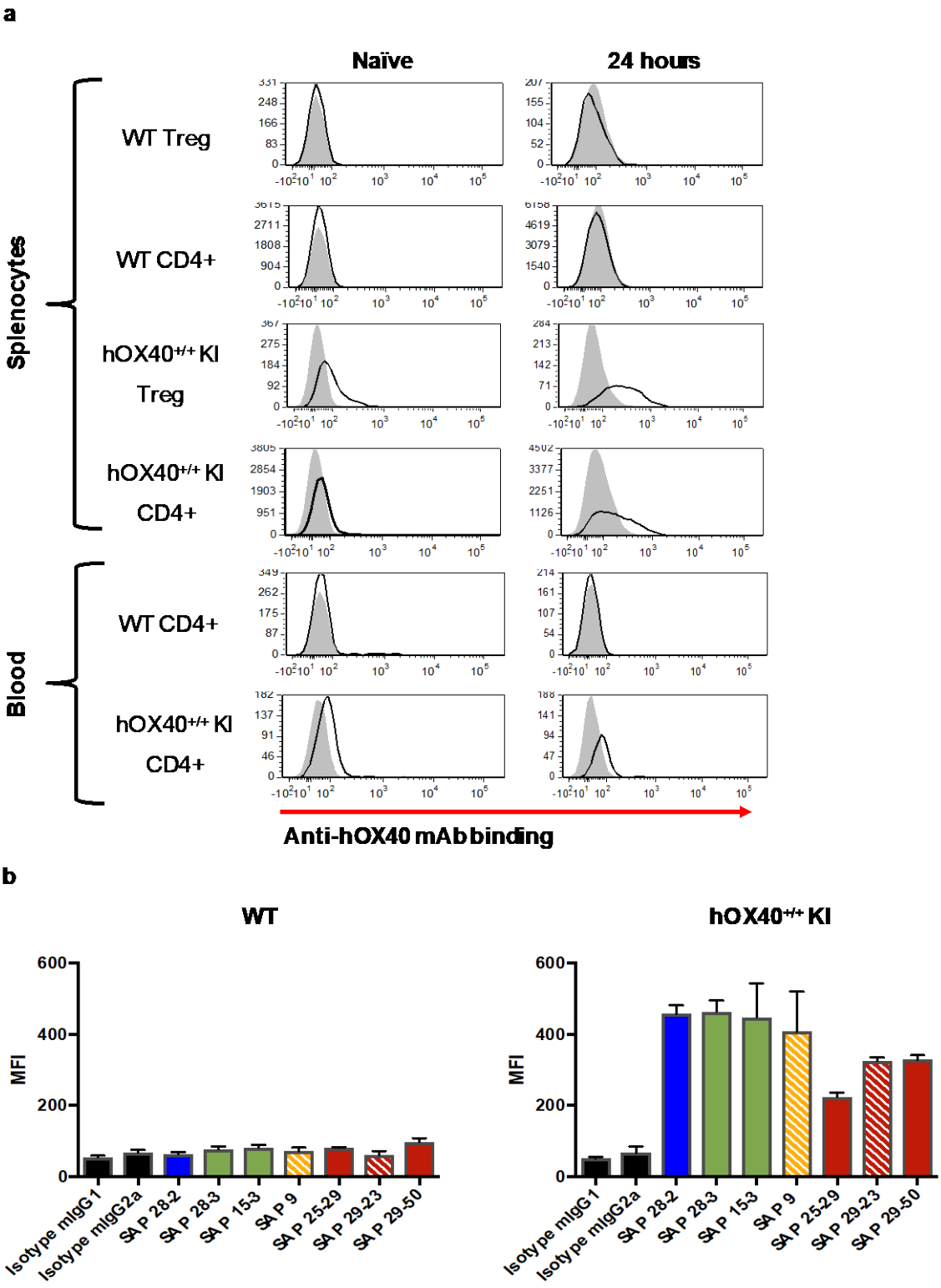

Figure 3.14 Binding of anti-hOX40 mAb to WT and hOX40$^{+/+}$ KI splenocytes and blood

Splenocytes were harvested and terminal bleeds performed on WT and hOX40$^{+/+}$ KI mice (N=3). Cells were activated *in vitro* with 0.1μg/ml anti-CD3 and 5μg/ml anti-CD28 for 24 hours. 20μg/ml of Fc blocker (2.4G2) was used before detection of anti-hOX40 mAb binding using a PE-conjugated anti-mouse Fc F(ab')$_2$ fragment. Antibody binding was detected using flow cytometry.
a) Histograms show a representative antibody binding (SAP 28-2 mIgG1) (black line) in comparison to an isotype control (grey shaded). b) Bar charts represent MFI indicating parental antibody binding in WT (left hand side) and hOX40$^{+/+}$ KI mice (right hand side) in the Treg population 24 hours after activation.mIgG1 mAb are represented by block colours and mIgG2a mAb by diagonal lines. Data is from one experiment with N=3 mice per group. Error bars represent mean±SEM.

It was seen that the panel of anti-human OX40 antibodies tested were able to bind to hOX40 in the KI mouse on both CD4+ and Treg cells in both the blood and the spleen (Figure 3.14). It was also revealed that none of the antibodies cross reacted with the mouse receptor on Tregs or CD4+ cells. CD8+ cells were also tested and demonstrated the same pattern (data not shown). These results confirmed that the anti-hOX40 mAb could be used within the hOX40 KI mouse and that the effects seen would be as a result of hOX40 stimulation alone, and not a combination of both mouse and human.

3.6 Binding domains of anti-hOX40 mAb

Having established the affinity of binding for the panel of hOX40 mAb as well as confirming their specific binding to the human receptor, the location of binding within the OX40 extracellular domain (ECD) was assessed. The ECD of human OX40 possesses three full cysteine rich domains (CRDs 1,2 and 4) and one partial CRD (CRD3) (Figure 3.15). It was previously confirmed that all of the antibodies developed using the hybridoma technique were targeted against hOX40, however it was unknown as to which specific CRD in OX40 that each bound to. Although all of the antibodies are capable of targeting the same receptor, it has been shown with other TNFR family members that binding domain/epitope can have substantial effects on functional activity [267, 328]. Likewise, antibody distance in relation to the cell membrane has also been shown to be important in Fc-mediated effector mechanisms [329]. Therefore, to determine which CRD each anti-hOX40 mAb bound, WT, ∆1, ∆1,2, ∆1,2,3 domain constructs were created (Dr C.Chan). An N-terminal CD20 peptide was included in the mutant ∆1,2,3 construct to confirm expression on the cell surface (illustrated in Figure 3.16). This was compared to the expression of a 4-1BB mutant domain construct, which expressed just the terminal 4th domain of 4-1BB with the same CD20 tag (4-1BB-1d), used previously in the lab and shown to express. Transient transfections of 293F cells were performed using a cationic based lipid transfection and screened after 24 hours using flow cytometry

.

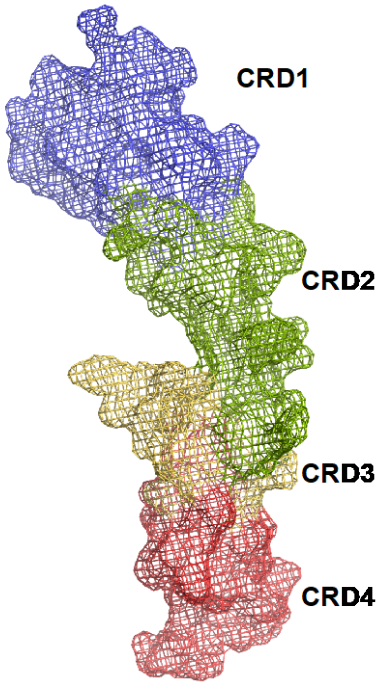

Figure 3.15 Crystal structure of hOX40

PDB file 2HEV was altered in Pymol to change the colour and structural representation of the hOX40 receptor. The receptor is rendered as a mesh surface with CRDs 1-4 coloured blue, green, yellow and red, respectively.

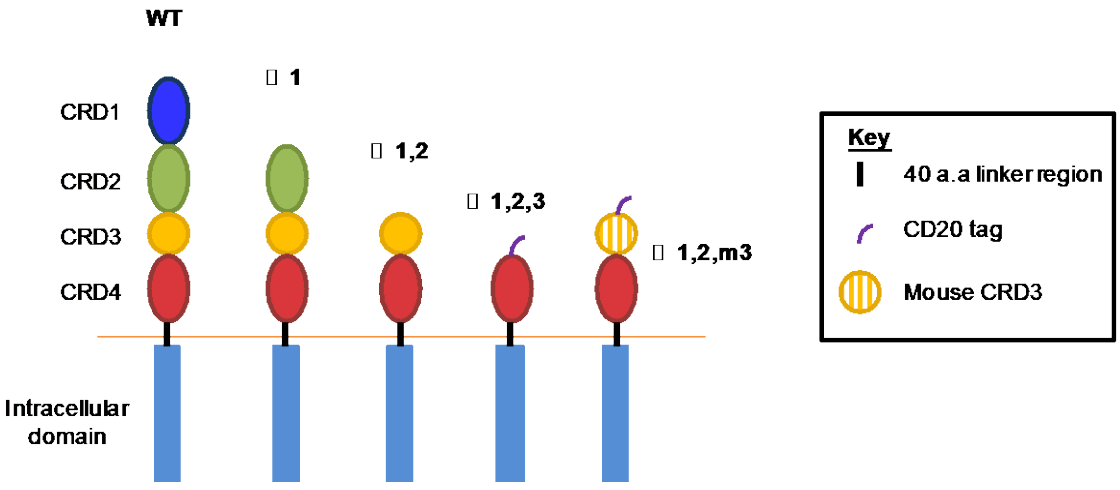

Figure 3.16 hOX40 domain constructs used in binding experiment

Schematic of the human OX40 domain constructs produced to establish binding location of anti-hOX40 mAb; constructs lacking 1(Δ1), 2 (Δ1,2) or 3 CRD (Δ1,2,3) domains, were created (by Dr C.Chan) from the WT human OX40 receptor and transiently transfected into 293F cells 24 hours prior to detection. Mouse CRD3 was used to stabilise and allow for expression of hCRD4.

Unfortunately, surface expression of the Δ1,2,3 construct did not occur as judged by a lack of expression of the CD20 tag in comparison to the positive control construct 4-1BB-1d (Figure 3.17a). Detection of the 4-1BB-1d construct confirmed that the transfection process was successful and the CD20 tag was able to be recognized by the anti-CD20 antibody. The absence of hOX40 Δ1,2,3 expression, is likely to be down to either mis-folding of the protein at the cell surface rendering it undetectable, or an inability to express the receptor altogether. From previous experiments (Figure 3.14) showing that the anti-hOX40 mAb don't cross react with the mouse receptor, we therefore utilized this knowledge and created a 4th mutant construct containing human CRD4 and mouse CRD3 again with the CD20 tag (illustrated in Figure 3.16). This time expression on the cell surface of transiently transfected 293F cells was successful (Figure 3.17b), as determined by FITC-labelled rituximab binding to a CD20-tag, therefore this construct was used in future experiments alongside the WT, Δ1 and Δ1,2 constructs. Figure 3.17c demonstrates that all four constructs were able to be expressed on the cell surface of 293F cells as detected by one of the seven OX40 mAb (SAP 25-29) at fairly equal levels ruling out this variable as something which could affect binding levels of the mAb. These four constructs were therefore used in subsequent binding experiments to help refine the binding epitope of the full panel of anti-hOX40 mAb

.

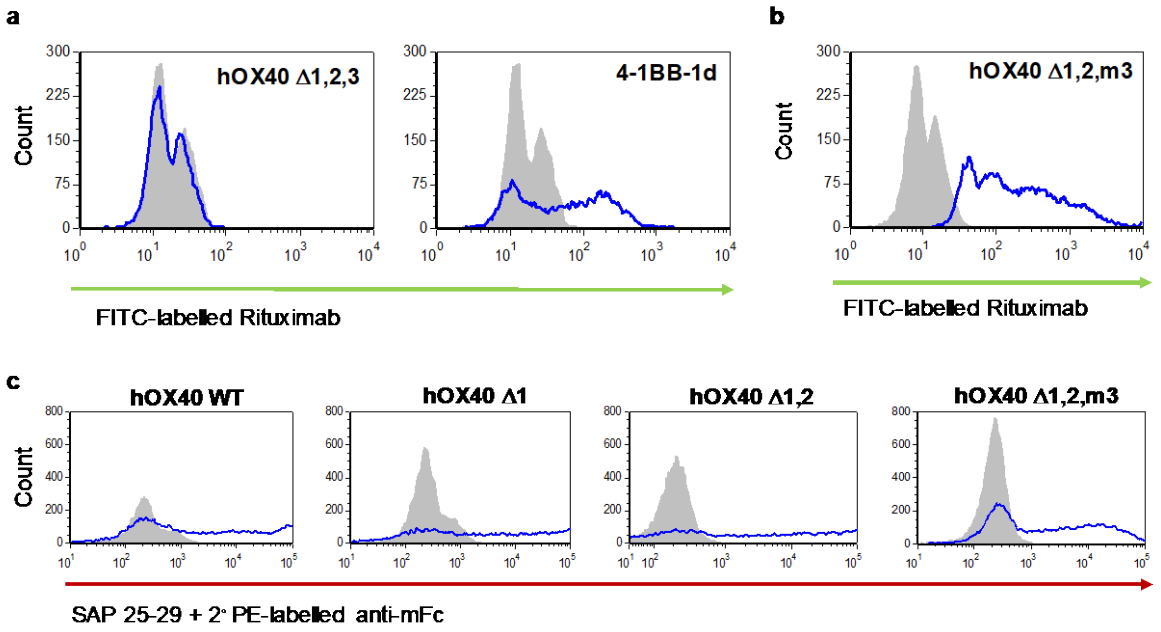

Figure 3.17 Expression of WT and mutant hOX40 constructs in 293F cells

Domain constructs were transfected into 293F cells via a cationic based lipid transfection and analysis of receptor expression was assessed 24 hours later using flow cytometry. Grey histograms represent binding of an irrelevant mAb, blue histograms represent expression of respective constructs. a) hOX40 Δ1,2,3 and 4-1BB-1d expression was detected via FITC-labelled rituximab binding to a CD20 epitope. b) Δ1,2,m3 expression was detected as described in a). c) Analysis of WT and all mutant domain constructs using SAP 25-29 and a secondary PE labelled anti-mFc to show equivalent binding.

Once the surface expression of all four constructs had been verified, the binding domains of the panel of anti-hOX40 mAb were determined and detected via flow cytometry. In these experiments unlabelled anti-hOX40 was added to the cells followed by the addition of a phycoerythrin (PE) conjugated anti-mouse F(ab')$_2$ fragment. Fluorescence detected in the FL-2 channel indicated binding which was compared to an isotype control (anti-4-1BB mAb) (Figure 3.18). Furthermore, determination of mAb binding to untransfected controls ruled out any non-specific binding of the mAb to anything other than the transfected OX40 constructs (Figure 3.18 Measuring anti-hOX40 mAb binding to 293F cells transfected with WT, Δ1 and Δ1,2, Δ1,2,m3 hOX40 constructs

The results show the ability of the mAb panel, collectively, to bind over all four CRDs of hOX40. SAP 28-2 was the only mAb binding to the N-terminal CRD1 domain, SAP 28-3 and SAP 15-3 bound CRD2, SAP 9 was the only mAb able to bind the partial CRD3 domain with the remaining mAb, SAP 25-29, SAP 29-23 and

SAP 29-50 all binding to CRD4 (Figure 3.18). This is further demonstrated in Figure 3.18 which shows the geometric mean of the PE fluorescence detected within the whole population. As expected, isotype switching of the mAb had no effect on binding domain (Figure 3.18 and Figure 3.19). Some residual binding was noted on a number of the constructs with varying mAb, however at much lower levels than mAb showing full binding and not consistently. In this particular experiment it was witnessed with mIgG2a mAb, however, in a repeat experiment mIgG1 mAb showed the residual binding and in another it was a mixture of both isotypes (data not shown). The underlying reasons for this variability is not clear.

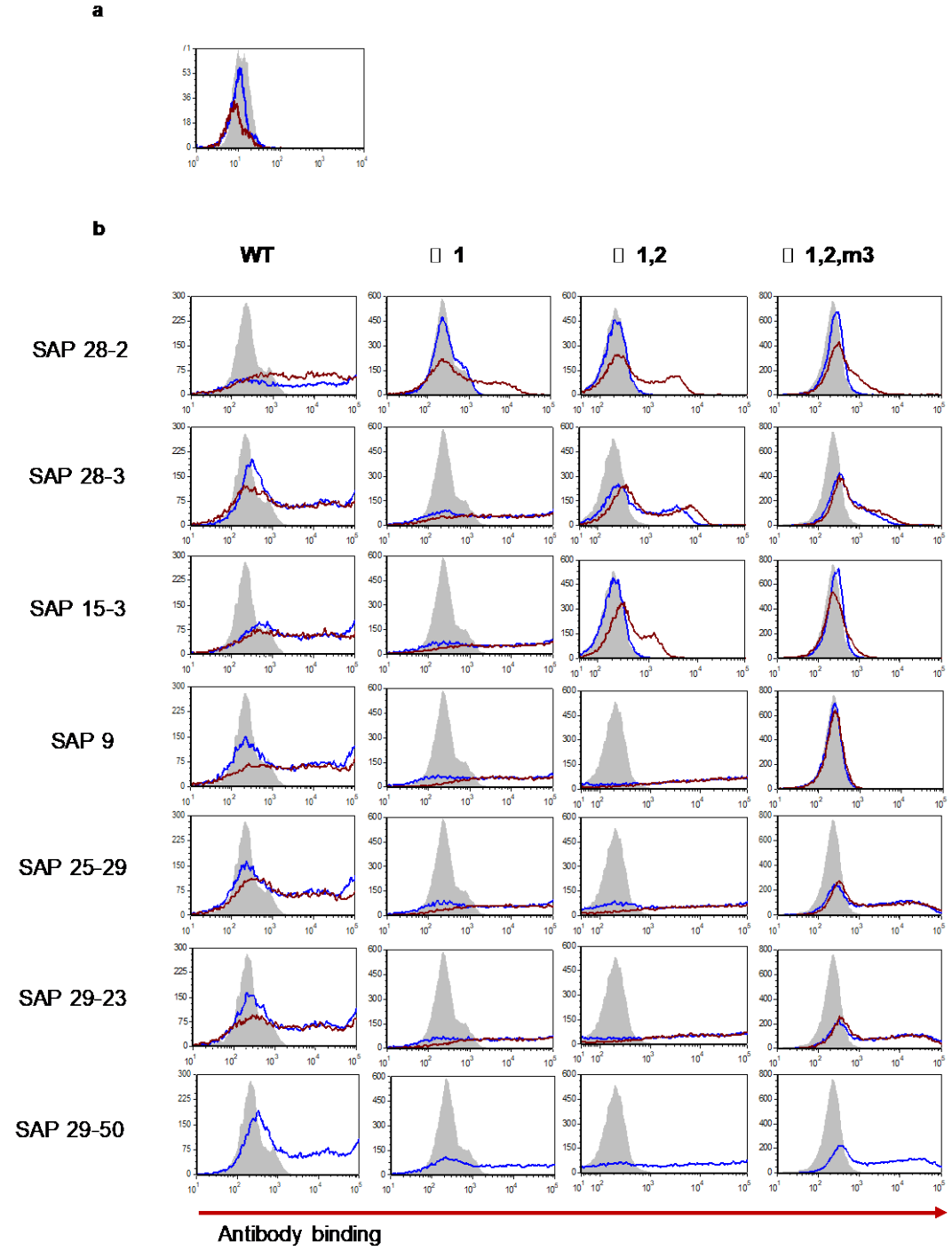

Figure 3.18 Measuring anti-hOX40 mAb binding to 293F cells transfected with WT, Δ1 and Δ1,2, Δ1,2,m3 hOX40 constructs

293F cells were transfected with either the WT, Δ1 or Δ1,2, Δ1,2,m3 constructs for 24 hours prior to analysis. Anti-hOX40 antibodies were added to 100μl of cells at a final concentration of 10μg/ml for 15 minutes at room temperature before washing and detection with a secondary PE-labelled anti-mouse F(ab')$_2$ fragment. a) Representative histogram of mIgG1 (blue) and mIgG2a (red) binding, detected by the seconardy PE mAb, on untransfected controls compared to an isotype control (grey shaded). b) Histograms demonstrate the binding of anti-hOX40 mAb to hOX40 compared to an isotype control (anti-4-1BB mIgG1/mIgG2a). Histograms show each SAP antibody from top to bottom; SAP 28-2, SAP 28-3, SAP 15-3, SAP 9 , SAP 25-29, SAP 29-23 and SAP 29-50 binding to either WT, Δ1, Δ1,2, Δ1,2,m3 hOX40 constructs, in order left to right. Data is representative of three independent experiments which all showed the same results.

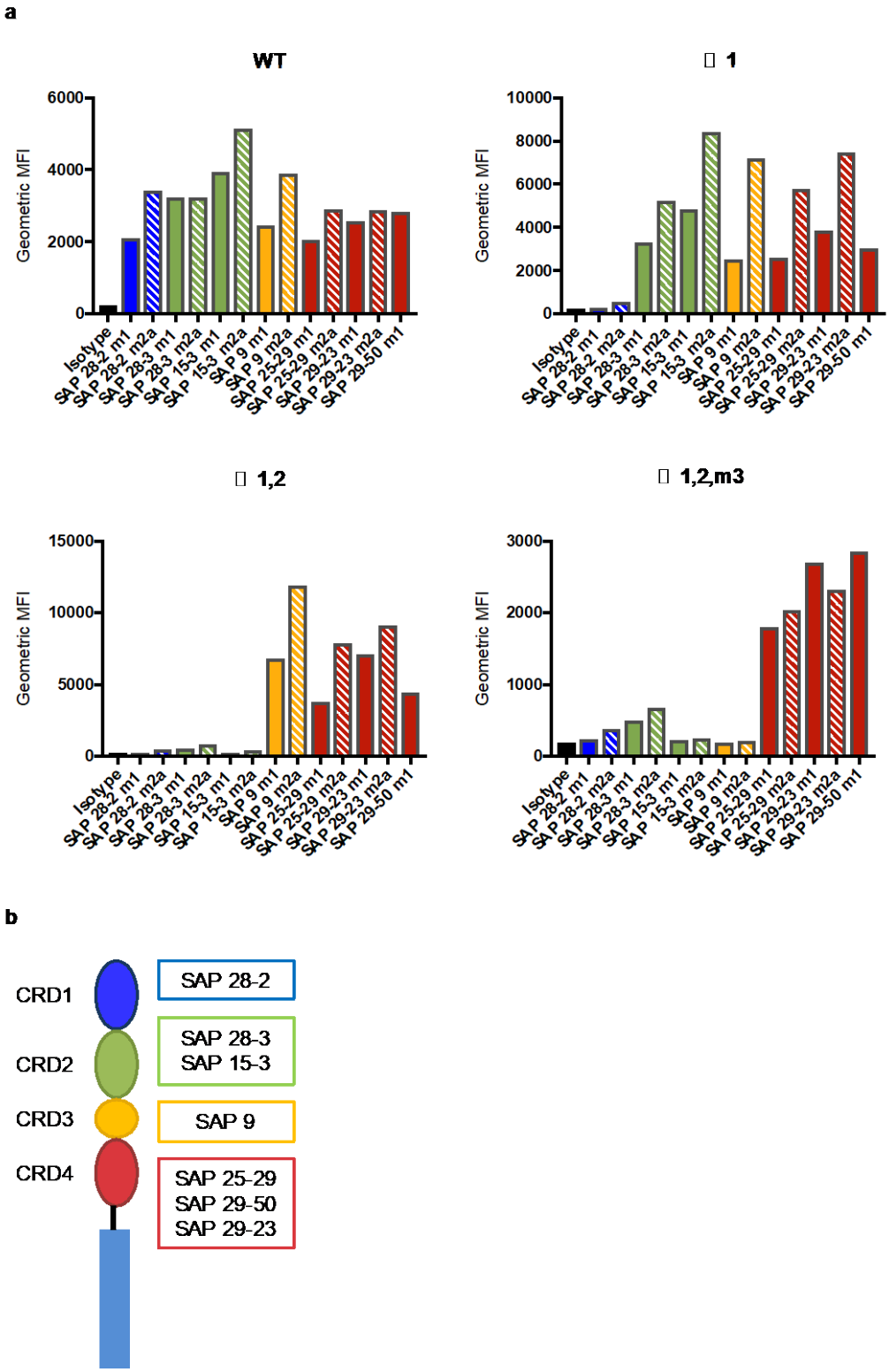

Figure 3.19 Determination of anti-hOX40 mAb domain binding categories

Geometric means of the PE fluorescence from the whole cell population, positive and negative, obtained from data in Figure 3.18 represented as bar charts. Each SAP mAb is shown as a mIgG1 (block colour) next the mIgG2a (dashed lines) isotype from left to right; SAP 28-2, SAP 28-3, SAP15-3, SAP 9 , SAP 25-29, SAP 29-23 and SAP 29-50 binding to either WT, Δ1, Δ1,2, Δ1,2,m3 hOX40 constructs. b) Schematic of hOX40 ECD and hOX40 mAb categorised into CRD binding groups.

To help better define where these various mAb bound, we took advantage of published data reporting the location of OX40L binding [16]. From the crystal structure of the hOX40/OX40L complex it is known that the ligand uses CRDs 1,2 and 3 for binding [16]. By performing binding assays in the presence of OX40L it was postulated that this may be a second method to confirm the mAb binding domains. This information may also come in useful once looking at the functionality of these mAb; i.e. do they require ligand binding for agonism?

SPR was again utilised, this time using only the parental mAb, to determine the ability of the anti-hOX40 mAb to bind hOX40 in the presence of the ligand. hOX40L carrying a His-tag was captured using an anti-His antibody, followed by injection of hOX40-hFc and the anti-hOX40 mAb in two separate steps. The sensogram in Figure 3.20 demonstrates successful binding of hOX40L to the chip as well as the binding of hOX40 to its ligand as governed by an increase in response units (RU). Out of the seven anti-hOX40 mAb tested, only the antibodies binding to CRD4 gave an increase in response units indicating binding in the presence of hOX40L. The remaining mAb gave a baseline level reading indicating an inability to bind in the presence of the ligand. These results correlate with the binding data described previously in Figure 3.18 and Figure 3.19.

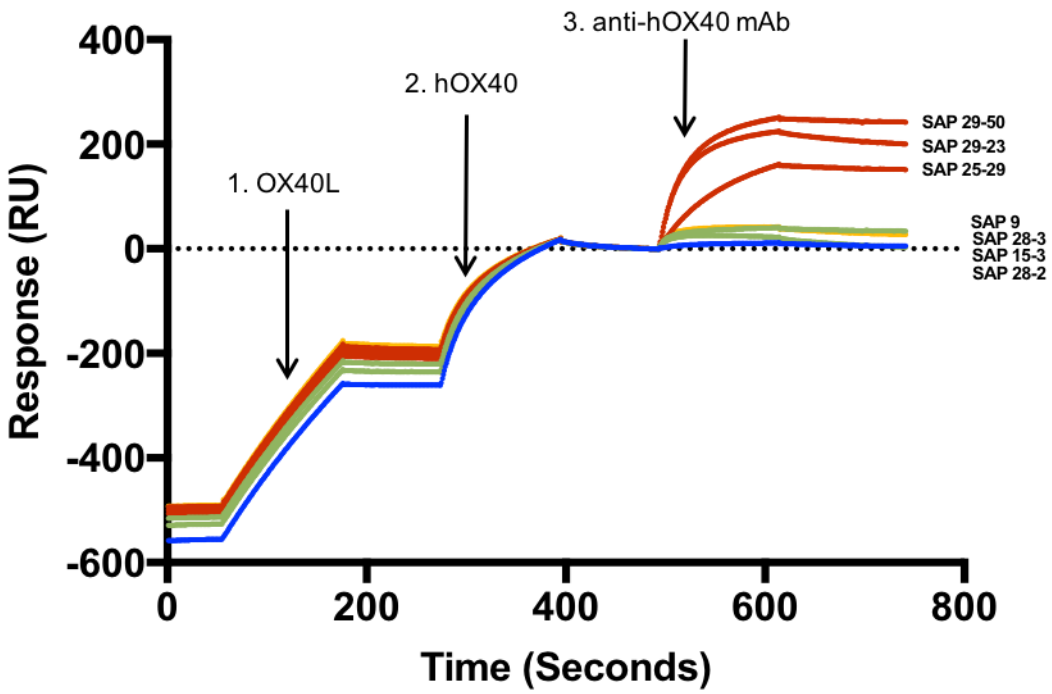

Figure 3.20 SPR analysis of anti-hOX40 mAb binding ability to hOX40 in the presence of hOX40L

Anti-His antibody was immobilised on a CM5 chip followed by capture of an hOX40L-His fusion protein. hOX40-hFc was then injected over the chip at 10μl/minute for 2 minutes followed by the sequential injection of an anti-human OX40 mAb, at the same flow rate. 10mM glycine (pH 1.5) was used for regeneration between antibodies, flow rate 30μl/minute for 1 minute. The sensogram firstly shows hOX40L binding, followed by hOX40 binding and lastly the anti-hOX40 mAb binding. Each line on the sensogram represents individual runs on the Biacore. Colours coordinate to domain binding of the mAb as determined previously; Blue = CRD1, Green = CRD2, Yellow = CRD3 and Red = CRD4.

To gain further understanding of the anti-hOX40 mAb binding domains an antibody cross-blocking experiment was conducted to identify if antibodies binding to the same domain were able to bind simultaneously or block one another giving insight into specific epitope binding. An antibody from each CRD binding domain was chosen for fluorescein isothiocyanate (FITC) conjugation; CRD1 = SAP 28-2, CRD2 = SAP 15-3, CRD3 = SAP 9 and CRD4 = SAP 29-50. 293F cells were transfected with WT hOX40 and the binding of mAb detected in the FL-1 channel. Following pre-exposure of the cells to an unlabelled anti-hOX40 antibody, the ability of the FITC-labelled anti-hOX40 mAb to bind hOX40 was compared with the binding of an isotype control (anti-4-1BB mAb).

As expected, all of the FITC-labelled anti-hOX40 mAb tested (SAP 28-2, SAP 15-3, SAP 9 and SAP 29-50) were cross-blocked by themselves, shown by a decrease in gMFI in comparison to the isotype control (Figure 3.21). SAP 15-3, a

CRD2 binding mAb, was also blocked from binding to hOX40 by the remaining CRD2 binder in the panel, SAP 28-3. Likewise, SAP 25-29 and SAP 29-23, which are both CRD4 binders, blocked the ability of SAP 29-50, also a CRD4 binder, to engage with hOX40. These blocking effects are summarized in Table 3.4.

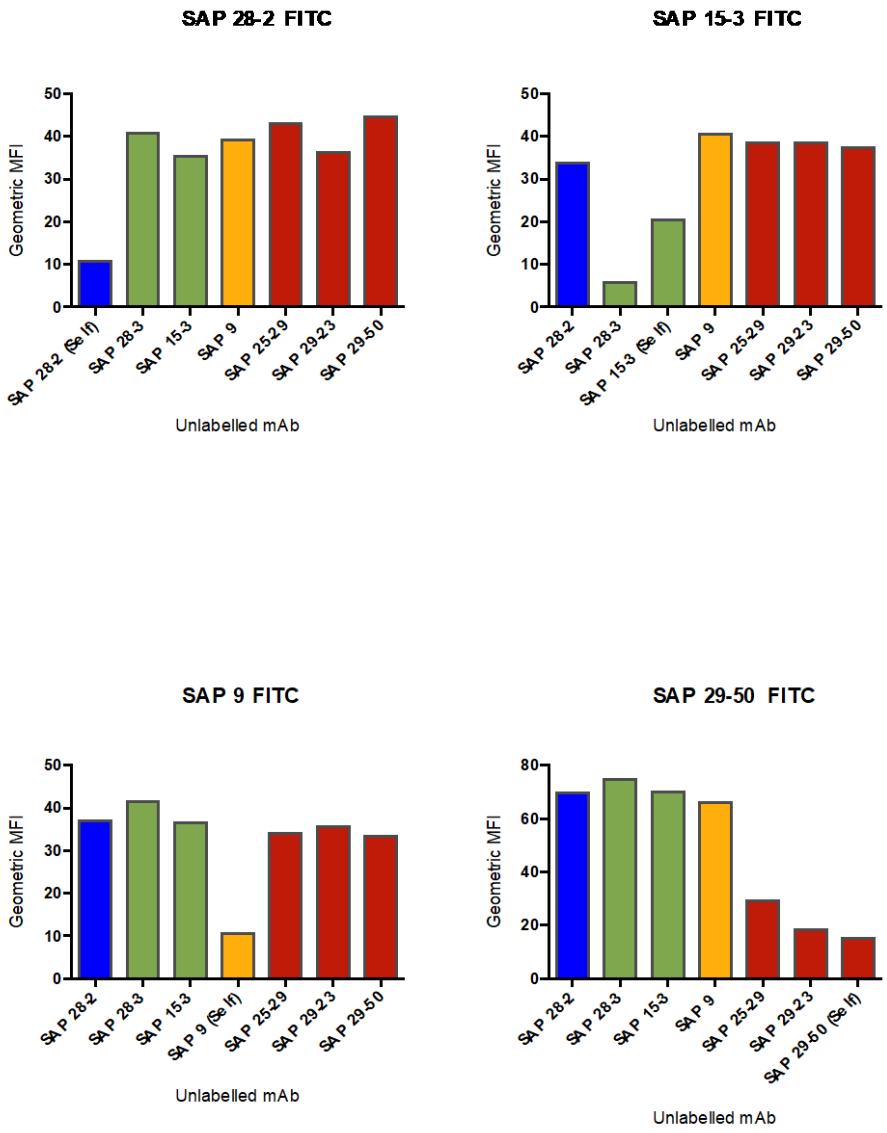

Figure 3.21 Cross blocking ability of the anti-hOX40 mAb

293F cells were transfected with WT hOX40 for 24 hours prior to analysis. 100μl of cells were incubated with unlabeled antibody at a concentration of 10μg/ml for 20 minutes at RT followed by the addition of FITC-labelled mAb at 5μg/ml. Binding of the secondary FITC labelled mAb was detected in the FL-1 channel on a FACSCalibur in comparison to a positive control (unlabelled isotype + FITC labelled mAb). Bar charts represent FITC geometric means (gMFI) of the whole cell population illustrating the ability of SAP 28-2, SAP 15-3, SAP 9 and SAP 29-50 to bind in the presence of themselves and the other anti-hOX40 mAb. Left to right; SAP 28-2, SAP 28-3, SAP 15-3, SAP 9, SAP 25-29, SAP 29-23, SAP 29-50.

		Competing IgG			
		SAP 28-2	SAP 15-3	SAP 9	SAP 29-50
Initial Binding IgG	Isotype	-	-	-	-
	SAP 28-2	x	-	-	-
	SAP 28-3	-	x	-	-
	SAP 15-3	-	x	-	-
	SAP 9	-	-	x	-
	SAP 25-29	-	-	-	x
	SAP 29-23	-	-	-	x
	SAP 29-50	-	-	-	x

Table 3.4 Cross blocking ability of the anti-hOX40 mAb

A table to summarise the blocking experiment above. 'X' indicates blocking of the FITC labelled mAb and '-'not blocked.

Having established the domain binding of each of the anti-hOX40 mAb the relationship with function was next assessed. To do this proliferation assays using human PBMCs were established.

3.7 Ability of anti-hOX40 antibodies to induce proliferation *in vitro*

To assess proliferation induction by anti-hOX40 mAb, human PBMCs were isolated from healthy donors, CFSE labelled and cultured at high density for 2 days prior to stimulation with sub-optimal plate bound anti-CD3 and the panel of anti-hOX40 mAb. After 5 days in culture, cells were harvested and proliferation determined by monitoring CFSE levels using flow cytometry. When a cell divides CFSE levels are diluted reducing the fluorescence seen. Therefore, the more dilution of the CFSE the greater the division/proliferation. This can be calculated by gating on the divided population seen in the isotype control compared the OX40 treated samples.

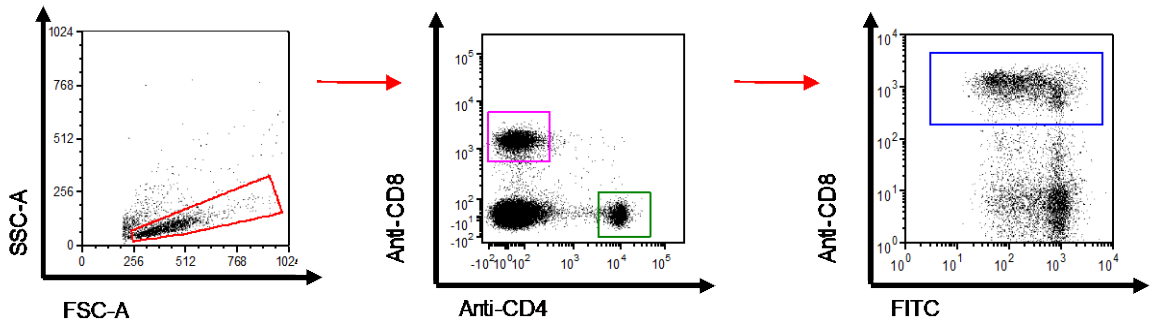

Figure 3.22 Gating strategy used in human PBMC proliferation assays

Human PBMCs were isolated, CFSE labelled and cultured at high density for 2 days prior to stimulation with 0.005μg/ml plate bound anti-CD3 (Clone: OKT3) and 5μg/ml anti-hOX40 mAb. Cells were harvested after 5 days in culture and FL-1 florescence observed using a flow cytometer. Dot plots show gating hierarchy; live lymphocytes, followed by CD4+ and CD8+ cells and lastly on FITC to monitor the division in each population.

In an initial assay comparing the panel of anti-hOX40 mAb as their parental isotypes, it was demonstrated by an increase in the percentage of proliferating cells, normalised to the irrelevant antibody, that SAP 28-2 (17.92%), SAP 28-3 (21.63%), SAP 15-3 (16.68%), SAP 25-29 (12.89%) and SAP 29-50 (16.35%) were able to act agonistically towards CD8+ lymphocytes (Figure 3.23). On the other hand, SAP 9 (-44.97%) and SAP 29-23 (-29.28%), normalised to the irrelevant antibody, caused a decrease in the proliferation of CD8+ lymphocytes. This was also demonstrated by the median CFSE fluorescence in the CD8+

population. SAP 9 and SAP 29-23 had a much higher CFSE median in comparison to the irrelevant indicating lack of division of the cells. In comparison, the other anti-hOX40 mAb showed a decrease in median CFSE fluorescence indicating dilution of the dye caused by cell division. It is important to highlight the difference in isotype between the mAb used within this assay; the five anti-hOX40 mAb causing an increase in proliferation were mIgG1s whereas SAP 9 and SAP 29-23 were mIgG2as. To determine if this difference in isotype ability to cause CD8+ proliferation was true for all mAb, the same experiment was carried out with the panel of mAb as both mIgG1 and mIgG2a isotypes. Figure 3.24 demonstrates that all mAb in our panel as mIgG1 were able to cause an increase in the proliferation of CD8+ and CD4+ cells above an irrelevant isotype control. Conversely, all mIgG2a versions of the mAb reduced the percentage of proliferating cells to levels below the irrelevant isotype control as seen in the initial assay (Figure 3.23 vs Figure 3.24)

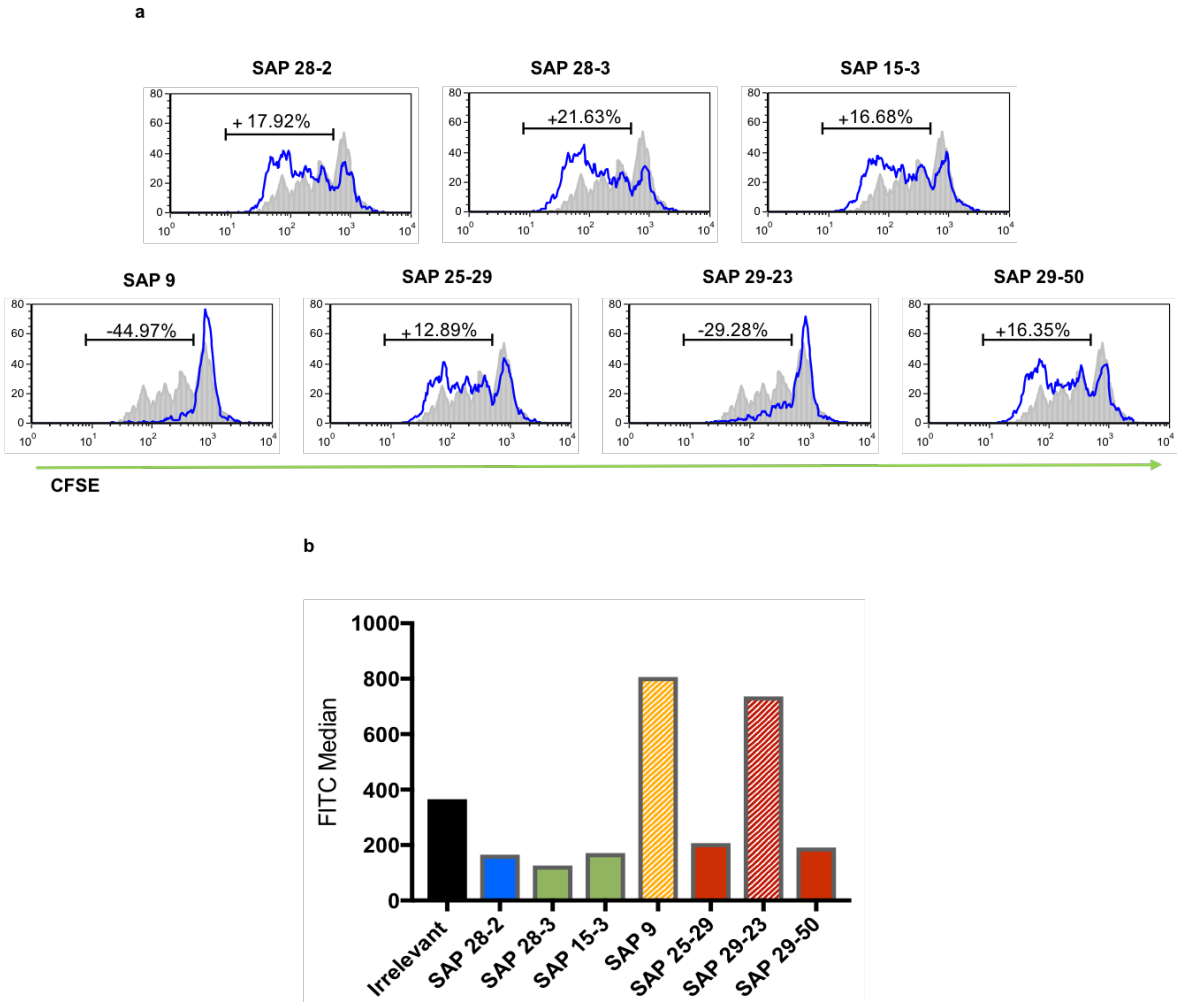

Figure 3.23 Proliferation of human PBMCs after stimulation with anti-CD3 and anti-hOX40 mAb

Human PBMCs were isolated, CFSE labelled and cultured at high density for 2 days prior to stimulation with 0.005μg/ml platebound anti-CD3 (Clone: OKT3) and 5μg/ml anti-hOX40 mAb. Cells were harvested after 5 days in culture and FL-1 florescence observed using a flow cytometer. a) Histograms show the ability of the anti-hOX40 mAb to cause proliferation (blue line) in comparison to an irrelevant antibody (grey) (Anti-saporin:DB7/12) c) Bar chart illustrating the median CFSE fluorescence in CD8+ cells. mIgG1 mAb are represented by block colour and mIgG2a mAb by diagonal lines. Data is from one individual experiment.

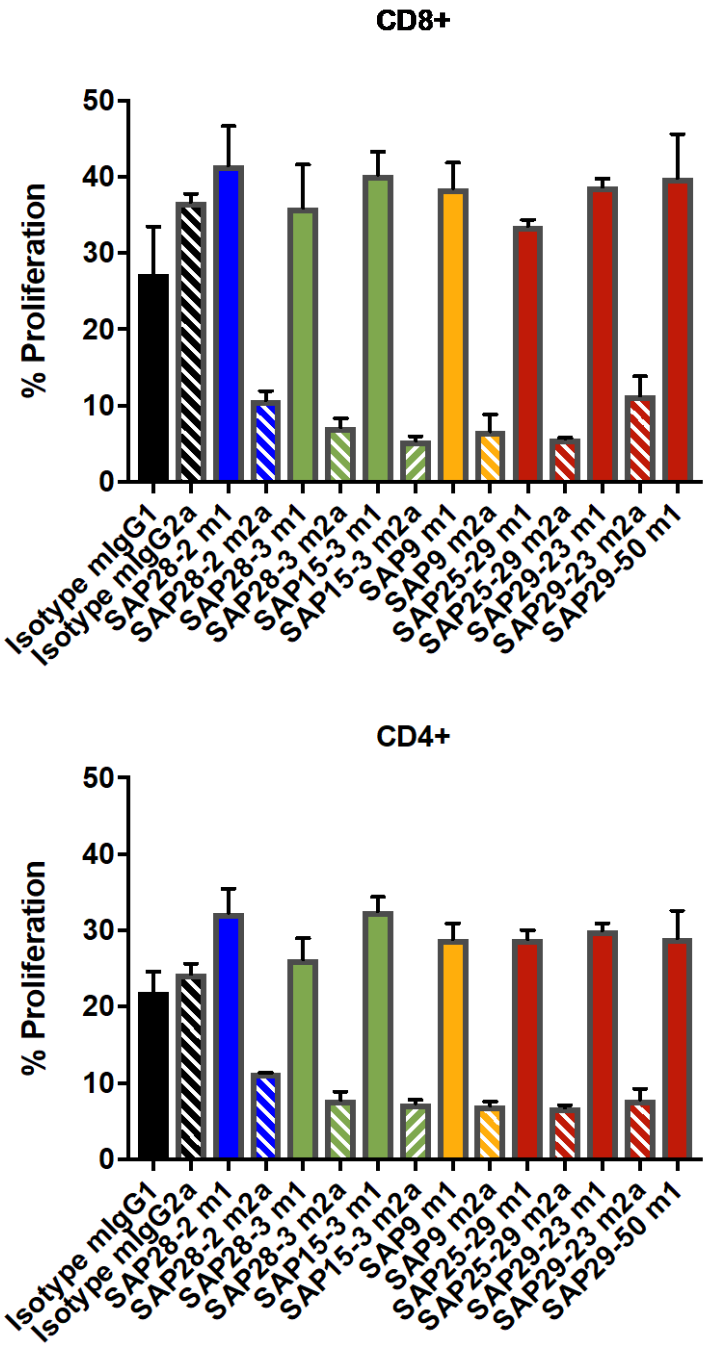

Figure 3.24 Comparison of human PBMC proliferation after stimulation with anti-CD3 and either a mIgG1 or mIgG2a anti-hOX40 mAb

Human PBMCs were isolated, CFSE labelled and cultured at high density for 2 days prior to stimulation with 0.005μg/ml platebound anti-CD3 (Clone: OKT3) and 5μg/ml anti-hOX40 mAb. Cells were harvested after 5 days in culture and FL-1 florescence observed using a flow cytometer. Bar charts illustrate the percentage of proliferation in the CD8+ population (top) and CD4+ population (bottom). mIgG1 mAb are represented by block colour and mIgG2a mAb by diagonal lines. Data is representative of two independent experiments showing similar results. Error bars represent mean±SEM of triplicate technical repeats.

3.8 Ability of anti-hOX40 mAb to signal via the NF-κB pathway *in vitro*

To determine if the proliferation ability of the anti-hOX40 mAb were linked to signalling strength evoked, an NF-κB reporter cell line was utilised. It has been identified that OX40 is capable of signalling via a number of downstream pathways, the most studied one being NF-κB [211, 238]. An NF-κB/Jurkat/GFP reporter cell line was therefore purchased and transfected with a hOX40ECD-CD40tail construct. Within this system Nf-κB transcription factor response elements sit upstream of a promoter controlling GFP expression, upon Nf-κB pathway activation the promoter is activated resulting in GFP fluorescence. The hOX40ECD-CD40tail construct was used as the CD40 intracellular domain had previously shown detectable signalling within experiments performed within the lab (X Yu, unpublished observations). Before we were able to perform the desired experiments a number of optimisation steps needed to be carried out.

Firstly, it was determined if the cells required CD3 stimulation (Clone:OKT3) to allow for signalling through OX40. Figure 3.24 clearly demonstrates that the cells do not require CD3 stimulation alongside anti-hOX40 mAb to produce a positive signal 24 hours post stimulation. The number of cells signalling (% +ve) was the same with and without OKT3 addition for all of the mAb tested (Figure 3.25). Likewise, the strength of the signalling within the positive cells (GFP gMFI) was the same for each mAb regardless of the presence of OKT3 (Figure 3.26). This result was also seen at 6 hours and 48 hours post addition of mAb (Figure 3.26).

a

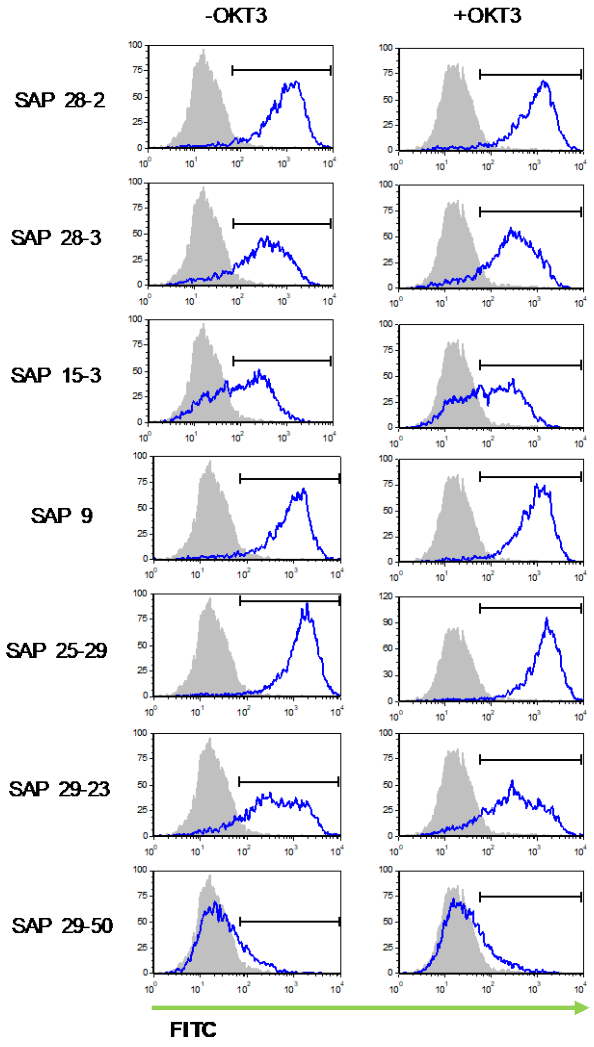

b

mAb	% +ve (–OKT3)	% +ve (+OKT3)
SAP 28-2	93.01	90.59
SAP 28-3	79.71	79.06
SAP 15-3	50.98	47.23
SAP 9	93.47	94.54
SAP 25-29	96.82	96.49
SAP 29-23	79.61	77.33
SAP 29-50	12.15	12.95

Figure 3.25 Signalling detection in NF-κB/Jurkat/GFP cells after anti-hOX40 -/+ anti-CD3 stimulation

Flat bottomed 96 well plates were coated overnight with anti-CD3 (Clone:OKT3) at 0.125μg/ml. 1x10^5 NF-κB/Jurkat/GFP cells were added per well followed by addition of anti-hOX40 mAb at 5μg/ml. Cells were harvested and FL-1 fluorescence monitored at 6, 24 and 48 hours post stimulation. a) Histograms show FL-1 fluorescence, resulting from GFP production, indicative of Nf-κB signalling, of anti-hOX40 mAb (blue line) compared to an isotype control (grey shaded) with and without anti-CD3 stimulation at 24 hours b) Percentage of positive cells with and without OKT3 at 24 hours.

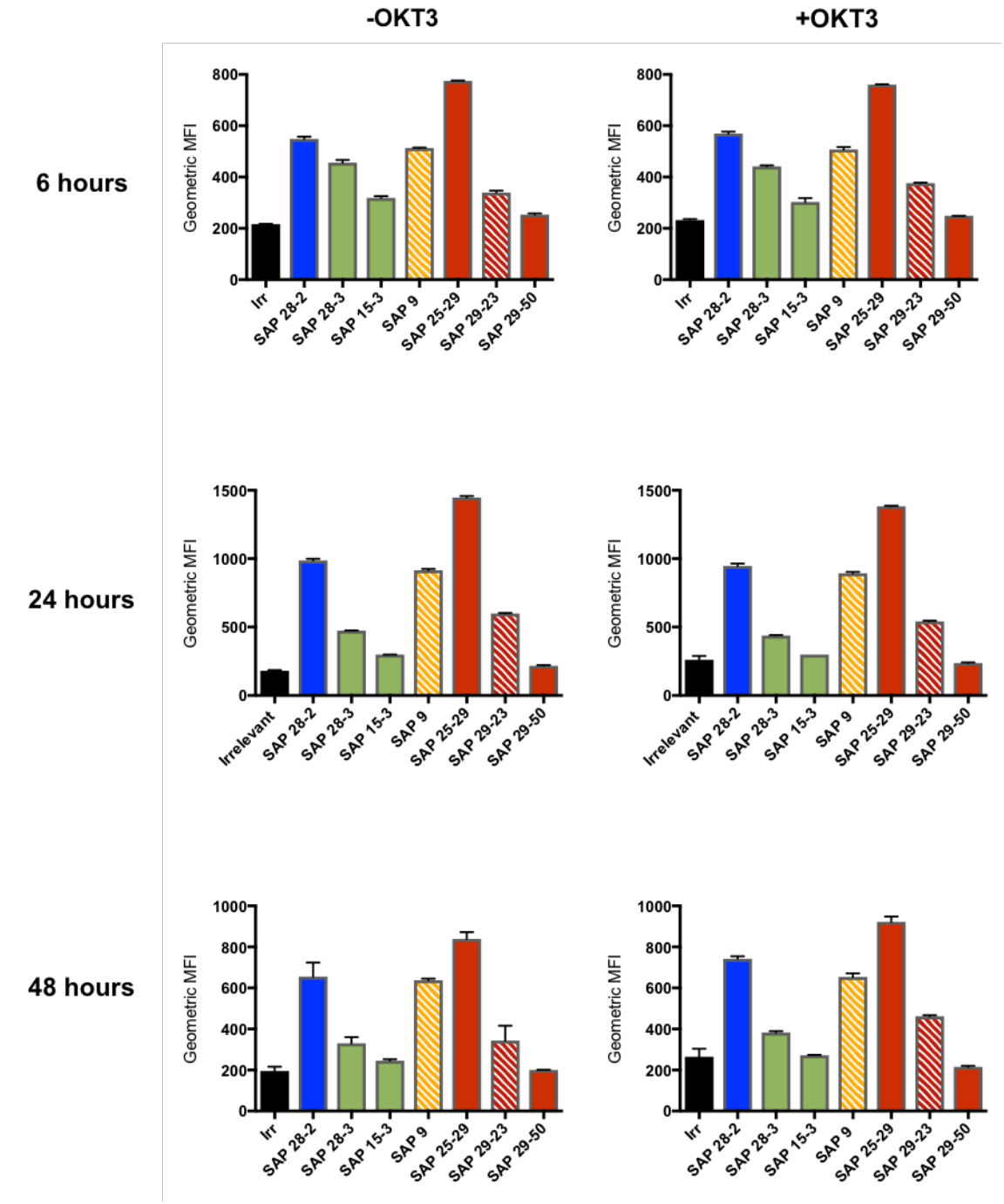

Figure 3.26 Signalling detection in NF-κB/Jurkat/GFP cells after anti-hOX40 +/- anti-CD3 stimulation at 6, 24 and 48 hours

Flat bottomed 96 well plates were coated overnight with anti-CD3 (Clone:OKT3) at 0.125μg/ml. $1x10^5$ NF-κB/Jurkat/GFP cells were added per well followed by addition of anti-hOX40 mAb at 5μg/ml. Cells were harvested and FL-1 fluorescence monitored at 6, 24 and 48 hours post stimulation. Bar charts illustrate the geometric means (gMFI) of the positive population of cells at 6, 24 and 48 hours (top to bottom), without and with OKT3 (L-R). Error bars indicate the mean with range of duplicate readings from one experiment. mIgG1 mAb are shown as block colours and mIgG2a mAb as dashed lines.

Secondly, the concentration of anti-hOX40 mAb needed to generate optimal signalling levels was optimised. To achieve this all mAb were subjected to a serial dilution in the range of 5μg/ml-0.0024μg/ml. Figure 3.27 demonstrates that the mAb differed in their ability to cause GFP fluorescence and hence signalling within the cells and this was affected by the concentration of mAb used. SAP 15-3 produced the highest gMFI amongst all the mAb and a concentration as low as 0.3125μg/ml could be used to elicit a signal above the irrelevant antibody (Figure 3.27). On the other hand, SAP 25-29 had the lowest gMFI and only at a concentration of 5μg/ml did it cause signalling above the irrelevant, however at much lower levels than SAP 15-3, as determined by GFP fluorescence (Figure 3.27). It was therefore decided to use 5μg/ml of anti-hOX40 mAb in subsequent experiments to allow detection of signalling with all mAb.

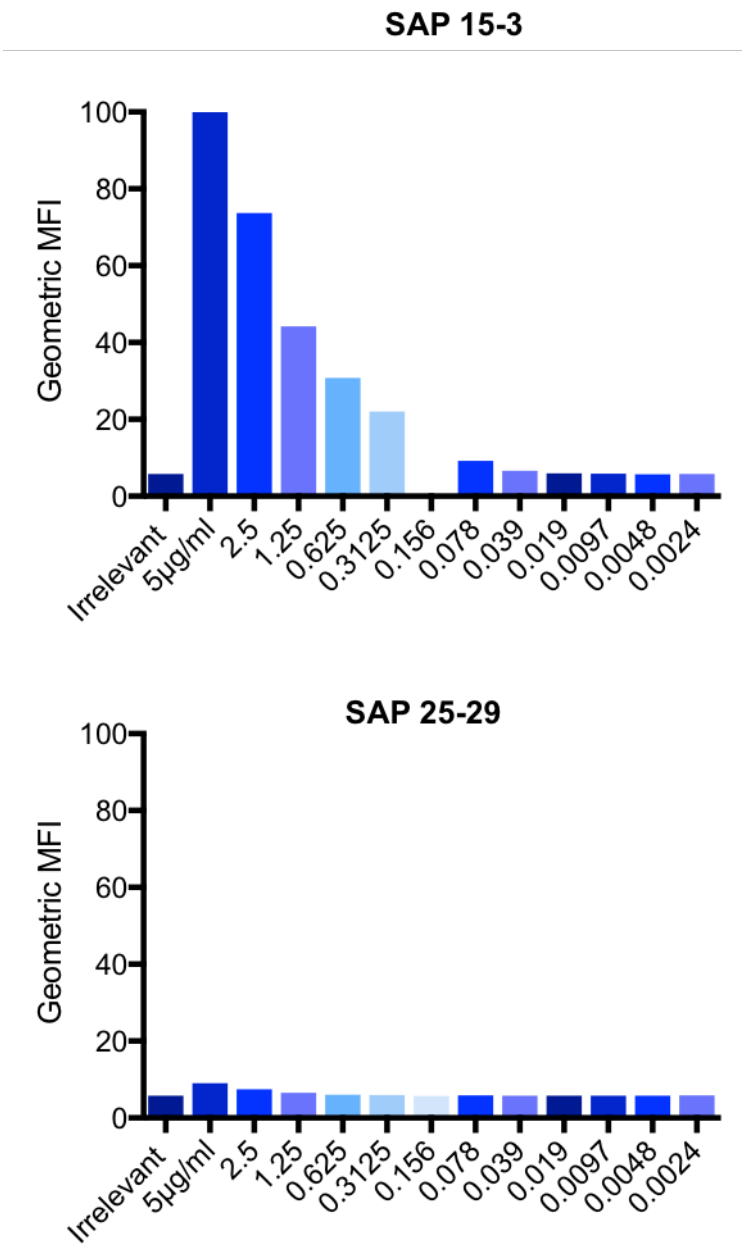

Figure 3.27 Serial dilution of anti-hOX40 mAb in NF-κB/GFP/Jurkat cell signalling assay

$1x10^5$ NF-κB/Jurkat/GFP cells were added per well into a flat bottomed 96 well plate. 5μg/ml of anti-hOX40 mAb was added to the top row and mAb were serially diluted down the plate. Cells were harvested at 6 hours post mAb addition and FL-1 fluorescence measured. Bar charts show the geometric mean of the whole cell population in comparison to a negative control antibody (Anti-4-1BB; SAP 1-2) from one experiment.

Lastly, the best time point to assess activity was determined. From the initial preliminary experiments, it was determined that GFP was induced as early as 6 hours post mAb addition which only increased marginally at 24 hours and was starting to decrease by 48 hours (Figure 3.26). As a result, GFP signal was assessed within the cells after stimulation with 5μg/ml anti-hOX40 mAb at 2, 4 and 6 hours. Two independent experiments showed the ability of the mAb to cause signalling as early as 2 hours post stimulation with increased GFP fluorescence over time (Figure 3.28).

Comparing the two experiments it was clear that the overall level of GFP induced was different as well as different mAb producing the strongest/weakest signals. For example, SAP 28-3 produced the strongest signal in experiment 1 and SAP 25-29 the weakest, conversely, SAP 15-3 produced the strongest signal in experiment 2 and SAP 25-29 was still the weakest.

It was apparent from these results that signalling strength did not necessarily marry with the mAb ability to cause proliferation. In the initial human PBMC proliferation assay using the panel of parental mAb SAP 28-3 caused the strongest proliferation out of the mIgG1 mAb and SAP 25-29 the weakest (Figure 3.23), which correlates with signalling strength in experiment 1 but not in experiment 2. Furthermore, in experiment 1 SAP 9 (mIgG2a) produced a higher GFP signal compared to most of the mAb however in the proliferation assay it caused a decrease below the isotype control like the other mIgG2a mAb. These results indicate that the mAb ability to cause proliferation of CD8+ cells in an *in vitro* assay are not correlated with Nf-κB signalling strength. This being said, however, the construct used had a CD40 intracellular tail which may not convey accurately the signalling which would be seen with an OX40 tail. Therefore these experiments need to be repeated with a full OX40 construct to determine if Nf-κB signalling influences the mAb ability to generate CD8+ proliferation.

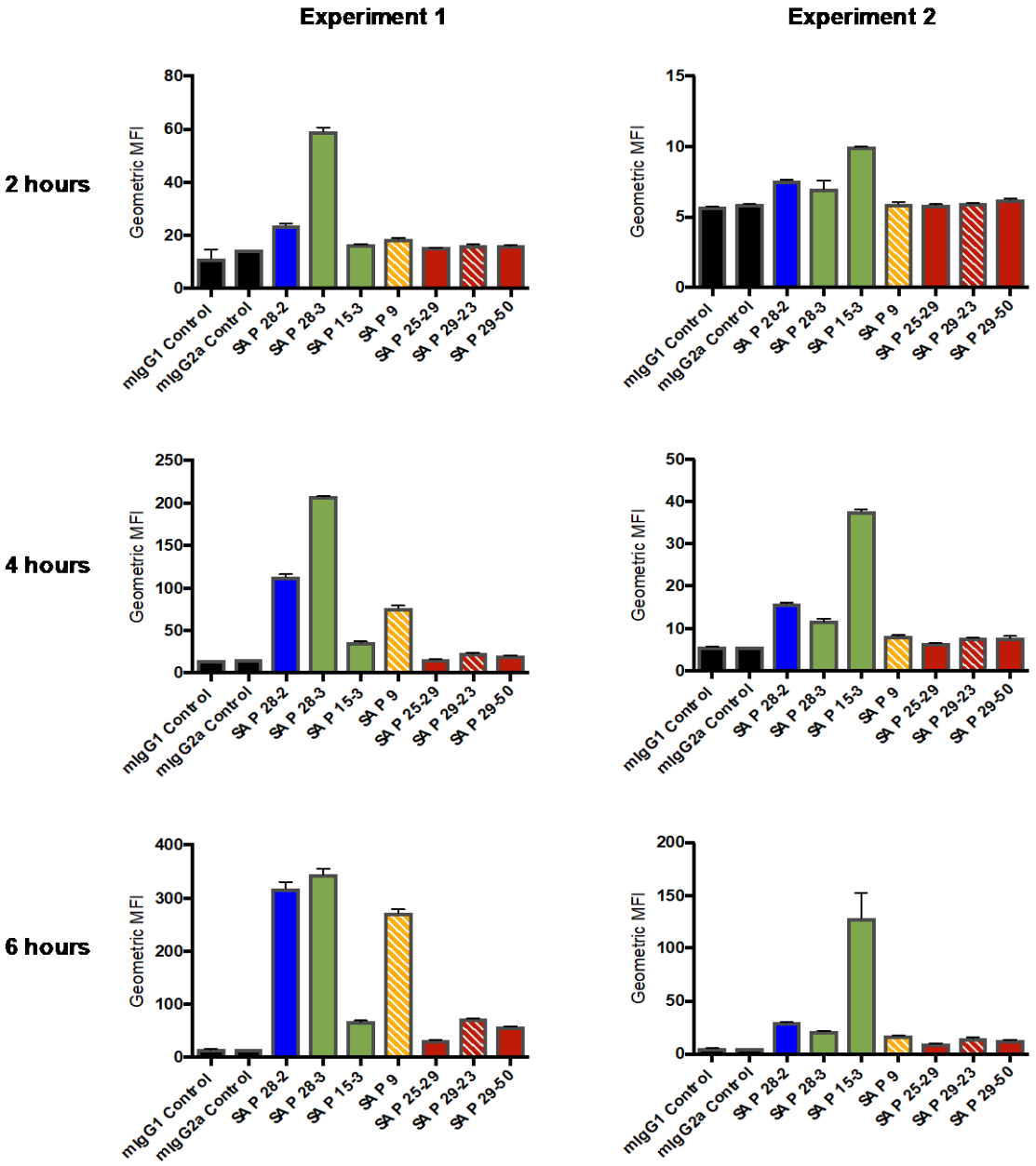

Figure 3.28 Kinetics of signalling detection at 2, 4 and 6 hours in NF-κB/GFP/Jurkat reporter cell line after anti-hOX40 stimulation

1x10^5 NF-κB/Jurkat/GFP cells were added per well into a flat bottomed 96 well plate. 5μg/ml of anti-hOX40 mAb was added to each well and GFP fluorescence measured in the FL-1 channel at 2, 4 and 6 hours post antibody addition. Bar charts illustrate the geometric mean (gMFI) GFP fluorescence of the whole cell population. Error bars indicate mean with range of duplicate wells containing the same sample. mIgG1 mAb are shown as block colours and mIgG2a mAb as dashed lines.

3.9 Chapter Discussion and future work

In this chapter a hOX40 KI mouse model was validated for the use of testing our panel of anti-hOX40 mAb *in vivo*. The panel of mAb were also characterised, initially this was done in terms of binding domain and antibody affinity followed by functional effects *in vitro*.

To enable investigation of the exact function of our panel of mAb in a therapeutically relevant system, a novel mouse model was developed where a chimeric hOX40 molecule was knocked into the mouse OX40 locus. A chimeric receptor was used instead of a fully human receptor to allow for physiological signalling within the mouse cell (mouse transmembrane and intracellular domain) as a result of anti-hOX40 mAb binding (human extracellular domain). To gain a better understanding of the mouse model, firstly expression profiles, of mouse and human OX40 were assessed at resting and activated states in the cells of the blood and spleen. OX40 expression was seen in a hierarchal fashion on T cell subsets, Tregs > CD4+ > CD8+, in both blood and spleen, with approximately half the expression of the human chimeric receptor observed in the $hOX40^{+/-}$ KI compared to $hOX40^{+/+}$ KI mice. Peak expression of the receptor was seen on day 1 after TCR activation in the CD4+ population and day 2 in the CD8+ population of T cells, within the range described in the literature [234]. Unfortunately, in some cases the Treg population was too small to obtain accurate expression data and so these experiments require repeating.

To determine the comparability of this model to human expression of OX40, human PBMCs from healthy donors were activated and expression assessed over 6 days. Human PBMCs showed the same hierarchal expression profile of OX40 as seen in the mouse and again the expression peaked between day 1 and day 2 post TCR activation. One thing to note is that the $hOX40^{+/+}$ KI mouse compared to a human shows an over-expression of the receptor when comparing levels on CD4 and CD8 T cells. Furthermore, the expression of hOX40 expression seen in both $hOX40^{+/-}$ KI and $hOX40^{+/+}$ KI mice within the Treg population is more like the expression seen in a mouse than in a human as it is constitutively expressed. This should be considered when interpreting results and when considering this KI model for immunotherapy experiments. It may therefore be wise to utilise the $hOX40^{+/+}$ KI mice for proof of concept experiments, and the $hOX40^{+/-}$ KI mice for

translational experiments, as although still slightly overexpressed, it appears closer to the human expression profile. Gaining this information on expression levels of hOX40 within the different genotypes of mice will allow the optimisation of our future experiments in terms of when to administer the anti-hOX40 mAb, as well as giving an indication as to whether expression levels influence the functional effects seen. To facilitate the interpretation of the *in vivo* studies, particularly in relation to the hOX40$^{+/-}$ KI mice, the ability of the anti-hOX40 mAb to bind the mouse receptor was determined; importantly none were shown to cross-react removing a possible complication in the interpretation of the data.

Before the study of our anti-hOX40 mAb *in vivo* their binding domains and affinities as well as their function *in vitro* in terms of proliferation and signalling was assessed. Proliferation assays using human PBMCs revealed that five of the parental mAb, SAP 28-2, SAP 28-3, SAP 15-3, SAP 25-29 and SAP 29-50 all possessed agonistic function towards the receptor. Conversely the remaining two antibodies, SAP 9 and SAP 29-23 acted in an antagonistic manner, reducing proliferation of hPBMCs. It is crucial to point out the difference in isotype between the antibodies, the 5 agonists were all mIgG1 and the 2 antagonists mIgG2a. It is well known that isotype influences affinity [330] and ability to bind FcγR [144] as well as influencing the activatory:inhibitory ratio (A:I) of an antibody which ultimately controls effector function [331, 332]. The differences between isotype of these anti-hOX40 mAb is explored in more detail in subsequent chapters within this thesis.

An interesting observation from the *in vitro* functional assay was that the mIgG2a antibodies were not just blocking proliferation of lymphocytes but were reducing proliferation to a level lower than the control, indicating a potential deleting ability. It has been observed in the literature that anti-hOX40 mAb might deliver at least some of their therapeutic effect by deletion of Tregs, causing a release of CD8 T cell mediated anti-tumour immunity [165].

Subsequently, the NF-κB signalling potential of these mAb was assessed using a GFP reporter cell line. Having established optimal conditions in terms of antibody concentrations and desirable time points, the antibody panel were examined. These experiments demonstrated no clear correlation between Nf-κB signalling potential and proliferative capability of the anti-hOX40 mAb. Having said this, both

the proliferation and signalling assays were only performed a number of times each, it would therefore be of benefit to repeat these experiments. Moreover, there are a number of potential caveats to these experiments that need to remembered; plate based assays are forced, artificial systems which may not depict what would happen *in vivo*. What these experiments did show us however, is that the signalling assay is functional when using our anti-hOX40 mAbs and it may potentially correlate with the mAb proliferation ability. It would therefore be of interest to perform this experiment with a construct that contains the OX40 tail in place of the CD40 tail as it may produce results more reflective of OX40 signalling.

SPR data classed all of the anti-hOX40 mAb being tested as high affinity (KD values $>10^{-9}$), regardless of isotype with the exception of SAP 28-2 mIgG2a. Rationale behind the large drop in affinity when this mAb was isotype switched from a mIgG1 to a mIgG2a is unclear. Further binding experiments, however, demonstrated that both isotype versions of this mAb were able to bind WT hOX40 on transiently transfected 293F cells to equal levels. Likewise, the parental mAb were tested on hOX40 KI cells from the mice and showed binding. Presumably therefore, the loss of binding reflects an artefact of the SPR experiment.

WT and domain mutant hOX40 constructs allowed identification of the specific binding domains of the anti-hOX40 mAb, in which again, isotype switching had no effect. These binding domains were also confirmed by a number of other experiments including SPR data, demonstrating the ability of the mAb to bind in the presence of the natural ligand, and antibody cross blocking experiments. SPR analysis of mAb and ligand binding demonstrated that only mAb binding to CRD4, a domain which the ligand does not occupy, could bind in conjunction with the ligand. Likewise, cross blocking experiments revealed that mAb binding the same domain could not bind simultaneously. There could be a number of reasons behind this. The difference in size between a mAb and the extracellular region of a TNFR is significant; 150kDa for an antibody compared to ~20kDa for the TNFR ECD. Figure 3.28 demonstrates the size of hCD40 (TNFRSF5) in complex with an antibody Fab fragment. Therefore, if one mAb is already bound to a specific domain it can be speculated that there is simply no room for a second mAb to bind to the same domain. Alternatively, if mAb share a similar/same binding epitope, as has been witnessed with CD20 mAb [333], it makes sense that two would not be able to occupy the same site at the same time. This rationale holds true for

explaining the ligand binding results also; if the ligand is occupying CRDs 1-3 it is reasonable to assume that it blocks/occupies binding sites or alters the structure of hOX40 in a way that inhibits mAb binding to these same domains. To definitively demonstrate this either structural data, identifying the contacting residues between mAb and ECD, or exhaustive mutational data (such as through alanine scanning mutagenesis) would be required.

The next chapter describes our attempts at creating crystals of hOX40 in complex with Fab fragments from the anti-hOX40 mAb, specifically those which bind CRDs 3 and 4. Obtaining crystal structures of these complexes would enable us to distinguish exact binding epitopes of the mAb and gain a better understanding of the steric changes that are potentially causing any functional difference in efficacy as described above.

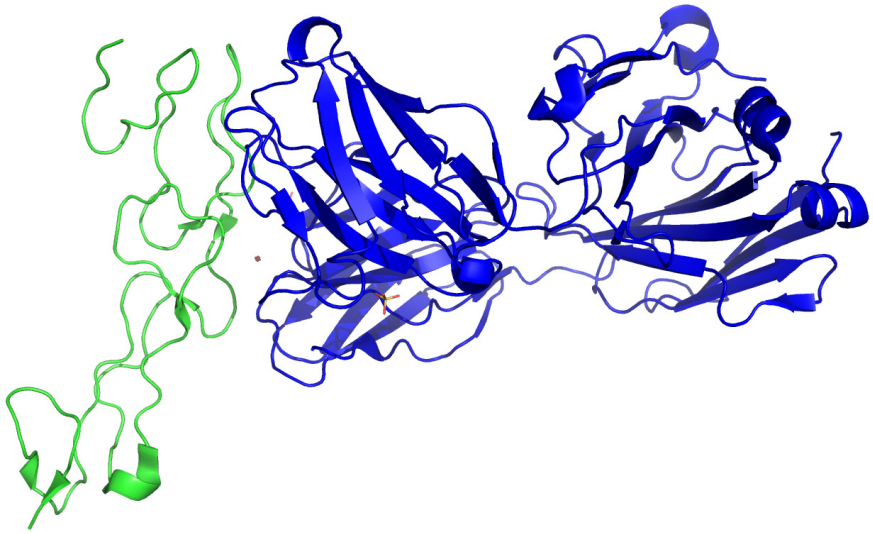

Figure 3.29 To-scale size of the crystal structure of a TNFR (CD40) ECD and Fab fragment of an antibody.

PDB file 5DMI was altered in Pymol to change the colour and structural representation of the complex. The CD40 ECD (green) and Fab fragment (blue) are rendered as ribbons.

Chapter 4 Generation of hOX40-Fab complexes to determine their crystal structure

4.1 Introduction

In the previous chapter the anti-hOX40 mAb were characterised in terms of their binding properties, affinities and function *in vitro*. A number of differences were observed between our panel of mAb and this included binding domains, affinity for the receptor and agonistic activity. To gain further insight into the reasons behind the diversity seen amongst the mAb it was of interest to determine their exact binding epitope and structural properties when in complex with hOX40.

It is well known that different mAb to the same target can elicit widely different activities, as evidenced, for example, by CD20 and CD40 targeting mAb [267, 334]. The specificity and affinity of a mAb towards a given epitope on a target antigen has been shown to influence the type and strength of effector function [329, 335]. For example, site-directed mutagenesis and epitope mapping have revealed differences in epitopes recognised by novel anti-CD20 and anti-CD40 antibodies and the resulting effector functions they possess [267, 335, 336]. Rituximab and ofatumumab, both type I anti-CD20 mAb, show differences in epitope binding correlating to strength of certain effector mechanisms such as CDC [335]. Furthermore, solving the crystal structure of a number of these antibodies in complex with the receptor revealed fundamental differences in their binding properties. Niederfellner et al. demonstrated that despite recognising an overlapping CD20 epitope type I and type II anti-CD20 antibodies, rituximab and GA101, bind in a different orientation to one another [337], which provides a potential molecular explanation to the differences in functional effects seen between type I and type II anti-CD20 antibodies. Likewise, Barr et al. have demonstrated with a panel of mouse anti-CD40 mAb that there is a strong correlation between specific binding site, relative to the natural ligand, CD154, and resultant activation signals delivered to B cells [328]. Interestingly this correlation was independent of isotype and affinity of the mAb. Yu et al. further demonstrated the importance of specific domain binding and the type of activity an anti-CD40 mAb elicits. They demonstrated that CRD1 binding mAb were strong agonists of

CD40 however, mAb binding epitopes closer to the membrane showed a decrease in agonistic activity [267]. Furthermore, those mAb binding CRDs 2-4 blocked CD40L and were potent antagonists. Collectively this evidence highlights the importance of determining specific epitope binding, as well as understanding ligand interaction, alongside other mAb characteristics such as affinities.

To date, these types of structure:function studies have yet to be performed amongst anti-hOX40 antibodies. From our panel of mAb comparing those which bound to CRD 3 or 4 were of particular interest. There were a number of reasons behind this; firstly, the difference in ability to bind in the presence of the ligand, secondly the differences in agonistic activity, and lastly the fact that CRD3 is only a partial domain. We therefore chose SAP 9 and SAP 29-50 as two potential candidate mAb for which to obtain crystal structures in complex with OX40; SAP 9 as it was our only CRD3 binding mAb, and SAP 29-50 as out of the CRD4 binding mAb we possessed the most material. Therefore, to determine the exact binding epitope and the structure of these mAb when in complex with hOX40 we bulk produced the extracellular domain of hOX40 as well as generating Fab fragments of both SAP 9 and SAP 29-50. These individual components were then made into hOX40:Fab complexes and set up in crystallographic trials

4.2 Cloning of OX40 construct

The DNA for the extracellular domain (ECD) of hOX40, containing a 6xHis-tag at the C-terminus, had previously been amplified by PCR (by Dr C.Chan). In order to confirm the identify of the insert, Zero Blunt TOPO PCR Cloning Kit (Figure 4.1) was used to create clones from the blunt end PCR products. As initial assessment of whether the ligation was successful, DNA was amplified in TOP 10 chemically competent *E.coli* cells and the resulting bacteria streaked onto an agar plate to allow selection of single colonies. Eight colonies were chosen from the agar plate, expanded, and the DNA isolated using a QIAprep miniprep kit. The plasmid DNA then underwent a restriction digest with EcoR1 followed by agarose gel electrophoresis to determine the size of the insert.

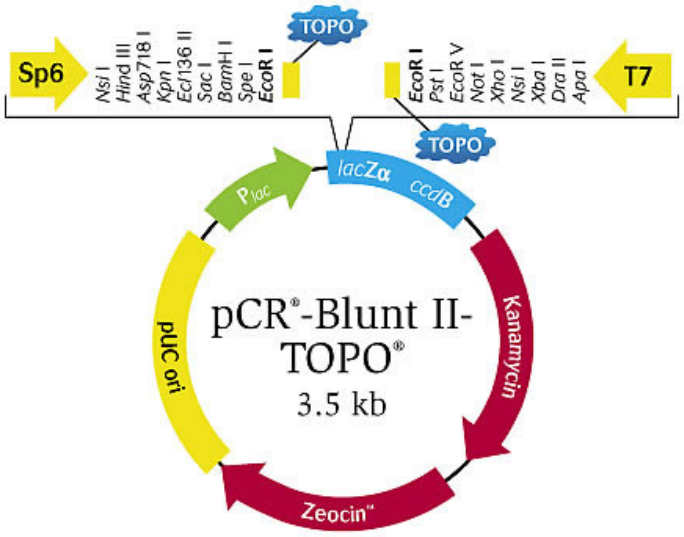

Figure 4.1 pCR-Blunt II-TOPO cloning vector map

Annotated vector map of the TOPO vector used for diagnostic steps in gene cloning. The vector contains T7 and Sp6 primers for DNA sequencing alongside two EcoRI sites which flank the cloning region. The toxic ccdB gene was used for positive selection, presence of an insert disrupts the gene and allows cell survival. The map was obtained from Thermo Fisher Scientific [338].

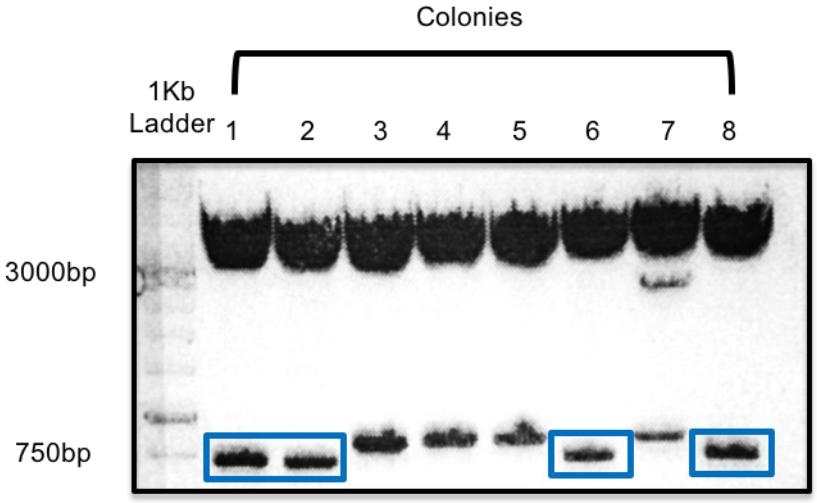

Figure 4.2 EcoRI digest of Top10 colonies transformed with human OX40 extracellular domain ligated into a TOPO-Blunt vector

hOX40 extracellular domain was ligated into a TOPO-Blunt vector. Ligated plasmids were transformed into Top10 cells followed by isolation using the Qiagen miniprep kit. Isolated plasmids were digested with EcoRI and the resulting products separated by gel electrophoresis on a 0.7% agarose gel stained with GelRed for DNA visualisation. The boxed bands represent the correct size gene insert that corresponds to hOX40 extracellular domain.

Figure 4.2 contains the diagnostic gel for the plasmid isolated from the transformed TOP 10 *E.coli*. All eight colonies showed a band at ~3500bp which corresponds to the size of the TOPO vector whilst wells 1, 2, 6 and 8, showed a band ~750bp which corresponds to the hOX40 ECD gene insert. In order to determine which insert was correct, conventional DNA sequencing (short chain termination method using BigDye terminatior v3.1) was performed and analysed (by Dr C.Chan) revealing that the insert in colony 1 matched the sequence for the hOX40 ECD. Following this the DNA from colony 1 was ligated into an expression vector, pcDNA3. In order to sub-clone the construct into the expression vector restriction digests were performed on the empty pcDNA3 vector, using restriction enzymes EcoRI and HindIII, and the TOPO vector, using EcoRI, containing the insert of interest. The digested products were run on a 0.7% agarose gel as before and the separated products excised followed by extraction of the DNA. A ligation reaction, mediated by T4 DNA ligase, was used to anneal the hOX40 ECD into the pcDNA3 expression vector. The resulting product was then used to transform chemically competent JM109 *E.coli* cells, and as before single colonies were selected from an agar plate, expanded and the DNA extracted. To confirm successful insertion of the DNA of interest into the expression vector a double

restriction digest using EcoRI and HindIII was performed followed by agarose gel electrophoresis. Figure 4.3 shows that that all six colonies that were selected contained clean, separate bands at molecular weights corresponding to the pcDNA3 vector (~3500bp) and hOX40 ECD (~750bp). Furthermore, DNA was excised from the gel followed by extraction using a maxiprep kit.

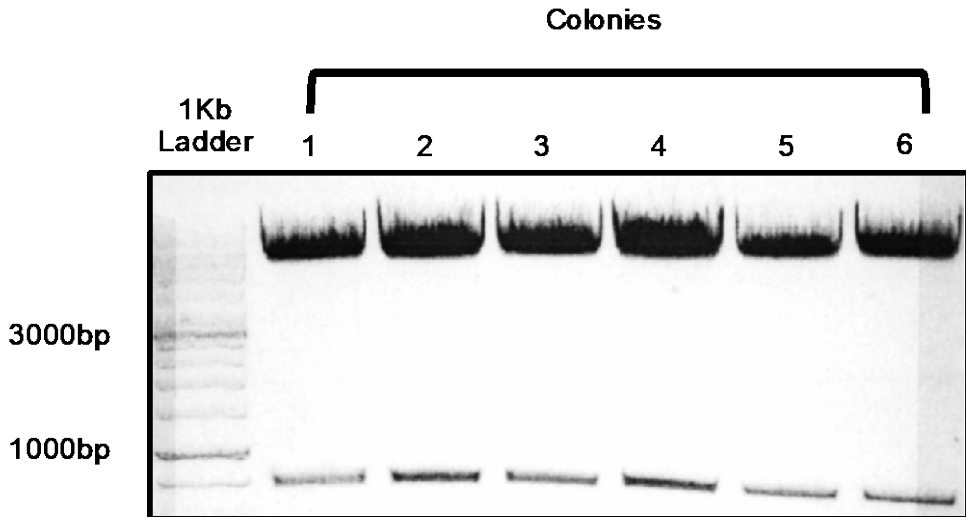

Figure 4.3 EcoRI and HindIII double digests of JM109 colonies transformed with human OX40 extracellular domain ligated into a pcDNA3 expression vector

hOX40 extracellular domain was ligated into a pcDNA3 expression vector. Ligated plasmids were transformed into JM109 cells followed by isolation using the Qiagen maxiprep kit. Isolated plasmids were digested with EcoRI and HindIII and the resulting products separated by gel electrophoresis on a 0.7% agarose gel stained with GelRed for DNA visualisation.

4.3 Protein expression in mammalian cells

Once the gene construct for the extracellular domain of hOX40 had been cloned protein expression was assessed. To achieve this, transient transfections into 293F cells were performed using 293Fectin, a cationic lipid transfection reagent. After a week, the hOX40-6His ECD was purified from 500ml of cell supernatant using immobilised metal affinity chromatography (IMAC) with a NTA-Ni^{2+} column.

The 6xHis-tag attached to the C-terminal of the hOX40 ECD construct allowed us to capture the protein using a Ni^{2+} column. Imidazole competes with the His-tag for interaction with the metal ion in the column therefore was used to elute the hOX40-6His ECD. A gradient approach to elution was decided upon (10-500mM) as some proteins will naturally have more than two histidines in a row allowing for binding to the column, the lower concentrations of imidazole will remove these contaminants so that the protein of interest elutes as a homogenous population.

Figure 4.4 shows the chromatogram from the purification of hOX40-6His ECD on a Ni^{2+} column. It is seen at concentrations of 10-40mM imidazole that contaminants are removed as a small amount of absorbance at 280nm is seen. However, although higher mAu values were detected when 250mM and 500mM of imidazole were used, these are values which you would expect of imidazole alone (imidazole at 500mM gives an mAu ~60-70). This result indicates a lack of hOX40 ECD presence, however it may also be due to lack of expression of the His-tag resulting in an inability to capture the protein of interest onto the column. To determine which of these explanations were correct SDS-PAGE and western blots were performed on fractions eluted from the column.

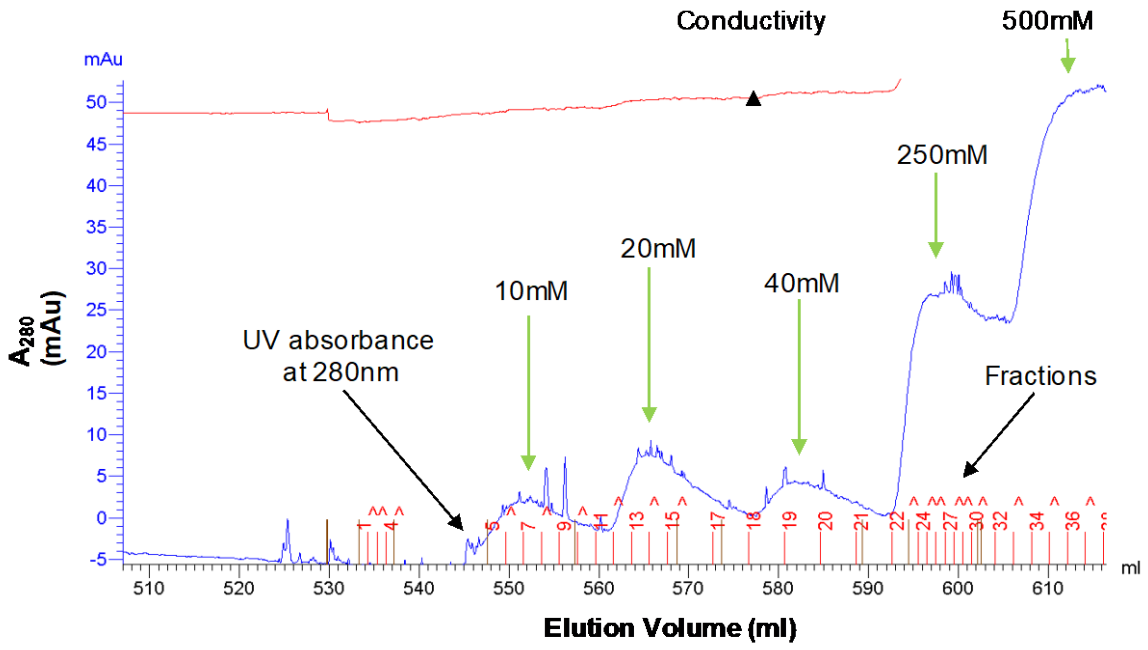

Figure 4.4 Immobilised metal affinity chromatography (IMAC) of hOX40-6His extracellular domain

hOX40-6His ECD transfected 293F cell supernatant were applied to a 1ml Ni^{2+} column. The protein was eluted with a gradient concentration of imidazole (10-500mM) indicated by the green arrows. 1ml fractions (red lines on x-axis) were collected at a flow rate of 3ml/min. The blue line represents UV absorbance at 280nm, indicative of protein. The red line represents conductivity in the sample, indicative of equilibration.

15µl samples were collected from fractions 7-36 and analysed using SDS-PAGE (Figure 4.5a). SDS-PAGE revealed a small amount of protein present at twice the expected molecular weight of hOX40 ECD (~40kDa). Western blot analysis, however, revealed that the 40kDa protein was in fact hOX40 (Figure 4.5b) with a His-tag present (Figure 4.5c). Given the low expression of hOX40 seen in transient transfections a stable cell line was created using Chinese ovarian hamster (CHO) cells. In a stable transfection the gene of interest is integrated into the genome resulting in passing on of the gene to the next generation as well as prolonged expression of the gene in comparison to a transient transfection. The transfected CHO cells were sub-cloned twice using a double dilution method across a 96 well plate to obtain a monoclonal cell population. Cells which were secreting the hOX40 ECD were selected using ELISA as a detection method. The pcDNA3 vector contains a geneticin antibiotic resistance gene which was used as a selective marker for transfected cells.

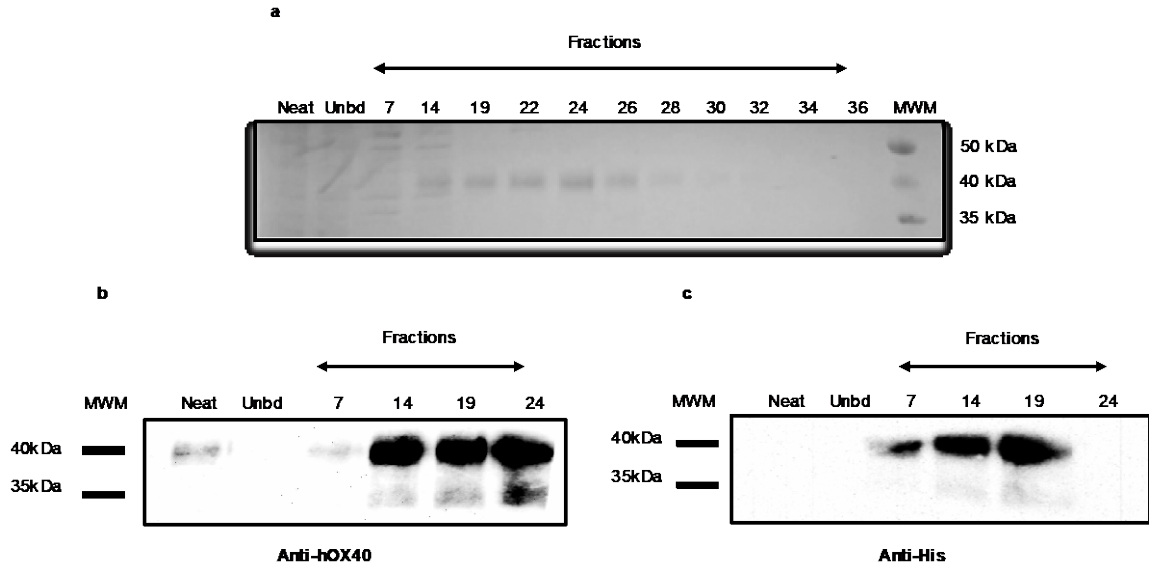

Figure 4.5 SDS-Page and western blot analysis of supernatant from a transient transfection of 293F cells with His-tagged hOX40 extracellular domain post IMAC

Fractions ranging from 7-36 were collected post IMAC (Figure 4.4) and hOX40-6His ECD presence and purity was analysed using SDS-Page and western blot.
a) 15µl of fractions in the range of 7-36 eluted from the Ni^{2+} column were loaded onto a 15% SDS gel alongside the 15µl of neat and unbound (Unbd) protein and 10µl of protein ladder (MWM). The gel was run at 150V for 1 ½ hours followed by imaging under white light. b) Fractions ranging from 7-24 were used for western blot. An SDS-Page gel was run as described above. The protein was then transferred onto a polyvinylidene fluoride (PVDF) membrane at 24V for 1 hour. The membrane was blocked with 5% (w/v) milk followed by probing with either an (1) anti-hOX40 mAb (SAP 29-50) detected using a goat anti-mouse HRP conjugated antibody or an (2) anti-His antibody (abcam;ab18184) detected using a goat anti-rabbit HRP antibody. The HRP antibodies were detected using ECL and the chemiluminescence measured using a coupled charged device (CCD).

CHO cells stably transfected with the hOX40-6His ECD that were positive secretors and originated from a single colony were expanded to produce a bulk culture. Cells were grown adherently for 2 months and the supernatant harvested weekly. A total volume of 700ml was collected and the same process of purification, as described above, using a Ni^{2+} column was performed (Figure 4.6a). Figure 4.6b shows an SDS-PAGE revealing a strong band at ~40kDa, as had been seen in the transient transfections, indicating hOX40 ECD presence, however another strong band was also witnessed at ~ 30kDa. To determine the identity of the bands a western blot was carried out checking for the presence of hOX40 ECD and the His-tag. Figure 4.6c shows that the ~40kDa band present is hOX40 however the ~30kDa band is a His rich protein separate to the hOX40 ECD. This result demonstrated that using a Ni^{2+} column as a method of purification for CHO cell supernatant was not suitable when a homogenous hOX40 population

is required, therefore an affinity column using an anti-hOX40 mAb was created. To produce the affinity column an anti-hOX40 mAb was coupled to CNBr activated sepharose beads and packed into a 10/300 column.

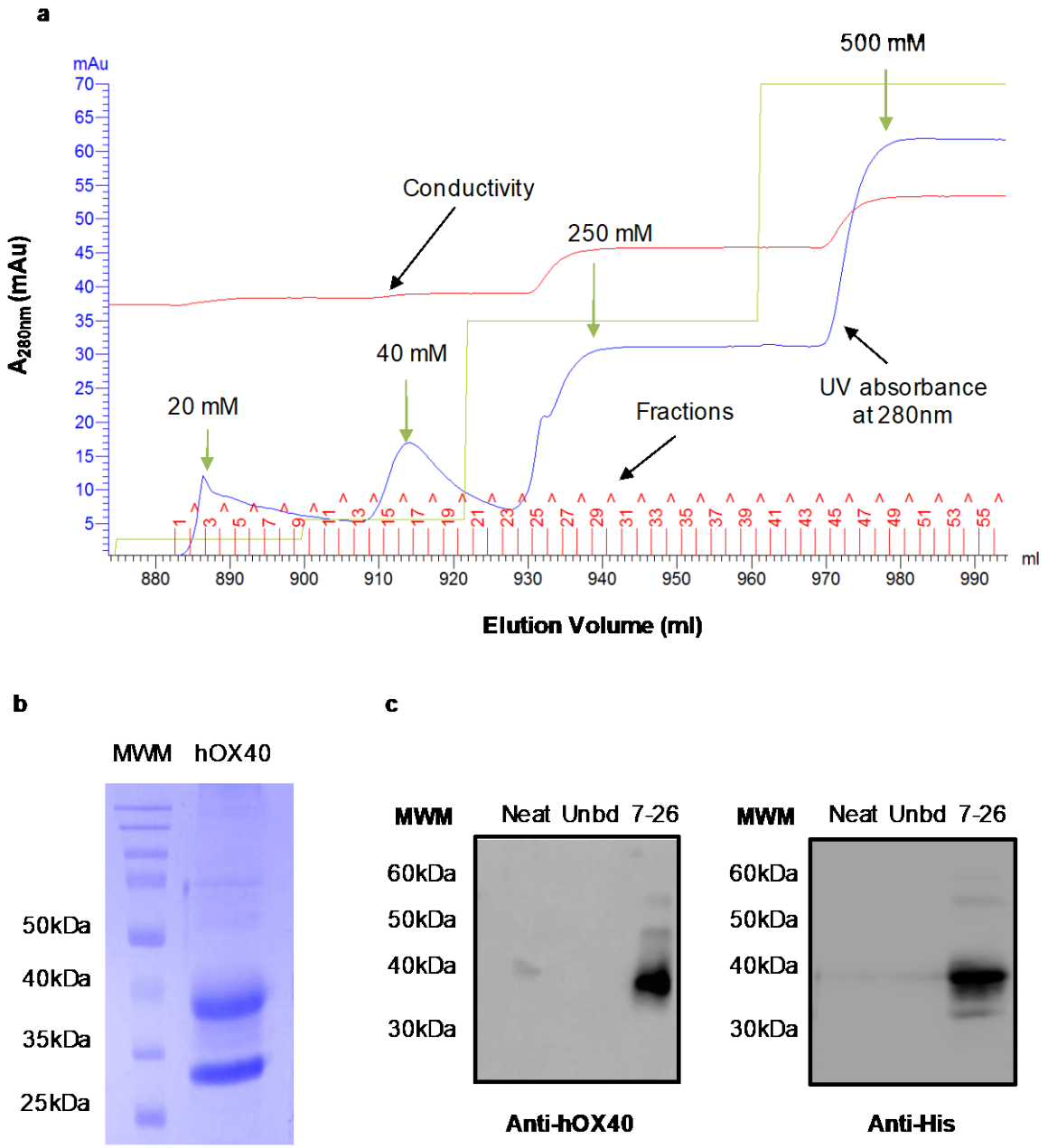

Figure 4.6 Purification of hOX40 extracellular domain from CHO cell supernatant using an Ni^{2+} column

a) 700ml of hOX40-6His transfected CHO cell supernatant was applied to a 6.2ml Ni^{2+} column. The protein was eluted with a gradient concentration of imidazole (20-500mM) indicated by the green arrows. 2ml fractions (red lines on x-axis) were collected at a flow rate of 4ml/min and fractions 7-26 were pooled and concentrated to 430µl ready for further analysis. b) The purity of hOX40 post Ni^{2+} column was analysed using SDS-Page. 15µl of concentrated hOX40 and 10µl of protein ladder (MWM) were loaded onto a 15% SDS gel and run at 150V for 1 ½ hours. The gel was imaged under white light. c) Samples from fractions 7-26 were used for western blot. An SDS-Page gel was run as described above. The protein was then transferred onto a polyvinylidene fluoride (PVDF) membrane at 24V for 1 hour. The membrane was blocked with 5% (w/v) milk followed by probing with either an (1) anti-hOX40 mAb (SAP 29-50) detected using a goat anti-mouse HRP conjugated antibody or an (2) anti-His antibody (abcam;ab18184) detected using a goat anti-rabbit HRP antibody. The HRP antibodies were detected using ECL and the chemiluminescence measured using a coupled charged device (CCD).

A new bulk culture of hOX40 ECD stably transfected CHO cells were prepared by thawing a previously frozen stock and sub-cloning as described above. CHO cells were grown adherently for 7 weeks and ~720ml of supernatant harvested weekly. The culture supernatant was concentrated from 5L to 300ml using a Vivaflow system producing a more manageable volume for ammonium sulphate (AS) precipitation. This step was carried out to remove large amounts of bovine serum which was used in the cell culture stage. The final volume after AS precipitation was 150ml which was then subjected to purification using the newly made anti-hOX40 affinity column.

Capture of the hOX40 ECD was successful using the anti-hOX40 affinity column. The red arrows on the chromatogram in Figure 4.7a indicate hOX40 elution from the column using glycine at pH 3. The purity, presence and size of hOX40 was confirmed using SDS-PAGE as before (Figure 4.7b). Due to the low capacity of a mAb column the flow through from the initial run was re-applied to the column until the peak highlighted by the red arrows decreased in height; this indicated that the column was no longer saturated/had reached its maximum binding capacity and so all of the hOX40 present had been captured and collected. The final amount of protein collected was 13.8mg; this is a suitable amount for crystallization trials therefore purification steps continued.

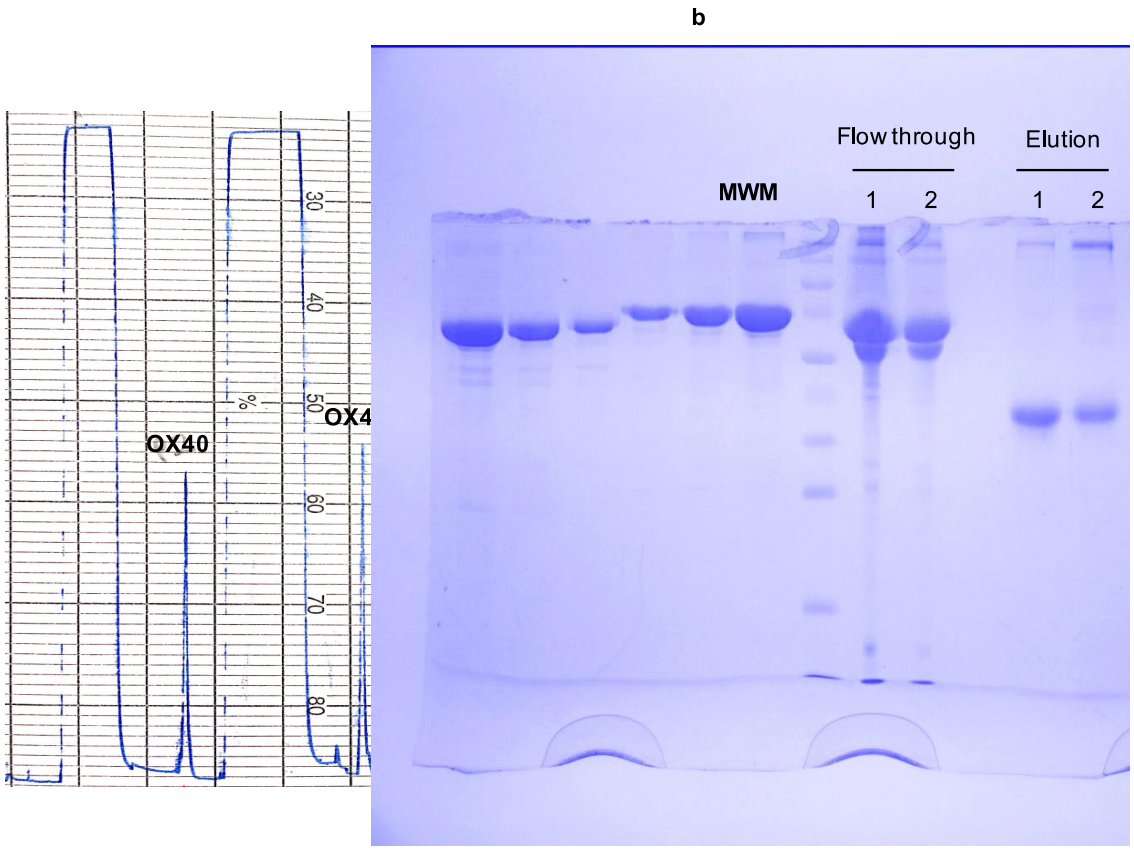

Figure 4.7 Affinity chromatography of hOX40 extracellular domain from stably transfected CHO cells

An anti-hOX40 mAb (SAP 29-50) was coupled to CNBr activated sepharose for 1 hour at RT to produce an anti-hOX40 affinity column. a) 150ml of CHO cell supernatant containing secreted protein was applied to the column at a flow rate of of 1ml/min and the flow through collected. Bound hOX40 protein was eluted using glycine pH 3, indicated by the red arrows. This process was repeated twice due to the low capacity nature of mAb columns. b) 15µl of sample from the flow through and elution's alongside 10µl of a molecular weight marker (MWM) were run on a 15% SDS gel at 150V for 1 ½ hours. The gel was imaged under white light.

Following affinity chromatography, size exclusion chromatography (SEC) was performed to remove any aggregates in the protein preparation. Figure 4.8a shows the chromatogram produced when using a Superdex 200, 26/600 column. Protein was eluted into 50mM HEPES pH 7.5 and 150mM KCl. SDS-PAGE was performed on fractions collected from the SEC which confirmed the presence of hOX40, again at ~40kDa, and specifically its high purity in fractions 23-30 compared to neat protein from the culture supernatant which had not undergone any purification (Figure 4.8b). As a result, fractions 23-30 were pooled and concentrated to a final volume of 4mls. The final protein concentration was 1.2mg/ml. This amount of protein was sufficient for complex formation and was taken forward to crystallisation trials.

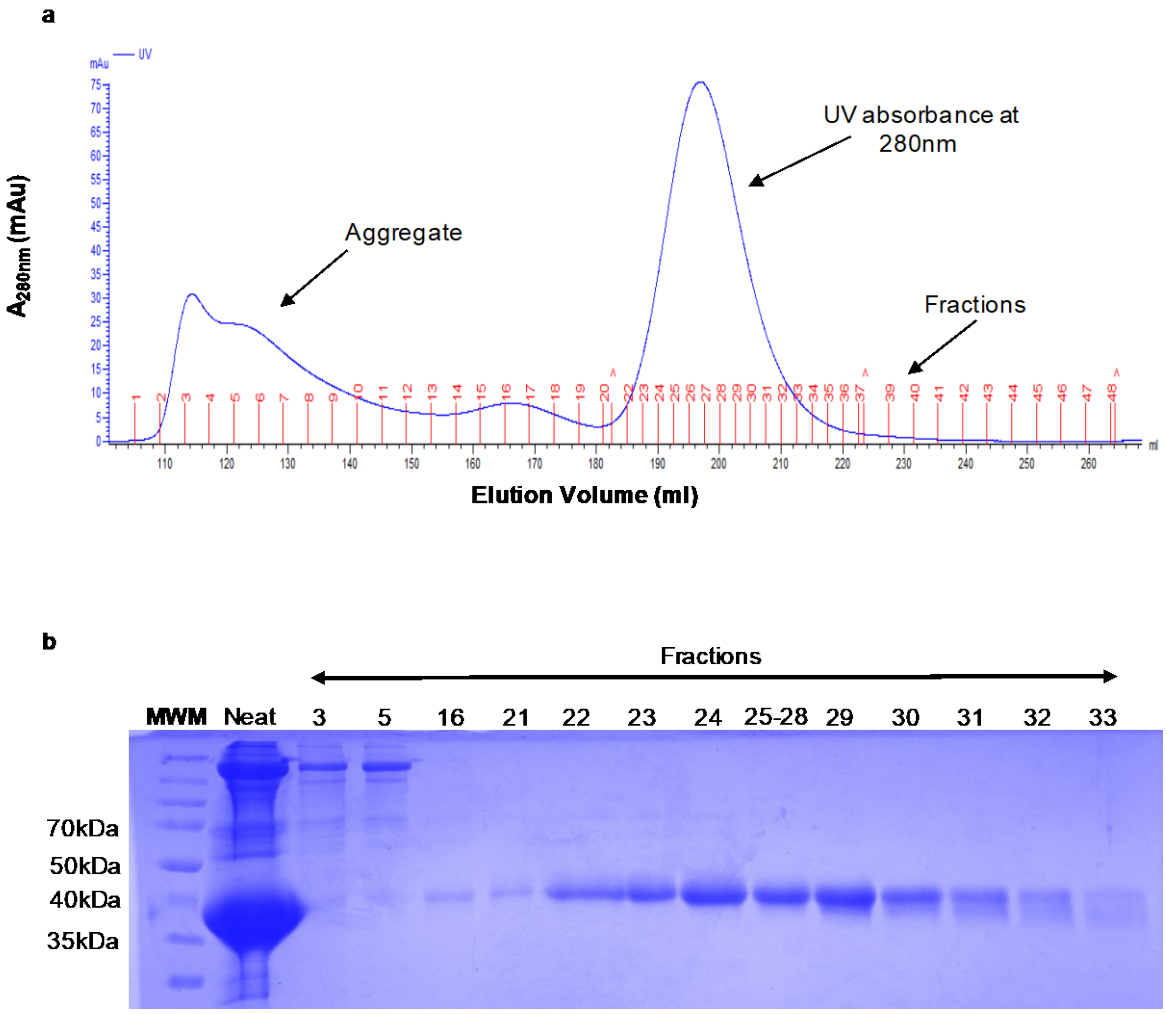

Figure 4.8 Purification and identification of hOX40 extracellular domain produced from stably transfected CHO cells

a) Gel filtration on a Superdex 200, 26/600 column of hOX40 ECD. Fractions (2.5mls) were collected at a flow rate of 4ml/min and analysed for absorbance at 280nm. Fractions 23-30 were pooled. b) SDS-page was carried out on fractions collected from gel filtration. 15µl of sample was loaded alongside 10µl of a molecular weight marker (MWM). The gel was run at 150V for 1 ½ hours and imaged under white light

.

4.4 Production of anti-hOX40 F(ab)

Fab fragments of two anti-hOX40 mAb, SAP 9 and SAP 29-50, were prepared. These specific mAb were chosen as results shown in Chapter 3 demonstrate differing abilities to bind in the presence of the natural ligand, as well as different abilities to act agonistically towards hOX40, affinities however were similar. It was therefore of interest to determine their crystal structures in complex with hOX40 ECD and discover to which exact epitope each mAb was binding. Removal of the Fc portion of the antibodies was performed using pepsin at pH 4.1; followed by reduction and alkylation to break the disulphide bonds between the two Fab arms. 20mgs of each mAb was used as starting material.

Pepsin digestion of both SAP 9 and SAP 29-50 was performed and monitored at hourly intervals using HPLC; Figure 4.9a shows the digest and purification of SAP 29-50. An increase in height in the right hand peak indicates $F(ab')_2$ formation whilst a decrease in the left hand peak indicates loss of full length IgG. Both digests were stopped after 3 hours as the height of the IgG peak had decreased substantially, and the $F(ab')_2$ peak was no longer increasing. Following digestion, SEC was performed on a 26/600, S200 column to remove any aggregates (Figure 4.9b). Fractions were eluted in 0.2M TE8 buffer. Fractions 45-47 containing $F(ab')_2$ fragments were pooled and concentrated to 1.5mls. The final protein concentration of SAP 29-50 $F(ab')_2$ was 3.49mg/ml. This was a substantial loss of protein from a starting point of 20mg, however was still enough to perform complex formation. Unfortunately, only 2mg of protein was recovered in the case of SAP 9, this amount was too little to continue with considering the multiple purification steps to follow.

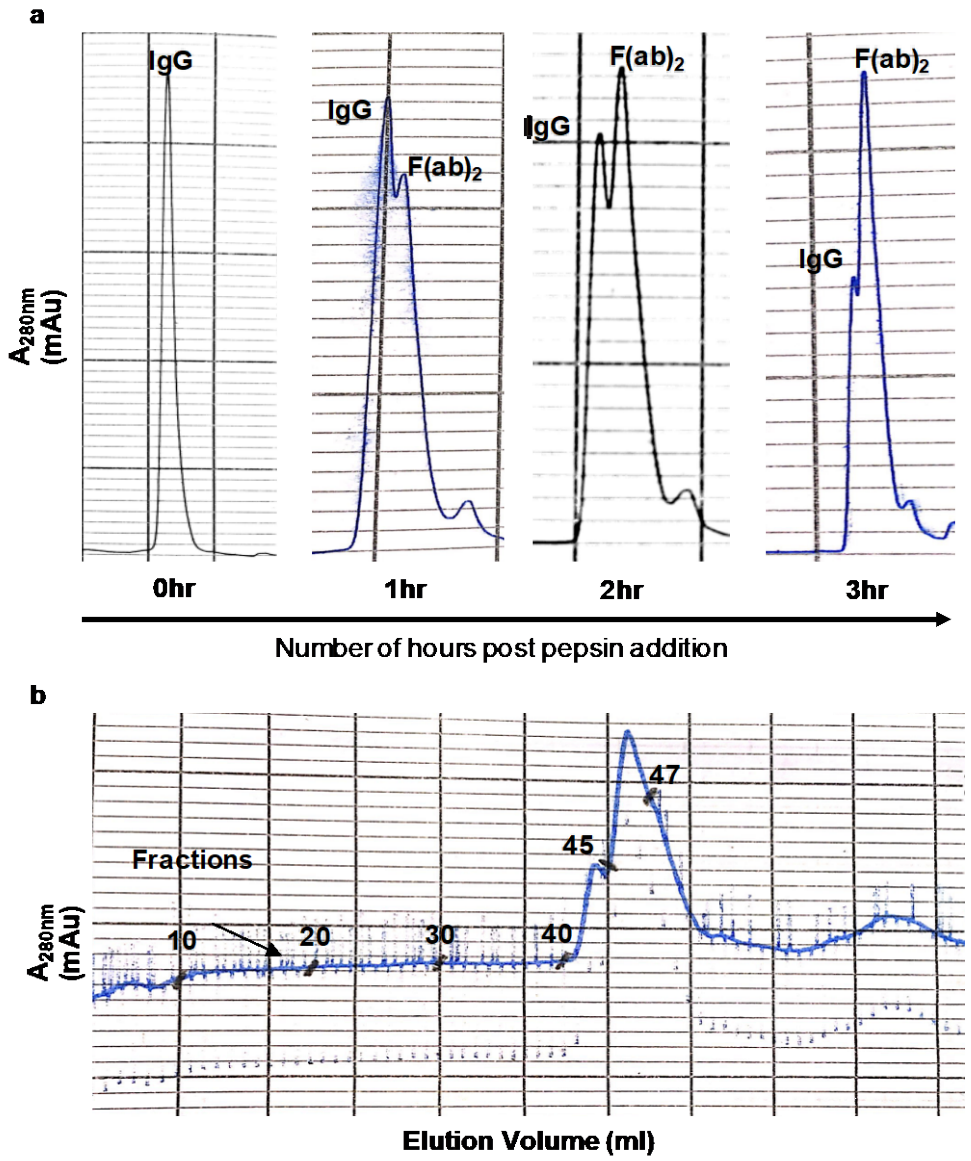

Figure 4.9 Fc digestion and F(ab')$_2$ purification of anti-hOX40 mAb SAP 29-50

Pepsin at pH 4.1 was used to digest the Fc portion of the mAb followed by gel filtration to remove any undigested IgG. a) 0.6mg of pepsin was added to the antibody. Samples were taken hourly and monitored on HPLC. Peaks representing full IgG and F(ab')$_2$ fragments are labelled. b) SEC was then performed on a 26/600, S200 column to remove any remaining IgG. The chromatogram shows absorbance at 280nm indicating protein presence. The F(ab')$_2$ fragments eluted in fractions 45-47, labelled on the trace, these were pooled and concentrated.

To determine the purity of the fractions collected from the gel filtration column a sample of SAP 29-50 F(ab')$_2$ was run on HPLC. Figure 4.10a shows a shoulder on the peak highlighted by the red circle. This shoulder indicates undigested antibody still present in the protein solution, therefore, the sample was passed down an anti-Fc column (Figure 4.10b) to remove remaining whole IgG. The HPLC trace in

Figure 4.10c demonstrates that the shoulder initially seen on the peak in Figure 4.10a was able to be removed using the anti-Fc column. The elution from the anti-Fc column were collected and concentrated to 1.7mls. The final protein concentration was 2.29mg/ml.

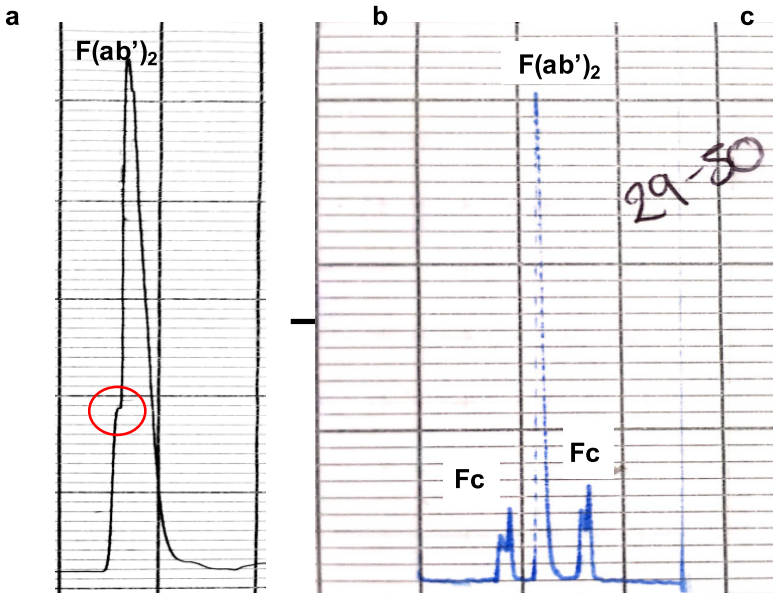

Figure 4.10 Removal of full length IgG and Fc fragments remaining after pepsin digestion of SAP 29-50

After pepsin digestion of full length IgG HPLC was run to check the purity of the sample. a) 20µl of digested IgG was applied to a mAbSec column and absorbance at 280nm recorded. The red circle highlights a shoulder in the peak indicating an impurity. b) The digested IgG was applied to an anti-Fc column to remove the shoulder. The anti-Fc column was run at a flow rate of 1ml/min and $F(ab')_2$ fragments were eluted in 1:5 Tris:NaCl, Fc fragments were eluted using glycine pH 3.0. c) Again, 20µl of sample was analysed on HPLC.

Following the successful production of a pure sample of SAP 29-50 $F(ab')_2$ fragments, a reduction-alkylation reaction was performed using DTT and IAA to generate Fab fragments. Figure 4.11 shows the HPLC trace of the sample post reaction; little $F(ab')_2$ remains whilst the peak representing the Fab fragments is large. The slight shoulder highlighted by the red circle was lost once the protein was dialysed into HEPES buffer. The digested sample was concentrated down to 2mls with a final concentration of 1.71mg/ml.

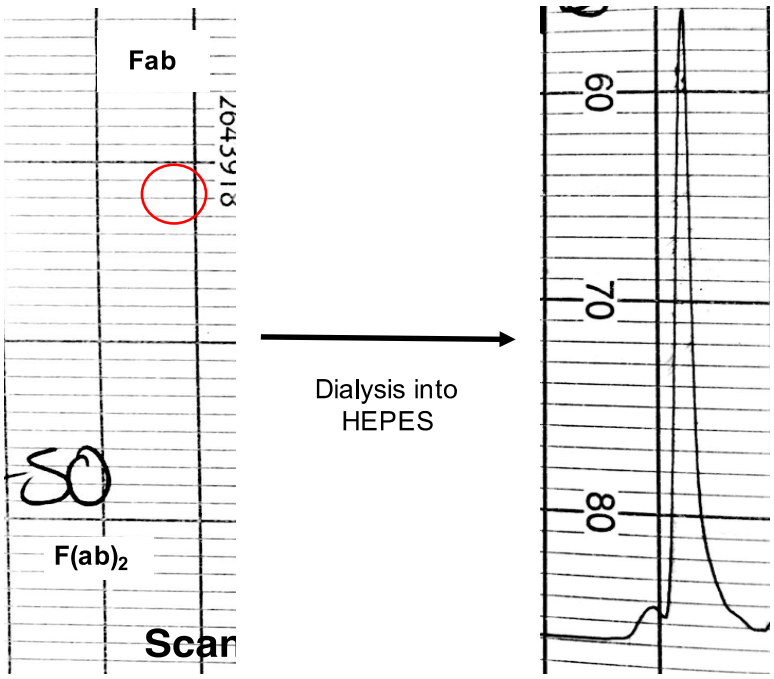

Figure 4.11 Dialysis of anti-hOX40 Fab fragments into HEPES buffer

SAP 29-50 Fab fragments were dialysed into 50mM HEPES pH7.5 and 150mM KCl before being complexed with hOX40 ECD.

Following reduction and alkylation of the F(ab')$_2$ fragments into Fab SEC was performed to remove any remaining F(ab')$_2$. As before with the hOX40 purification a 26/600, Superdex 200 column was used and the Fab fragments eluted in 50mM HEPES pH 7.5 and 150mM KCl (Figure 4.12). Fractions 25-29 were pooled and concentrated down to a final volume of 2mls with a concentration of 0.95mg/ml.

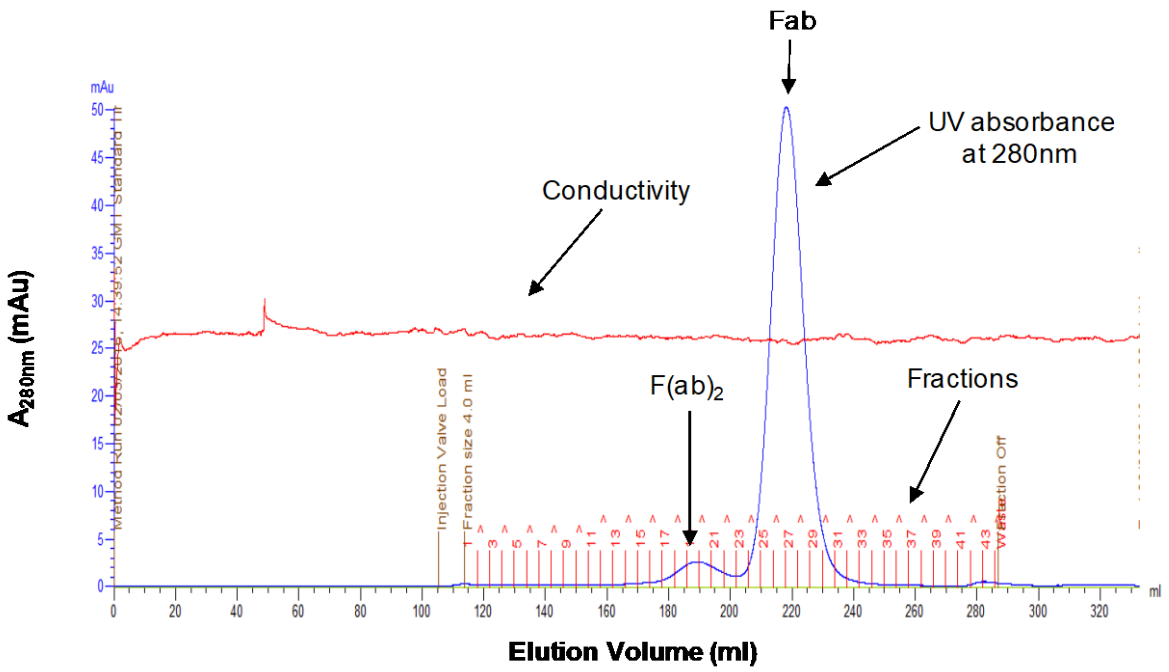

Figure 4.12 Purification of anti-hOX40 Fab fragments post reduction and alkylation from $F(ab)_2$ fragments

Gel filtration on a Superdex 200, 26/600 column after digestion and reduction of SAP 29-50 IgG. Fractions (4mls) were collected at a flow rate of 4ml/min and the absorbance at 280nm, indicating protein, was analysed. Fractions 25-29 were pooled.

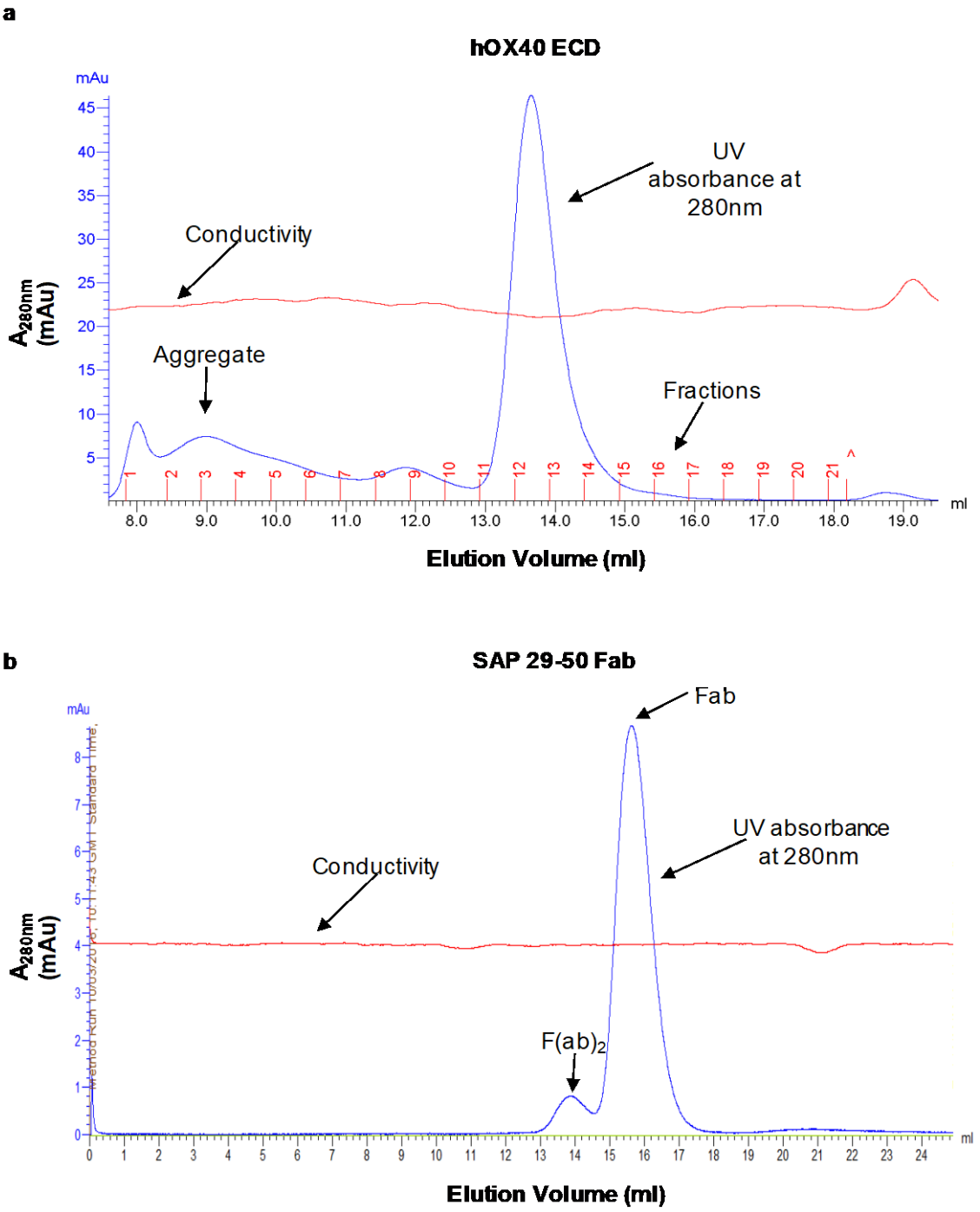

Figure 4.13 Gel filtration trials for hOX40 ECD and SAP 29-50 Fab fragment on a Superdex 200, 10/300 column

Gel filtration trial runs of hOX40 ECD and SAP 29-50 Fab fragments on a Superdex 200, 10/300 column at a flow rate of 0.3ml/min. No fractions were collected. a) hOX40 ECD elution profile. Elution volume = 13.6mls. b) SAP 29-50 Fab elution profile. Elution volume = 15.8mls.

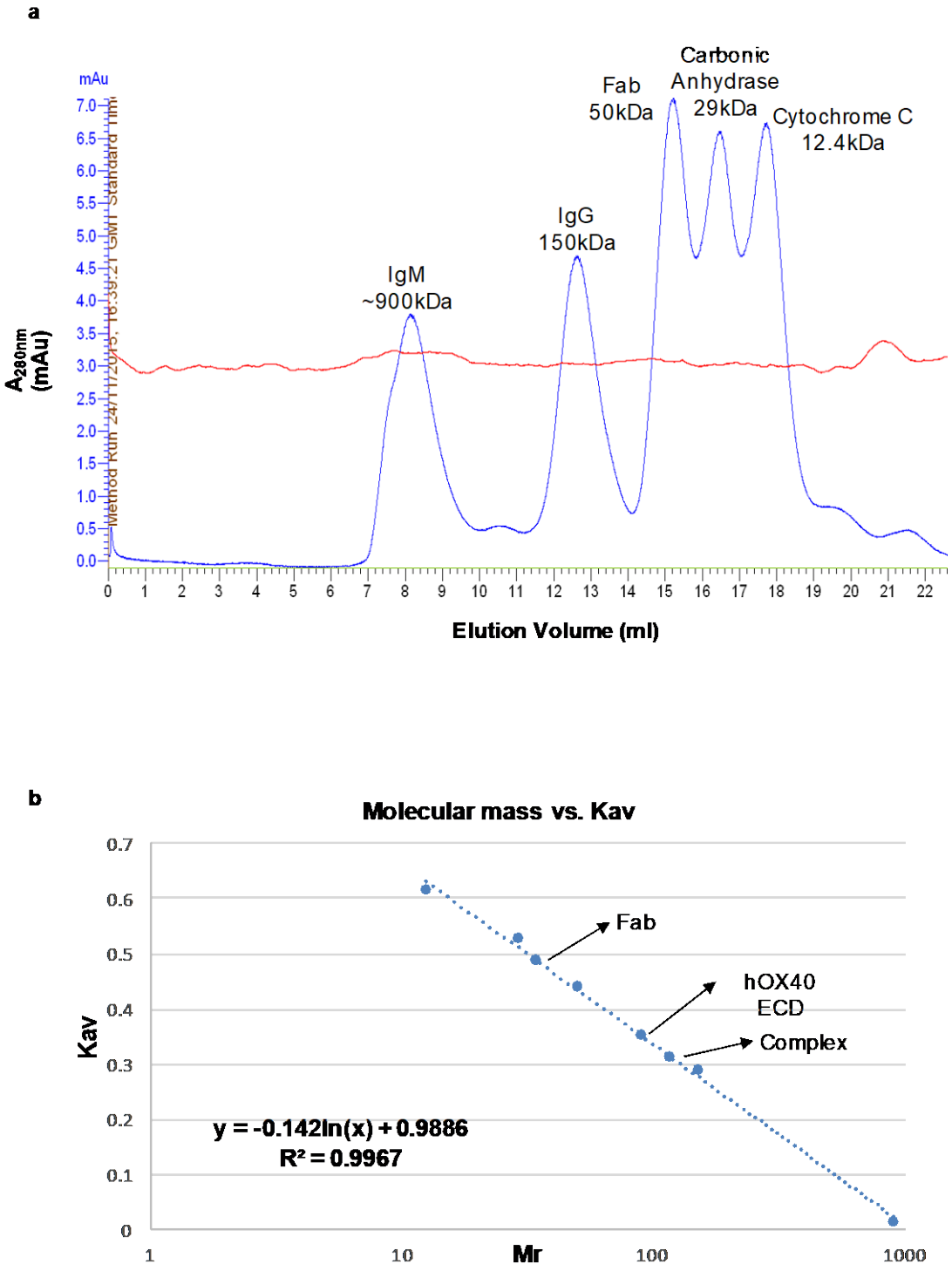

Figure 4.14 Calibration of a Superdex 200, 10/300 column using a number of protein standards and the calculation of their Kav values

a) 5 protein standards labelled on the chromatogram were applied to a Superdex 200, 10/300 column and the elution volumes measured. A flow rate of 0.3ml/minute was used and no fractions were collected. b) From the void volume of the column (Vo), the total column volume (Vc) and the elution volume of the specific protein (Ve), Kav values for each molecular mass standard were calculated using the equation below. Kav values were plotted against the log of the molecular mass (Mr) in kDa and a line of best fit drawn. The equation from the line of best fit was used to determine the Kav values of proteins with unknown Mr, and from this an estimate of their molecular weight was achieved.

Figure 4.14a shows the chromatogram produced by the calibration proteins on a Superdex 200, 10/300 column. From their elution volumes their Kav values were calculated and plotted against their molecular mass (Mr), shown in Figure 4.14b. Kav is known as the partition coefficient and gives a value for the proportion of pores available to the protein. It is calculated using the equation below where Ve represents the elution volume of the individual protein, Vo the void volume of the column and Vc the total column volume.

$$Kav = \frac{Ve - Vo}{Vc - Vo}$$

Using the equation formulated from the line of best fit and elution volumes seen in Figure 4.13 the molecular mass of both hOX40 ECD and SAP 29-50 Fab were estimated. For hOX40 ECD, the elution volume correlated to an estimated molecular mass of 89.9 kDa. This value is over 4x the expected Mr from sequence analysis (21kDa) (Protparam). For SAP 29-50 Fab, the elution volume correlated to an estimated Mr of 34 kDa. This value is slightly smaller than expected for a Fab fragment (~50kDa). It must be remembered, however, that gel filtration is not only affected by the size of a protein but also its shape. Long, non-spherical molecules will run at a higher apparent molecular mass in comparison to a globular protein with the same actual molecular mass. This is due to their differing abilities to enter and leave the pores in the column matrix.

Following this, hOX40 ECD and SAP 29-50 Fab were prepared in complex at molar ratios of 1:1.5 and a 1:1.25 of hOX40:Fab, respectively. These ratios were chosen due to previous work in the lab which showed ratios in this range to be correct for complex formation between a receptor and Fab fragment. Complex formation was visualised using SEC (Figure 4.15). At both ratios of hOX40:Fab tested a peak was observed with an elution volume of 13mls. Calculating the Kav value of this protein using the equation in Figure 4.14 an estimated Mr of 116.7 kDa is produced. This value is the sum of the estimated molecular masses observed when hOX40 ECD and SAP 29-50 Fab were applied separately to the column. Therefore, this peak was indicative of complex formation between hOX40

ECD and the Fab fragment. The smaller peak eluting at ~15.5mls in Figure 4.15 indicated remaining unbound Fab fragments.

The peak representing complex formation in both chromatograms had the same absorbance value (18mAu), indicating no change in amount of complex generated between the two ratios. However, the peak representing unbound Fab fragments was reduced from 7 mAu to 3 mAu between the 1:1.5 and the 1:1.25 ratio. This suggests that the likely hOX40:Fab ratio is 1:1 seeing as there were Fab fragments unbound in both ratios tested, however to ensure all hOX40 ECD was bound by Fab, a ratio of 1:1.25 hOX40:Fab was used in subsequent complex formation.

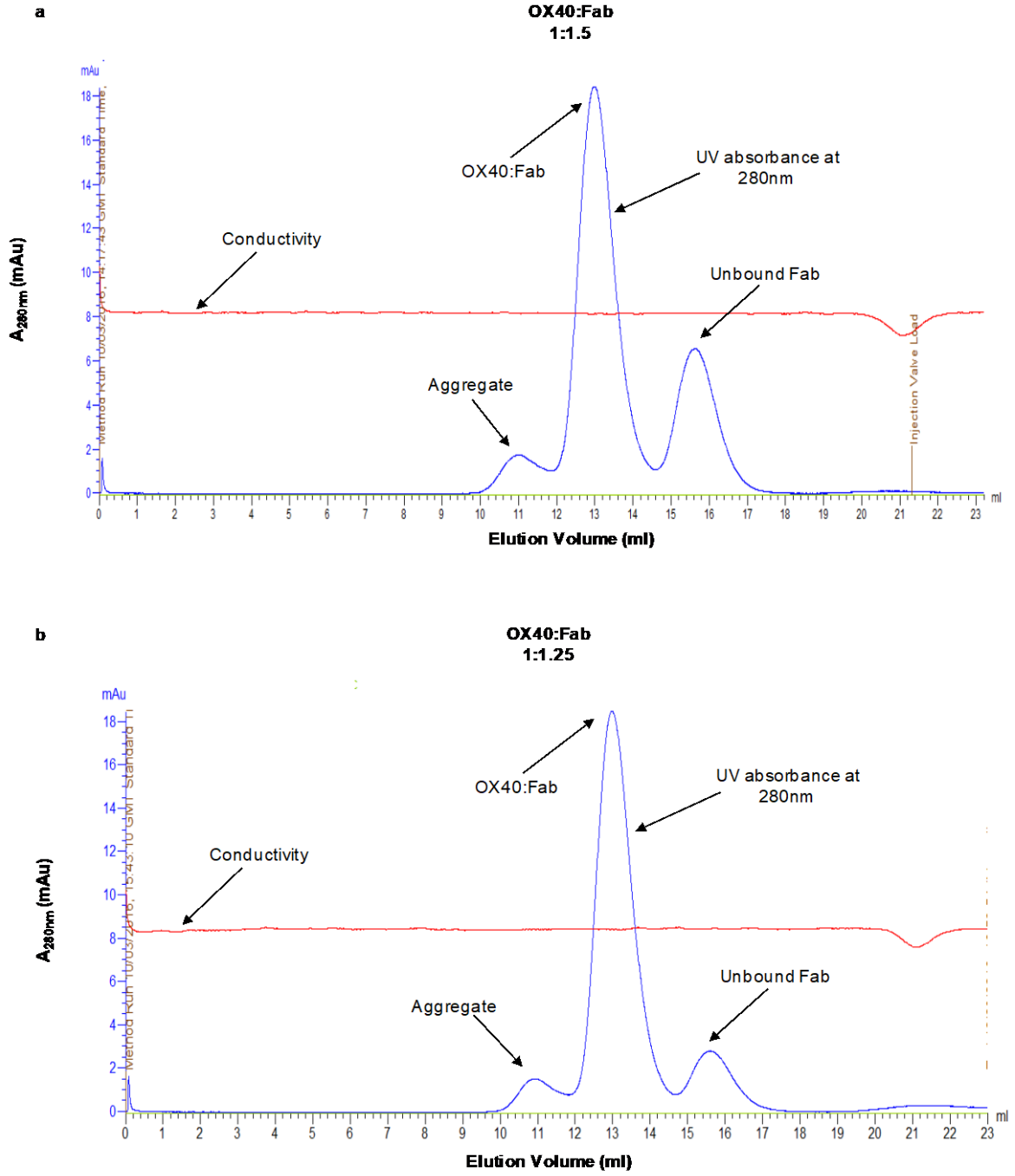

Figure 4.15 Gel filtration trials of hOX40:Fab complexes at molar ratios 1:1.5 and 1:1.25 on a Superdex 200, 10/300 column

1:1.5 and 1:1.25 hOX40:Fab complexes were applied to a Superdex 200, 10/300 column at a flow rate of 0.3ml/min. No fractions were collected. a) hOX40:Fab ratio at 1:1.5 elution profile. Elution volume = 13mls. b) hOX40:Fab ratio at 1:1.25 elution profile. Elution volume = 13mls.

As a result of the trial runs of complex formation the remaining hOX40 ECD and SAP 29-50 Fab fragments were combined at a 1:1.25 ratio and applied to a Superdex 200, 10/300 column in two consecutive runs shown on the chromatogram in Figure 4.16. Two runs were performed as the sample volume was larger than the total injection volume that a 10/300 column can withstand. Protein was eluted into 50mM HEPES pH 7.5 and 150mM KCl. Fractions 24-29 from the initial run and 47-52 from the second were pooled and concentrated down to 70µl. The final concentration of protein was 14mg/ml. This amount of protein was sufficient to set up 1 crystallisation trial using the sitting drop method and mother liquor components that were successful in crystallising the original hOX40-OX40L complex [16].

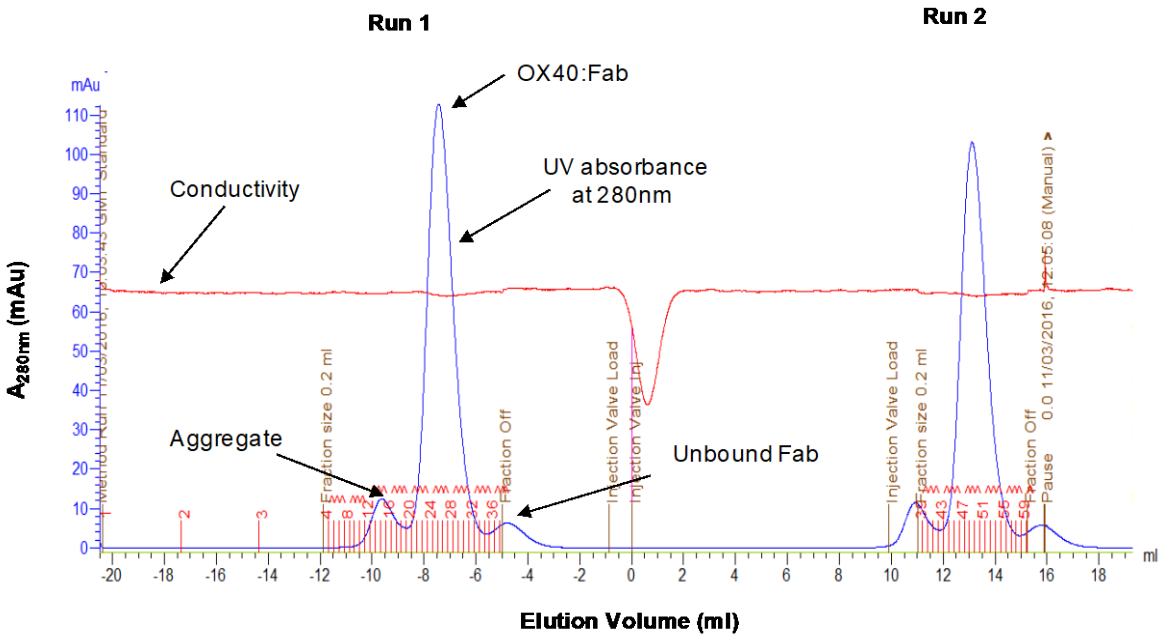

Figure 4.16 Gel filtration of a 1:1.25 hOX40:Fab complex

Gel filtration of a 1:1.25 hOX40:Fab complex on a Superdex 200, 10/300 column. Fractions (0.2mls) were collected at a flow rate of 0.3ml/min and analysed for absorbance at 280nm. Fractions 24-29 were pooled from the initial run and fractions 47-52 from the second run.

Unfortunately, no crystal formation was achieved in this trial. As a result, this avenue of the project was no longer pursued due to the amount of material and time required to generate it.

4.5 Discussion

In this chapter, production of a recombinant extracellular domain of human OX40 was produced with an N-terminal poly-His tail alongside Fab fragments of two anti-hOX40 monoclonal antibodies, SAP 9 and SAP 29-50. Stable transfections in CHO cells produced a higher yield of the hOX40 ECD in comparison to transient transfections in 293F cells.

The purification process of hOX40 from CHO cell supernatant revealed a number of unexpected molecular masses of the protein. Sequence analysis using Protparam provides a molecular mass for the extracellular domain of hOX40 as 19.9kDa. Interestingly, when applied to SDS-Page analysis the protein detected by western blot as hOX40 ECD was running as a 40kDa protein (Figure 4.6). Similarly, the elution volume recorded for hOX40 ECD when applied to a Superdex 200, 10/300 gel filtration column revealed an estimated Mr of ~4.5x the expected Mr from sequence analysis (Figure 4.3). These results leave it unclear as to what state hOX40 is in in solution e.g monomer, dimer etc.

This larger apparent Mr seen on gel filtration columns has also been observed within our lab with other receptors such as CD40 and CD32b. All of these receptors, including OX40, possess glycosylation, this is known to increase the Mr of full length OX40 from 30kDa to 50kDa [211] so may explain the larger Mr seen when the protein is subjected to SEC. This additional apparent shift in mass (~20kDa) would explain the size of the OX40-ECD seen on western blot (i.e. 19.9 + 20 kDA = ~40 kDa). A way of testing this (i.e the presence of carbohydrates on the size of hOX40 ECD) would be to remove the sugars enzymatically and apply glycosylated and non-glycosylated hOX40 to both SDS-PAGE and gel filtration. Likewise, a reducing and non-reducing gel could be run to determine if disulphide bonds are having any affect on the Mr of hOX40 ECD. Structural methods may also be exploited to determine the nature of hOX40 in solution.

Small angle x-ray scattering (SAXS) was performed on a series of hOX40 dilutions and analysis (By Emma Sutton) revealed that hOX40 seems to be behaving as a monomer in solution, and is comparable to the monomeric crystal structure (Figure 4.17). Unfortunately, the data was not sufficient to determine the molecular mass of hOX40. Further structural methods utilised in this chapter were X-ray

crystallography, to determine the specific binding epitopes of the anti-hOX40 mAbs.

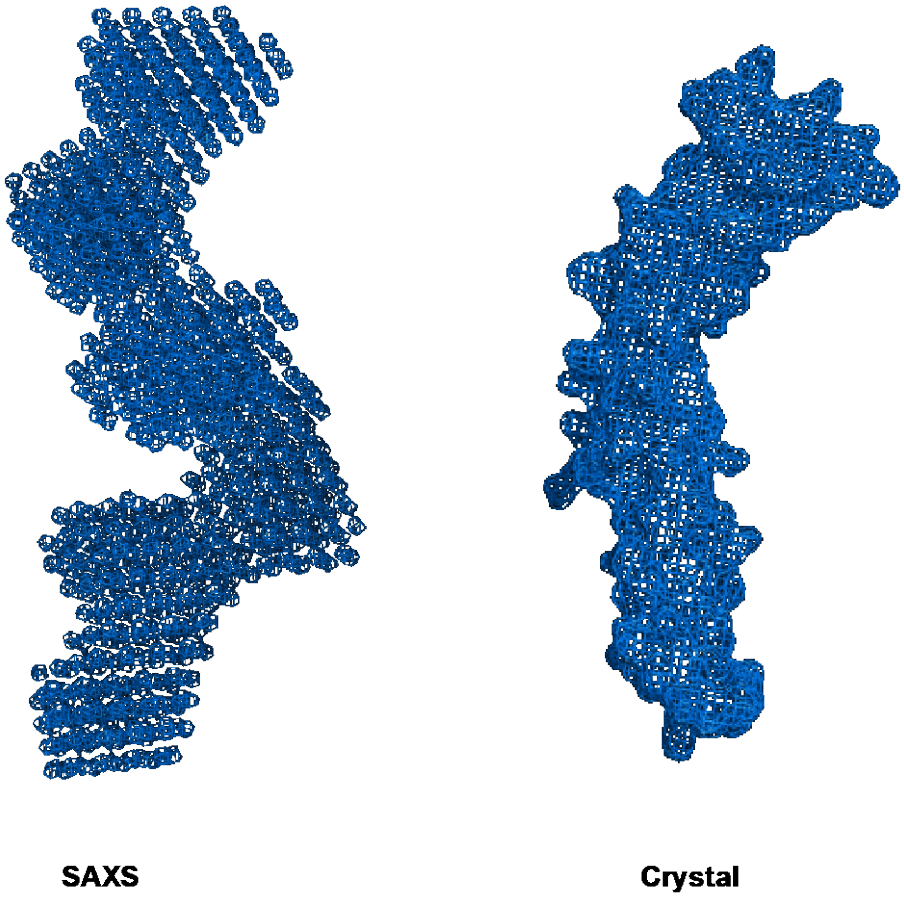

Figure 4.17 Structure of hOX40 ECD from SAXS and crystal data.

SAXS data initially analysed using ScÅtter followed by *ab-initio* bead modelling conducted using the ATSAS software. hOX40 crystal structure was obtained from the PBD (2HEV) and image generated using Pymol software.

Complex formation between hOX40 ECD and anti-hOX40 Fab fragments for use in crystal trials was successful and revealed that the ratio of binding was likely 1:1. The estimated molecular mass of the complex derived from its Kav value revealed it was the sum of the estimated Mr of hOX40 ECD and Fab fragment eluding that one hOX40 was binding to one Fab fragment. The complexes were set up in a crystal trial containing conditions previously used in the hOX40:OX40L crystal structure determination [16]. Unfortunately, no crystals were formed and it was

decided that this structural avenue of the project would no longer be pursued to make time to characterise the anti-hOX40 mAb *in vivo*.

If this avenue of research were to be taken forward we would have produced larger quantities of hOX40 ECD and the two mAb so that we were able to generate larger amounts of complex allowing a number of different crystal screens to be set up side by side. Having more than one screen set up would increase our chances of crystal formation and structure determination of hOX40 in complex with a Fab fragment. We could also use the method of seeding to increase our chances of crystal formation. Crystal seeding is the process of adding homogeneous or heterogeneous crystals to a crystallising solution to give a nucleation point encouraging new crystals to grow. Using crystals from similar complexes would benefit this process as it is likely they could have the same space group and other physical properties; CD40-Fab complexes have been resolved within the lab. Furthermore, we would have also tried to generate complexes with Fab fragments of anti-hOX40 mAb which bound to CRDs 1 and 2. This would be particularly interesting in light of our *in vivo* studies in which we have witnessed differences in the strength of depleting ability and agonistic activity in relation to mAb domain binding. Other TNFR family members, as discussed in the introduction to this chapter, have shown differences in activity dependant on domain binding but also specific epitope binding, is this the same for OX40? Does ligand binding affect mAb functionality? These questions could be answered if we were able to generate crystal structures of hOX40 ECD with one mAb from each CRD binding domain.

Chapter 5 Characterisation of anti-hOX40 mAb using an OT-I model

5.1 Introduction

The successful translation of an effective anti-hOX40 mAb into the clinic is still yet to be achieved. As discussed in Chapter 3, a number of clinical trials are underway testing the efficacy of anti-hOX40 mAb for treating a wide range of cancers. When developing mAb for use as a therapeutic in human patients there are a wide range of important factors to consider; for example, half-life, isotype and effector function of the mAb. Moving a mAb from 'bench to bedside' is a labour intensive, multi-step process to ensure the optimal mAb has been selected for administration into humans.

Initial mAb were produced using the hybridoma technique in which mouse splenocytes were fused with mouse myeloma cells, the mAb generated were therefore murine [131]. Technology advances however, have allowed the development of chimeric and fully humanized mAb to overcome the difficulties of administering a murine mAb into human patients. However, before considering these obstacles there are other important factors to consider when designing a successful therapeutic agent. Conventionally, mAb have two separate functions; 1) to bind to a specific antigen governed by the complementary determining regions and 2) to engage Fc receptors and elicit effector functions. Target specificity controlled by the variable region of the mAb is obviously of paramount importance, however it is also apparent that the constant region of a mAb plays a crucial role in antibody function, which, for IgG mAb, is largely mediated through its interaction with Fcγ receptors. As discussed in the Introduction, antibody isotype choice has important consequences and can be used to influence the desired effector function of the mAb; for example promoting agonism or deletion. It was therefore of interest in this chapter to explore the effects of both mIgG1 and mIgG2a anti-hOX40 mAb *in vivo* as potential agonist and depleting mAb, respectively.

Before testing these mAb in a tumour setting an OT-I transfer model was used to elucidate the effects of the anti-hOX40 mAb on the major T cells subsets. By crossing the OT-I mice with hOX40$^{+/+}$ KI mice, OT-I/hOX40$^{+/-}$ KI transgenic T cell

bearing mice were generated. These mice have an MHC-I-restricted TCR specific for residues 257-264 of ovalbumin (Ova), and concurrently express the human OX40 chimeric receptor in a heterozygous manner. The splenocytes from these mice allowed us to monitor an Ova specific proliferative response in the CD8+ T cell population and from that determine the effects of the anti-hOX40 mAb. OT-I cells can be tracked in the peripheral blood and lymphoid organs in recipient animals using H2- K^b $OVA_{257-264}$ tetramers [339]. These tetramers consist of four MHC molecules, each of which are bound to a SIINFEKL peptide and a fluorochrome. These tetramers bind with high affinity to SIINFEKL-specific CD8+ T cells allowing detection via flow cytometry. OT-I transfer experiments therefore allowed us to observe the T cell immune response dynamics to antigen (Ova) concurrent with stimulation through our anti-hOX40 mAb in a setting simpler than a tumour model

.

5.2 OT-I T cell adoptive transfer model

Following characterisation and validation of the hOX40 KI mouse as a suitable model to look at anti-hOX40 mAb *in vivo*, an OT-I transfer model (Figure 5.1) was used to determine if the anti-hOX40 mAb functions observed i*n vitro* matched those *in vivo*; i.e. mIgG1 mAb increasing CD8+ T cell proliferation and mIgG2a mAb inhibiting proliferative capacity (Figure 3.24).

$1x10^5$ OT-I/hOX40$^{+/-}$ KI splenocytes were given to either WT C57BL/6 or hOX40 $^{+/+}$ KI mice via i.v. injection 1 day prior to administration of Ova and the anti-hOX40 mAb via an i.p. route. To monitor the kinetics of CD8+ OT-I cell expansion after immunisation with Ova within the periphery, blood samples were taken from mice at regular intervals and the OT-I cells detected using the tetramer stain described in Section 5.1 (Figure 5.1a). Furthermore, this model was used to determine any significant changes in the number of different T cell populations after anti-hOX40 mAb treatment. To achieve this, spleens were harvested on day 4 post Ova and mAb administration and the numbers of CD4+, CD8+ Treg and OT-I populations assessed (Figure 5.1b). The activation status of the OT-I cells was checked prior to administration using CD62L as a marker for naïve cells and CD44 as a marker for activated cells. OT-I cells were only administered to mice if >80% were naïve ($CD62L^{hi}CD44^{lo}$) (Figure 5.1c).

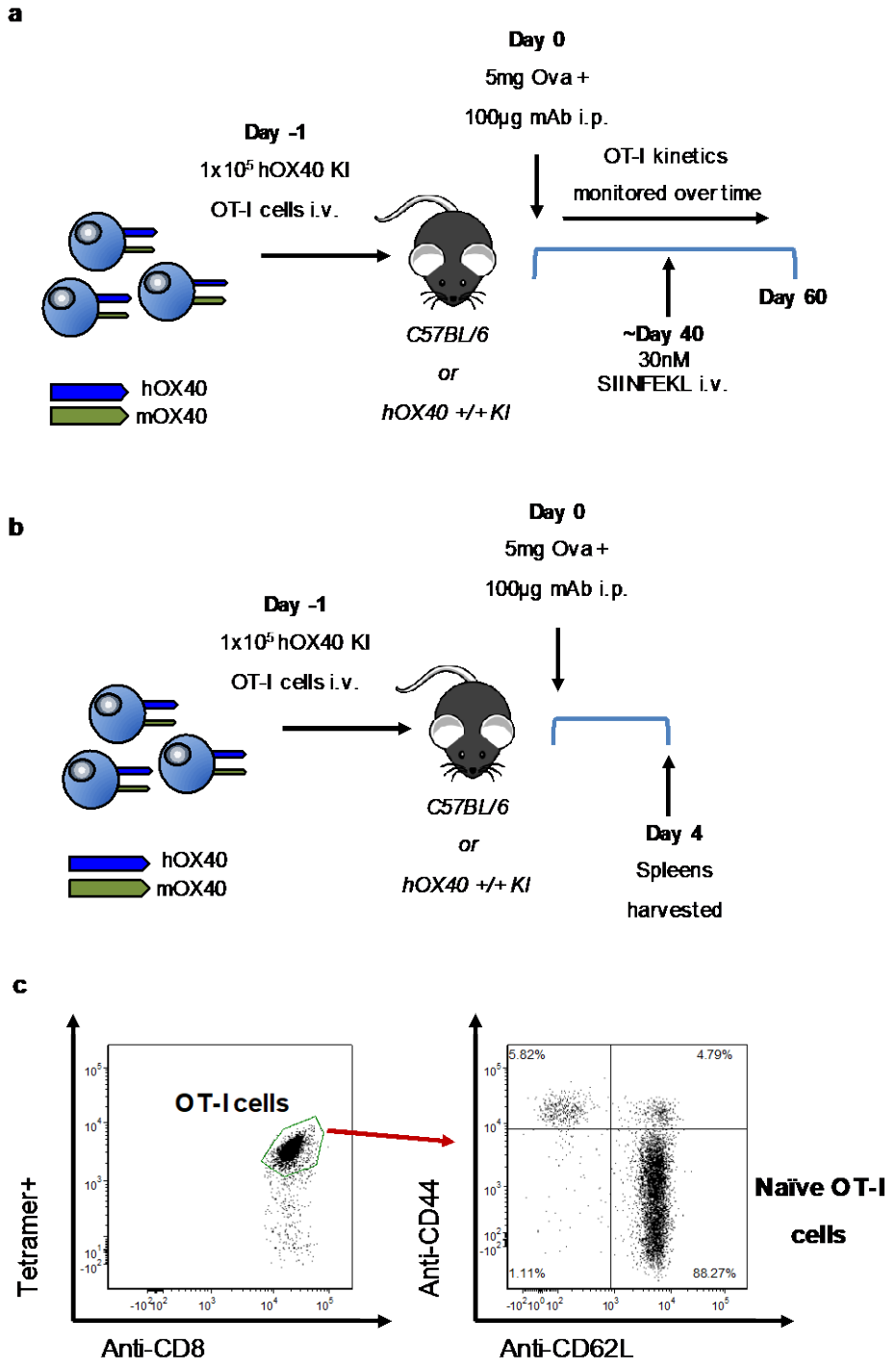

Figure 5.1 Schematic of the OT-I transfer model

$1x10^5$ OT-I cells from OT-1/hOX40$^{+/-}$ KI mice were given to mice via i.v. injection. A day later 5mg Ova and 100µg of an anti-hOX40 mAb were administered via i.p. injection then either: a) OT-I cells kinetics were monitored using flow cytometry over the following 6-8 weeks to assess the primary response, resting memory phase and memory phase after mice had been re challenged with 30nM SIINFEKL peptide via i.v. injection at ~day 40. b) Spleens were harvested from mice on day 4 and cell populations assessed using flow cytometry. c) OT-1/hOX40$^{+/-}$ KI splenocytes were tested for their levels of activation before administration to the mice using CD62L as a marker for naïve cells and CD44 as a marker for activated cells. Cells were only administered to mice if >80% were CD62L^{hi}CD44^{lo} (Naïve OT-I cells).

5.3 Effect of anti-hOX40 mAb on OT-I cells within hOX40$^{+/+}$ KI mice

In Chapter 3 we demonstrated that dependent on isotype, anti-hOX40 mAb were able to cause either proliferation (mIgG1) or inhibition of CD8 cells (mIgG2a) *in vitro*. To test if this held true *in vivo,* OT-I/hOX40$^{+/-}$ KI cells were adoptively transferred into hOX40$^{+/+}$ KI mice followed by vaccination with Ova and our panel of anti-hOX40 mAb (spanning the domains of OX40) as both a mIgG1 and a mIgG2a. Kinetics of OT-I cell expansion within the periphery were monitored using SIINFEKL-tetramer. Figure 5.2 demonstrates the ability of both mIgG1 and mIgG2a anti-hOX40 mAb to expand OT-I T cells in the blood compared to Ova alone. This was unexpected in terms of the mIgG2a, when considering the effects of the mAb in the human PBMC proliferation assay (Figure 3.24). Figure 5.2 and Figure 5.3a demonstrate that the kinetics of OT-I expansion in the primary response were very similar when comparing mIgG1 and mIgG2a treated mice, with the exception of SAP 28-2. All of the mIgG1 mAb induced a mean peak frequency (day 7) of OT-I cells between 51-68% of total CD8+ cells (Figure 5.3a). The mIgG2a mAb caused a slightly higher peak mean frequency of OT-I cells, 63-72% of total CD8+ cells, with the exception of SAP 28-2 whose peak mean frequency was 26% (Figure 5.3a).

One difference noted between mIgG1 and mIgG2a treated mice was the strength of the memory response. Figure 5.2 shows that the mIgG1 treated mice produced a stronger re-expansion of OT-I cells upon rechallenge in comparison to mice treated with the equivalent mAb as a mIgG2a. Figure 5.3b highlights that at the peak of the memory response mIgG1 anti-hOX40 mAb generally produced a higher frequency of OT-I cells post rechallenge in comparison to mIgG2a mAb, (SAP 28-2; 34% vs. 2%, SAP 9; 28% vs. 15%, SAP 25-29; 57% vs. 10%, SAP 29-23; 47% vs. 6%), with the exception of SAP 15-3 (10% vs. 18%). These differences between isotype were statistically significant in SAP 28-2 and SAP 25-29 treated mice. This interesting observation seen between mIgG1 and mIgG2a memory responses was therefore further explored in Section 5.4.

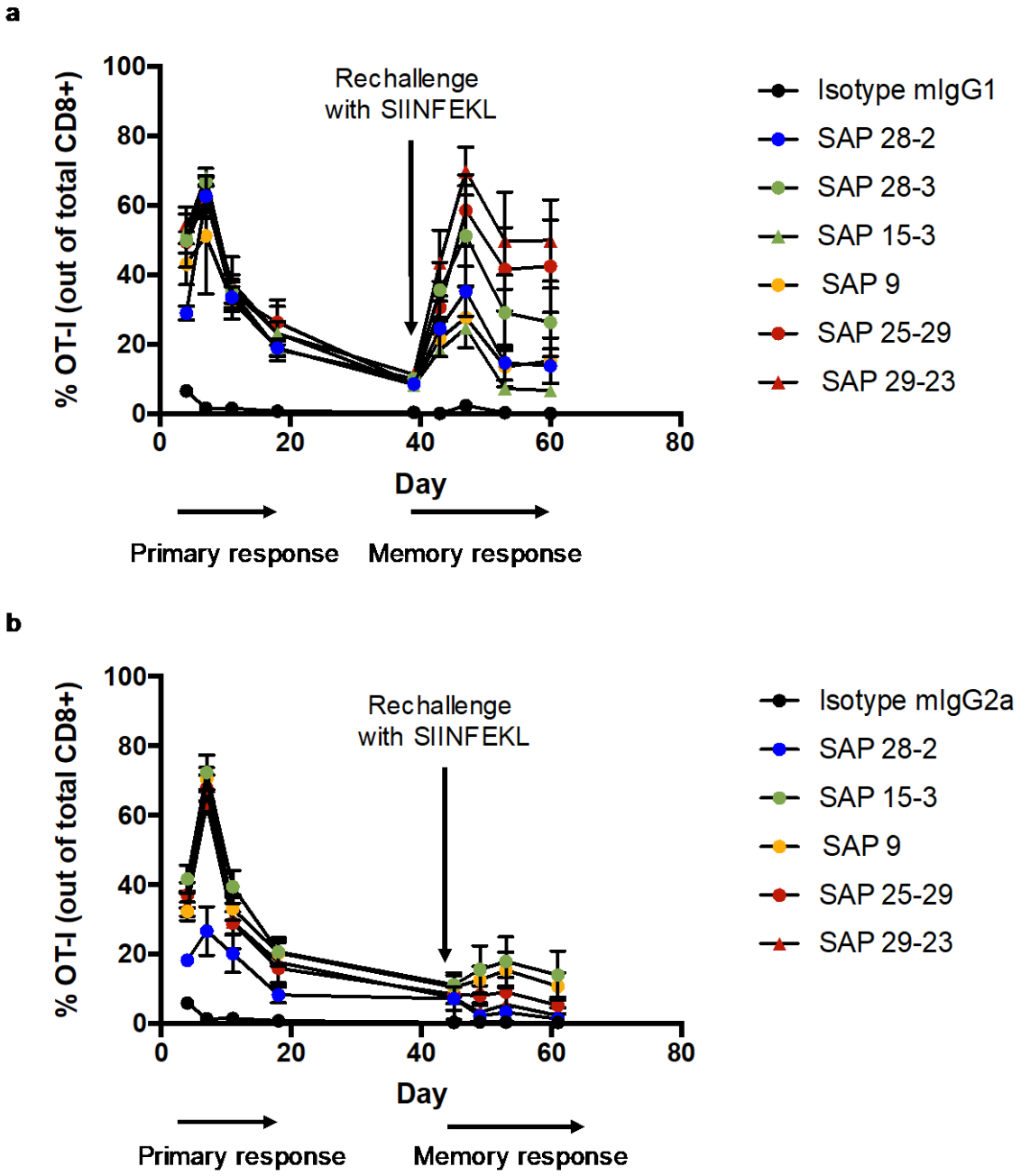

Figure 5.2 Measurement of OT-I kinetics in the blood of hOX40$^{+/+}$ KI mice after immunisation with Ova in the presence of anti-OX40 mAb

1x10^5 OT-I cells (in whole splenocyte population) from OT-1/hOX40$^{+/-}$ KI mice were given to hOX40$^{+/+}$ KI mice via i.v. injection. A day later mice were administered 5mg Ova and 100μg of anti-hOX40 mAb (mIgG1 or mIgG2a) via i.p. injection. a) mIgG1 treated mice. Blood was drawn on days 4, 7, 11 and 18 to monitor the primary response. Mice were bled on day 39 to check OT-I levels were low enough for a re-challenge with 30nM SIINFEKL peptide which took place on day 40. Blood was then drawn on days 43, 47, 53 and 60 to monitor the memory response. b) mIgG2a treated mice. Blood was drawn on days 4, 7, 11 and 18 to monitor the primary response. Mice were bled on day 45 to check OT-I levels were low enough for a re-challenge with 30nM SIINFEKL peptide which took place on day 46. Blood was then drawn on days 49, 53 and 61 to monitor the memory response. OT-I cells were detected in the blood using CD8 and the tetramer as markers. Data is a combination of 2 independent experiments with N=6 mice per treatment group. Error bars represent mean±SEM.

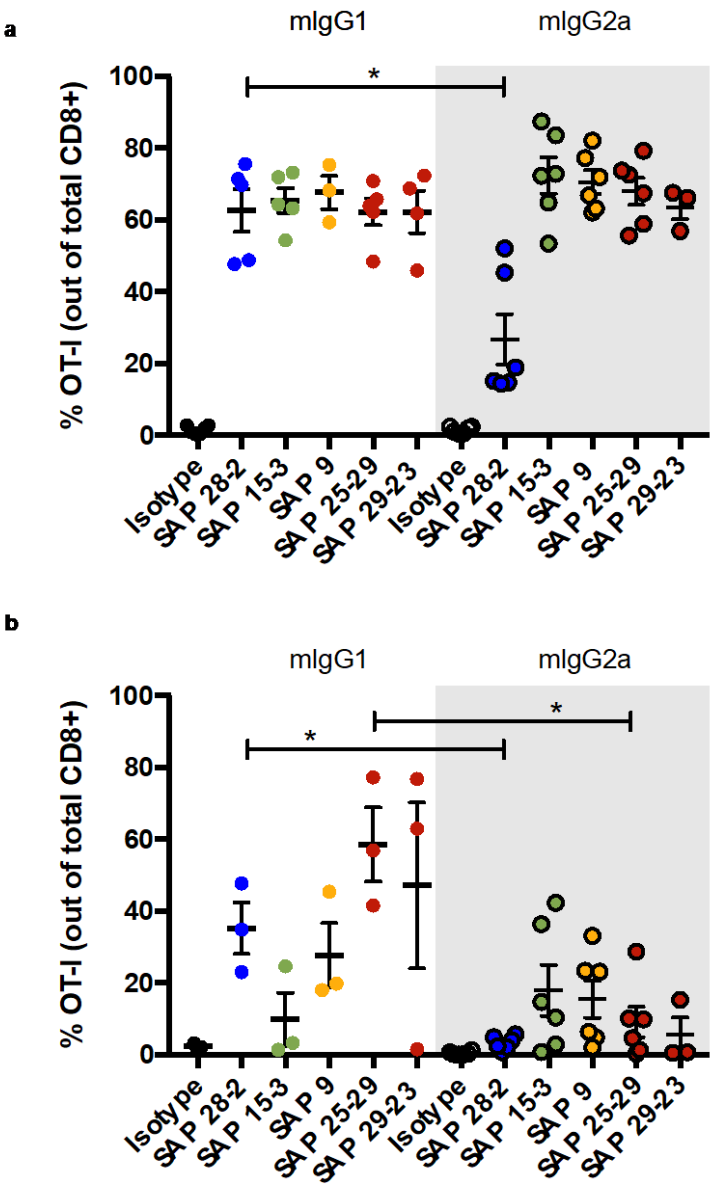

Figure 5.3 Frequency of OT-I cells in hOX40$^{+/+}$ KI mice at the peak of the primary and memory response after immunisation with Ova in the presence of anti-hOX40 mAb (mIgG1 vs. mIgG2a)

Data from Figure 5.2; a) Day 7 (peak of primary response) and b) Day 47 (mIgG1) and Day 53 (mIgG2a) (peak of memory response). Data is a combination of 2 independent experiments with N=3-6 mice per group. Error bars represent mean±SEM. Statistical significance was evaluated using a Mann-Whitney test; * P≤ 0.05, ** P≤ 0.01, *** P ≤ 0.001.

As a result of this unexpected expansion of OT-I cells in the periphery of mIgG2a treated mice (given their apparent lack of agonism on human cells *in vitro*) it was of interest to determine the affect of these mAb, compared to mIgG1, within the spleen of vaccinated hOX40$^{+/+}$ KI mice. The same experimental set up as described above was used however in this case spleens were harvested on day 4

post vaccination with Ova and the anti-hOX40 mAb (mIgG1 and mIgG2a). The number of cells present in different T cell subsets in the spleen was assessed using flow cytometry and the gating strategy shown in Figure 5.4. Data is displayed on the graphs colour coordinated into domain binding categories; CRD1=Blue, CRD2=Green, CRD3=Yellow and CRD4=Red.

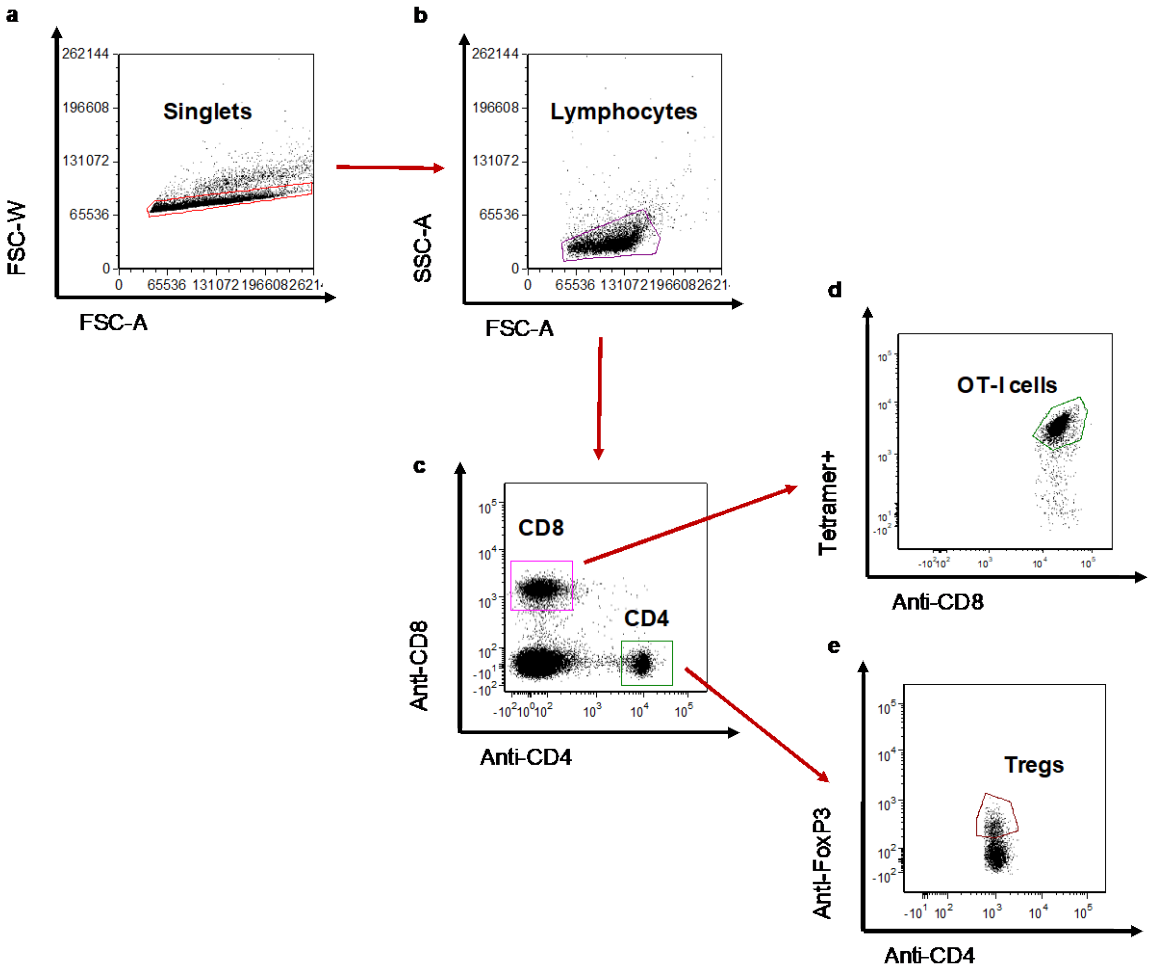

Figure 5.4 Gating strategy used to analyse T cell populations in flow cytometry

Processed splenocytes and blood samples were labelled with CD4, CD8 and Tetramer fluorescently labelled antibodies for 20 minutes at RT before cells were fixed, permeabilised and stained with a fluorescently labelled FoxP3 antibody. Cell samples were assessed using a FacsCanto and gating was performed in a hierarchal fashion. a) Cells were firstly gated on a FSC-A/FSC-W plot to determine singlets. b) Cells were then gated using a FSC-A/SSC-A plot to determine lymphocytes followed by gating on c) CD8 and CD4 markers. Lastly, CD8+ cells were gated on CD8/tetramer to observe Tetramer+ OT-I cells (d) and CD4+ cells were gated on CD4/FoxP3 to observe Tregs (e).

The data demonstrated that in terms of OT-I cell expansion the results seen in the spleen matched those seen in the periphery; both mIgG1 and mIgG2a mAb were able to cause expansion of OT-I cells above isotype control treated mice (Figure 5.5 and Figure 5.6). However, the level of expansion in mIgG2a treated mice was statistically lower in 4/6 treatment groups when compared to the mIgG1 mAb (Figure 5.8) unlike in the blood when both mAb isotypes reached very similar peak levels of expansion. Furthermore, this expansion in the spleen was not seen with every mAb as it was in the periphery (Figure 5.5 and Figure 5.6 vs.Figure 5.2).

In contrast to the expansion of OT-I cells, Figure 5.6 demonstrates that the mIgG2a mAb were able to significantly reduce the number of Tregs and total CD4+ cells in what seemed to be a hOX40 expression dependent manner, as OX40 expression follows the hierarchy Treg>CD4+>CD8+ (as described in Chapter 1; Section 3.2). On the other hand, the general trend in the mIgG1 treated mice was expansion of most of the T cell populations (CD8+, Tregs and OT-I cells) (Figure 5.5). This preference for expansion versus deletion between the different isotypes resulted in significant differences in absolute numbers within all T cell subsets, in particular amongst the Treg and OT-I populations (Figure 5.8). The CD8:Treg ratio was unchanged in the mIgG1 treated mice (Figure 5.7) and this was due to the mAb causing expansion, to some extent, of all populations. On the other hand the CD8:Treg ratio in mIgG2a treated mice was increased significantly with all mAb, apart from SAP 28-2 (Figure 5.7), and this was due to the mAb ability to strongly deplete the Treg population. NK and NKT sub-populations were also assessed but showed little change when compared to isotype treated mice (data not shown).

mIgG1

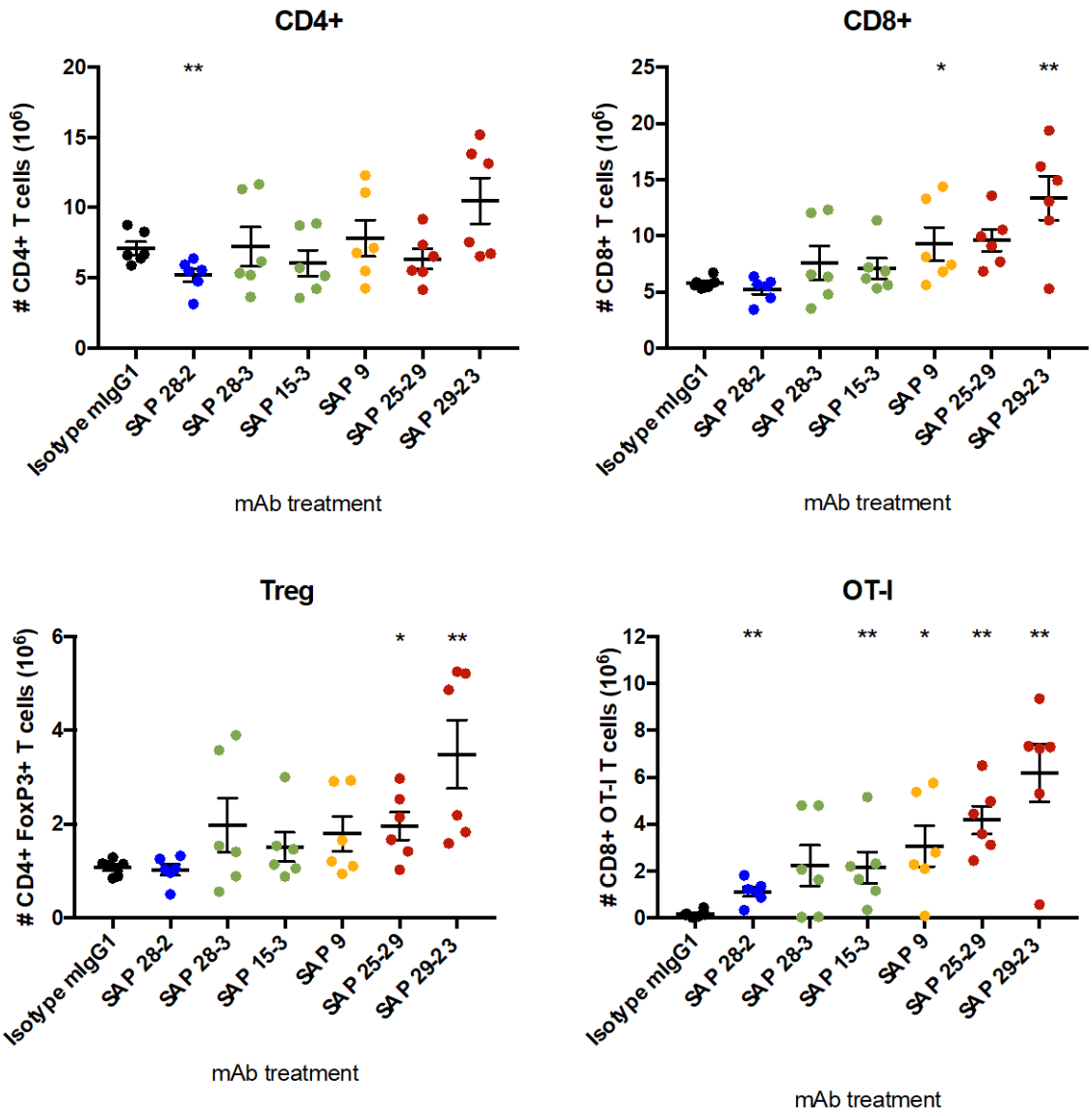

Figure 5.5 Numeration of T cell subsets in the spleens of hOX40$^{+/+}$ KI mice after vaccination with Ova and mIgG1 anti-hOX40 mAb

The same experimental set up as described in Figure 5.2 was used. Spleens were harvested from mice on day 4 post vaccination with Ova and a mIgG1 anti-hOX40 mAb. Cell populations (CD4+, CD8+, Treg and OT-I) were numerated using flow cytometry. Data is combined from two individual experiments with N=6 mice per treatment group. Each dot represents an individual mouse. Error bars represent mean±SEM. Statistical significance was evaluated using a Mann-Whitney test; * P≤ 0.05, ** P≤ 0.01, *** P ≤ 0.001.

mIgG2a

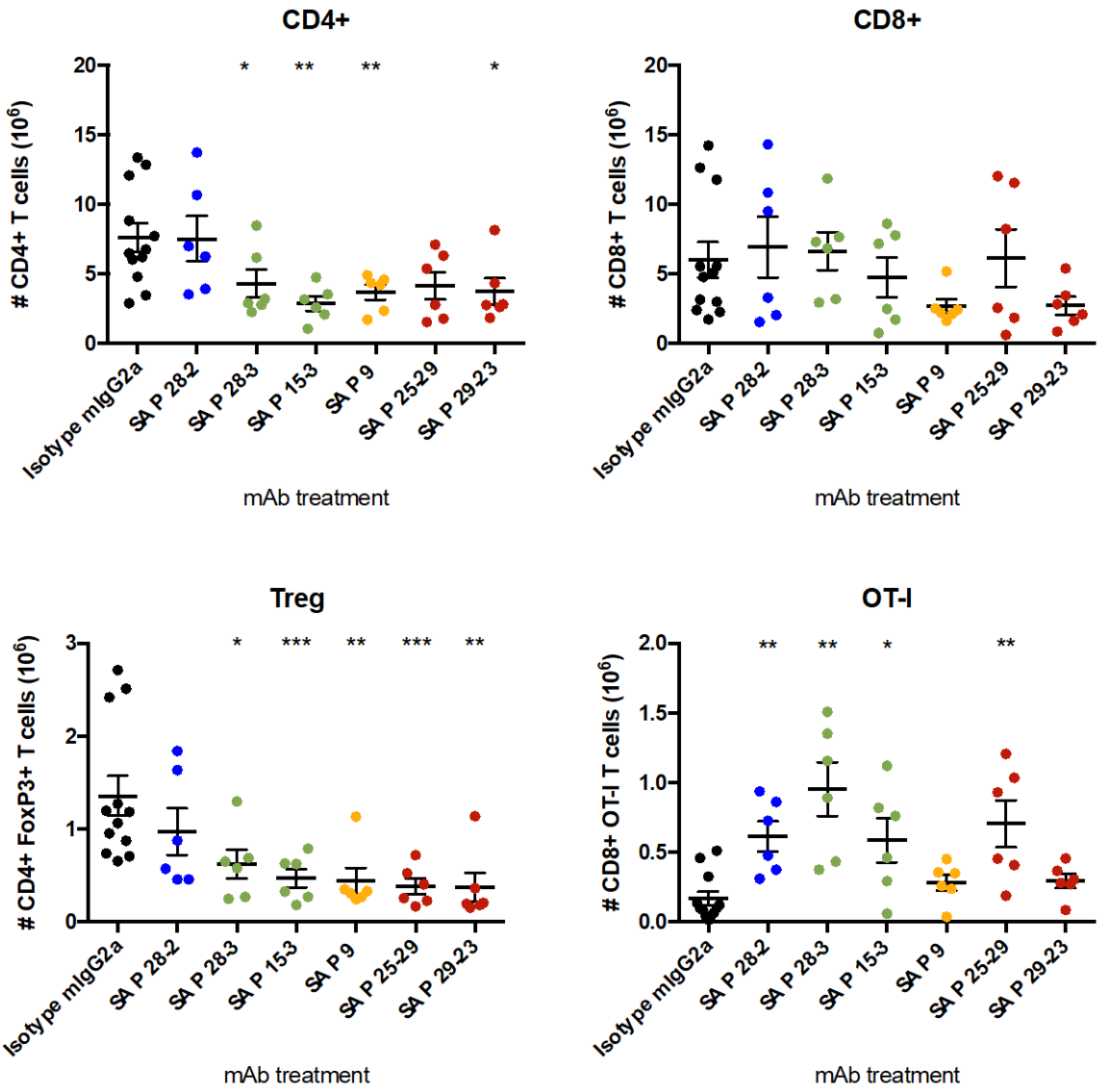

Figure 5.6 Numeration of T cell subsets in the spleens of hOX40$^{+/+}$ KI mice after vaccination with Ova and mIgG2a anti-hOX40 mAb

The same experimental set up as described in Figure 5.2 was used. Spleens were harvested from mice on day 4 post vaccination with Ova and a mIgG2a anti-hOX40 mAb. Cell populations (CD4+, CD8+, Treg and OT-I) were numerated using flow cytometry. Data is combined from two individual experiments with N=6 mice per treatment group. Each dot represents an individual mouse. Error bars represent mean±SEM. Statistical significance was evaluated using a Mann-Whitney test; * P≤ 0.05, ** P≤ 0.01, *** P ≤ 0.001.

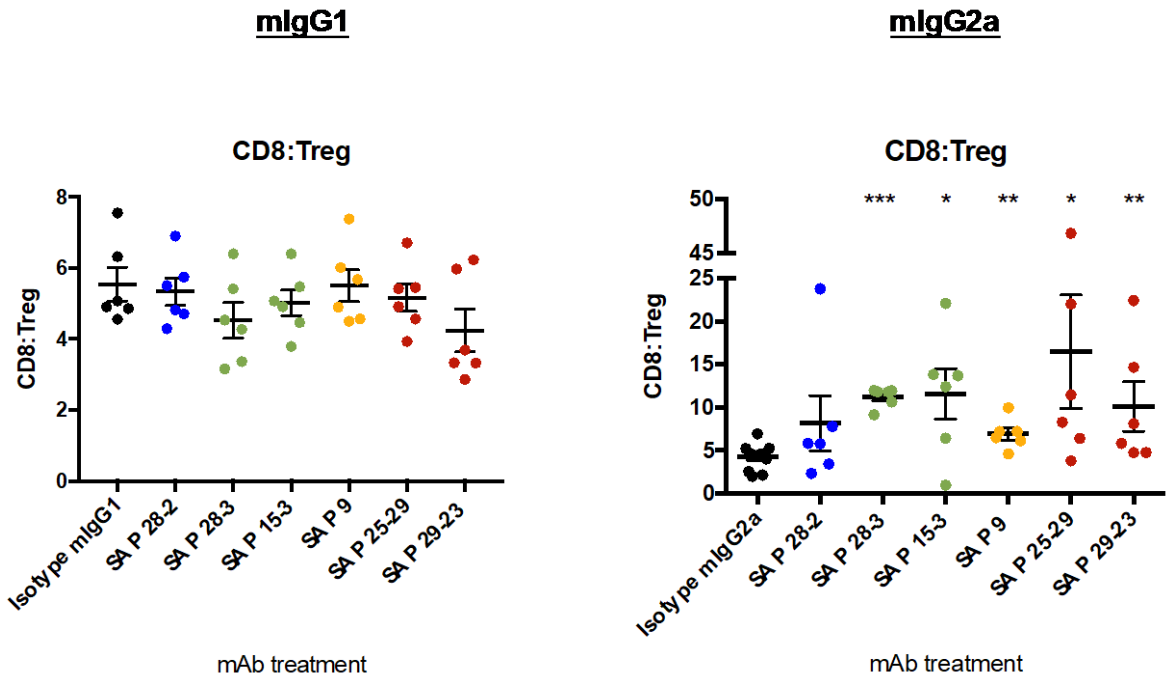

Figure 5.7 CD8:Treg in the spleens hOX40$^{+/+}$ KI mice treated with Ova and anti-hOX40 mAb

The CD8:Treg ratio was determined by dividing the number of CD8+ cells by the number of CD4+FoxP3+ cells from numbers documented in Figure 5.5 and Figure 5.6.

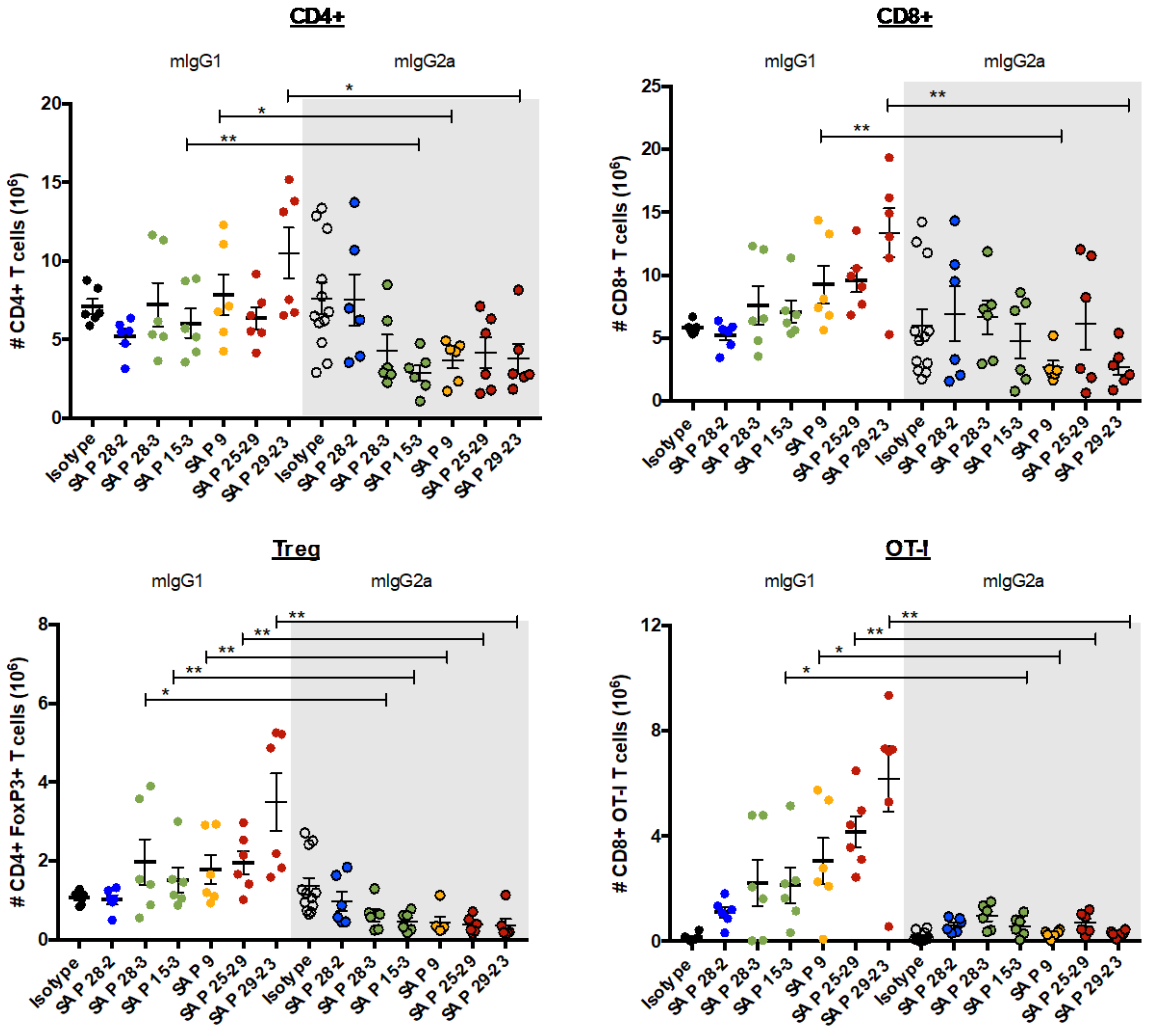

Figure 5.8 Numeration of T cell subsets in the spleens of hOX40$^{+/+}$ KI mice comparing mIgG1 and mIgG2a treated mice

The same experimental set up as described in Figure 5.2 was used. Spleens were harvested from mice on day 4 post vaccination with Ova and anti-hOX40 mAb. Cell populations (CD4+, CD8+, Treg and OT-I) were numerated using flow cytometry. Data is combined from two individual experiments with N=6 mice per treatment group. Each dot represents an individual mouse. Error bars represent mean±SEM. Statistical significance between mIgG1 and mIgG2a treated mice was evaluated using a Mann-Whitney test; * P≤ 0.05, ** P≤ 0.01, *** P ≤ 0.001.

Most notably, the results from these experiments demonstrated an element of domain bias, in some populations, in terms of strength of deletion/agonism. For example, Treg depletion in mIgG2a treated mice and OT-I expansion in mIgG1 treated mice was strongest as mAb binding moved closer to the membrane (i.e CRD4 (Red) binding mAb were stronger than CRD1 (Blue) mAb). This was not seen previously in the blood, therefore, to assess this further we grouped our splenic data into CRD 1+2 binding mAb (SAP 28-2, SAP 28-3 and SAP 15-3) and CRD 3+4 binding mAb (SAP 9, SAP 25-29 and SAP 29-23).

Figure 5.9 demonstrates that the increase in the number of CD4+, CD8+, Treg and OT-I cells with mIgG1 antibodies was larger when mice were treated with anti-hOX40 mAb which bind to CRDs 3+4 in comparison to mAb which bind CRDs 1+2. Likewise, in the Treg population in mIgG2a treated mice there was a greater amount of depletion in mice treated with mAb binding to CRD 3 or 4 in comparison to those binding CRD 1 or 2. There was little to no effect seen in the CD4+ and CD8+ populations when comparing the different mAb with respect to domain binding. This grouping of the results also highlighted that although there was an increase in the number of OT-I cells above the isotype control treated mice with the mIgG2a mAb, indicating their expansion, this was reduced with mAb binding CRD 3 or 4. This however was not the case in the periphery where CRD 3+4 binding mAb were overlapping in terms of OT-I expansion with mAb binding CRD 1+2 (Figure 5.9). This indicates that dependant on location the mAb can have different effects.

As a result of the domain binding bias observed, four mAb from our panel were used in subsequent experiments, one which bound to each CRD of hOX40. This enabled a reduction in the size of experiments and provided a focus on the comparison between domain binding as well as isotype

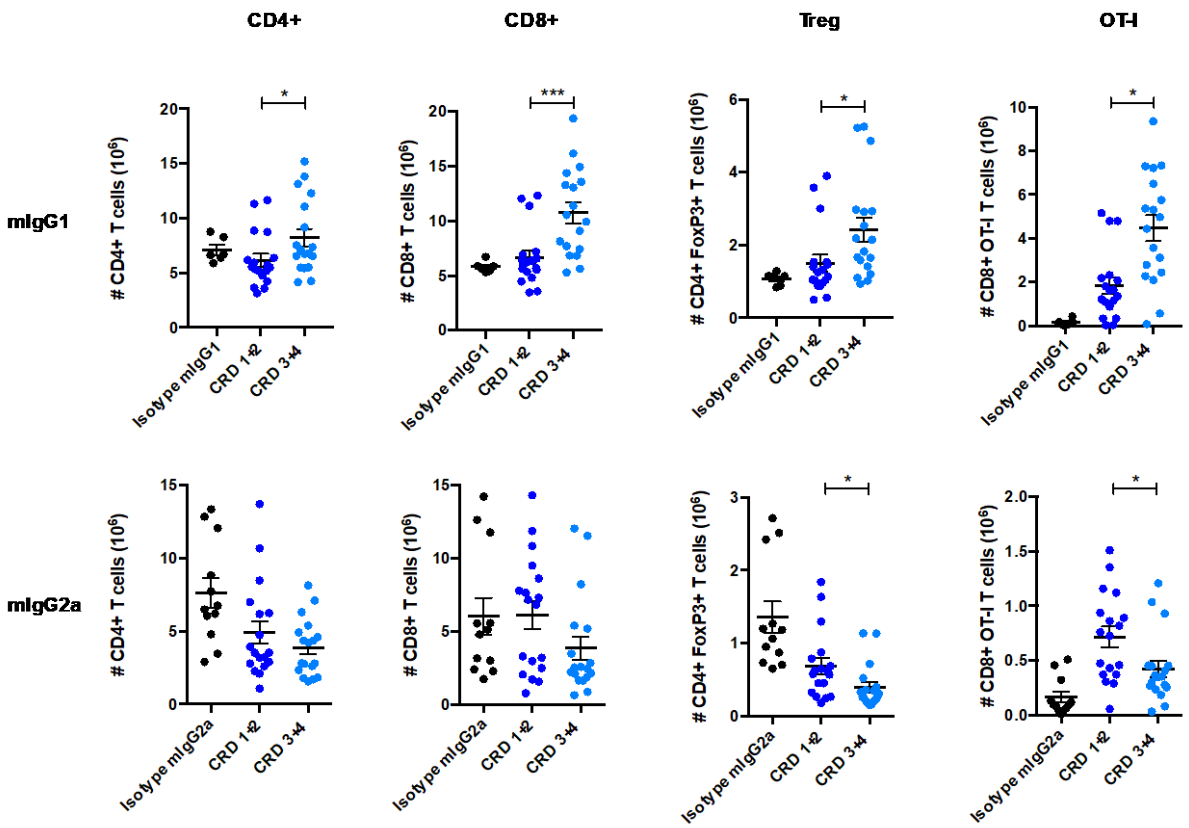

Figure 5.9 Number of T cell subsets within the spleen of hOX40$^{+/+}$ KI mice after treatment with anti-hOX40 mAb grouped into CRD binding domains

Data from Figure 5.4 grouped into CRD binding categories CRD 1+2 (SAP 28-2, SAP 28-3 and SAP 15-3) and CRD 3+4 (SAP 9, Sap 25-29 and SAP 29-23). Graphs from left to right show CD4+, CD8+, Treg and OT-I numbers. The top row represents mIgG1 treated mice and the bottom mIgG2a treated mice. Each dot represents an individual mouse. Error bars represent mean±SEM. Statistical significance was evaluated using a Mann-Whitney test; * P≤ 0.05, ** P≤ 0.01, *** P ≤ 0.001.

5.4 Memory cell phenotype

The results generated in the initial OT-I kinetics model (Figure 5.1) highlighted a discrepancy between the mIgG1 and mIgG2a treated mice; the memory responses generated when mice were re-immunised with SIINFEKL peptide. Mice that had been vaccinated with mIgG1 anti-hOX40 mAb produced a robust re-expansion of OT-I cells upon rechallenge, reaching levels comparable to the primary response in some cases, for example after SAP 25-29 and SAP 29-23 treatment (CRD4 binding mAb). On the other hand, the memory response generated when mice had been vaccinated with a mIgG2a mAb was much weaker, with some of the responses being 10x less than the peak reached during the primary expansion (e.g. SAP 29-23; primary = 63%, memory = 5%).

To understand this difference in memory response further we phenotyped the OT-I T cells in the blood at both the primary and memory stages using the gating strategy shown in Figure 5.10. We first assessed the proportions of short-lived effector cells, SLECs ($CD127^{lo}KLRG1^{hi}$), and memory precursor effector cells, MPECs ($CD127^{hi}KLRG1^{lo}$), as defined by the expression of CD127 and KLRG1 during the primary response [89]. Granzyme B was also assessed as an indicator of cytotoxic potential of the cells. As shown in Figure 5.11 and Table 5.1, the frequencies of MPECs in the blood was higher in the mIgG1 treated mice versus the mIgG2a treated mice. In some cases, the difference was significant; SAP 28-2; 64% vs 46% and SAP 25-29; 64% vs 30% (Figure 5.12). Conversely there was only a 6% difference between SAP 15-3 mIgG1 and mIgG2a; 51% vs. 45% and only a 4% difference with SAP 9; 49% vs. 45%. On the other hand, the frequencies of SLECs in the blood was higher in mIgG2a treated mice compared to mIgG1 treated mice (Table 5.1), however not significant (Figure 5.12). Likewise, the percentage of OT-I cells producing granzyme B was higher in mIgG2a treated mice versus mIgG1 treated mice (Figure 5.11). Again, this was only statistically significant in SAP 28-2 and SAP 25-29 treatment groups (Figure 5.12). Interestingly, the domain correlation previously seen between strength of agonism/depletion in the OT-I splenocyte data also presented itself here particularly in the mIgG2a treated mice; mAb binding CRD 3 or 4 generated a larger percentage of SLECs and Granzyme B+ cells in comparison to mAb binding CRD 1 or 2 (Figure 5.11). To observe this more clearly the mAb were again

grouped according to domain binding; CRDs 1+2 (SAP 28-2 and SAP 15-3) and CRDs 3+4 (SAP 9 and SAP 25-29) and examined with respect to the proportions of SLECs, MPECs and granzyme B producing cells on Day 18. Figure 5.13 shows that mAb binding CRDs 3+4 produced a higher frequency of granzyme B producing OT-I cells; this was true for both mIgG1 and mIgG2a vaccinated mice. Likewise, mIgG2a treated mice also produced a higher frequency of SLECs with mAb binding to CRDs 3+4, this was not the case for mIgG1 treated mice which showed no statistical significance between CRD 1+2 and CRD 3+4 binding mAb. However, there was an upward trend observed as is seen with the mIgG2a mAb which correlated with the domain related increase in granzyme B production, as was seen in the mIgG2a treated mice. There was no significant difference seen between the percentage of MPECs produced regardless of domain binding or isotype.

This difference in proportions of SLECs to MPECs seen between mIgG1 and mIgG2a treated mice supports the data observed in the OT-I kinetics in terms of strength of memory response. mIgG1 treated mice have a higher percentage of MPECs in comparison to mIgG2a treated mice which may be a potential reason for the stronger memory response witnessed in the periphery of mIgG1 vs mIgG2a treated mice.

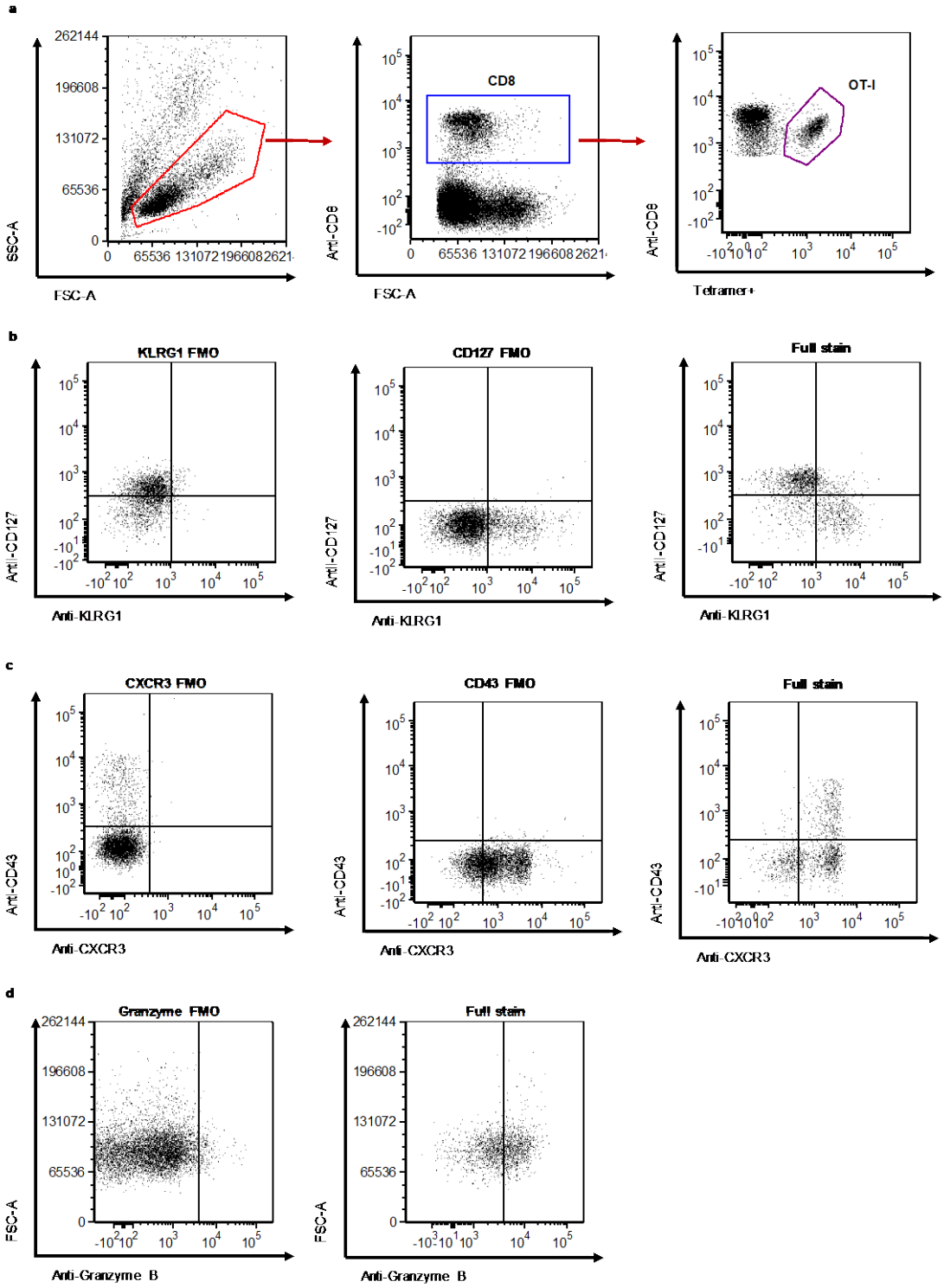

Figure 5.10 Gating strategy used to analyse effector and memory populations in OT-I kinetics

a) To allow detection of OT-I cells blood samples were labelled with CD8 and Tetramer fluorescently labelled antibodies before sequentially being gated on lymphocytes, CD8 cells and lastly OT-I cells. b) Dot plots from left to right showing FMO controls for KLRG1 staining, CD127 staining and a double stained sample, respectively c) Dot plots from left to right showing FMO controls for CXCR3 staining, CD43 staining and a double stained sample, respectively. d) Dot plots from left to right showing an FMO control and a fully stained sample for Granzyme B staining.

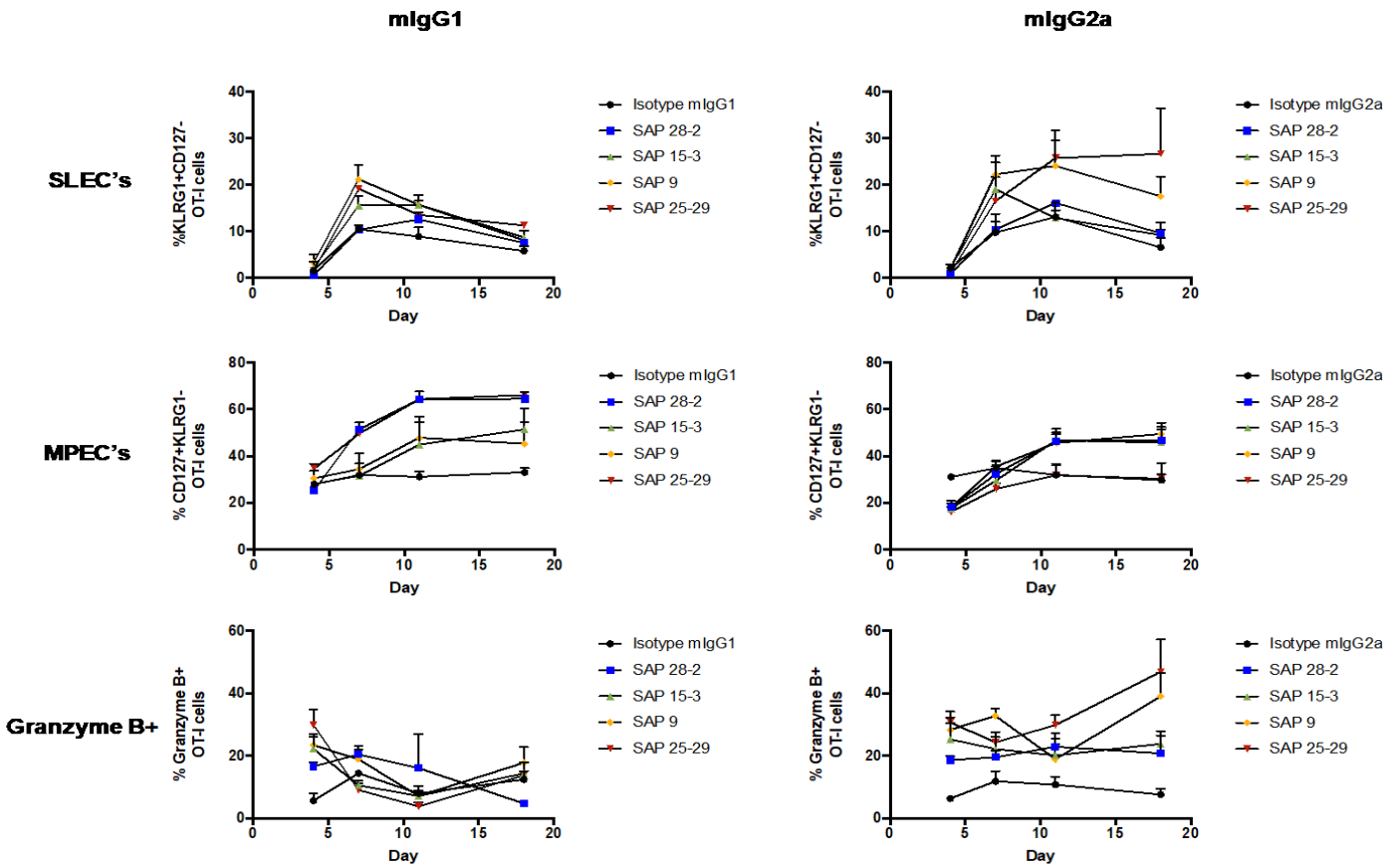

Figure 5.11 Detailed phenotyping of OT-I cells in the primary response to Ova and anti-hOX40 mAb stimulation

$1x10^5$ OT-I cells (in whole splenocytes population) from OT-1/hOX40$^{+/-}$ KI mice were given to hOX40$^{+/+}$ KI mice via i.v. injection. A day later mice were administered 5mg Ova and 100μg of anti-hOX40 mAb (mIgG1 or mIgG2a) via i.p. injection. Blood was drawn on days 4, 7, 11 and 18 and OT-I cells phenotyped using markers KLRG1, CD127 and granzyme B. Error bars represent mean±SEM with N=4 mice per treatment group

Antibody	% MPECs		% SLECs		% Granzyme B	
	mIgG1	mIgG2a	mIgG1	mIgG2a	mIgG1	mIgG2a
SAP 28-2	64.4% ± 3%	46.6% ± 4.8%	7.5% ± 0.6%	9.6% ± 2.3%	4.6% ± 0.3%	20.7% ± 5.6%
SAP 15-3	51.4% ± 8.9%	45.7% ± 6.6%	8.7% ± 0.7%	9.2% ± 1.1%	14.3% ± 3.6%	23.8% ± 4%
SAP 9	66% ± 1%	49.4% ± 4.8%	8.1% ± 2%	17.5% ± 4.2%	17.7% ± 5%	38.9% ± 7.5%
SAP 25-29	45.2% ± 9.2%	30.3% ± 6.8%	11.3% ± 0.3%	26.6% ± 9.7%	13.6% ± 4%	46.8% ± 10.4%

Table 5.1 Percentage of MPECs, SLECs and Granzyme B producing OT-I cells in mIgG1 and mIgG2a anti-hOX40 treated hOX40$^{+/+}$ KI mice

The mean percentage ±SEM was taken from day 18 of the primary response (Figure 5.11) in hOX40$^{+/+}$ KI mice after treatment with anti-hOX40 mAb (mIgG1 and mIgG2a). N = 4 mice per treatment group.

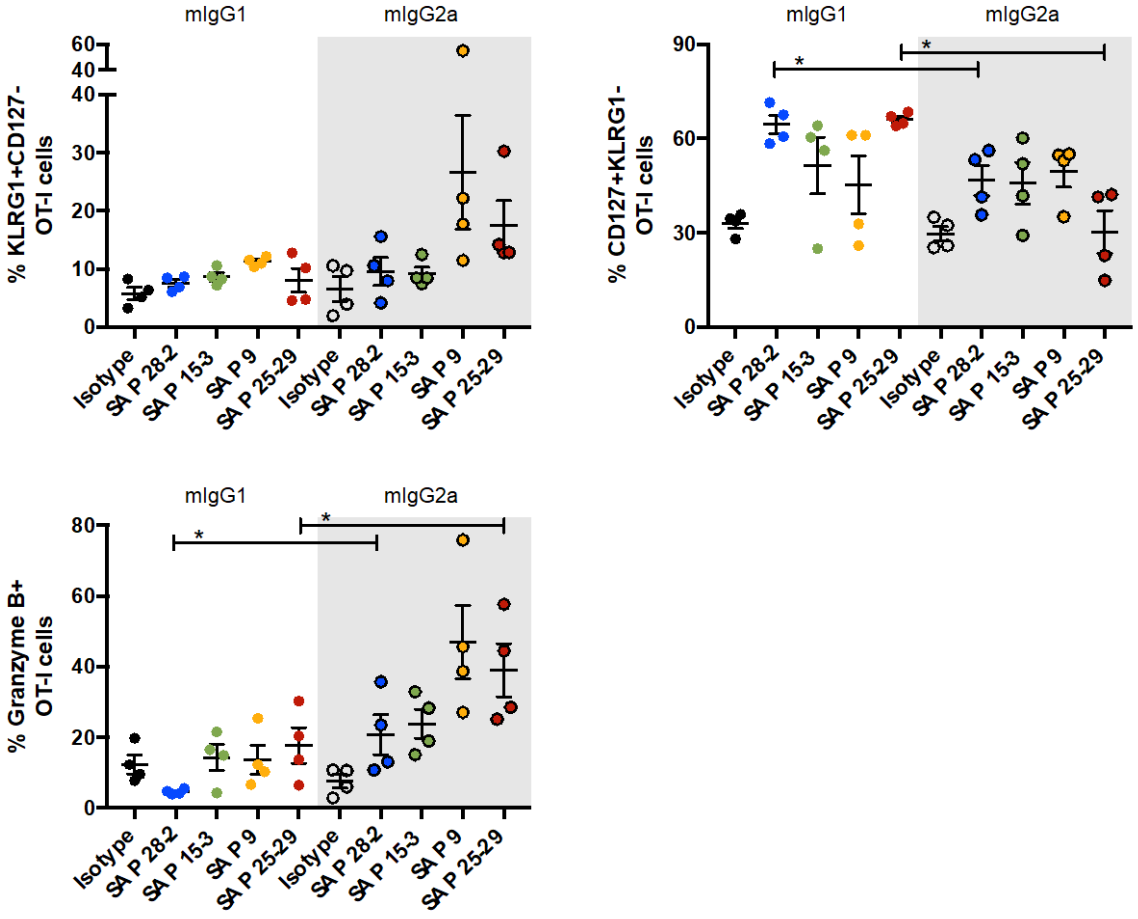

Figure 5.12 Comparison of the percentage of SLECs, MPECs and Granzyme B producing OT-I cells between mIgG1 and mIgG2a anti-hOX40 treated mice on day 18 post treatment.

Day 18 data from Figure 5.11 grouped into mIgG1 (white background) and mIgG2a (grey background) treated groups. Error bars represent mean±SEM. Statistical significance was evaluated using a Mann-Whitney test; ns = non-significant * P≤ 0.05, ** P≤ 0.01, *** P ≤ 0.001.

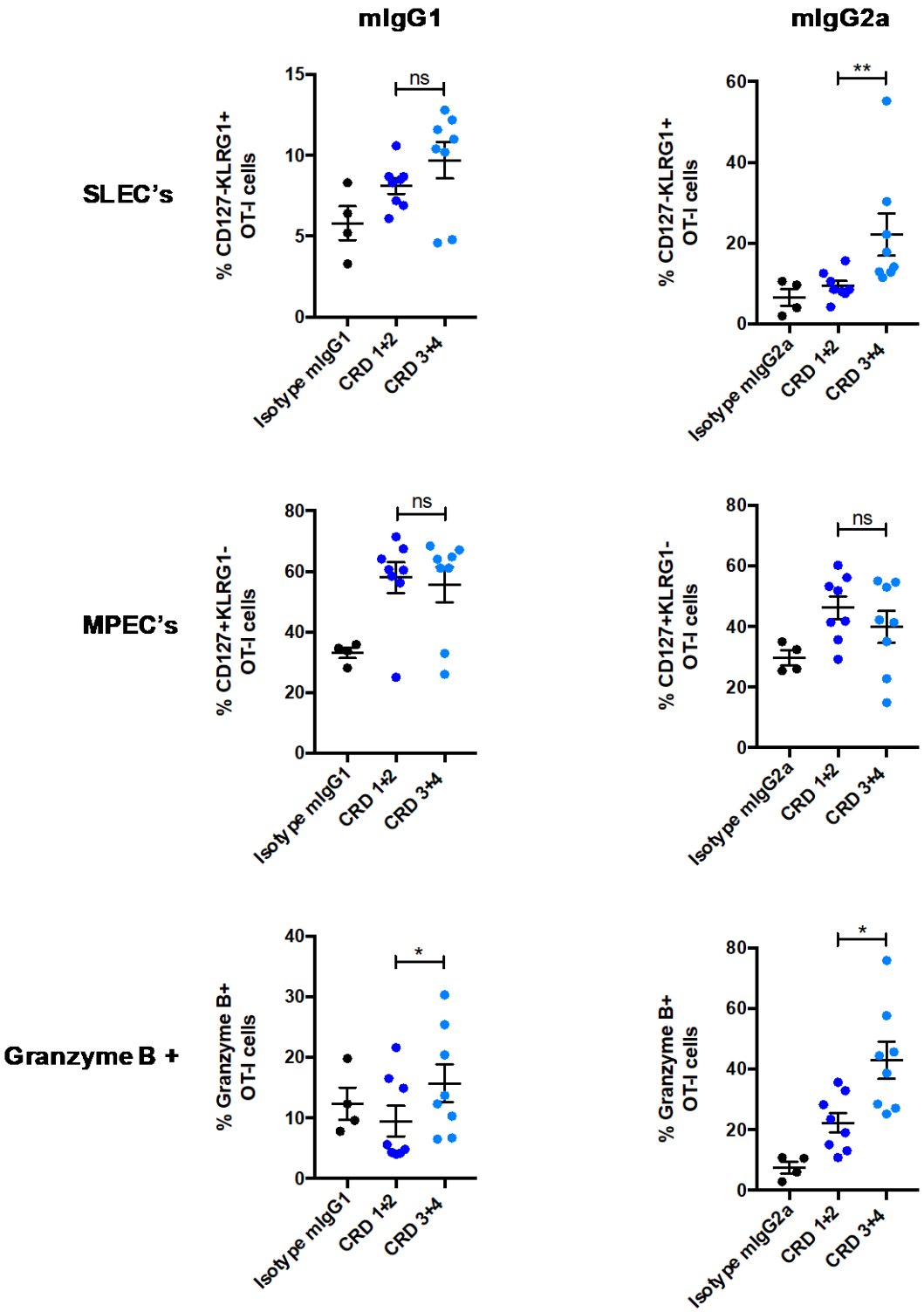

Figure 5.13 Percentage of SLECs, MPECs and Granzyme B producing OT-I cells in the periphery of hOX40$^{+/+}$ KI mice after treatment with anti-hOX40 mAb grouped into CRD binding domains

Day 18 data from Figure 5.11 grouped into CRD binding categories CRD 1+2 (SAP 28-2 and SAP 15-3) and CRD 3+4 (SAP 9 and Sap 25-29). Error bars represent mean±SEM. Statistical significance was evaluated using a Mann-Whitney test; ns = non-significant * P≤ 0.05, ** P≤ 0.01, *** P ≤ 0.001.

It has been shown previously in a number of infection models that the relative frequencies of these three subpopulations (SLEC, MPEC and GzB+) in the primary response does not always correlate with the accumulation of CD8+ T cells during a recall response [89, 340]. It was therefore decided to use the markers, CXCR3 and CD43, which have been shown in a different model [119], to define three distinct populations of memory cells based on expression of these markers rather than the central- and effector- memory T cell classification using CD62L [341]. These authors documented, in a lung infection model, a hierarchy of recall response amongst the memory sub-populations (CXCR3hiCD43lo > CXCR3hiCD43hi > CXCR3loCD43lo) which inversely correlated with effector markers such as KLRG1 [119].

In the memory phase (Day 74-78) of the OT-I model, mice that had been treated with anti-OX40 mIgG1 m Ab generally gave rise to a higher frequency of cells with a phenotype that matched those reported previously to have a greater capacity to proliferate (CXCR3hiCD43lo and CXCR3hiCD43hi), in comparison to those mice that had been treated with a mIgG2a isotype (Figure 5.14, Figure 5.15, Figure 5.16, Figure 5.17). This difference in frequencies between mIgG1 and mIgG2a treated mice was sustained from the contraction period in the primary response (D18), into the resting memory period (D39), and within the memory response itself (D74-D78). There were however some exceptions; SAP 15-3 treated mice at day 18 produced similar levels of CXCR3hiCD43lo and CXCR3hiCD43hi OT-I cells regardless of isotype (mIgG1 = 79% and mIgG2a = 80%, respectively). Likewise, at peak expansion after rechallenge with SIINFEKL peptide, mIgG1 and mIgG2a SAP 25-29 treated mice showed similar levels of highly proliferative OT-I cells (mIgG1 = 84% and mIgG2a = 85%, respectively). Interestingly, despite having the smallest memory recall amongst the mIgG2a treated mice (Figure 5.2), SAP 28-2 treated mice at day 74 showed the opposite to what was witnessed with all other mAb, 91% of OT-I cells in mIgG2a treated mice presented with a phenotype suggesting highly proliferative cells (CXCR3hiCD43lo), whereas 82% of OT-I cells in the mIgG1 treated mice had this same phenotype. This data indicates that CXCR3/CD43 expression is not influenced by mAb domain binding.

Hikono et al. previously described CD8+ CXCR3loCD43lo expressing cells as effector-like memory cells [119]. In the OT-I model employed here, a trend in the frequency of these cells and the mAb isotype was observed, however it was not as

clear cut as with the highly proliferative cells described above. SAP 9 mIgG2a treated mice produced a higher frequency of CXCR3loCD43lo expressing OT-I cells than mIgG1 treated mice at day 18, day 39, day 74 and day 78 (Figure 5.16). However, this was only true for the other mAb (SAP 28-2, SAP 15-3 and SAP 25-29) at day 39 and day 78. On days 18 and 74, mIgG1 and mIgG2a treated mice produced the same or similar levels of CXCR3loCD43lo OT-I cells (Figure 5.14, Figure 5.15, Figure 5.17). This data did not seem to be skewed by domain binding.

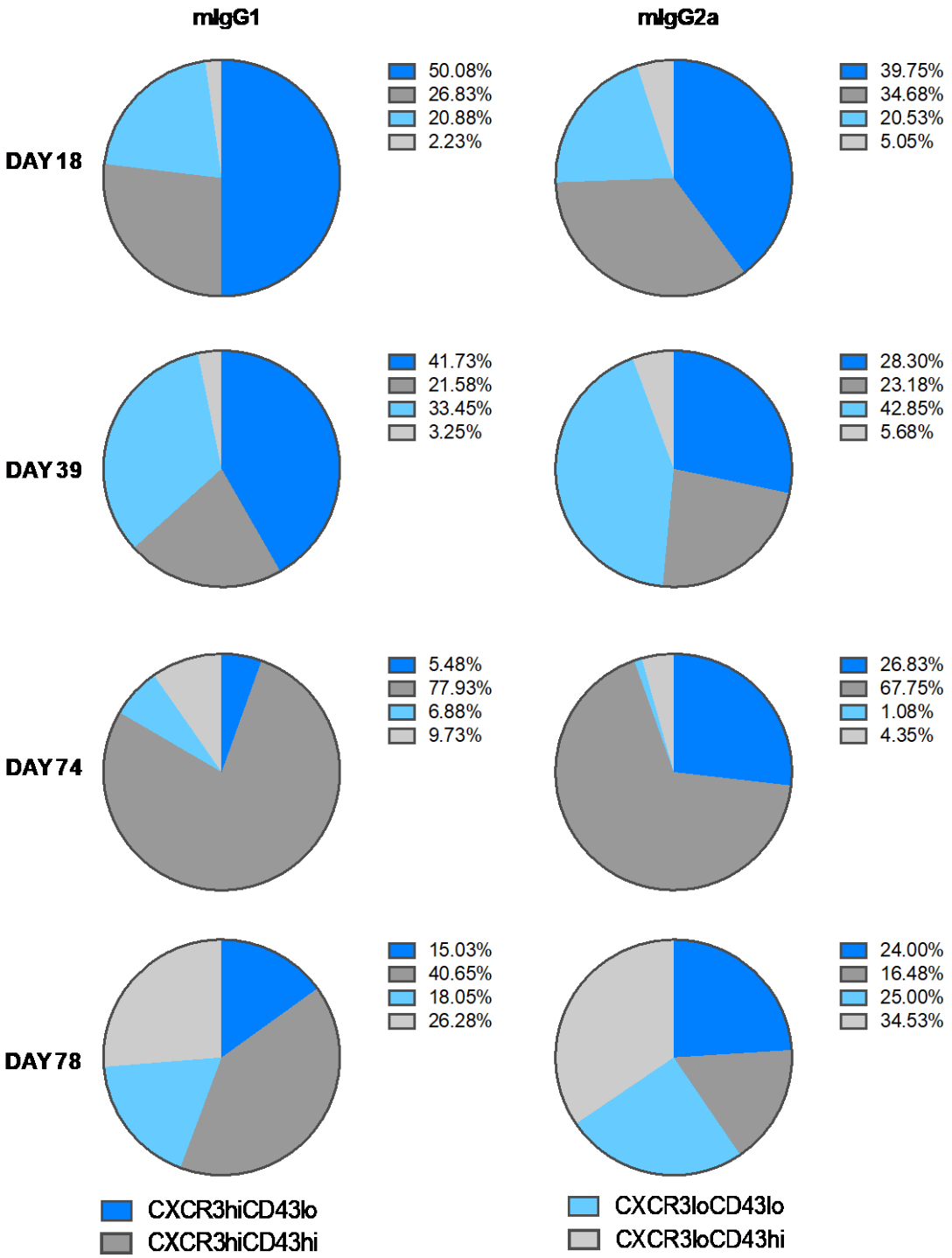

Figure 5.14 Phenotypic analysis of memory OT-I cells in SAP 28-2 mIgG1 and mIgG2a treated hOX40$^{+/+}$ KI mice

1x10^5 OT-I cells (in whole splenocytes population) from OT-1/hOX40$^{+/-}$ KI mice were given to hOX40$^{+/+}$ KI mice via i.v. injection. A day later mice were administered 5mg Ova and 100μg of anti-hOX40 mAb (mIgG1 or mIgG2a). Once OT-I cells were <10% of the total CD8+ population mice were re-challenged with 30nM SIINFEKL peptide. Subsequently mice were bled on days 74, 78, 85 and 92 (post initial vaccination) and OT-I cells phenotyped using markers CXCR3 and CD43 to categorise memory populations as described in a previous model [119]. Percentages represent the % of OT-I cells out of the total CD8+ population in SAP 28-2 treated mice. Pie charts on the left represent populations in mIgG1 treated mice on days 18, 39, 74 and 78 and pie charts on the right mIgG2a treated mice at the same time points. Data is from an individual experiment with N=4 mice per treatment group.

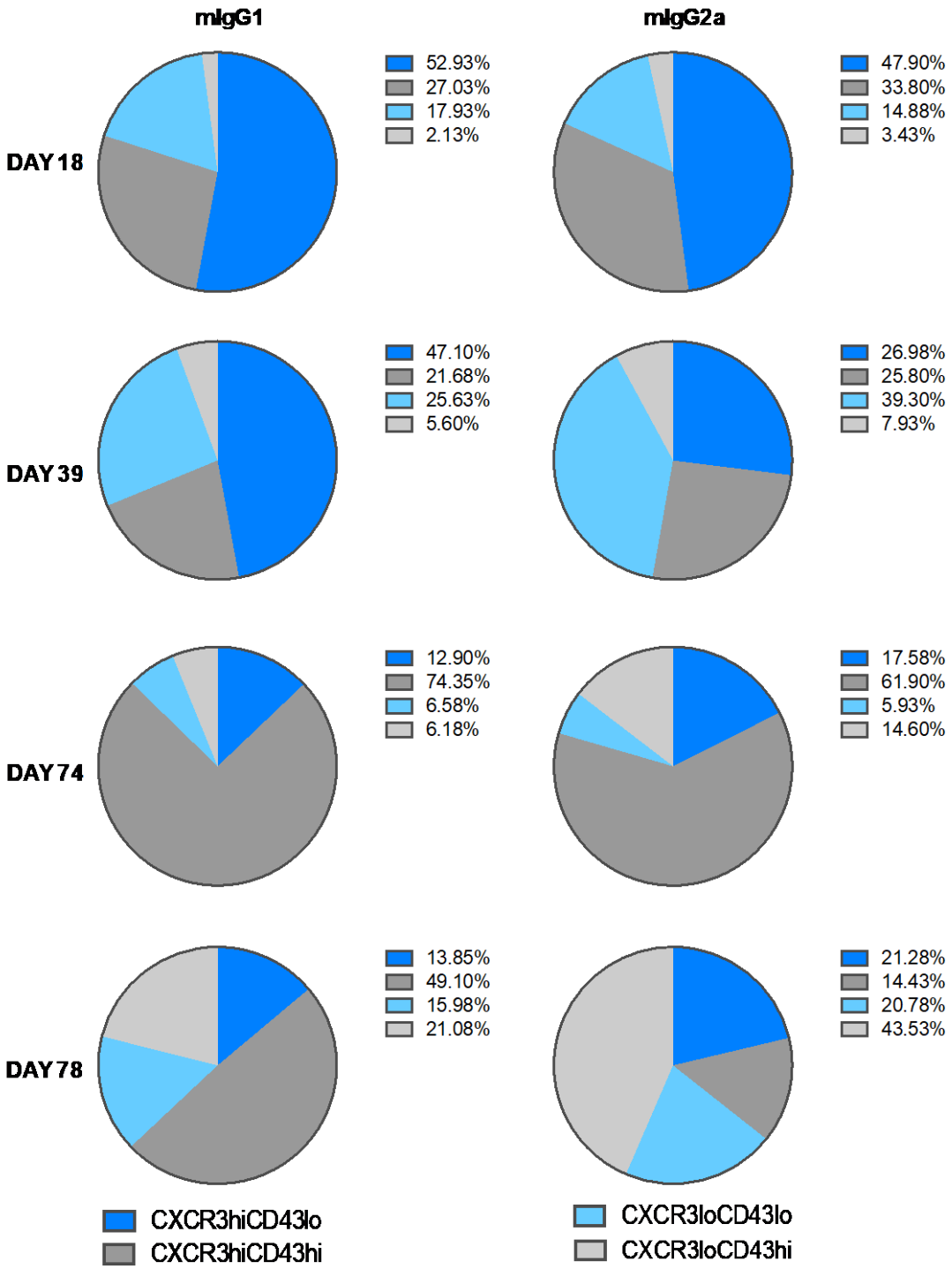

Figure 5.15 Phenotypic analysis of memory OT-I cells in SAP 15-3 mIgG1 and mIgG2a treated hOX40$^{+/+}$ KI mice

The same experimental set up as described in Figure 5.14 was used. Percentages represent the % of OT-I cells out of the total CD8+ population in SAP 15-3 treated mice. Pie charts on the left represent populations in mIgG1 treated mice on days 18, 39, 74 and 78 and pie charts on the right mIgG2a treated mice at the same time points. Data is from an individual experiment with N=4 mice per treatment group.

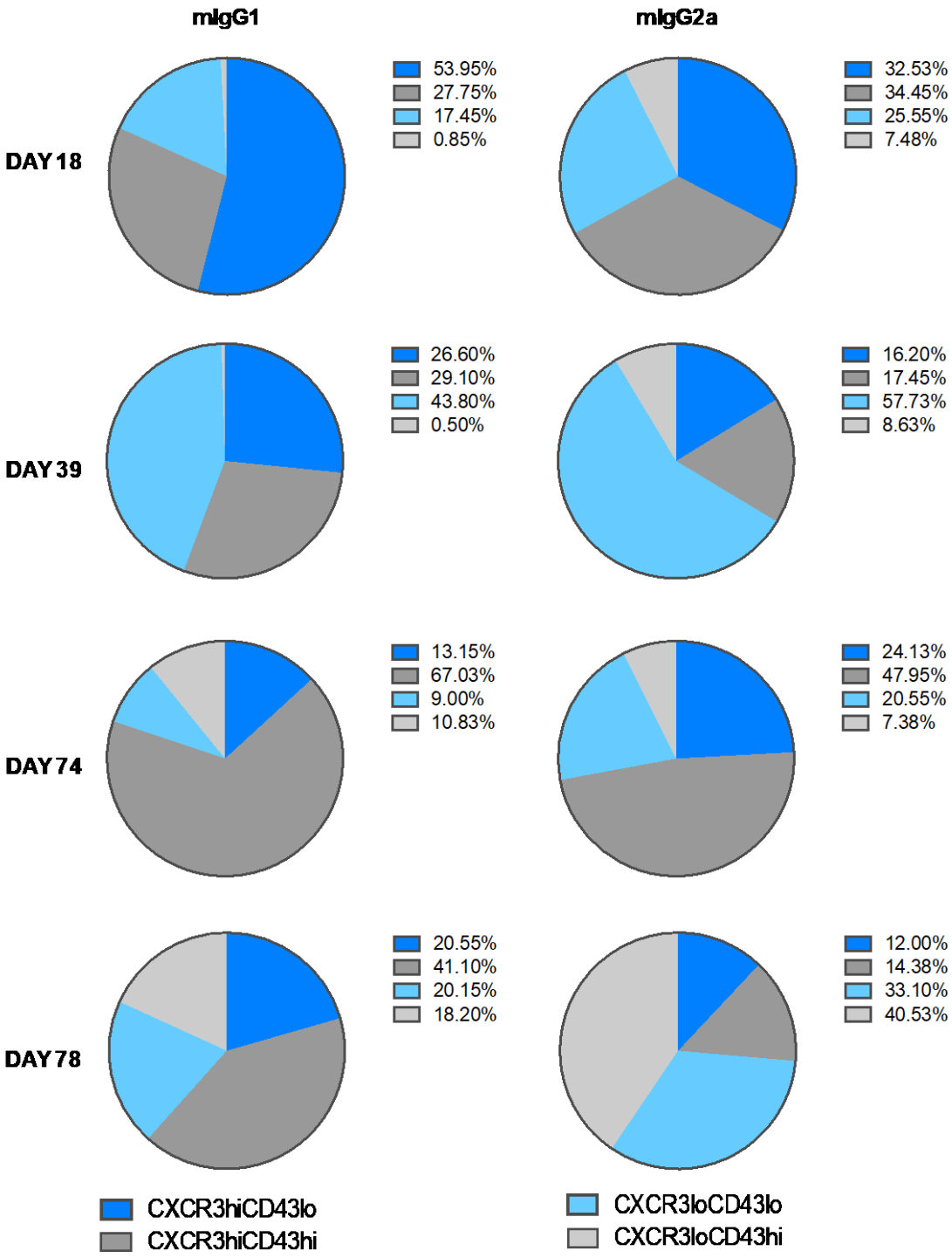

Figure 5.16 Phenotypic analysis of memory OT-I cells in SAP 9 mIgG1 and mIgG2a treated hOX40$^{+/+}$ KI mice

The same experimental set up as described in Figure 5.14 was used. Percentages represent the % of OT-I cells out of the total CD8+ population in SAP 9 treated mice. Pie charts on the left represent populations in mIgG1 treated mice on days 18, 39, 74 and 78 and pie charts on the right mIgG2a treated mice at the same time points. Data is from an individual experiment with N=4 mice per treatment group.

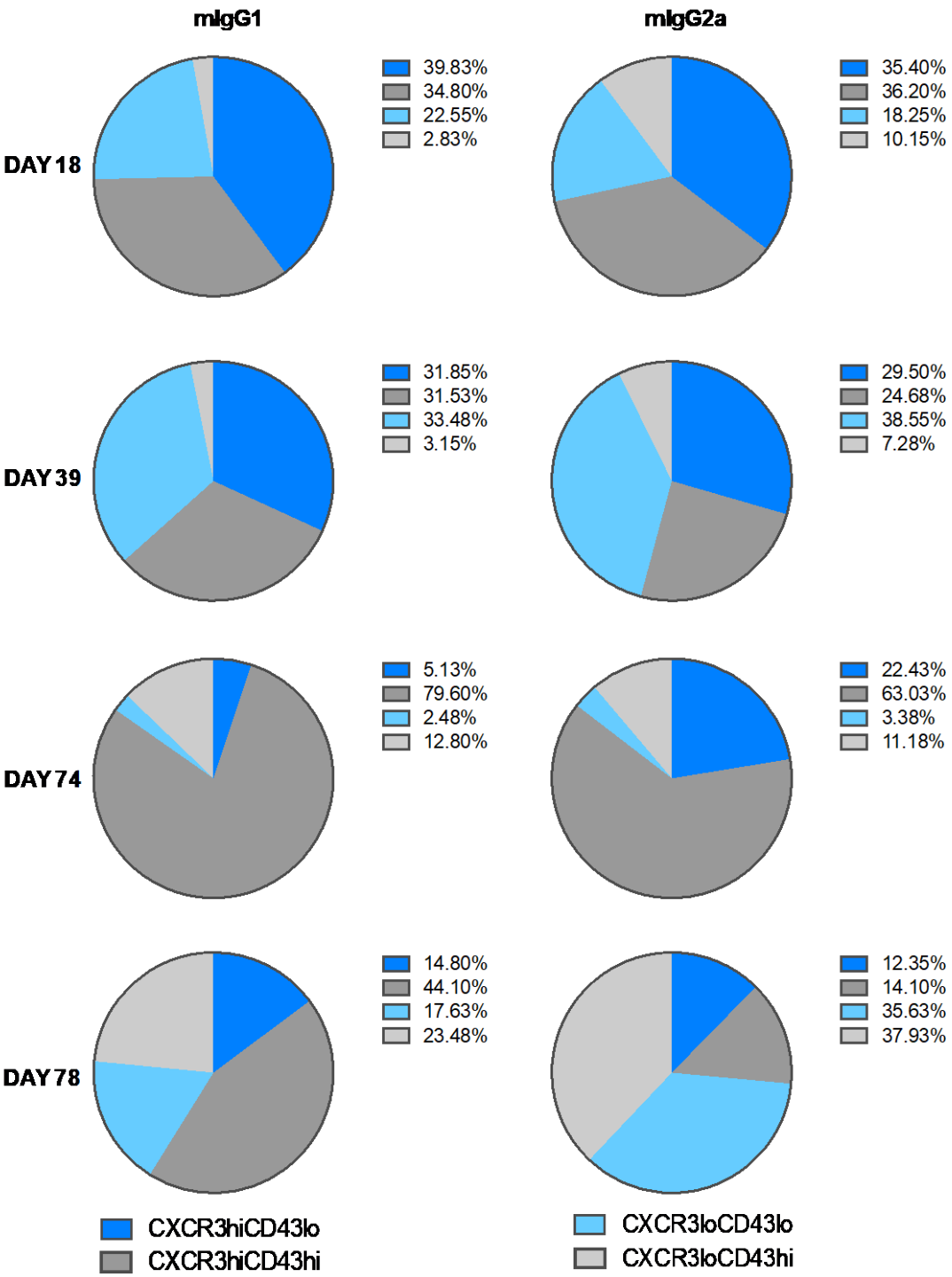

Figure 5.17 Phenotypic analysis of memory OT-I cells in SAP 25-29 mIgG1 and mIgG2a treated hOX40$^{+/+}$ KI mice

The same experimental set up as described in Figure 5.14 was used. Percentages represent the % of OT-I cells out of the total CD8+ population in SAP 25-29 treated mice. Pie charts on the left represent populations in mIgG1 treated mice on days 18, 39, 74 and 78 and pie charts on the right mIgG2a treated mice at the same time points. Data is from an individual experiment with N=4 mice per treatment group.

5.5 Effect of anti-hOX40 mAb on OT-I cells within WT C57BL/6 mice

To probe the mechanisms underpinning the ability of both mIgG1 and mIgG2a mAb to cause expansion of antigen specific T cells in the OT-I model, in both the periphery (Figure 5.2) and the spleen (Figure 5.5 and Figure 5.6) CD8+ OT-I/hOX40$^{+/-}$ KI cells were purified and transferred into WT C57BL/6 mice. In doing this the anti-hOX40 mAb would only be able to act directly on the transferred OT-I cells which express the hOX40 receptor in a heterozygote manner. Figure 5.18 demonstrates that whilst mIgG1 mAb were able to act directly on the transferred OT-I cells and cause their expansion following Ova immunisation, the mIgG2a mAb were no longer able to cause expansion of the OT-I cells as had been seen previously in the hOX40$^{+/+}$ KI mouse (Figure 5.2). This result suggests that the mIgG2a mAb need to act on supporting cells/non-CD8+ cells to allow for the expansion of OT-I cells in the periphery.

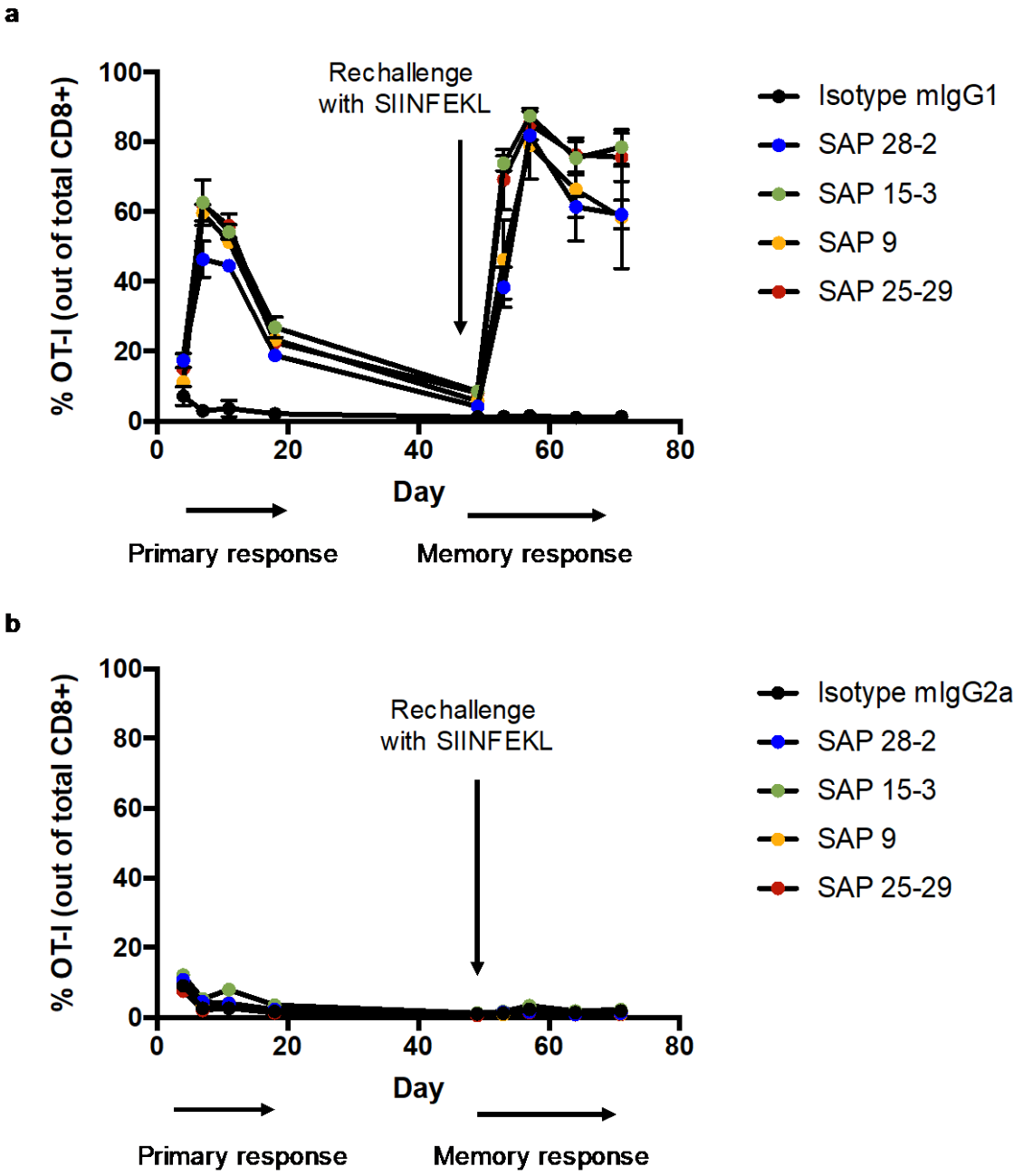

Figure 5.18 Measurement of OT-I kinetics in the blood of WT C57BL/6 mice after immunisation with Ova in the presence of anti-OX40 mAb

$1x10^5$ OT-I cells (purified from splenocytes) from OT-1/hOX40$^{+/-}$ KI mice were given to WT C57BL/6 mice via i.v. injection. A day later mice were administered 5mg Ova and 100μg of anti-hOX40 mAb (mIgG1 or mIgG2a) via i.p. injection. a+b) Blood was drawn on days 4, 7, 11 and 18 to monitor the primary response. Mice were bleed on day 49 to check OT-I levels were low enough for a re-challenge with 30nM SIINFEKL peptide which took place on day 50. Blood was then drawn on days 53, 57, 64 and 71 to monitor the memory response. OT-I cells were detected in the blood using CD8 and the tetramer as markers. Data is representative of 2 independent experiments with N=3 mice per treatment group. Error bars represent mean±SEM.

5.6 Endogenous response to anti-hOX40 mAb in hOX40$^{+/+}$ KI mice

As a more rigorous test of the T cell immunity produced by the anti-hOX40 mAb, the ability of the mAb to elicit an endogenous response was assessed *in vivo,* by measuring the response of hOX40$^{+/+}$ KI mice after the administration of Ova and our mIgG2a anti-hOX40 mAb (SAP 15-3 and SAP 25-29) in the absence of the OT-I cells. The repertoire of CD8+ cells in C57BL/6 mice contains a small proportion of SIINFEKL specific cells. There is an expansion of this population after immunisation with Ova alone [342] so it was of interest to assess if the anti-hOX40 mAb were able to elicit the same effects as had been seen when mice had received adoptively transferred OT-I cells. hOX40$^{+/+}$ KI mice were therefore immunized with Ova and either SAP 15-3 mIgG2a or SAP 25-29 mIgG2a.

Figure 5.19 demonstrates that treatment with mIgG2a anti-hOX40 significantly reduced the number of CD4+ and Treg cells within the spleen as had been witnessed previously in mice that had received an OT-I adoptive transfer. Interestingly, the CD8+ population was also depleted which had not been previously witnessed in mice which had a transfer; this population of T cells was previously unaffected (Figure 5.6). Furthermore, there was a trend indicating expansion of SIINFEKL-Tetramer + cells, even if small, suggesting that these mAb maintain the ability to elicit expansion of CD8+ Ova specific cells despite the initial low numbers. Having a lower number of antigen specific cells more closely represents the tumour microenvironment giving promise that our mAb would be therapeutically beneficial. The CD8:Treg ratio was also significantly increased in both anti-OX40 treatment groups, again providing evidence that these mAb have the potential to be beneficial in a tumour setting; explored in the following chapter.

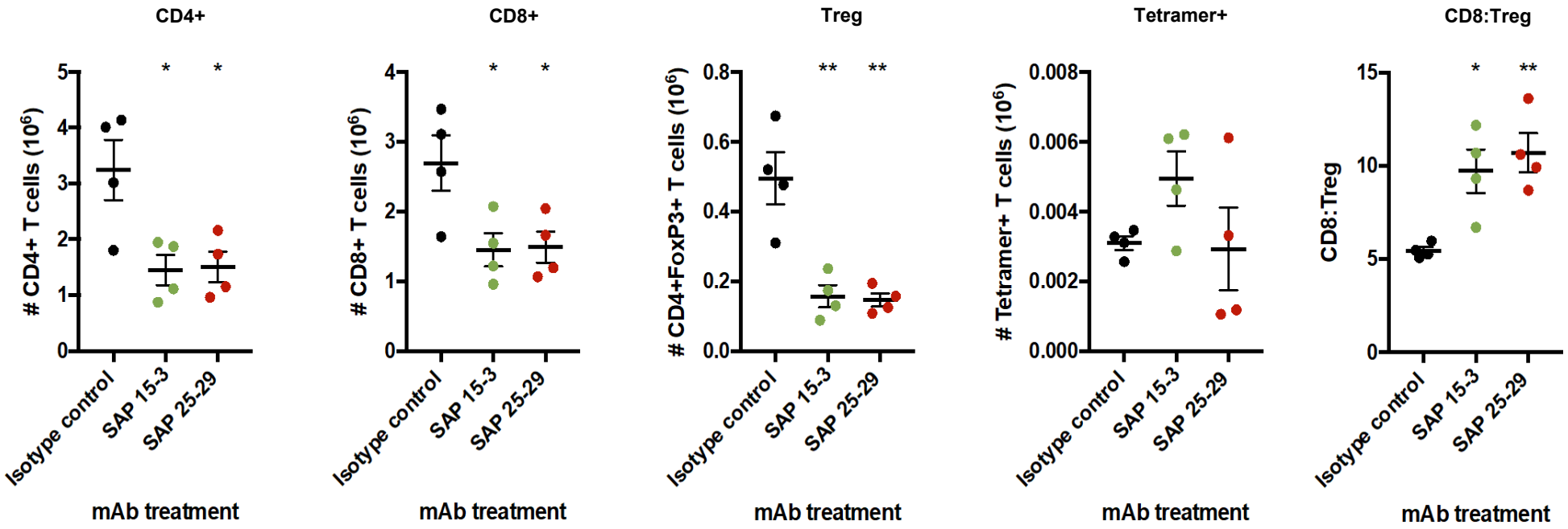

Figure 5.19 Endogenous response of hOX40$^{+/+}$ KI mice to Ova and anti-hOX40 mAb vaccination

hOX40$^{+/+}$ KI mice were vaccinated with 5mg Ova and 100μg anti-hOX40 mAb (mIgG2a) via i.v injection. Spleens were harvested on day 4 post vaccination and T cell populations (Left to right: CD4+, CD8+, CD4+FoxP3+, Tetramer+ and CD8:Treg) numerated using flow cytometry. Each dot represents an individual mouse with N=4 per treatment group. Error bars represent mean±SEM. Statistical significance was evaluated using an unpaired students t-test; * P≤ 0.05, ** P≤ 0.01, *** P ≤ 0.001.

5.7 Discussion

It is well known that an antibodies Fc region, and hence isotype, dictate effector function of a mAb due to differences in Fc receptor interaction [157]. Isotype choice has been shown to be important for therapeutic success dependent upon which effector mechanism is required i.e. direct tumour targeting, receptor blocking, receptor agonism etc. Initially the results presented in Chapter 3 revealed the classical difference in effect between a mIgG1 and mIgG2a TNFR targeting mAb; in a human PBMC proliferation assay mIgG1 mAb caused an increase in proliferation of CD8+ T cells, on the other hand mIgG2a mAb resulted in a decrease in the percentage of proliferating cells compared to the isotype control (Chapter 3, Figure 3.24). This was shown to be due to isotype as when mAb were isotype switched, those changing from a mIgG1 to a mIgG2a lost their ability to cause proliferation and in contrast, when switching a mIgG2a to a mIgG1, proliferation of CD8 T cells was gained.

Surprisingly, data from *in vivo* studies reported here indicated a difference in effect. In the setting of an OT-I/hOX40$^{+/-}$ KI transfer into hOX40$^{+/+}$ KI mice both mIgG1 and mIgG2a anti-hOX40 mAb were able to cause expansion of CD8+ OT-I T cells within the periphery to similar levels with the exception of SAP 28-2 which produced a significantly lower percentage of OT-I cells as a mIgG2a compared to a mIgG1. This difference in OT-I cells could be linked to the fact that this mAb, when isotype switched from a mIgG1 to a mIgG2a, exhibited a reduced affinity to hOX40 as shown by SPR analysis (Figure 3.13). This however did not hold true when comparing mIgG1 and mIgG2a binding to transfected cells (Figure 3.18) and thus may reflect an artefact of SPR making it difficult to conclude if lack of binding is an explanation for the reduced agonism or whether the mIgG2a mAb actually has lower activity in comparison to the mIgG1 mAb. Upon numerating the sub populations of T cells within the spleen of these mice revealed that the mIgG2a anti-hOX40 mAb caused depletion of cells, specifically Tregs and CD4+ T cells with little to no affect on the CD8 population. The strength of deletion seen amongst these T cell subsets appears to be linked to the levels of hOX40 expression. In Chapter 3; Section 3.2 it was shown that there was a hierarchal expression pattern of hOX40 on T cell subsets; Treg>CD4+ >CD8+. The greatest amount of deletion in the Treg population supports previously published data

[165], suggesting that preferential depletion of this subset is due to their higher levels of receptor expression. Conversely, mIgG1 anti-hOX40 mAb caused expansion of the T cell subsets in a manner not correlated to receptor expression.

From these experiments a domain trend in terms of agonistic and depleting ability was also observed. mAb which bound to CRDs 3+4 were stronger depleters as a mIgG2a mAb and more potent agonists as a mIgG1 mAb when compared to antibodies which bound to CRDs 1+2 of hOX40. Why specific binding domains correlate with stronger effector functions is not immediately clear. However, Cleary et al. demonstrated recently with the TNFR family member 4-1BB that ADCC was favoured by mAb binding more membrane proximal epitopes, conversely ADCP favoured a slightly more distal epitope [329]. Rationale behind this was that for efficient ADCC small immune synapses were required to maximise the exposure of the target cell to cytotoxic granules, therefore it is favourable to bind a membrane proximal domain. On the other hand, ADCP relies on the formation of a stable multimeric complex between the Ag, mAb and FcγR followed by the formation of the phagosome which when binding a highly membrane proximal domain may result in steric hindrance, hence a more membrane distal domain was favourable. This same notion could be applicable to hOX40 due to the broadly similar structure and size of TNFR family members. Further work is required to explain why mAb binding CRDs 3+4 are favourable for both agonism and depletion when targeting hOX40. It would be interesting to investigate the type of Fc-mediated effector function used by these anti-hOX40 mAb to determine if what was seen with 4-1BB holds true for other TNFR family members.

We know from previous studies that the ability of IgG isotypes to bind certain FcγR, which subsequently controls effector function, varies [144, 343]. It has been shown that mAb targeting TNFR receptors rely upon activatory FcγR interaction for the deletion of target cells and upon the inhibitory receptor for agonistic activity [155, 165]. mIgG2a mAb have a higher specificity for the activatory receptors in contrast to mIgG1 mAb which favour interaction with the inhibitory receptor. This is therefore the most likely reason for the ability of our mIgG2a anti-hOX40 mAb to cause depletion of target cells. This superior affinity for the activatory FcγRs over mIgG1 mAb and resultant deletion of suppressive Tregs may also explain the mechanism behind their ability to expand OT-I cells in the blood and spleen of $hOX40^{+/+}$ KI mice. Therefore, to dissect the mechanisms behind the ability of both

isotypes of mAb to cause expansion of OT-I cells, OT-I/hOX40$^{+/-}$ cells were adoptively transferred into WT mice. By doing this the anti-hOX40 mAb were no longer able to bind to cells within the host mouse but only to the transferred OT-I cells. We found that mIgG1 anti-hOX40 mAb were able to expand OT-I cells in the periphery as had been seen previously in the huOX40 $^{+/+}$ KI mice, however the mIgG2a mAb were no longer able to cause any expansion of these cells above isotype control. This suggests that the mIgG1 mAb are able to cause direct agonism of the OT-I /hOX40$^{+/-}$ cells resulting in their expansion, whereas the mIgG2a mAb require hOX40 expressing non-CD8 cells to generate expansion of OT-I/hOX40$^{+/-}$ cells. It is likely the depletion of these surrounding non-CD8 cells, in particular Tregs, alleviate suppression of the antigen specific cells and allow for their expansion.

A striking difference observed in our OT-I model between mice treated with the different isotypes of anti-hOX40 mAb was the strength of re-expansion of OT-I cells after mice had been rechallenged with SIINFEKL peptide. mIgG1 mAb produced a robust response whereas mIgG2a mAb did not. To begin to understand why this was the OT-I cells were phenotyped within the primary, resting memory and memory phases of the response. We assessed the proportion of SLECs and MPECs within the primary response as defined by the expression of CD127 and KLRG1 alongside analysing the expression of CXCR3 and CD43 to determine three distinct memory populations. In a previous model, a hierarchy of recall response amongst the memory sub-populations (CXCR3hiCD43lo > CXCR3hiCD43hi > CXCR3loCD43lo) was proposed [119]. We found that within the primary response there was only a slight difference in the MPEC populations, described by CD127^{hi}KLRG1^{lo} expression, between the mIgG1 and mIgG2a treated mice. However, from as early as day 18 and through to day 92 we discovered that mice treated with a mIgG1 anti-hOX40 mAb generated a higher percentage of CXCR3^{hi}CD43^{lo} and CXCR3^{hi}CD43^{hi}, highly proliferative cells in comparison to mice treated with a mIgG2a mAb. These findings would explain the disparity seen in the levels of memory cells generated in mice treated with mIgG1 versus mIgG2a mAb. On the other hand, a higher percentage of SLECs and granzyme B producing cells were generated in the primary response of mIgG2a treated mice, as well as a higher frequency of effector-like memory cells as described by CXCR3^{lo}CD43^{lo} expression from day 18 through to day 92. This opposing difference in balance between the percentages of potent effector and

effector-like cells (generally higher in mIgG2a treated mice) versus the percentage of highly proliferative cells (generally higher in mIgG1 treated mice) together with the OT-I splenic data highlight the disparity between the mechanisms of the two different isotypes of mAb.

As with the splenic OT-I data, a domain trend was also observed when assessing the percentage of SLECs and granzyme B+ cells in the primary OT-I response. Anti-hOX40 mAb binding CRDs 3+4 produced a higher % of granzyme B+ OT-I cells with both isotypes and with mIgG2a treated mice a higher percentage of SLECs were produced with CRD 3+4 binding mAb. This data, along with the OT-I splenic data, highlights the possibility that in the case of the anti-hOX40 mAb examined here, binding domain may be just as important a consideration as isotype when deciding upon the most appropriate therapeutic mAb.

A good indicator of prolonged survival in both mouse and human tumours is a high CD8:Treg ratio [344]. Within the spleen of our mIgG2a treated mice there was a statistically significant increase in the CD8:Treg ratio in 4/6 treatment groups, whereas there was no change between isotype and treatment in the mIgG1 treated mice. This evidence would suggest that potentially a mIgG2a anti-hOX40 mAb would provide better therapy in a cancer setting compared to a mIgG1 anti-hOX40 mAb. However, this increase in CD8:Treg ratio would have to hold true inside the tumour as this is where it has been described to be most beneficial [345, 346]. The results from the experiment where endogenous OT-I responses were examined suggest that this may be true as the mIgG2a mAb in this set up still maintain the ability to increase the CD8:Treg ratio in a setting that more closely represents a tumour (i.e. where frequency of antigen specific cells is low). However, the total number of CD8+ T cells was reduced with the mIgG2a isotype which was not seen in experiments where mice had received an adoptive transfer of OT-I cells. Although in terms of the CD8:Treg ratio this decrease had no effect, it is important to bear in mind that when moving forward into the tumour models mice will not receive an adoptive transfer of cells or be vaccinated with Ova in conjunction with the anti-hOX40 mAb treatment. This may therefore have an impact on the CD8 response to mAb, as has been suggested by the results from the endogenous experiment.

Within the next chapter these various aspects were assessed in a tumour model i.e. if one isotype of mAb and therefore one particular effector function provides

more efficient therapy and also whether the domain binding preferences witnessed in this chapter play a role in a therapeutic setting.

Chapter 6 Efficacy of anti-hOX40 mAb in mouse tumour models

6.1 Introduction

There is substantial preclinical evidence suggesting that anti-OX40 mAb may provide successful cancer immunotherapy; both as a monotherapy and in combination with other agents (reviewed in [278, 319]). As discussed in the Introduction and Chapter 3, there are several agonistic anti-OX40 mAb being tested in early phase clinical trials, however conflicting results between *in vitro* and *in vivo* data, as well as conflicts between effects seen in murine models and human patients, highlights the need for more comprehensive studies of the mAb so that their biology and mechanism of action are more thoroughly understood.

In Chapter 4, it was shown that OX40 antibodies with a mIgG2a isotype had the potential to affect the CD8:Treg ratio. It has been previously documented that this ratio of cells is of particular importance within tumours. It is reported that a high CD8:Treg within human tumours is associated with prolonged survival [346] which is further supported by mouse models in which depletion of Tregs and thus increasing the CD8:Treg ratio allows for anti-tumour immunity and rejection of tumour [347]. However, somewhat paradoxically, more recent analysis of human cancers has shown that dependent on the type of cancer, high FoxP3+ Treg infiltration can be associated with improved survival [348]. Thus it will be important to understand how OX40 antibodies affect this ratio and impacts on therapeutic potential.

It is also important to note that whilst anti-hOX40 monotherapy has shown benefit in small immunogenic tumours [221, 349], efficacy against larger, metastatic, immunologically ‘cold’ tumours, a situation much closer to that of human patients, is much less impressive [349]. Hence, as with other targets, attempting to combine anti-hOX40 immunotherapies with other agents is being trialled to overcome these obstacles. Pre-clinical data has demonstrated the benefit of combining anti-mOX40 reagents, namely OX86, with three other therapeutic strategies. Firstly, increasing antigen release through surgery [276], radiotherapy [350], chemotherapy [274] and vaccination [351]. Secondly, via adoptive T cell therapy

[352], and lastly via tackling immunosuppression through checkpoint blockade [282, 283]. It has also been shown that combinations with anti-4-1BB mAb can synergise with anti-OX40 mAb to stimulate antigen specific CD8 T cells resulting in robust effector function and rejection of established tumours [353]. It is therefore unsurprising that 10 out of the 11 current anti-hOX40 clinical trials being recruited for are in combination with other agents; be it another mAb, chemotherapy or radiotherapy.

Therefore, it was desirable to further understand the effects of our panel of mAb in a tumour setting and compare them with the data in the OT-I model (discussed in Chapter 5). Furthermore, it was desired to determine if alterations in the proportion of different T cell subsets was beneficial to the eradication of tumour and whether there was a preference for either isotype or domain binding of the mAb, or both in terms of therapeutic efficacy. In addition, the efficacy of the panel of mAb was compared with current clinically-relevant anti-hOX40 mAb.

6.2 E.G7-Ova tumour model

To evaluate the immunotherapeutic potential of the panel of anti-hOX40 mAb the E.G7-Ova lymphoma model was chosen (Figure 6.1). This particular tumour model was decided upon for a number of reasons. Firstly, the model had been previously used in anti-OX40 preclinical studies by other groups [281] and within our lab, secondly, the tumour cells express Ova therefore antigen specific cytotoxic T cell responses can be measured through SIINFEKL Tetramer staining, as had been done in the OT-I transfer model. Lastly, the tumour has a high level of immune infiltrate, as shown by others [354] and ourselves (data not shown), and would therefore be a good starting point to test the ability of our immunomodulating mAb.

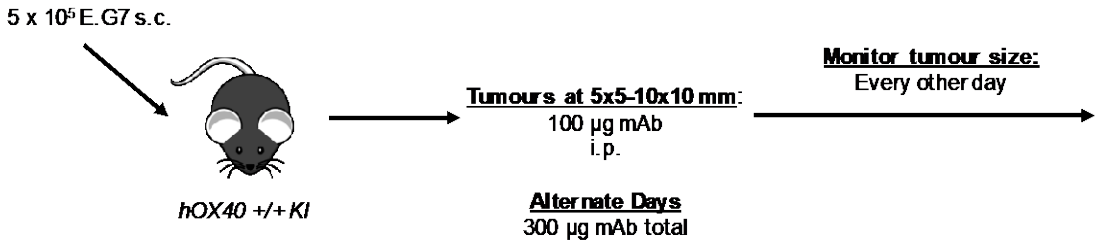

Figure 6.1 E.G7-Ova lymphoma model

hOX40$^{+/+}$ KI mice were inoculated with 5x10^5 E.G7-Ova tumour cells s.c. into the flank. Tumours were allowed to reach a size of between 5x5 and 10x10mm before mice were treated with a total of 300µg anti-hOX40 mAb (100µg on alternate days i.e. Mon, Wed and Fri). Tumour size was measured every other day until mice reached a terminal end point which was deemed a tumour size of 20x20mm.

mAb which bound to each CRD of hOX40 as either a mIgG1 or a mIgG2a isotype, were first examined. hOX40$^{+/+}$ KI mice were inoculated with E.G7-Ova lymphoma cells and subsequently treated with anti-hOX40 mAb once established tumours were formed (5x5 - 10x10 mm). Figure 6.2 shows that anti-hOX40 mAb, as both mIgG1 and mIgG2a, were able to elicit significant therapy in comparison to isotype control treated mice in an E.G7-Ova tumour model, as mice were able to eradicate established tumours in all treatment groups. Amongst the mAb there were no obvious isotype or domain binding preferences (Figure 6.3) suggesting both agonism and depletion may be important in this particular tumour setting. Interestingly, the difference in percent survival between mIgG1 and mIgG2a

isotypes was largest with SAP 28-2 (60% vs. 25%, respectively) and SAP 25-29 (45% vs. 64.7%, respectively), although not statistically significant (Figure 6.3). These mAb bind CRDs at opposite ends of the extracellular domain of hOX40; SAP 28-2 binds CRD1 and SAP 25-29 CRD4. The difference in percent survival between mIgG1 vs mIgG2a was very slight in mice that had been treated with SAP 15-3 (20% vs. 27.7%, respectively) and SAP 9 (33.3% vs. 27.7%, respectively); mAb which bind to the middle two CRDs; SAP 15-3 binds CRD2 and SAP 9 CRD3 (Figure 6.3). Importantly, mice also appeared to form durable memory responses as upon re-challenge with the same number of tumour cells no mice developed tumour in comparison to naïve mice which succumbed to tumour growth (Figure 6.4). Tumour free survival was observed as long as 9 weeks post secondary inoculation.

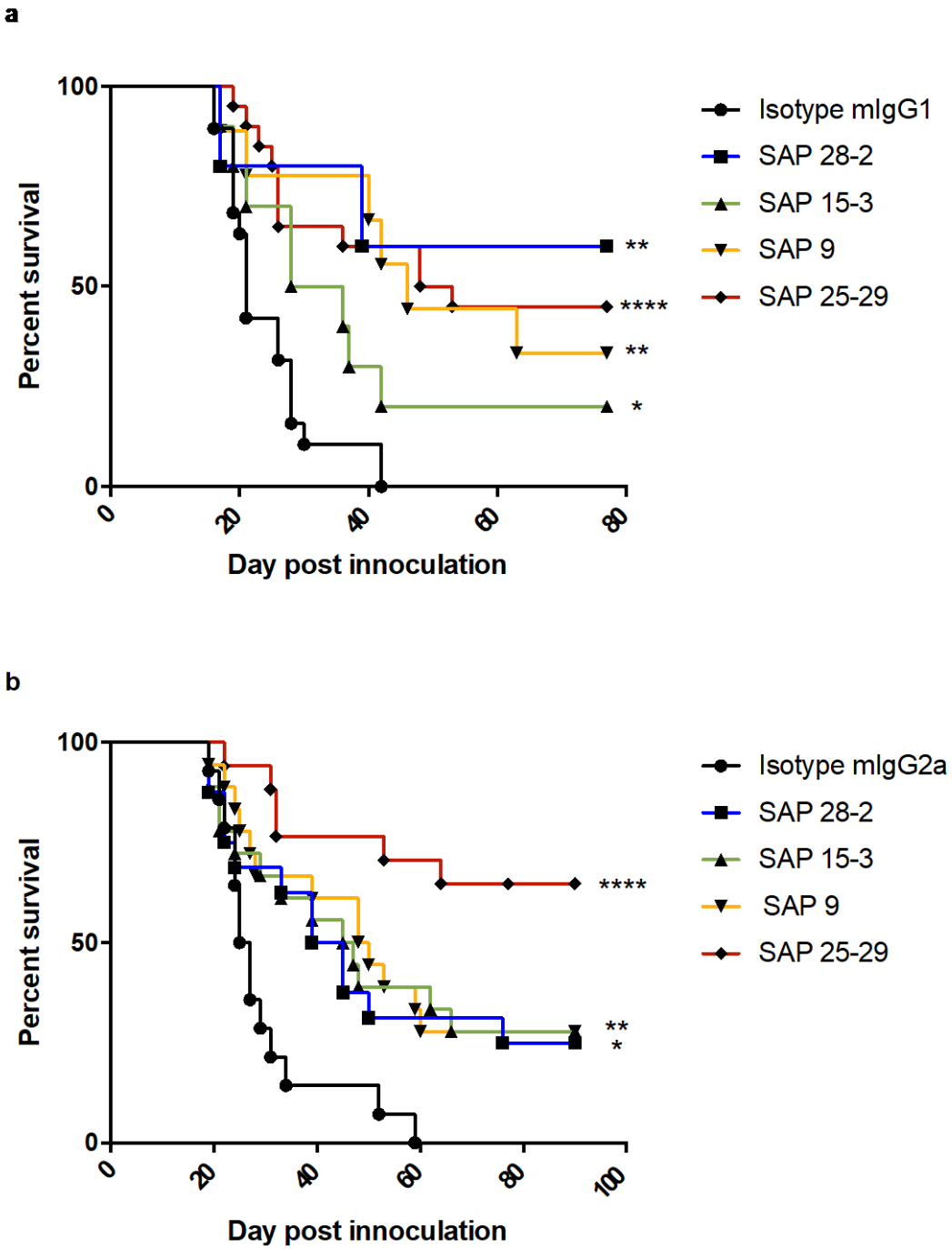

Figure 6.2 Therapeutic effect of anti-hOX40 mAb in an E.G7-Ova lymphoma model

hOX40$^{+/+}$ KI mice were inoculated with 5x10^5 E.G7-Ova tumour cells s.c. Once tumours had reached 5x5-10x10mm mice were treated with a total of 300μg anti-hOX40 mAb (dosing schedule described in Figure 6.1). Survival curves show a) pooled data from 2 individual experiments of mIgG1 treated mice, N=10-20 mice per treatment group and b) pooled data from 3 individual experiments of mIgG2a treated mice, N=16 mice per treatment group. Statistical significance was evaluated using a Log-rank (Mantel-Cox) test; * P≤ 0.05, ** P≤ 0.01, **** P ≤ 0.0001.

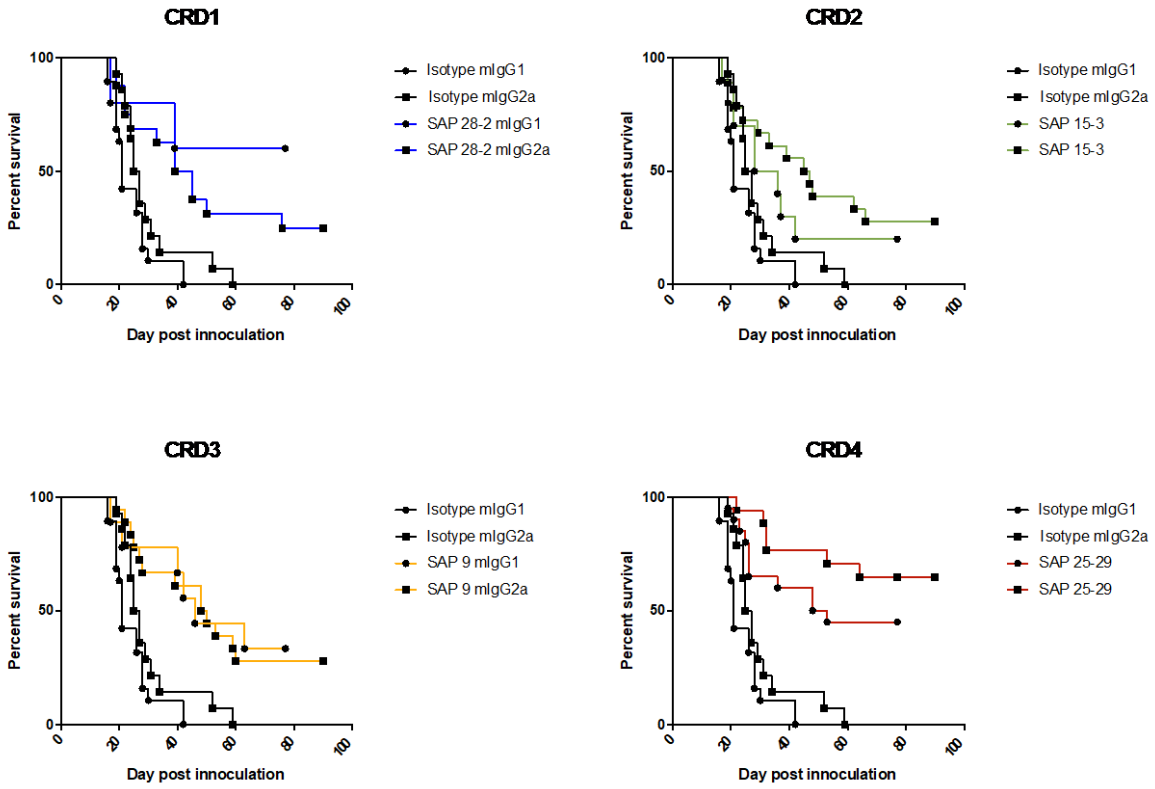

Figure 6.3 Comparison of the therapeutic effect of mIgG1 and mIgG2a anti-hOX40 mAb binding different CRDs in an E.G7 tumour model

Data from Figure 6.2 separated into binding domain treatment groups comparing mIgG1 and mIgG2a versions of the same mAb.

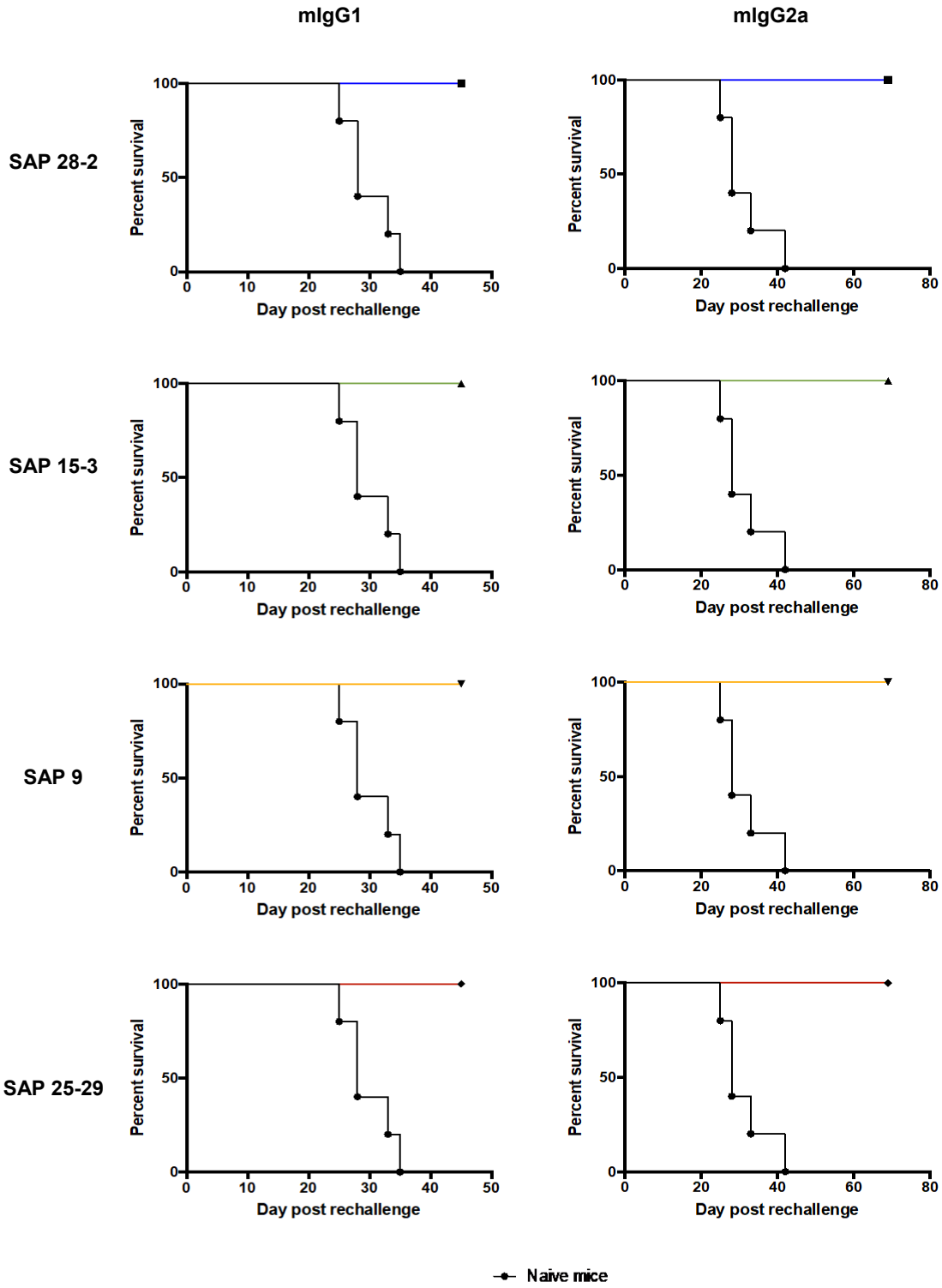

Figure 6.4 E.G7-Ova rechallenge of tumour free hOX40$^{+/+}$ KI mice and naïve hOX40$^{+/+}$ KI mice

All surviving, tumour free mice for the experiment outlined in Figure 6.2 were rechallenged with 5x10^5 E.G7-Ova tumour cells s.c. Naïve mice (N=5) were also inoculated as a positive control. Survival curves on the left show pooled data from 2 individual experiments of mIgG1 treated mice. N numbers per treatment group (top to bottom) as follows; SAP 28-2, N=3, SAP 15-3, N=2, SAP 9, N=3 and SAP 25-29, N=9. Graphs on the right show pooled data from 3 individual experiments of mIgG2a treated mice. N numbers per treatment group (top to bottom) as follows; SAP 28-2, N=4, SAP 15-3, N=5, SAP 9, N=5 and SAP 25-29, N=11.

To determine if the reason for tumour free survival of mice was down to changes in T cell populations, as had been seen in the OT-I model (Chapter 5), mice were again inoculated with E.G7-Ova lymphoma cells and treated with anti-hOX40 mAb before organs were harvested 4 days post final treatment and T cell numbers obtained. Specifically, numbers in blood, spleen, ndLN and tdLN were examined, alongside those in the tumour itself normalised to the tumour weight (g) to take into account the different tumour sizes. However, cell numbers recovered from tumours were very small and heterogeneous therefore it was difficult to observe any clear trends within the tumour infiltrating lymphocytes (TILs). Optimisation of the digestion process may improve TIL recovery and may be something that is looked at by the lab in future. Therefore, more attention was concentrated upon the blood, spleen, ndLN and tdLN. Furthermore, the overall numbers of Tetramer+ cells were small due to these cells being endogenous rather than adoptively transferred as was done in the OT-I model.

Within the blood, spleen, ndLN and tdLN an increase in the number of CD4+ T cells was seen when mice had been treated with a mIgG1 mAb in comparison to an isotype control; this was most significant within the spleen (

Figure 6.5). In contrast, in the mIgG2a treated mice a decrease in the number of CD4+ T cells was observed in comparison to the isotype control in the blood and spleen, with little to no change in the lymph nodes with the exception of SAP 15-3 which decreased the number of CD4+ cells in the tdLN (

Figure 6.5). Similarly, a general increase in the number of CD8+ T cells was seen amongst the organs in mIgG1 treated mice compared to isotype control treated mice (Figure 6.6), whereas only within the spleen and tdLN of SAP 15-3 treated mice did we observe an obvious decrease in the number of CD8+ T cells. A clear trend indicating an increase in the number of Treg cells was seen within the blood, spleen and both sets of lymph nodes in mIgG1 treated mice in comparison to the isotype control group (Figure 6.7). A decrease in the number of these cells was seen in the blood and spleen of mIgG2a treated mice whereas there was little to no change in the number of Tregs in comparison to the isotype control within the lymph nodes (Figure 6.7). As mentioned above, there were only a small number of tetramer+ cells in these mice however a trend was observed indicating an increase in the population, especially within the tdLN, in mIgG1 treated mice (Figure 6.8).

Interestingly, an increase was also seen in mIgG2a treated mice within the tdLN, however a decrease was seen in the spleen and little to no change was seen in the tetramer+ population within the blood and ndLN compared to isotype control (Figure 6.8). Figure 6.9 shows that the CD8:Treg ratio in mIgG1 treated mice was unchanged in the lymph nodes and TILs, however there was a decrease in the spleen and within one treatment group in the blood (SAP 25-29). The CD8:Treg ratio in the mIgG2a treated mice was increased in all organs compared to the isotype control with the exception of the ndLN in which only SAP 28-2 treated mice demonstrated this increase (Figure 6.9). The tables in Figure 6.5-Figure 6.9show the statistical significance between the change in absolute numbers of T cell populations within the organs of mice treated with different isotypes (mIgG1 vs. mIgG2a) of the same anti-hOX40 mAb. The most significant differences were seen in the Treg populations due to the mIgG1 causing strong expansion of cells whereas the mIgG2a were causing depletion (Figure 6.7). Likewise, mAb binding the most membrane proximal domains of hOX40 (CRD3 and CRD4) produced the most significant differences in all cell populations across all organs between mIgG1 and mIgG2a treated mice. In summary, this data demonstrated trends in the mIgG1 and mIgG2a treated mice that were consistent with data from the OT-I model; i.e. mIgG1 mAb showing expansion of T cells, whilst mIgG2a mAb show trends of depletion. This data is summarised in Table 6.1. Furthermore, significant differences were seen between mIgG1 and mIgG2a versions of the same mAb with a link again to domain binding.

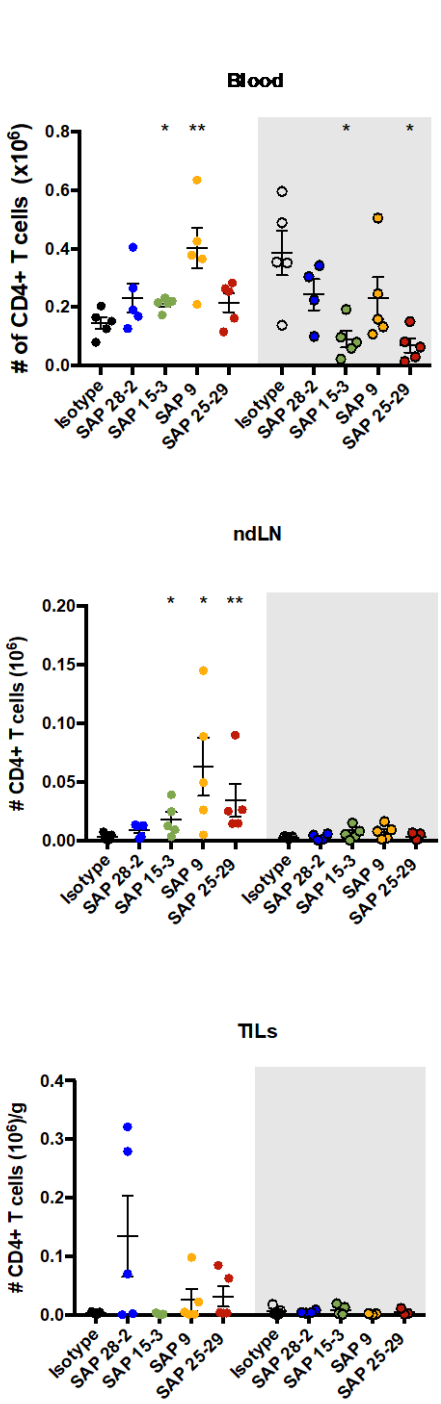

	mIgG1 vs mIgG2a			
	SAP 28-2	SAP 15-3	SAP 9	SAP 25-29
Blood	ns	*	ns	*
Spleen	*	**	**	**
ndLN	ns	ns	ns	**
tdLN	ns	**	ns	**
TILs	ns	ns	ns	ns

Figure 6.5 Numeration of CD4+ T cells within organs of E.G7-Ova tumour bearing hOX40$^{+/+}$ KI mice after treatment with anti-hOX40 mAb (mIgG1 and mIgG2a)

hOX40$^{+/+}$ KI mice were inoculated with 5x10^5 E.G7-Ova tumour cells s.c. Once tumours reached a size of between 5x5 -10x10mm mice were subsequently treated with a total of 300μg of anti-hOX40 mAb (mIgG1 and mIgG2a) as described in Figure 6.1. Day 4 post final treatment organs were harvested from mice and T cell subsets numerated using flow cytometry. Graphs show the number of CD4+ T cells in the blood, spleen, ndLN, tdLN and TILs. The white background on the graphs highlights the mIgG1 treated mice and the grey shaded background mIgG2a treated mice. mAb are ordered on the graph according to domain binding (CRD1-4, respectively). Statistical analysis shown on the graphs is between isotype control and treatment groups whereas that shown in the table is between mIgG1 and mIgG2a versions of the same mAb. Data is representative of 2 independent experiments with N=5/6 mice per treatment group. Each dot represents an individual mouse. Error bars represent mean±SEM. Statistical significance was evaluated using a Mann-Whitney test; * P≤ 0.05, ** P≤ 0.01, *** P ≤ 0.001

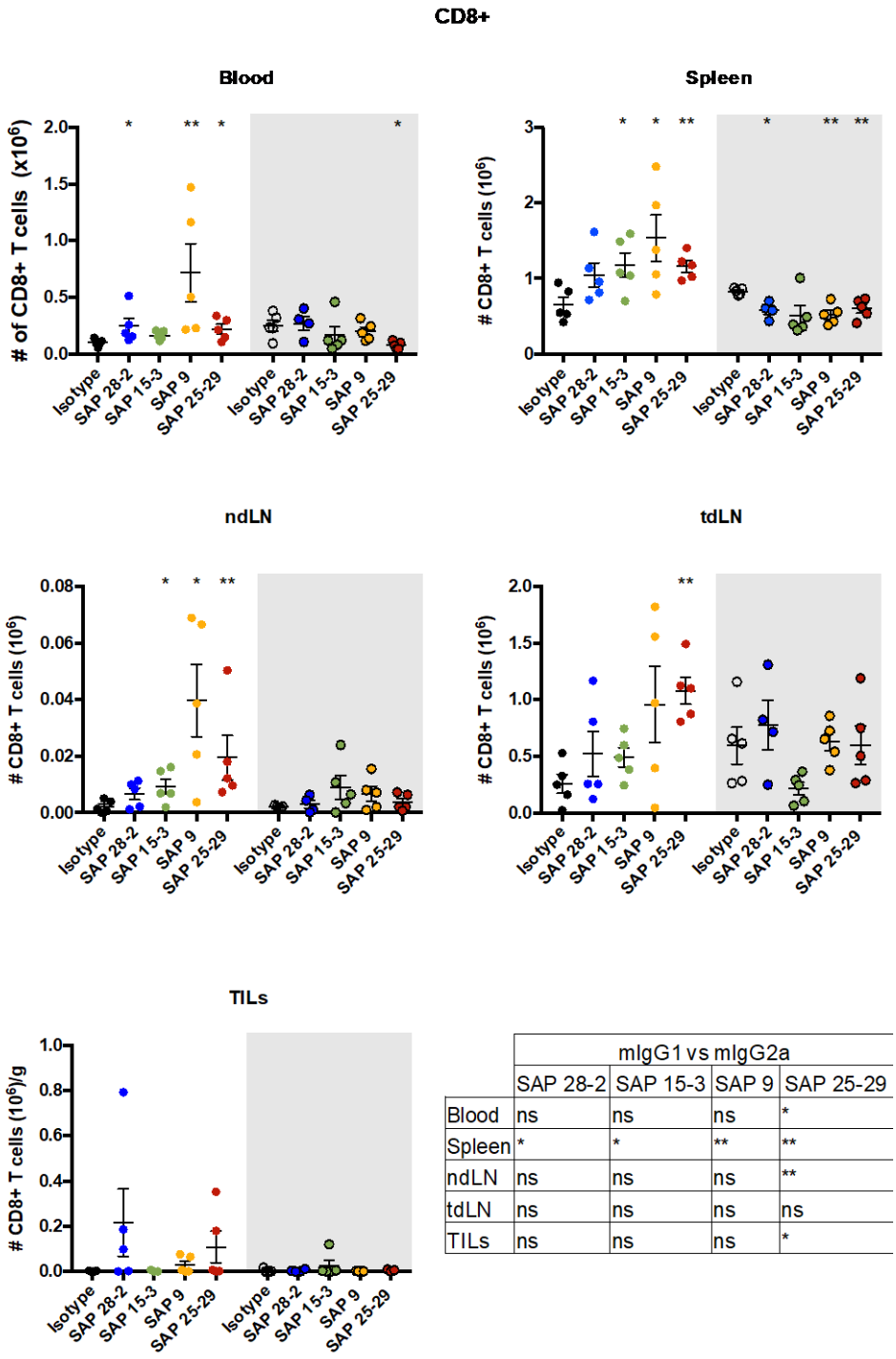

	mIgG1 vs mIgG2a			
	SAP 28-2	SAP 15-3	SAP 9	SAP 25-29
Blood	ns	ns	ns	*
Spleen	*	*	**	**
ndLN	ns	ns	ns	**
tdLN	ns	ns	ns	ns
TILs	ns	ns	ns	*

Figure 6.6 Numeration of CD8+ T cells within organs of E.G7-Ova tumour bearing hOX40$^{+/+}$ KI mice after treatment with anti-hOX40 mAb (mIgG1 and mIgG2a)

The same experimental set up as described in Figure 6.5 was used. Graphs show the number of CD8+ T cells in the blood, spleen, ndLN, tdLN and TILs. The white background on the graphs highlights the mIgG1 treated mice and the grey shaded background mIgG2a treated mice. mAb are ordered on the graph according to domain binding (CRD1-4, respectively). Statistical analysis shown on the graphs is between isotype control and treatment groups whereas that shown in the table is between mIgG1 and mIgG2a versions of the same mAb Data is representative of 2 independent experiments with N=5/6 mice per treatment group. Each dot represents an individual mouse. Error bars represent mean±SEM. Statistical significance was evaluated using a Mann-Whitney test; * P≤ 0.05, ** P≤ 0.01, *** P ≤ 0.001.

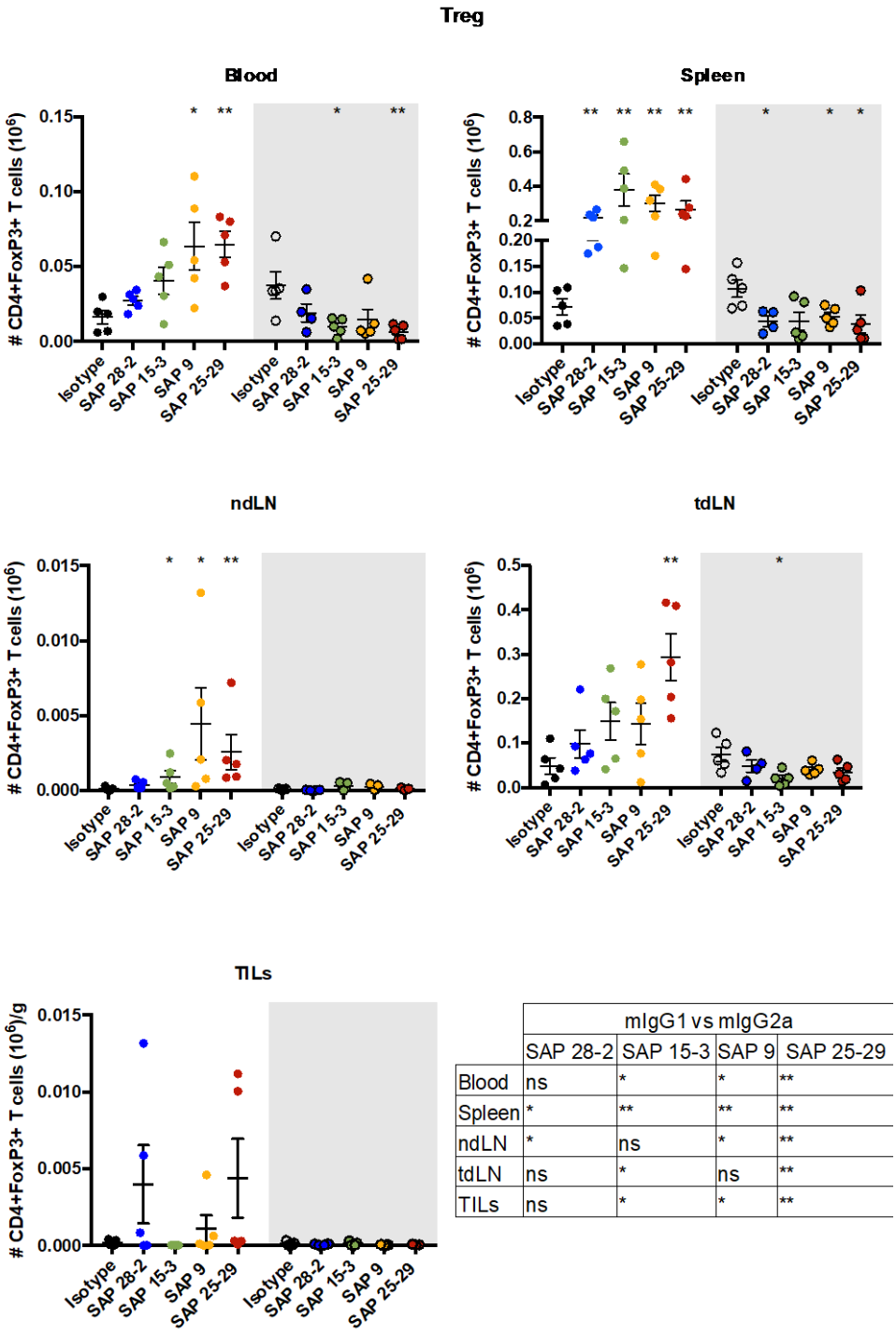

	mIgG1 vs mIgG2a			
	SAP 28-2	SAP 15-3	SAP 9	SAP 25-29
Blood	ns	*	*	**
Spleen	*	**	**	**
ndLN	*	ns	*	**
tdLN	ns	*	ns	**
TILs	ns	*	*	**

Figure 6.7 Numeration of Tregs within organs of E.G7-Ova tumour bearing hOX40$^{+/+}$ KI mice after treatment with anti-hOX40 mAb (mIgG1 and mIgG2a)

The same experimental set up as described in Figure 6.5 was used. Graphs show the number of Treg cells in the blood, spleen, ndLN, tdLN and TILs. The white background on the graphs highlights the mIgG1 treated mice and the grey shaded background mIgG2a treated mice. mAb are ordered on the graph according to domain binding (CRD1-4, respectively). Statistical analysis shown on the graphs is between isotype control and treatment groups whereas that shown in the table is between mIgG1 and mIgG2a versions of the same mAb Data is representative of 2 independent experiments with N=5/6 mice per treatment group. Each dot represents an individual mouse. Error bars represent mean±SEM. Statistical significance was evaluated using a Mann-Whitney test; * P≤ 0.05, ** P≤ 0.01, *** P ≤ 0.001.

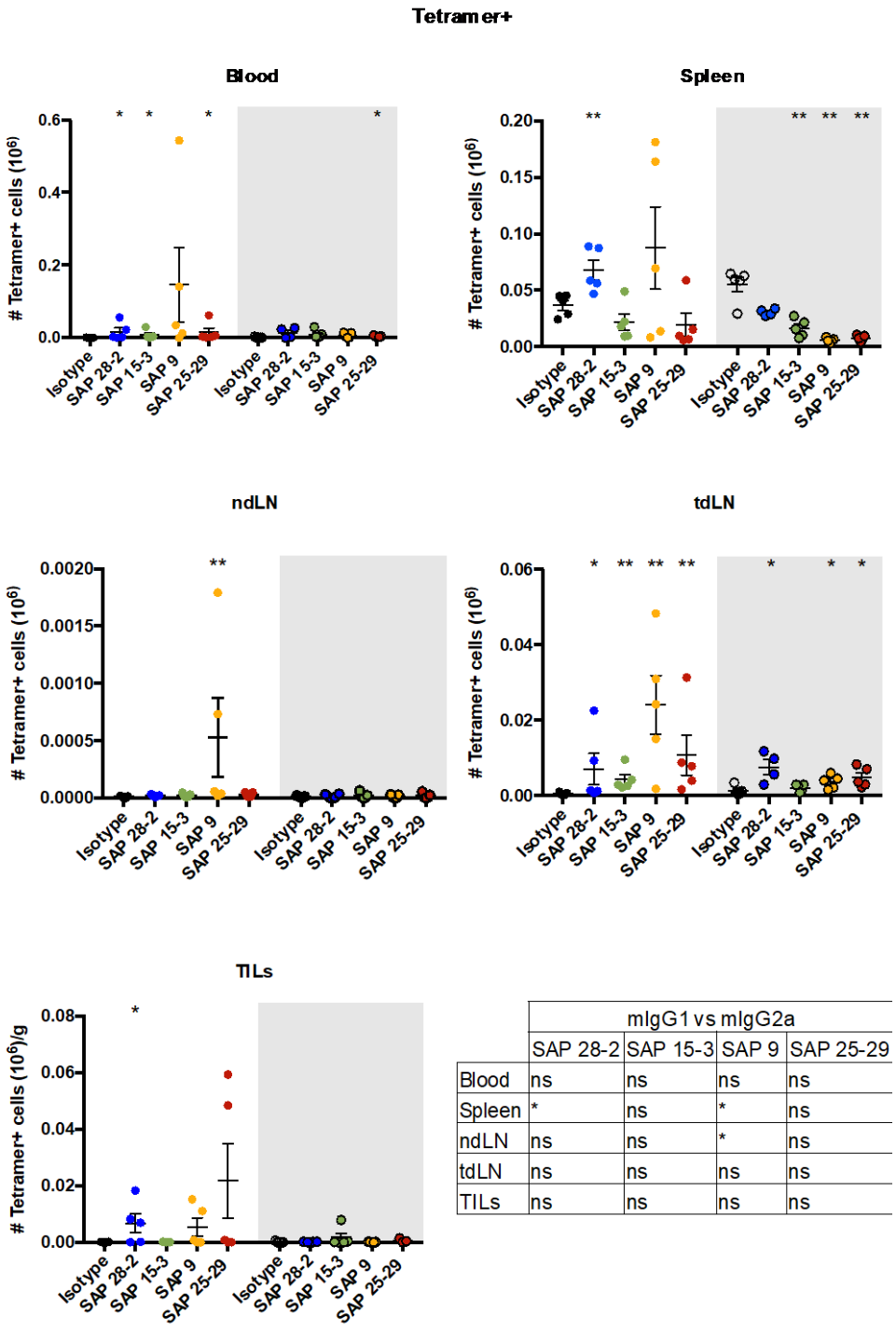

	mIgG1 vs mIgG2a			
	SAP 28-2	SAP 15-3	SAP 9	SAP 25-29
Blood	ns	ns	ns	ns
Spleen	*	ns	*	ns
ndLN	ns	ns	*	ns
tdLN	ns	ns	ns	ns
TILs	ns	ns	ns	ns

Figure 6.8 Numeration of Tetramer+ cells within organs of E.G7-Ova tumour bearing hOX40$^{+/+}$ KI mice after treatment with anti-hOX40 mAb (mIgG1 and mIgG2a)

The same experimental set up as described in Figure 6.5 was used. Graphs show the number of Tetramer+ cells in the blood, spleen, ndLN, tdLN and TILs. The white background on the graphs highlights the mIgG1 treated mice and the grey shaded background mIgG2a treated mice. mAb are ordered on the graph according to domain binding (CRD1-4, respectively). Statistical analysis shown on the graphs is between isotype control and treatment groups whereas that shown in the table is between mIgG1 and mIgG2a versions of the same mAb Data is representative of 2 independent experiments with N=5/6 mice per treatment group. Each dot represents an individual mouse. Error bars represent mean±SEM. Statistical significance was evaluated using a Mann-Whitney test; * P≤ 0.05, ** P≤ 0.01, *** P ≤ 0.001

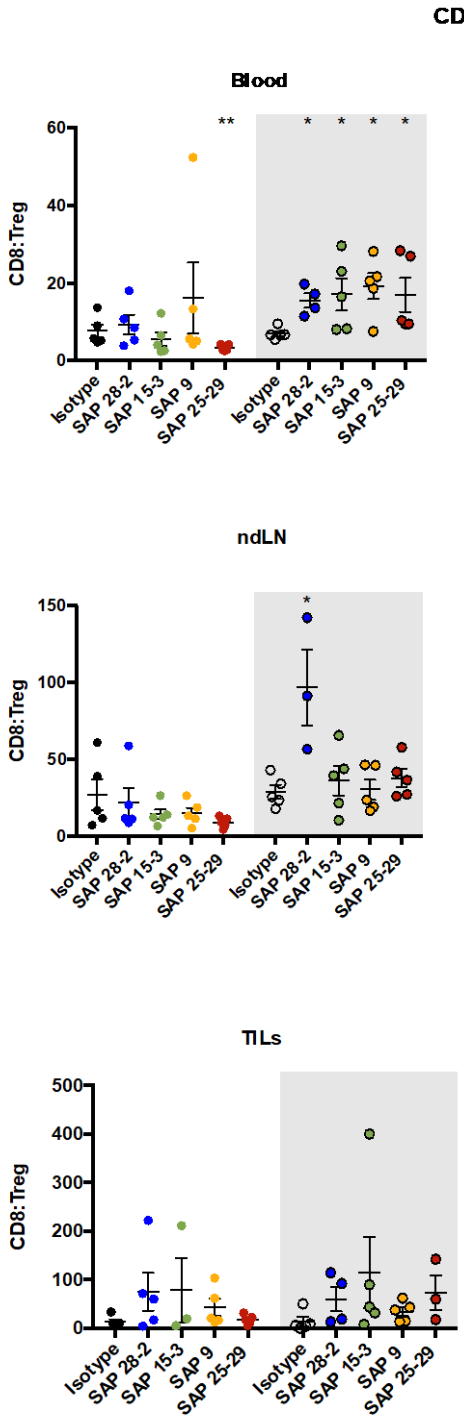

	mIgG1 vs mIgG2a			
	SAP 28-2	SAP 15-3	SAP 9	SAP 25-29
Blood	ns	*	ns	**
Spleen	*	*	**	*
ndLN	ns	ns	ns	**
tdLN	ns	*	**	**
TILs	ns	ns	ns	ns

Figure 6.9 CD8:Treg ratio within organs of E.G7-Ova tumour bearing hOX40$^{+/+}$ KI mice after treatment with anti-hOX40 mAb (mIgG1 and mIgG2a)

The same experimental set up as described in Figure 6.5 was used. Graphs show the CD8:Treg ratio in the blood, spleen, ndLN, tdLN and TILs. The white background on the graphs highlights the mIgG1 treated mice and the grey shaded background mIgG2a treated mice. mAb are ordered on the graph according to domain binding (CRD1-4, respectively). Statistical analysis shown on the graphs is between isotype control and treatment groups whereas that shown in the table is between mIgG1 and mIgG2a versions of the same mAb Data is representative of 2 independent experiments with N=5/6 mice per treatment group. Each dot represents an individual mouse. Error bars represent mean±SEM. Statistical significance was evaluated using a Mann-Whitney test; * P≤ 0.05, ** P≤ 0.01, *** P ≤ 0.001

		Cell type				
Organ	Isotype	CD4	CD8	Treg	Tetramer+	CD8:Treg
Blood	mIgG1	↑ 1	↑ 1	↑ 1	↑ 1	— 0
	mIgG2a	↓ -1	— 0	↓ -1	— 0	↑ 1
Spleen	mIgG1	↑	↑	↑	—	↓
	mIgG2a	↓	↓	↓	↓	↑
ndLN	mIgG1	↑ 1	↑ 1	↑ 1	— 0	↓ -1
	mIgG2a	— 0	— 0	— 0	— 0	— 0
tdLN	mIgG1	↑	↑	↑	↑	—
	mIgG2a	—	—	↓	↑	↑

Table 6.1 General trend regarding the change in T cell numbers within multiple organs of E.G7-Ova bearing mice after anti-hOX40 treatment (mIgG1 and mIgG2a)

Data from Figures 6.4-6.6 tabulated and the general trend in terms of T cell numbers within treatment groups in comparison to the isotype control group indicated by symbols; green arrow = increase, orange line = little/no change and red arrow = decrease.

When analysing this data, a correlation between domain binding and strength of function was observed similar to that seen in the OT-I model. Data was therefore combined into CRD binding groups as before; CRD 1+2 (SAP 28-2 and SAP 15-3) and CRD 3+4 (SAP 9 and SAP 25-29).

Figure 6.10 - Figure 6.13 demonstrate that E.G7-Ova bearing mice treated with mIgG1 mAb binding CRDs 3+4 evoked greater expansion of certain T cell subsets within a number of organs. CD4+ and CD8+ T cell expansion was favoured by mAb binding CRDs 3+4 compared to those binding CRDs 1+2 in the tdLN and ndLN. This trend was also seen within the blood for both CD4+ and CD8+ populations and within the spleen for CD8+ T cells, although this was not statistically significant (Figure 6.11). Likewise, Treg expansion was greater in mice treated with CRD 3+4 binding mIgG1 anti-hOX40 mAb in both the blood and ndLN (Figure 6.12). A trend was observed in the tdLN indicating CRD 3+4 binding mAb expand tetramer+ cells to a greater level than CRD 1+2 binding mAb (Figure 6.13). Only within the tetramer+ population in the spleen was a domain bias observed in terms of cell depletion that was statistically significant in mIgG2a treated mice (Figure 6.17). A trend was seen amongst the TILs in the CD4+ and Treg population indicating a larger amount of depletion with CRD 3+4 binding mAb over CRD1+2 binding mAb, however this was not statistically significant (Figure

6.14 and Figure 6.16). Within all other cell populations across all organs the number of cells in CRD 1+2 treated mice was similar to mice treated with CRD 3+4 binding mAb. These results demonstrate that the link between domain binding and strength of effector function (CRD 3+4 binding mAb being stronger agonists and depleters than CRD 1+2 binding mAb) could also be observed in organs other than the spleen and within a tumour setting. This same correlation however was not observed amongst all cell types within all organs.

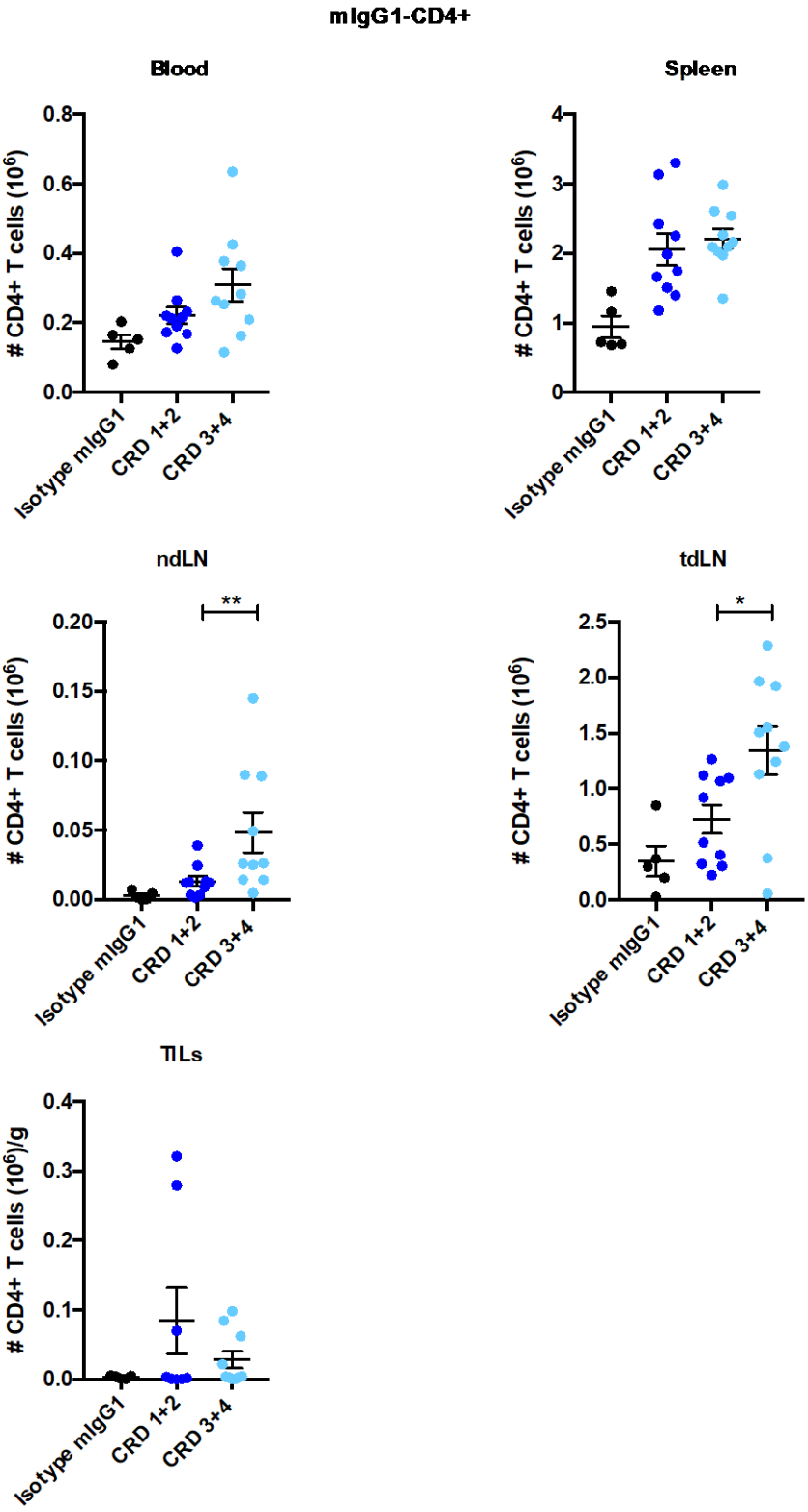

Figure 6.10 Number of CD4+ T cells within organs of E.G7-Ova bearing hOX40$^{+/+}$ KI mice after treatment with mIgG1 anti-hOX40 mAb grouped into CRD binding domains

Data from mIgG1 treated mice in Figure 6.5 were grouped into CRD binding categories CRD 1+2 (SAP 28-2 and SAP 15-3) and CRD 3+4 (SAP 9 and SAP 25-29). Each dot represents an individual mouse. Error bars represent mean±SEM. Statistical significance was evaluated using a Mann-Whitney test; * P≤ 0.05, ** P≤ 0.01, *** P ≤ 0.001.

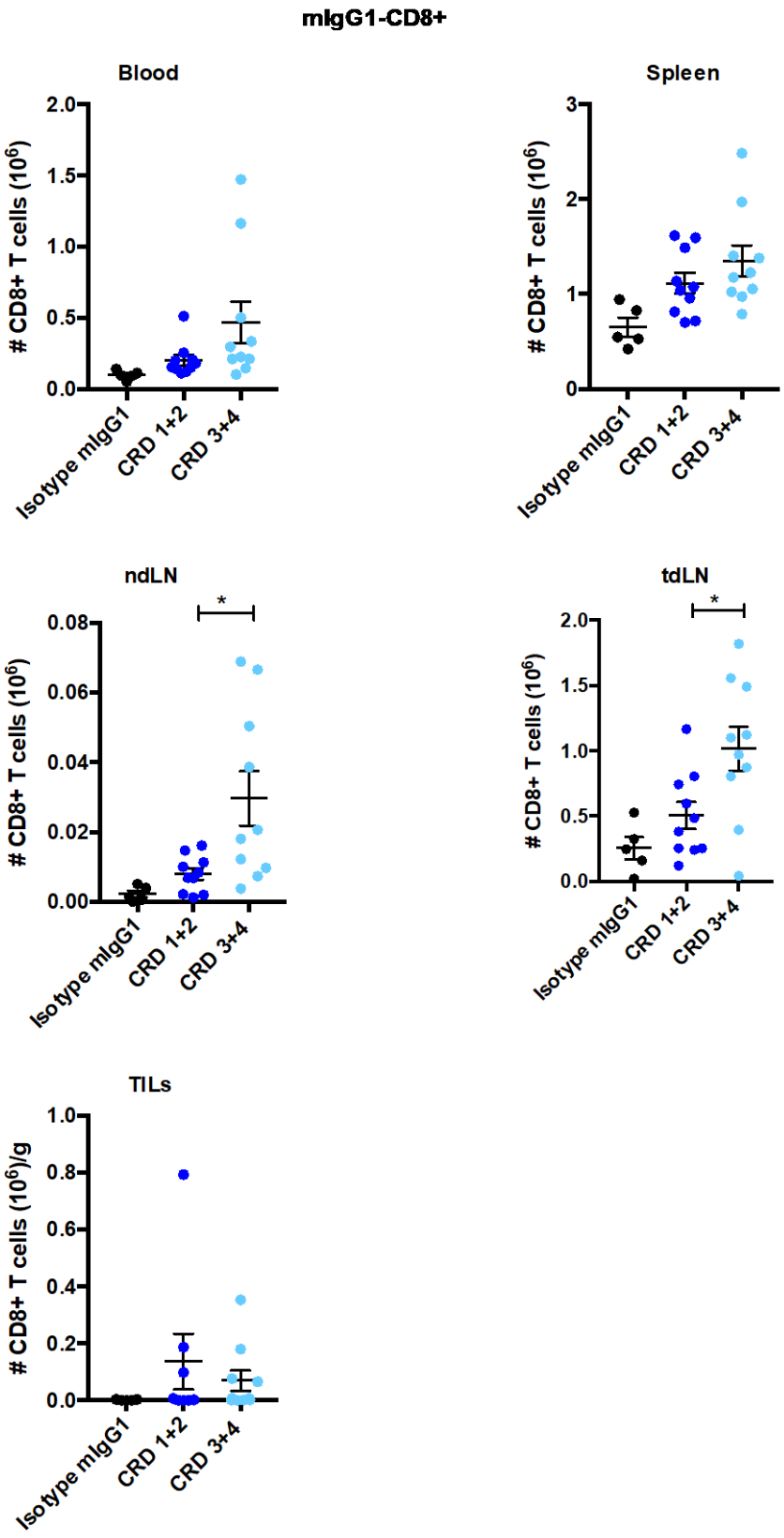

Figure 6.11 Number of CD8+ T cells within organs of E.G7-Ova bearing hOX40$^{+/+}$ KI mice after treatment with mIgG1 anti-hOX40 mAb grouped into CRD binding domains

Data from mIgG1 treated mice in Figure 6.6 were grouped into CRD binding categories CRD 1+2 (SAP 28-2 and SAP 15-3) and CRD 3+4 (SAP 9 and SAP 25-29). Each dot represents an individual mouse. Error bars represent mean±SEM. Statistical significance was evaluated using a Mann-Whitney test; * P≤ 0.05, ** P≤ 0.01, *** P ≤ 0.001.

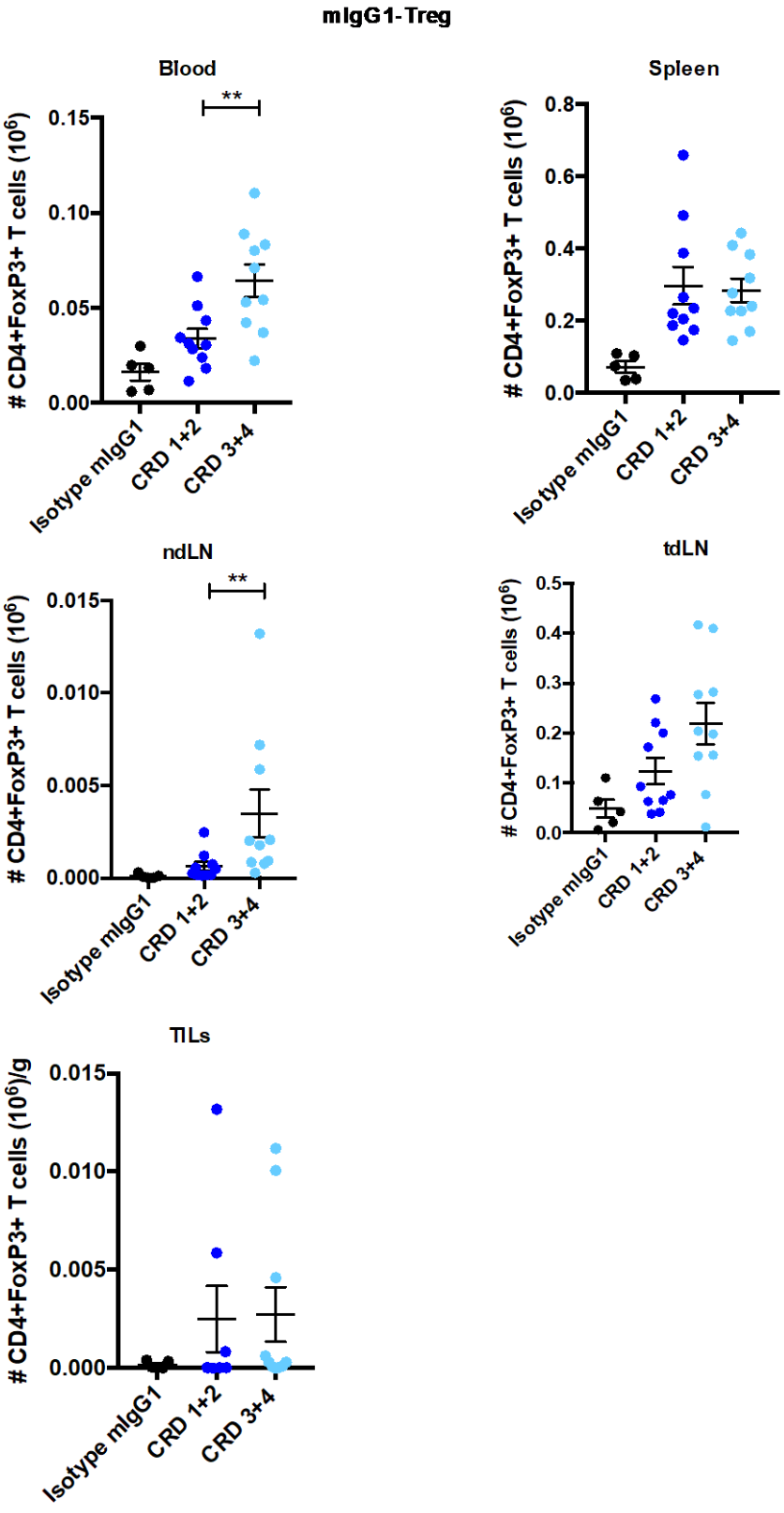

Figure 6.12 Number of Treg cells within organs of E.G7-Ova bearing hOX40$^{+/+}$ KI mice after treatment with mIgG1 anti-hOX40 mAb grouped into CRD binding domains

Data from mIgG1 treated mice in Figure 6.7 were grouped into CRD binding categories CRD 1+2 (SAP 28-2 and SAP 15-3) and CRD 3+4 (SAP 9 and SAP 25-29). Each dot represents an individual mouse. Error bars represent mean±SEM. Statistical significance was evaluated using a Mann-Whitney test; * P≤ 0.05, ** P≤ 0.01, *** P ≤ 0.001.

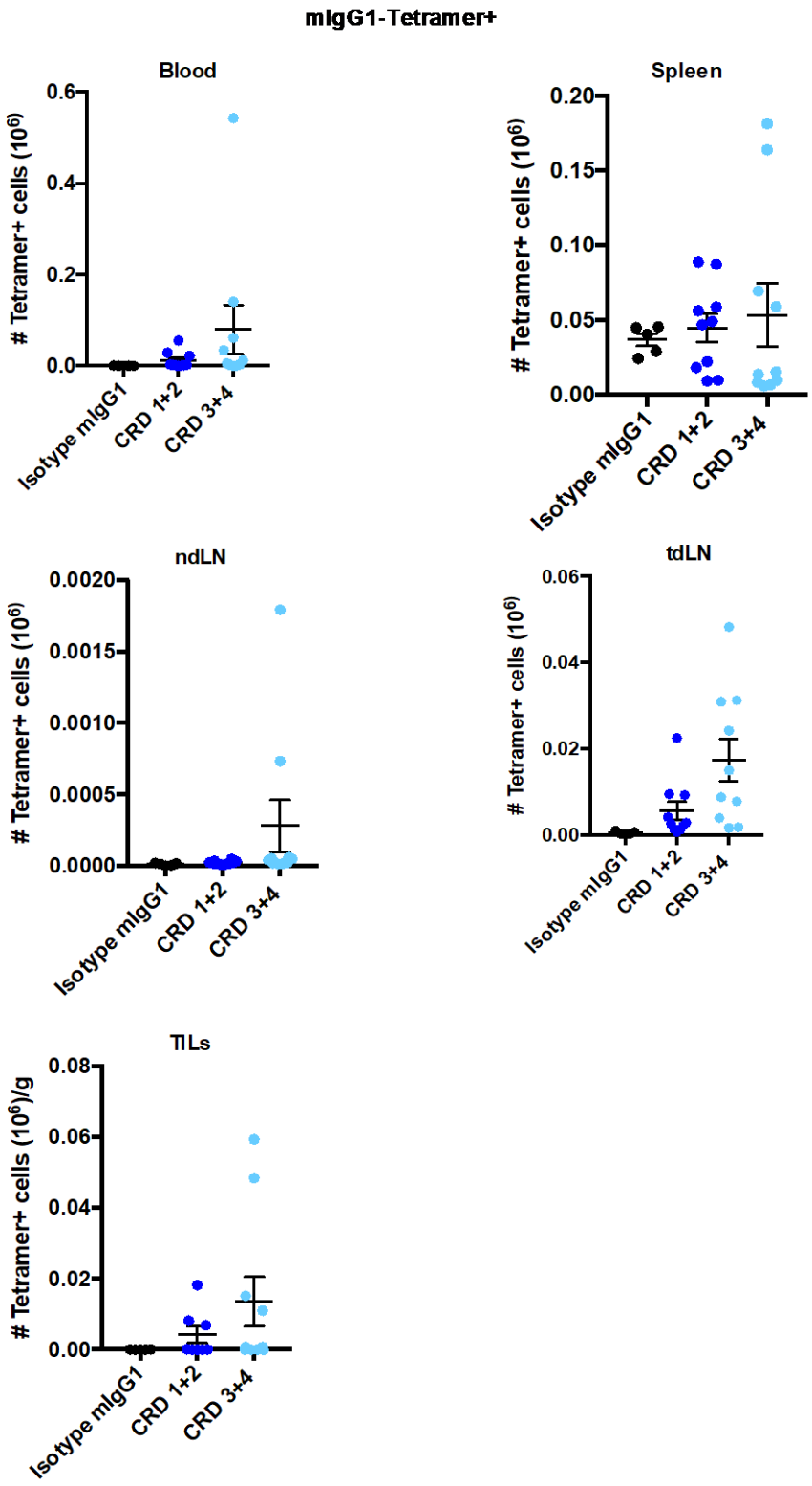

Figure 6.13 Number of Tetramer+ T cells within organs of E.G7-Ova bearing hOX40$^{+/+}$ KI mice after treatment with mIgG1 anti-hOX40 mAb grouped into CRD binding domains

Data from mIgG1 treated mice in Figure 6.8 were grouped into CRD binding categories CRD 1+2 (SAP 28-2 and SAP 15-3) and CRD 3+4 (SAP 9 and SAP 25-29). Each dot represents an individual mouse. Error bars represent mean±SEM. Statistical significance was evaluated using a Mann-Whitney test; * P≤ 0.05, ** P≤ 0.01, *** P ≤ 0.001.

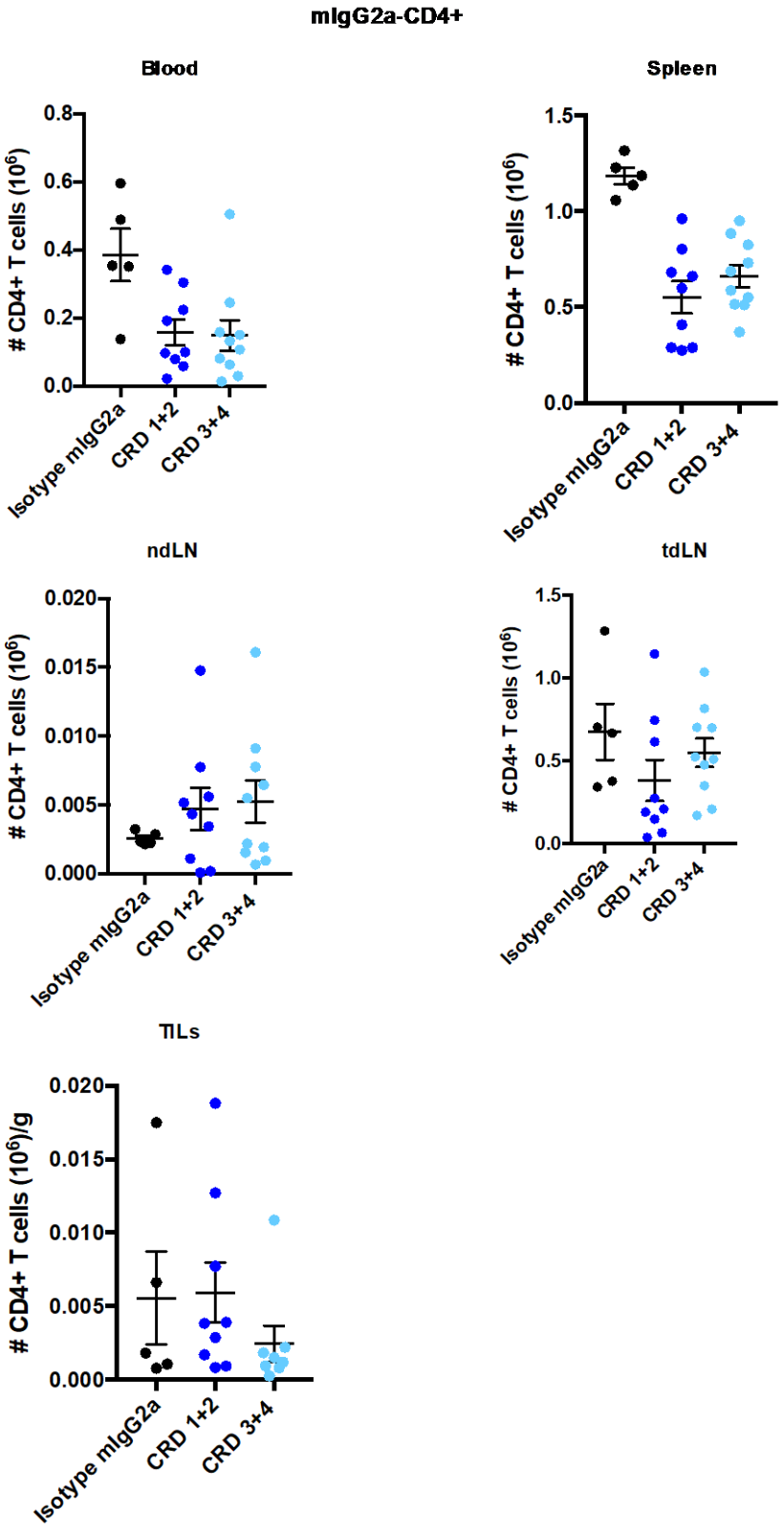

Figure 6.14 Number of CD4+ T cells within organs of E.G7-Ova bearing hOX40$^{+/+}$ KI mice after treatment with mIgG2a anti-hOX40 mAb grouped into CRD binding domains

Data from mIgG2a treated mice in Figure 6.5 were grouped into CRD binding categories CRD 1+2 (SAP 28-2 and SAP 15-3) and CRD 3+4 (SAP 9 and SAP 25-29). Each dot represents an individual mouse. Error bars represent mean±SEM. Statistical significance was evaluated using a Mann-Whitney test; * P≤ 0.05, ** P≤ 0.01, *** P ≤ 0.001.

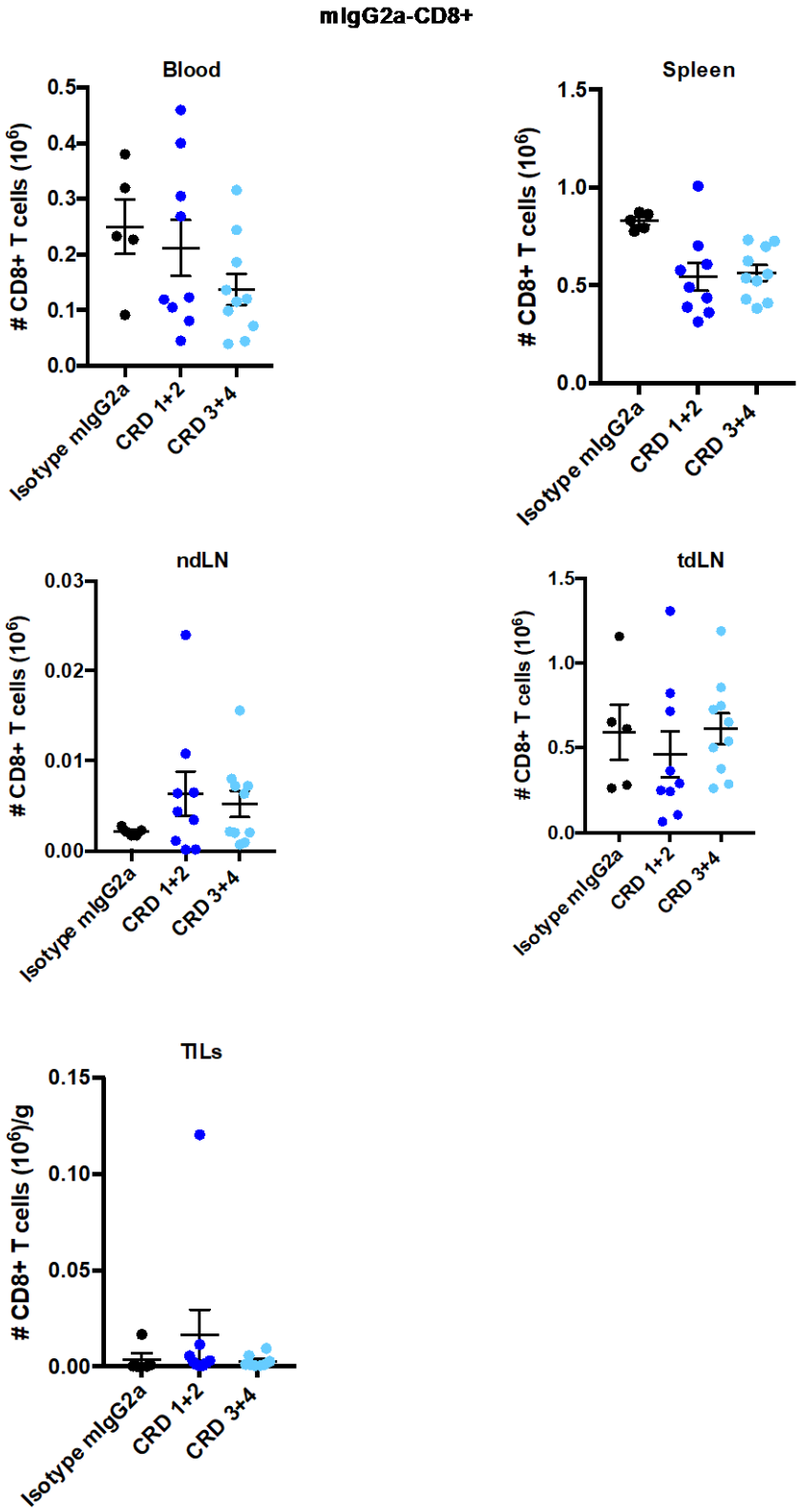

Figure 6.15 Number of CD8+ T cells within organs of E.G7-Ova bearing hOX40$^{+/+}$ KI mice after treatment with mIgG2a anti-hOX40 mAb grouped into CRD binding domains

Data from mIgG2a treated mice in Figure 6.6 were grouped into CRD binding categories CRD 1+2 (SAP 28-2 and SAP 15-3) and CRD 3+4 (SAP 9 and SAP 25-29). Each dot represents an individual mouse. Error bars represent mean±SEM. Statistical significance was evaluated using a Mann-Whitney test; * P≤ 0.05, ** P≤ 0.01, *** P ≤ 0.001.

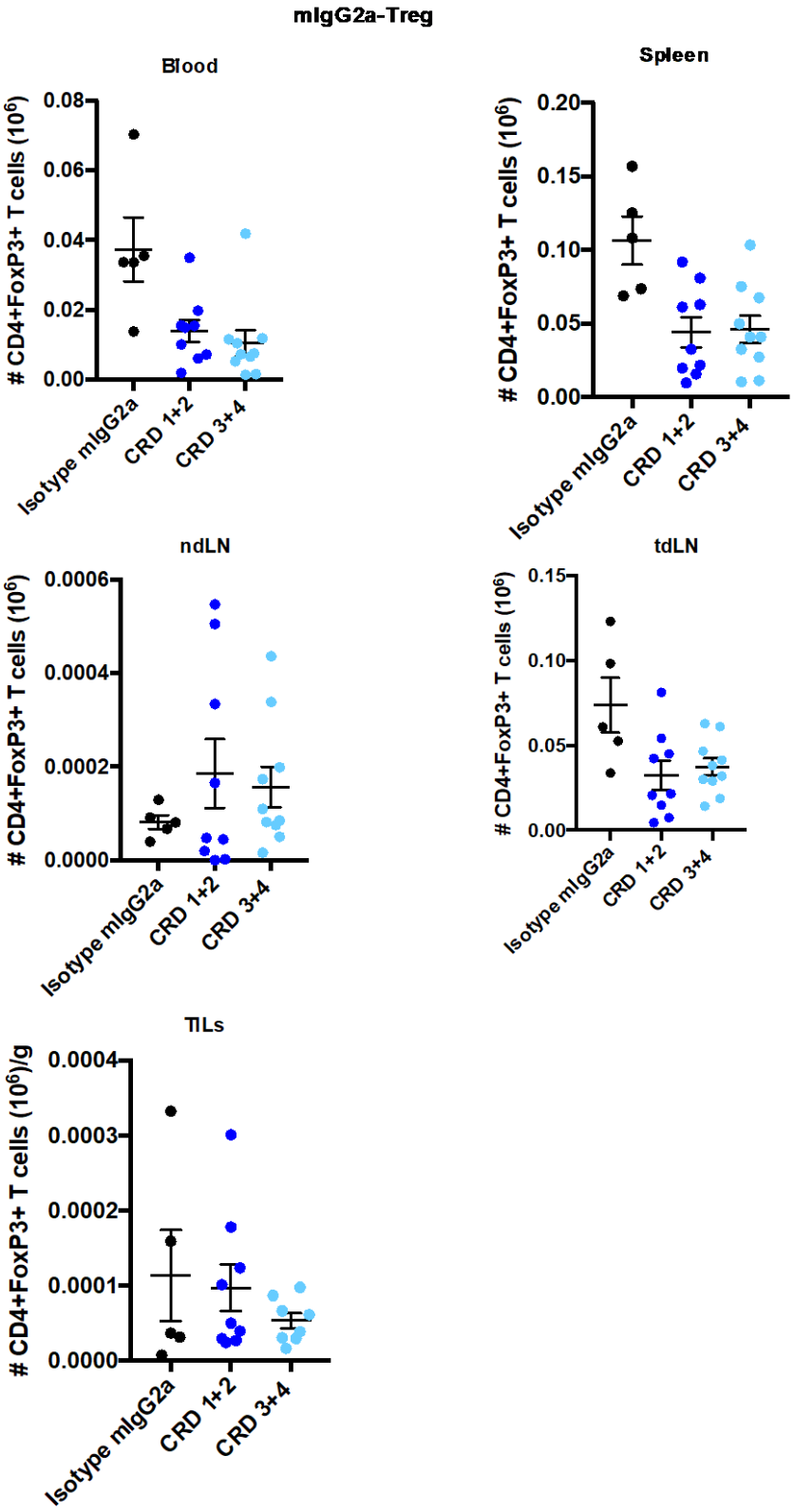

Figure 6.16 Number of Treg cells within organs of E.G7-Ova bearing hOX40$^{+/+}$ KI mice after treatment with mIgG2a anti-hOX40 mAb grouped into CRD binding domains

Data from mIgG2a treated mice in Figure 6.7 were grouped into CRD binding categories CRD 1+2 (SAP 28-2 and SAP 15-3) and CRD 3+4 (SAP 9 and SAP 25-29). Each dot represents an individual mouse. Error bars represent mean±SEM. Statistical significance was evaluated using a Mann-Whitney test; * P≤ 0.05, ** P≤ 0.01, *** P ≤ 0.001.

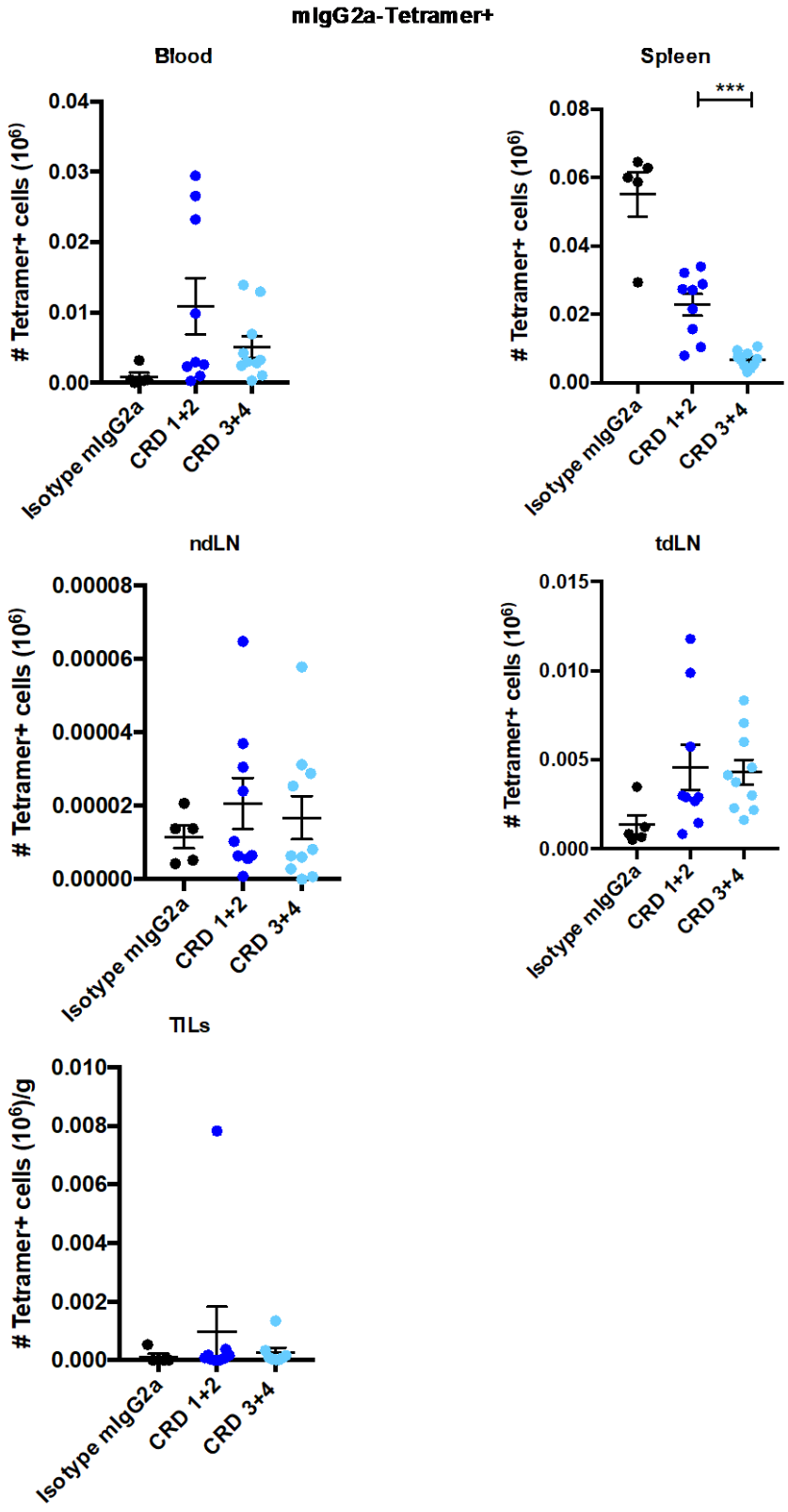

Figure 6.17 Number of Tetramer+ T cells within organs of E.G7-Ova bearing hOX40$^{+/+}$ KI mice after treatment with mIgG2a anti-hOX40 mAb grouped into CRD binding domains

Data from mIgG2a treated mice in Figure 6.8 were grouped into CRD binding categories CRD 1+2 (SAP 28-2 and SAP 15-3) and CRD 3+4 (SAP 9 and SAP 25-29). Each dot represents an individual mouse. Error bars represent mean±SEM. Statistical significance was evaluated using a Mann-Whitney test; * P≤ 0.05, ** P≤ 0.01, *** P ≤ 0.001.

6.3 Detailed phenotyping of T cell subsets in E.G7-Ova tumour model

Despite the functional differences of the mIgG1 and mIgG2a anti-hOX40 mAb, demonstrated in both the OT-I and E.G7-Ova tumour setting, both isotypes were able to cause efficient therapy to a fairly similar level and both produced a memory response demonstrated by the survival of mice after a tumour rechallenge (Figure 6.4). To understand why this was, T cell subsets within the different organs of tumour bearing mice were phenotyped for various functional markers. Expression of T-bet and Eomes were analysed as they regulate CD8+ T cell differentiation as discussed in the main introduction (Chapter 1; Section 1.3.7); example stains are shown in Figure 6.18. Furthermore, levels of granzyme B were also determined as the expression of granzyme B has been shown to be promoted/correlated with T-bet and Eomes expression and is a marker of effector cell function; an example stain is shown in Figure 6.19 indicating that either an FMO or isotype control stain could be used to set the negative population as both produced similar percentages of positive cells.

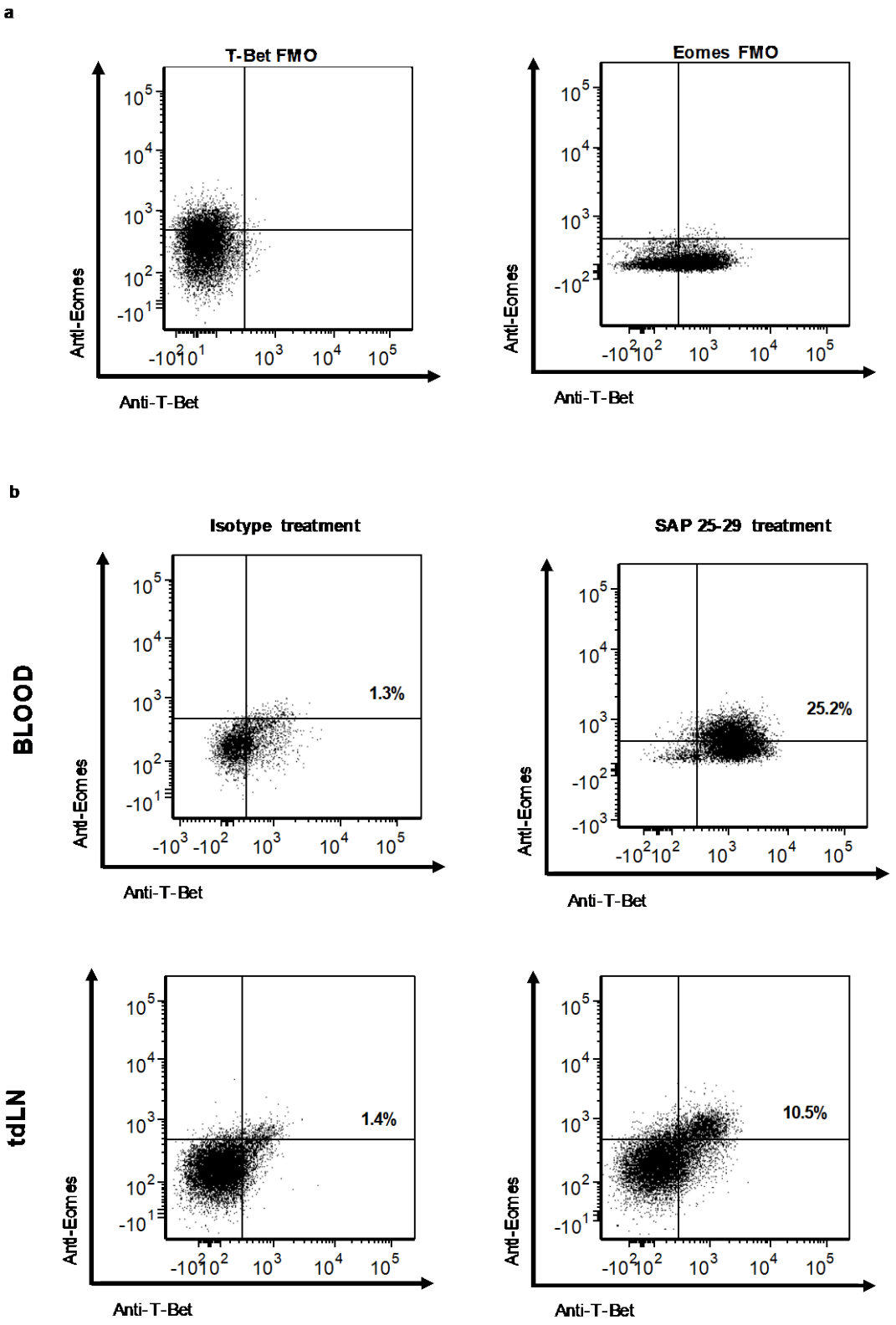

Figure 6.18 FMOs and example stains for T-Bet and Eomes markers

The gating strategy shown in Figure 5.4 was used to gate on CD4+ and CD8+ lymphocytes and the dot plots in (a) were used as negative controls for determining the expression of T-bet and Eomes in these populations. b) Dot plots show the expression of T-bet and Eomes in the CD8+ T cell population in both the blood (top) and tdLN (bottom) of an exemplar mouse from the mIgG1 isotype control treatment group (left) and the mIgG1 SAP 25-29 treatment group (right)

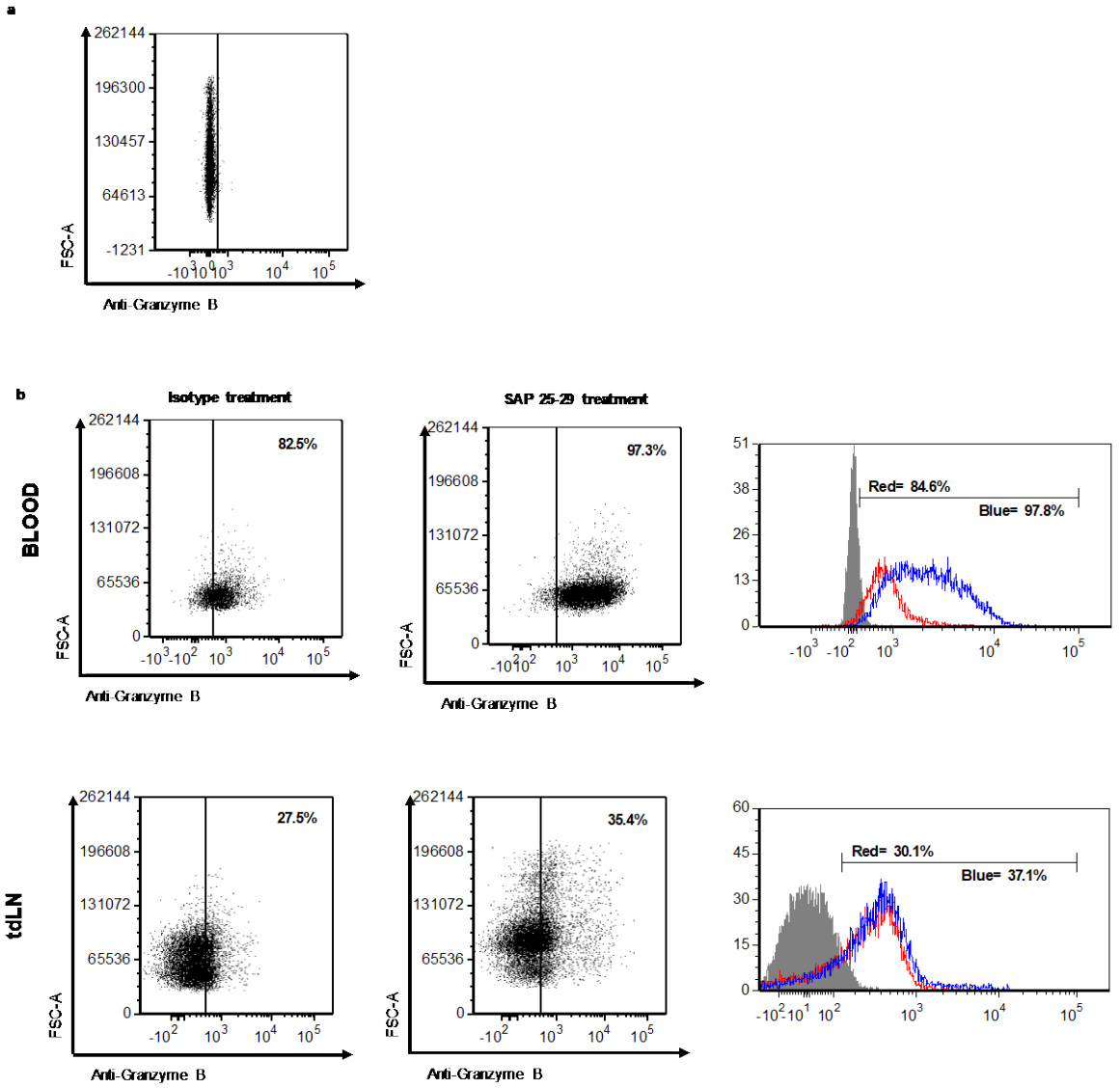

Figure 6.19 FMO and example stain for granzyme B expression

The gating strategy shown in Figure 5.4 was used to gate on CD4+ and CD8+ lymphocytes and the dot plot in (a) was used as a negative control for determining the expression of granzyme B in these populations. b) Dot plots show the expression of granzyme B in the CD8+ T cell population in both the blood (top) and tdLN (bottom) of an exemplar mouse from the mIgG1 isotype control treatment group (left) and the mIgG1 SAP 25-29 treatment group (right). Histograms show granzyme B expression, compared to an isotype control (grey shaded), in an isotype control treated mouse (red line) and a 25-29 treated mouse (blue line).

Examination of the expression of T-bet and Eomes on CD4+ and CD8+ T cells within the blood, spleen, ndLN, tdLN and TILs of anti-hOX40 mAb treated mice revealed that generally, double positive (DP) cells increased in the CD4 and CD8 populations when mice were treated with either a mIgG1 or a mIgG2a anti-hOX40 mAb (Figure 6.20 and Figure 6.21). Within the CD4+ population the increase in DP cells was greater in mIgG1 treated mice and most statistically significant in comparison to the isotype control treatment within the spleen (Figure 6.20). The CD4+ TIL data was rather variable making it difficult to draw any conclusions. Amongst the CD8+ T cells mIgG1 treated mice showed a significant increase in the percentage of DP cells within all organs, including TILs compared to the isotype control treated mice (Figure 6.21). Similarly, this increase was also seen within the blood, spleen, ndLN and tdLN of mIgG2a treated mice but in contrast to mIgG1 treated mice, not within the TILs. The levels of DP cells within the CD8+ population were similar between mIgG1 and mIgG2a anti-hOX40 treated mice, unlike the CD4+ population which showed a preference albeit only within some organs and with certain treatment groups, for mIgG1 (Figure 6.21 vs. Figure 6.20).

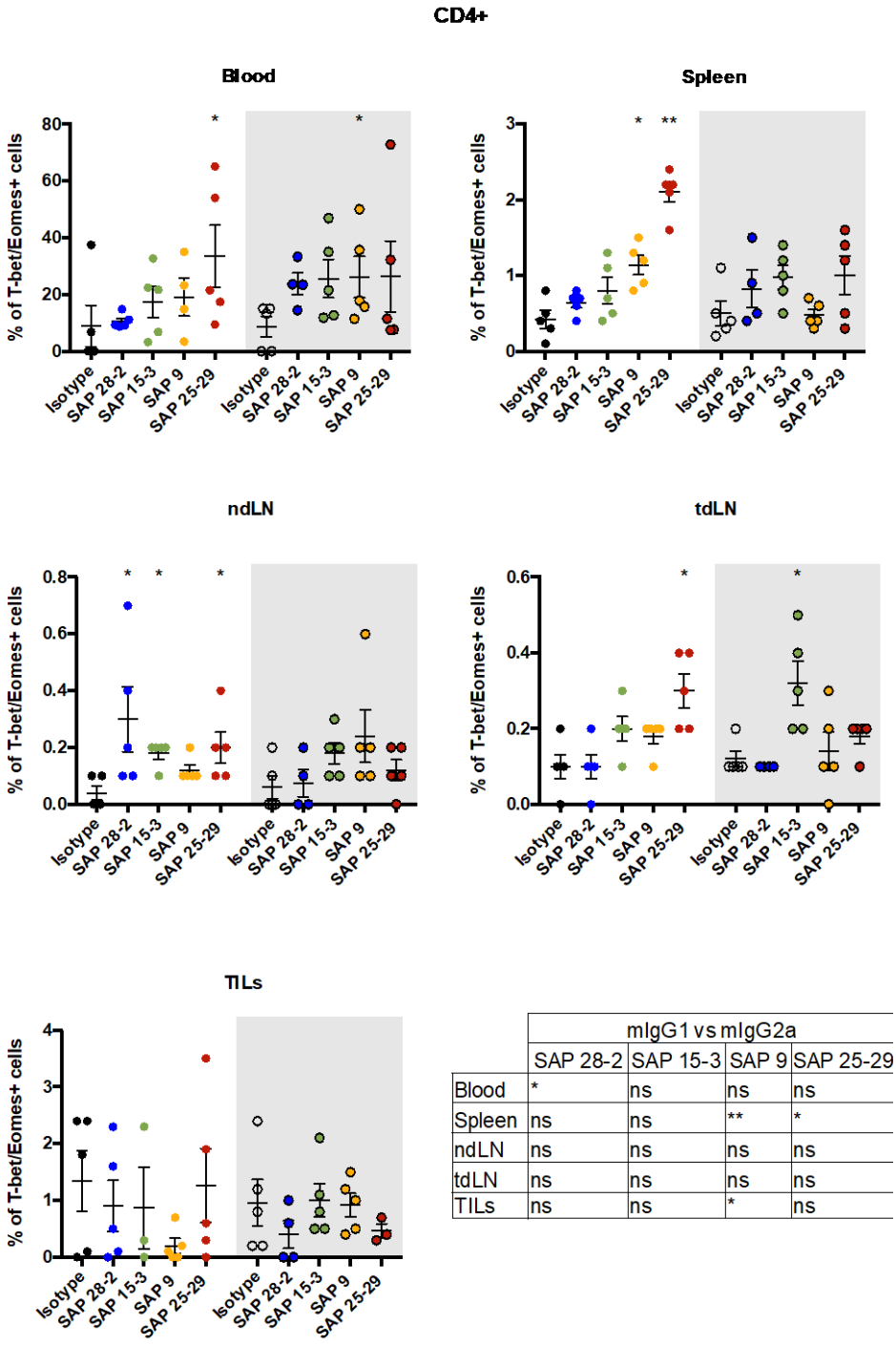

	mIgG1 vs mIgG2a			
	SAP 28-2	SAP 15-3	SAP 9	SAP 25-29
Blood	*	ns	ns	ns
Spleen	ns	ns	**	*
ndLN	ns	ns	ns	ns
tdLN	ns	ns	ns	ns
TILs	ns	ns	*	ns

Figure 6.20 Expression of T-bet/Eomes within CD4+ T cell populations from organs of E.G7-Ova bearing mice treated with anti-hOX40 mAb (mIgG1 and mIgG2a)

hOX40$^{+/+}$ KI mice were inoculated with 5x10^5 E.G7-Ova tumour cells s.c. Once tumours reached a size of between 5x5-10x10mm mice were subsequently treated with a total of 300ug of anti-hOX40 mAb (mIgG1 and mIgG2a) as shown in Figure 6.1. Day 4 post final treatment organs were harvested from mice and the expression of T-bet and Eomes within the CD4+ and CD8+ T cell populations was assessed using flow cytometry The white background on the graphs highlights the mIgG1 treated mice and the grey shaded background mIgG2a treated mice. mAb are ordered on the graph according to domain binding (CRD1-4, respectively). Statistical analysis shown on the graphs is between isotype control and treatment groups whereas that shown in the table is between mIgG1 and mIgG2a versions of the same mAb Each dot represents an individual mouse. Data represents one individual experiment with N=5 mice per treatment group. Error bars represent mean±SEM. Statistical significance was evaluated using a Mann-Whitney test; * P≤ 0.05, ** P≤ 0.01, *** P ≤ 0.001.

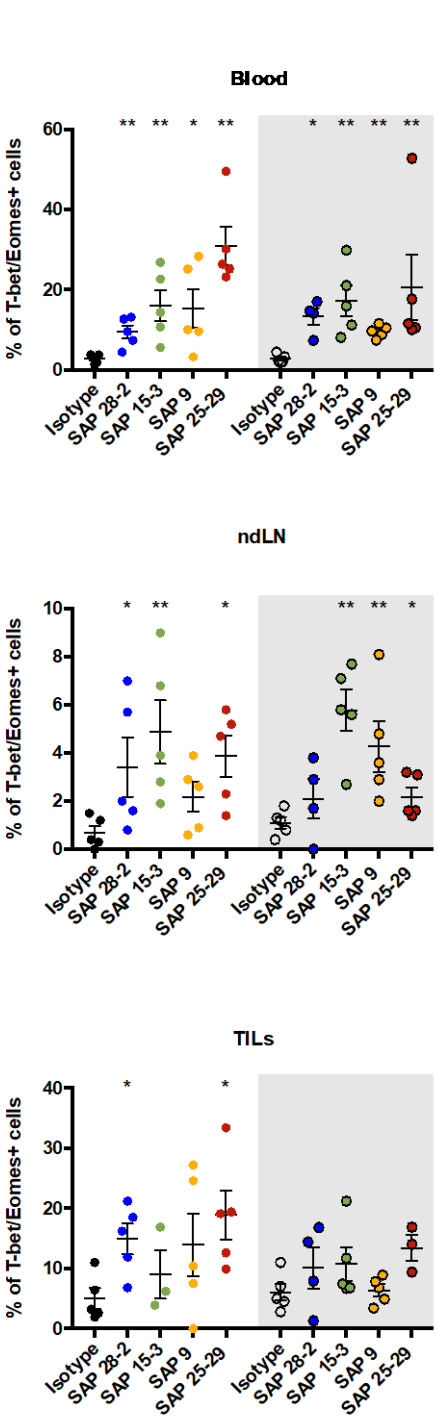

	mIgG1 vs mIgG2a			
	SAP 28-2	SAP 15-3	SAP 9	SAP 25-29
Blood	ns	ns	ns	ns
Spleen	ns	ns	ns	ns
ndLN	ns	ns	ns	ns
tdLN	*	ns	ns	ns
TILs	ns	ns	ns	ns

Figure 6.21 Expression of T-bet/Eomes within CD8+ T cell populations from organs of E.G7-Ova bearing mice treated with anti-hOX40 mAb (mIgG1 and mIgG2a)

The same experimental set up as described in Figure 6.20 was followed. The white background on the graphs highlights the mIgG1 treated mice and the grey shaded background mIgG2a treated mice. mAb are ordered on the graph according to domain binding (CRD1-4, respectively). Statistical analysis shown on the graphs is between isotype control and treatment groups whereas that shown in the table is between mIgG1 and mIgG2a versions of the same mAb Each dot represents an individual mouse. Data represents one individual experiment with N=5 mice per treatment group. Error bars represent mean±SEM. Statistical significance was evaluated using a Mann-Whitney test; * P≤ 0.05, ** P≤ 0.01, *** P ≤ 0.001.

When observing the percentage of granzyme B expressing CD4 and CD8 cells the levels were much more uniform between the mIgG1 and mIgG2a treated anti-hOX40 treated mice in comparison to the levels of T-bet and Eomes expression seen between the two isotype groups (Figure 6.22 and Figure 6.23). Within the CD4+ population of mIgG1 treated mice an increase in granzyme B+ cells was observed but only within the spleen (Figure 6.22). Likewise, in mIgG2a treated mice an increase in granzyme B+ CD4 cells was seen in the spleen and also within the blood. No change was seen in the lymph nodes with either mAb isotype, however a decrease in granzyme B expression was seen in CD4+ TILs of mIgG2a treated mice (Figure 6.22). Amongst CD8+ cells an increase in granzyme B was witnessed in the blood and TILs of mIgG1 treated mice, however within the lymph nodes and spleen levels stayed similar between isotype control treated mice and anti-hOX40 treated mice (Figure 6.23). In mIgG2a treated mice there was a statistically significant increase in granzyme B expression the blood, this trend was also observed within the spleen, ndLN and TILs, however this was more variable. The levels of granzyme B producing CD8+ and CD4+ T cells did not seem to be affected by antibody isotype as no significant difference was observed between the percentage of positive cells produced in mIgG1 and mIgG2a treatment groups (Figure 6.22 and Figure 6.23). To draw more solid conclusions from this data a repeat of the experiment would be needed to increase N numbers. This experiment, therefore, is currently being repeated within the lab.

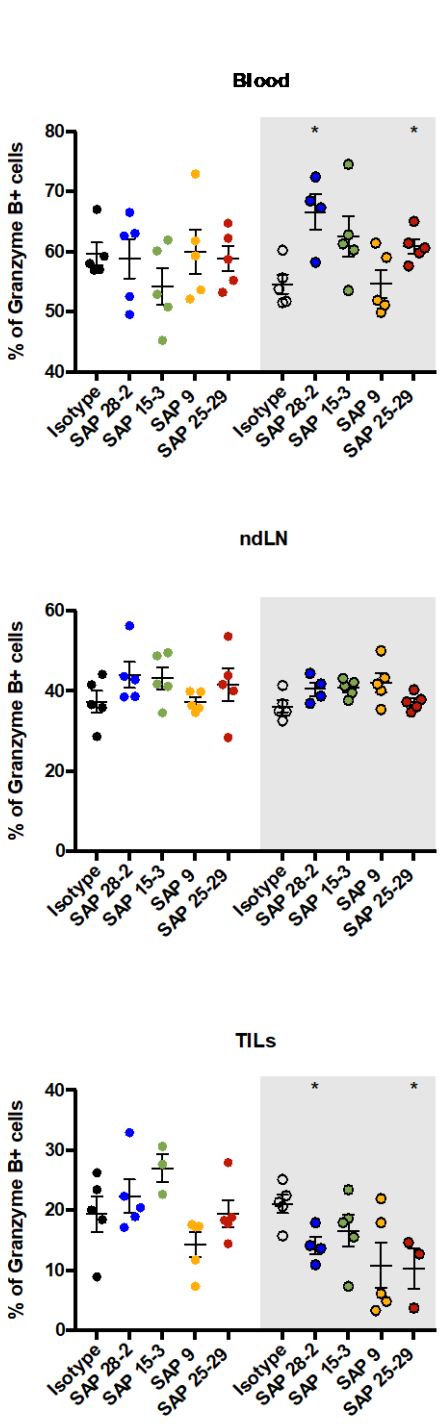

	mIgG1 vs mIgG2a			
	SAP 28-2	SAP 15-3	SAP 9	SAP 25-29
Blood	ns	ns	ns	ns
Spleen	ns	ns	ns	ns
ndLN	ns	ns	ns	ns
tdLN	ns	ns	ns	ns
TILs	ns	ns	ns	ns

Figure 6.22 Percentage of Granzyme B+ CD4+ T cell populations from organs of E.G7-Ova bearing mice treated with anti-hOX40 mAbs (mIgG1 and mIgG2a)

The same experimental set up as described in Figure 6.20 was used. Levels of Granzyme B within the CD4+ and CD8+ T cell populations was assessed using flow cytometry in blood, spleen, ndLN, tdLN and TILs. The white background on the graphs highlights the mIgG1 treated mice and the grey shaded background mIgG2a treated mice. mAb are ordered on the graph according to domain binding (CRD1-4, respectively). Statistical analysis shown on the graphs is between isotype control and treatment groups whereas that shown in the table is between mIgG1 and mIgG2a versions of the same mAb Each dot represents an individual mouse. Data represents one individual experiment with N=5 mice per treatment group. Error bars represent mean±SEM. Statistical significance was evaluated using a Mann-Whitney test; * P≤ 0.05, ** P≤ 0.01, *** P ≤ 0.001.

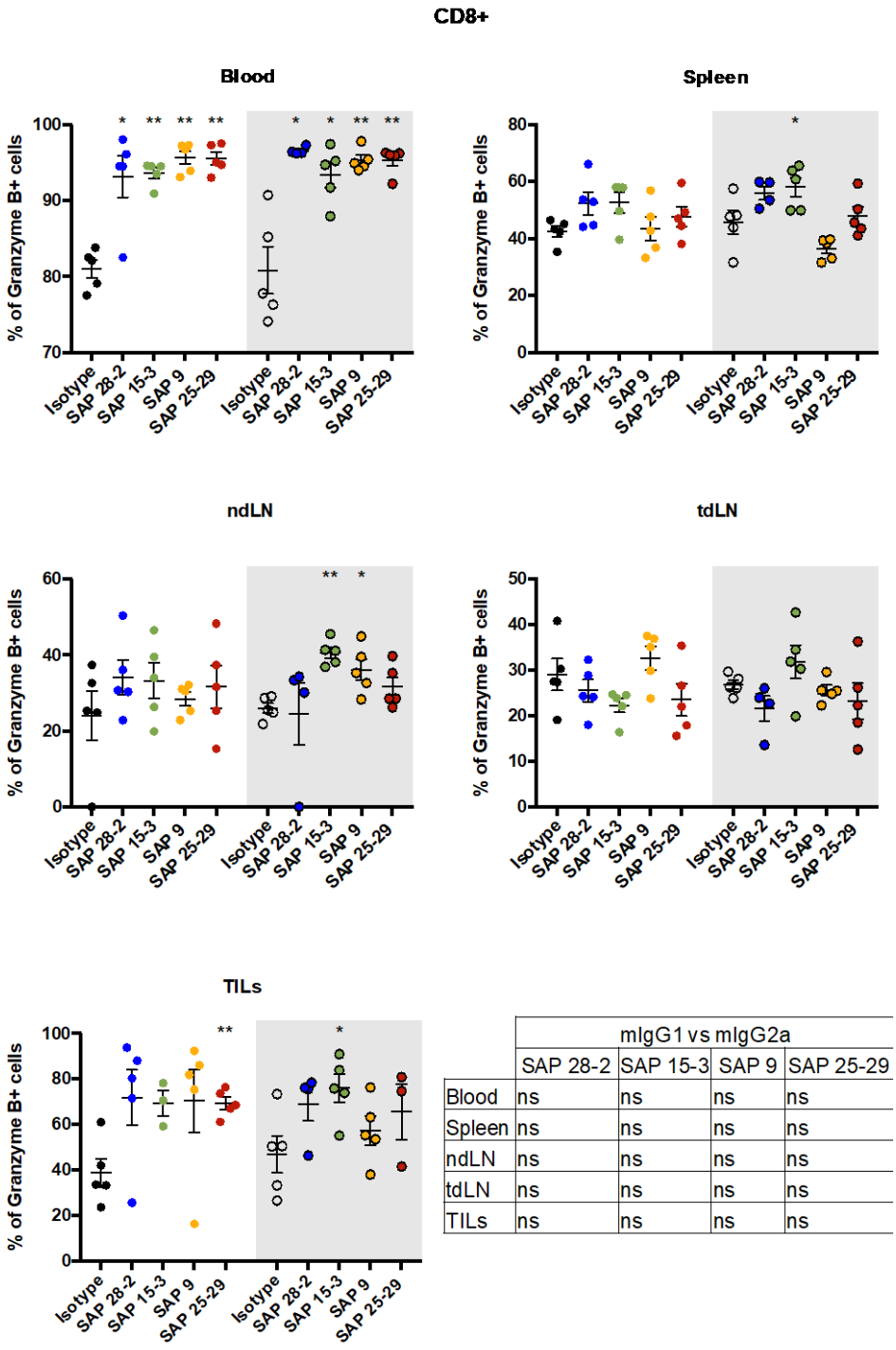

	mIgG1 vs mIgG2a			
	SAP 28-2	SAP 15-3	SAP 9	SAP 25-29
Blood	ns	ns	ns	ns
Spleen	ns	ns	ns	ns
ndLN	ns	ns	ns	ns
tdLN	ns	ns	ns	ns
TILs	ns	ns	ns	ns

Figure 6.23 Percentage of Granzyme B+ CD8+ T cell populations from organs of E.G7-Ova bearing mice treated with anti-hOX40 mAbs (mIgG1 and mIgG2a)

The same experimental set up as described in Figure 6.20 was used. Levels of Granzyme B within the CD8+ T cell populations was assessed using flow cytometry in blood, spleen, ndLN, tdLN and TILs. The white background on the graphs highlights the mIgG1 treated mice and the grey shaded background mIgG2a treated mice. mAb are ordered on the graph according to domain binding (CRD1-4, respectively). Statistical analysis shown on the graphs is between isotype control and treatment groups whereas that shown in the table is between mIgG1 and mIgG2a versions of the same mAb Each dot represents an individual mouse. Data represents one individual experiment with N=5 mice per treatment group. Error bars represent mean±SEM. Statistical significance was evaluated using a Mann-Whitney test; * P≤ 0.05, ** P≤ 0.01, *** P ≤ 0.001

From this initial experiment, however, a domain trend was seen in terms of the percentage of DP cells generated by each of the mAb. Although not as robust as the correlation seen between domain binding and mAb function observed in both the OT-I model and the previous E.G7-Ova tumour phenotyping (Figure 6.10-Figure 6.13) there was an element of the previous trend seen within the data. The data from mAb binding to CRDs 1+2 and those binding CRDs 3+4 from the spleen was therefore compared as before. Figure 6.24 demonstrates that the increase in T-Bet/Eomes DP cells in the CD4+ T cell population was greater with mIgG1 mAb binding CRDs 3+4 than mAb binding CRDs 1+2. A trend was also observed in the CD8+ T cells, however CRD 3 binding mAb, SAP 9, increased the percentage of DP cells to the same extent as mAb binding CRDs 1+2 hence the lack of statistical significance (Figure 6.24). Conversely, there seemed to be no domain bias when mice had been treated with mIgG2a versions of the mAb. These results highlighted that the correlation between domain binding and T-bet/Eomes expression is not as clear as that seen between domain binding and strength of mAb agonistic or depleting ability. Furthermore, mAb isotype seemed to be influencing whether or not a domain trend was observed.

Collectively, these results show that all of the anti-hOX40 mAb, irrespective of isotype or domain binding, are able to produce functional effector cells, as well as cells expressing transcription factors important for T cell effector and memory formation within a tumour environment. These results, however, did not further our understanding of the mechanisms behind the ability of both isotypes to generate therapeutic benefit.

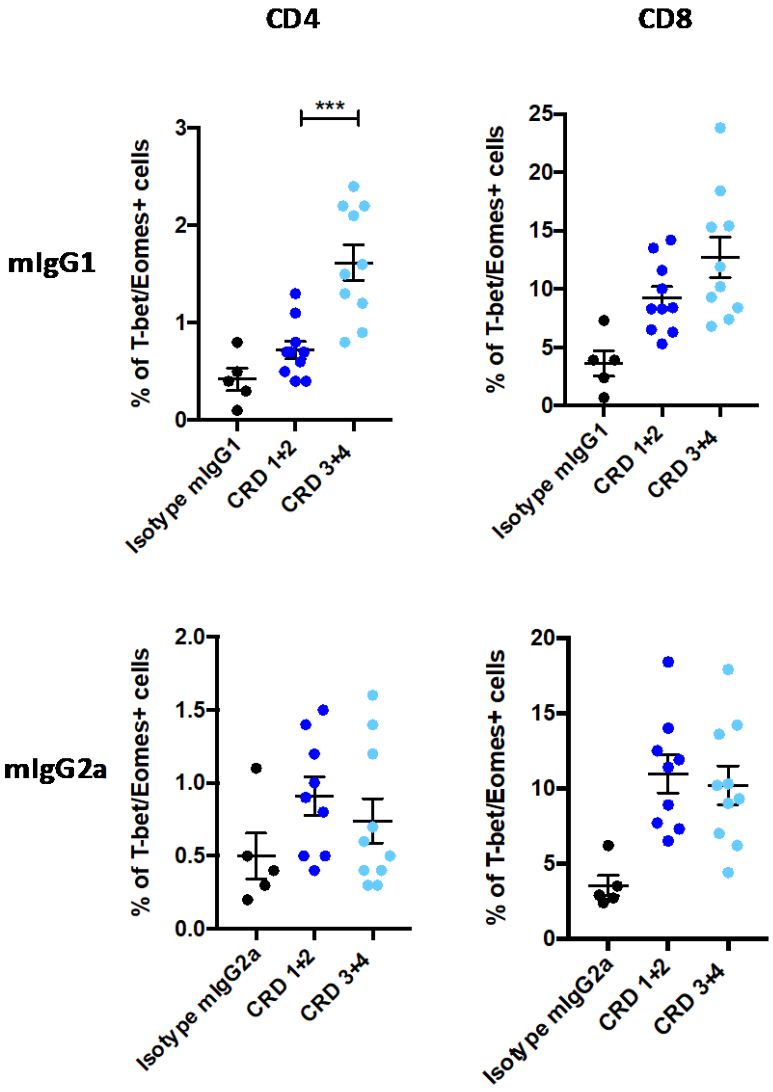

Figure 6.24 Expression of T-bet/Eomes within CD4+ and CD8+ T cell populations in the spleen of E.G7-Ova bearing hOX40$^{+/+}$ KI mice treated with anti-hOX40 mAb (mIgG1 and mIgG2a) grouped into CRD binding domains

Data from Figure 6.20 and Figure 6.21 was grouped into CRD binding categories CRD 1+2 (SAP 28-2 and SAP 15-3) and CRD 3+4 (SAP 9 and SAP 25-29). Graphs show percentage of T-bet/Eomes double positive CD4+ and CD8+ cells in spleen (left to right) in mIgG1 and mIgG2a treated mice (top to bottom). Each dot represents an individual mouse. Error bars represent mean±SEM. Statistical significance was evaluated using a Mann-Whitney test; * P≤ 0.05, ** P≤ 0.01, *** P ≤ 0.001

.

6.4 MCA-205 tumour model

To assess whether the ability of both isotypes of anti-hOX40 mAb to elicit therapy was applicable across multiple models, a second model was examined; the subcutaneous MCA-205 sarcoma cell line. As SAP 25-29 was seen to display a significant therapeutic difference between mIgG1 and mIgG2a in the E.G7-Ova tumour model, as well as demonstrating strong agonistic activity as a mIgG1 and strong depleting ability as a mIgG2a in the OT-I model, studies were performed with this mAb. hOX40$^{+/+}$ KI mice were therefore inoculated with MCA-205 cells and subsequently treated with SAP 25-29 (mIgG1 or mIgG2a) using the same dosing schedule as described in Figure 6.1. In contrast to the initial E.G7-Ova model, a higher percentage of survival was seen when mice were treated with the mIgG1 isotype in comparison to the mIgG2a mAb (33.3% vs. 16.6%, respectively) (Figure 6.25). The overall survival of mice in general was also lower in this model compared to the E.G7-Ova model. These results demonstrate that for any given target not only is isotype choice important but the type of tumour needs to also be considered, due to differences in immune infiltrate etc., when developing the most efficacious form of therapy.

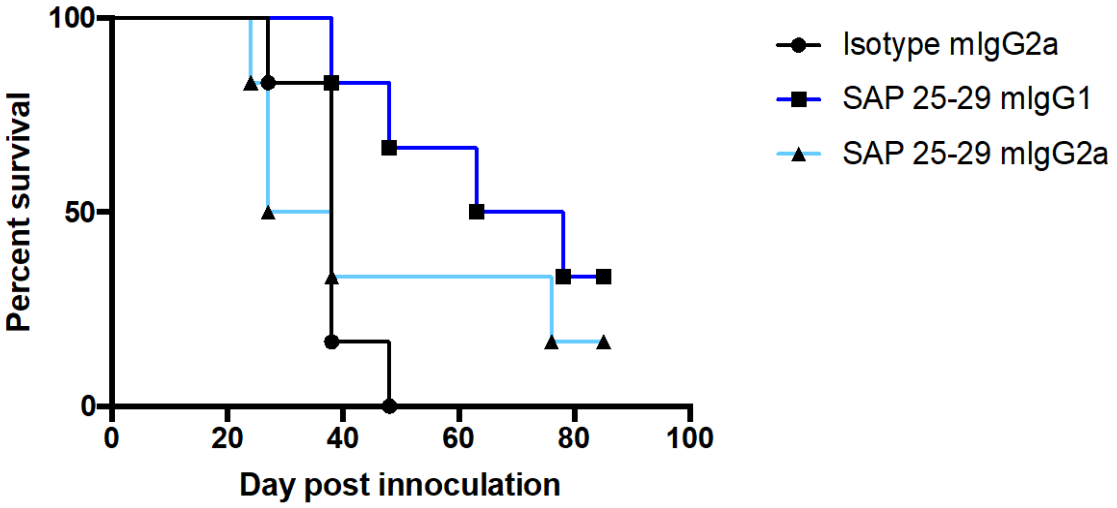

Figure 6.25 Comparison of the therapeutic effect of anti-hOX40 mAb SAP 25-29 as a mIgG1 and mIgG2a in the MCA-205 tumour model

$5x10^5$ MCA-205 tumour cells were injected s.c. in to the flank of $hOX40^{+/+}$ KI mice. Once tumours had reached 3x3-6x6mm mice were treated with a total of 300μg anti-hOX40 mAb. Mice were culled once a terminal end point had been reached which was decided as 15x15mm tumour size. Data is representative of 2 independent experiments with N=6 mice per treatment group.

6.5 Comparison of in-house anti-hOX40 mAb to clinically-relevant anti-hOX40 mAb

To gain an understanding of the translational potential of our panel of anti-hOX40 mAb, their therapeutic potential was compared with a series of anti-hOX40 mAb that are currently in clinical trials. To do this, several clinically-relevant mAb were identified from patent published sequences: MedImmune (9B12) (CRD3), GSK (106-222) (CRD2), Genentech (MOXR0916) (CRD4) and produced. First, these mAb were investigated for their therapeutic potential and functional ability as mIgG2a. To date the focus of anti-hOX40 mAb in the clinic has been on their agonistic ability, it was therefore of interest to determine the depleting ability of these mAb, and also to test whether the in-house mAb were superior in any way to the current clinically-relevant mAb. To achieve this hOX40$^{+/+}$ KI mice were inoculated with E.G7-Ova tumour cells followed by treatment with the in-house or clinically-relevant anti-hOX40 mAb using the dosing schedule illustrated in Figure 6.1. Figure 6.26 demonstrates that the in-house anti-hOX40 mIgG2a mAb, with the exception of SAP 15-3, were at least as therapeutically active as the clinically-relevant anti-hOX40 mAb in the E.G7-Ova tumour model. Consistent with results from the previous E.G7-Ova survival experiments (Figure 6.2), SAP 25-29 treated mice had the highest percent survival (83%) compared to all other mAb. In this particular experiment SAP 28-2 provided the second best therapy (66%) followed closely by SAP 9 (61%) and lastly SAP 15-3 (50%). Out of the clinically relevant anti-hOX40 mAb GSK and Genentech provided the same amount of therapy as SAP 15-3, with 50% of mice surviving, whereas MedImmune's mAb produced only half that amount of therapy with 25% of mice surviving. It should be noted that all of the clinically relevant mAb are human antibodies grafted onto a mouse IgG2a Fc, as opposed to the SAP antibodies which are all murine.

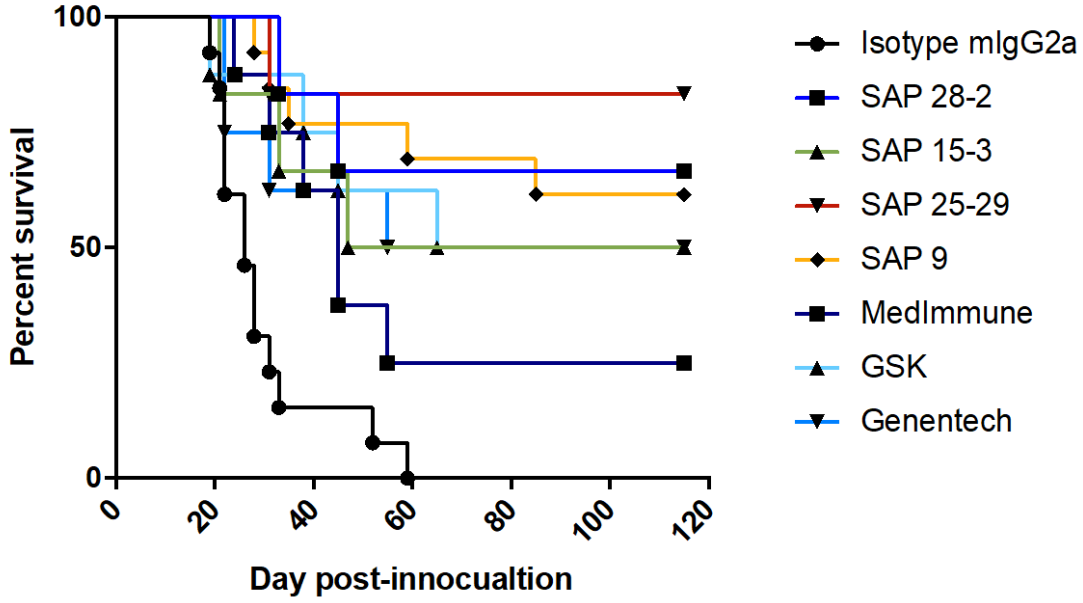

Figure 6.26 Therapeutic effect of in-house anti-hOX40 mAb versus clinically-relevant anti-hOX40 mAb in an E.G7-Ova tumour model

$5x10^5$ E.G7-Ova tumour cells were injected s.c. in to the flank of $hOX40^{+/+}$ KI mice. Once tumours had reached 5x5-10x10mm mice were treated with a total of 300μg anti-hOX40 mAb. Mice were culled once a terminal end point had been reached which was decided as 20x20mm tumour size. Graph shows survival curves from one independent experiment with N=6 mice per treatment group.

In order to compare if the clinically-relevant mAb function in a similar manner to the in-house mAb, $hOX40^{+/+}$ KI mice were again inoculated with E.G7-Ova tumour cells and subsequently treated with anti-hOX40 mAb using the dosing regime shown in Figure 6.1. 4 days post final treatment organs were harvested and T cell populations numerated using flow cytometry. Within the spleen and ndLN isotype control treated mice showed great variability in CD4, CD8 and Treg numbers making it difficult to draw any firm conclusions from the data (Figure 6.27-Figure 6.29). The isotype control treated mice within the tdLN, however, were a lot tighter, so although data was still quite variable within treatment groups a general trend indicating increase in T cell numbers could be seen (Figure 6.27-Figure 6.29). Data obtained from the blood was much clearer, especially in the SAP treated groups. A decrease in the number of total CD4+ cells (Figure 6.27) as well as Tregs (Figure 6.29) was observed. CD8+ numbers were more variable but hinted at a decrease in all anti-hOX40 treated groups (Figure 6.28). Within the blood, the SAP mAb seemed to be better depleters than the clinically-relevant mAb tested and within the Treg population this seemed to follow the same domain trend witnessed throughout the research (CRD 3+4 better depleters than CRD 1+2).

This was not true however for the clinically relevant mAb. In terms of Treg depletion in the blood MedImmune (CRD3 binder) was the strongest depleter, followed by GSK (CRD2 binder) and lastly Genentech (CRD4 binder). Again only a small number of cells were able to be recovered from TILs making the data very difficult to interpret. Some treatment groups also only contained 2 mice per group due to tumours being too small or non-existent because of the effects of treatment. Nevertheless, the CD8:Treg ratios were increased in the blood, ndLN and tdLN, although not statistically significant, although this trend was not so clear in the spleen and tumour again due to variability and lack of cells, respectively (Figure 6.30). SAP 9 mIgG1 was included within this experiment as a point of comparison however it did not differ dramatically from the isotype control in most cases due to the caveats in this experiment as described above.

From this data it could be concluded with caution that the SAP mAb cause better depletion and increase the CD8:Treg ratio in a favourable manner more so than any of the clinically-relevant mAb tested. This would explain the more efficacious therapy observed in Figure 6.26, however to conclude this with confidence and determine any domain related bias amongst the clinically-relevant mAb further repeat experiments would need to be carried out. Furthermore, it would also be of interest to test the in-house and clinically-relevant mAb as mIgG1 isotypes to determine if the SAP anti-hOX40 mAb are superior agonists than the current clinically-relevant mAb. Unfortunately, due to time-restrictions, these experiments were not performed.

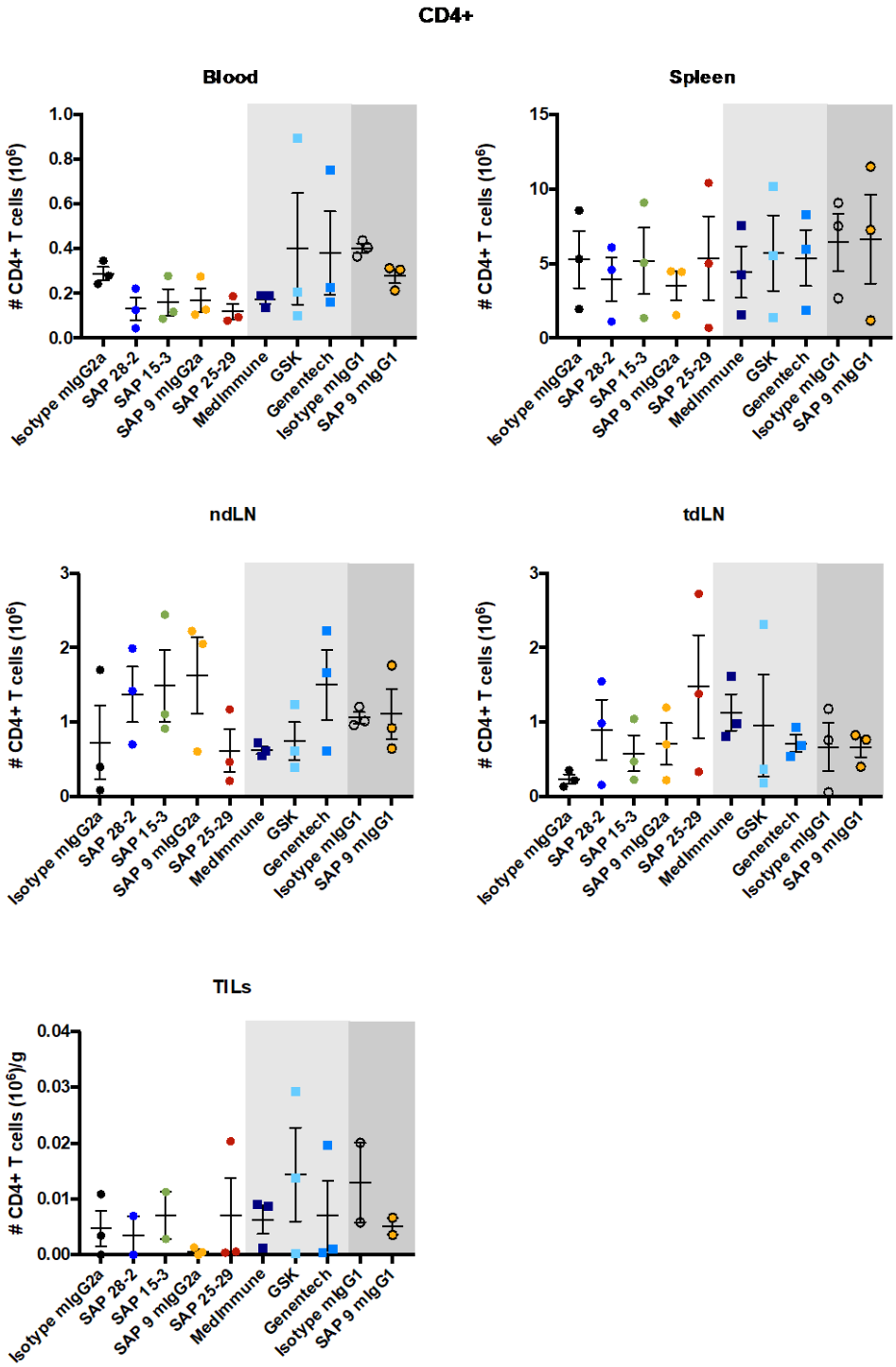

Figure 6.27 Numeration of CD4+ T cells within multiple organs from E.G7-Ova bearing hOX40$^{+/+}$ KI mice after treatment with anti-hOX40 mAb (In-house vs clinically-relevant)

hOX40$^{+/+}$ KI mice were inoculated with 5x10^5 E.G7-Ova tumour cells s.c. Once tumours reached a size of between 5x5 -10x10mm mice were subsequently treated with a total of 300μg of anti-hOX40 mAb (mIgG1 and mIgG2a). Day 4 post final treatment organs were harvested from mice and T cell subsets numerated using flow cytometry. Graphs show the number of CD4+ T cells in blood, spleen, ndLN, tdLN and TILs. TIL numbers are normalised to tumour weight (g). The white background on the graphs highlights the in-house anti-hOX40 treated mice, the light grey shaded background the clinically-relevant anti-hOX40 treated mice and the dark grey background SAP 9 mIgG1 treated mice. In-house SAP mAb are ordered on the graph according to domain binding (CRD1-4, respectively). Data is representative of 1 independent experiment with N=2/3 mice per treatment group. Each dot represents an individual mouse. Error bars represent mean±SEM

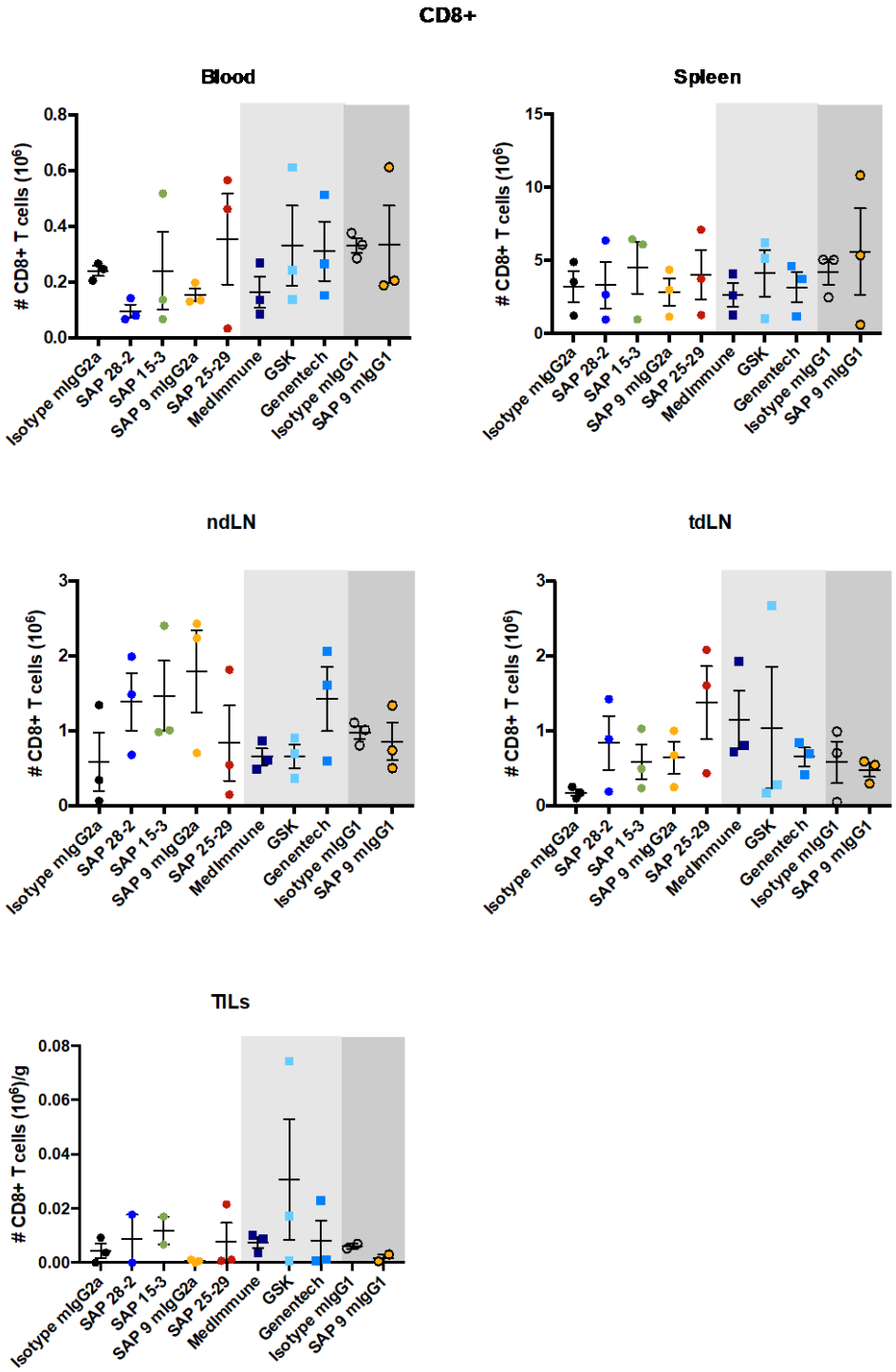

Figure 6.28 Numeration of CD8+ T cells within multiple organs from E.G7-Ova bearing hOX40$^{+/+}$ KI mice after treatment with anti-hOX40 mAb (In-house vs clinically-relevant)

The same experimental set up as described in Figure 6.27 was used. Graphs show the number of CD8+ T cells in blood, spleen, ndLN, tdLN and TILs. The white background on the graphs highlights the in-house anti-hOX40 treated mice, the light grey shaded background the clinically-relevant anti-hOX40 treated mice and the dark grey background SAP 9 mIgG1 treated mice. In-house SAP mAb are ordered on the graph according to domain binding (CRD1-4, respectively). Data is representative of 1 independent experiment with N=2/3 mice per treatment group. Each dot represents an individual mouse. Error bars represent mean±SEM.

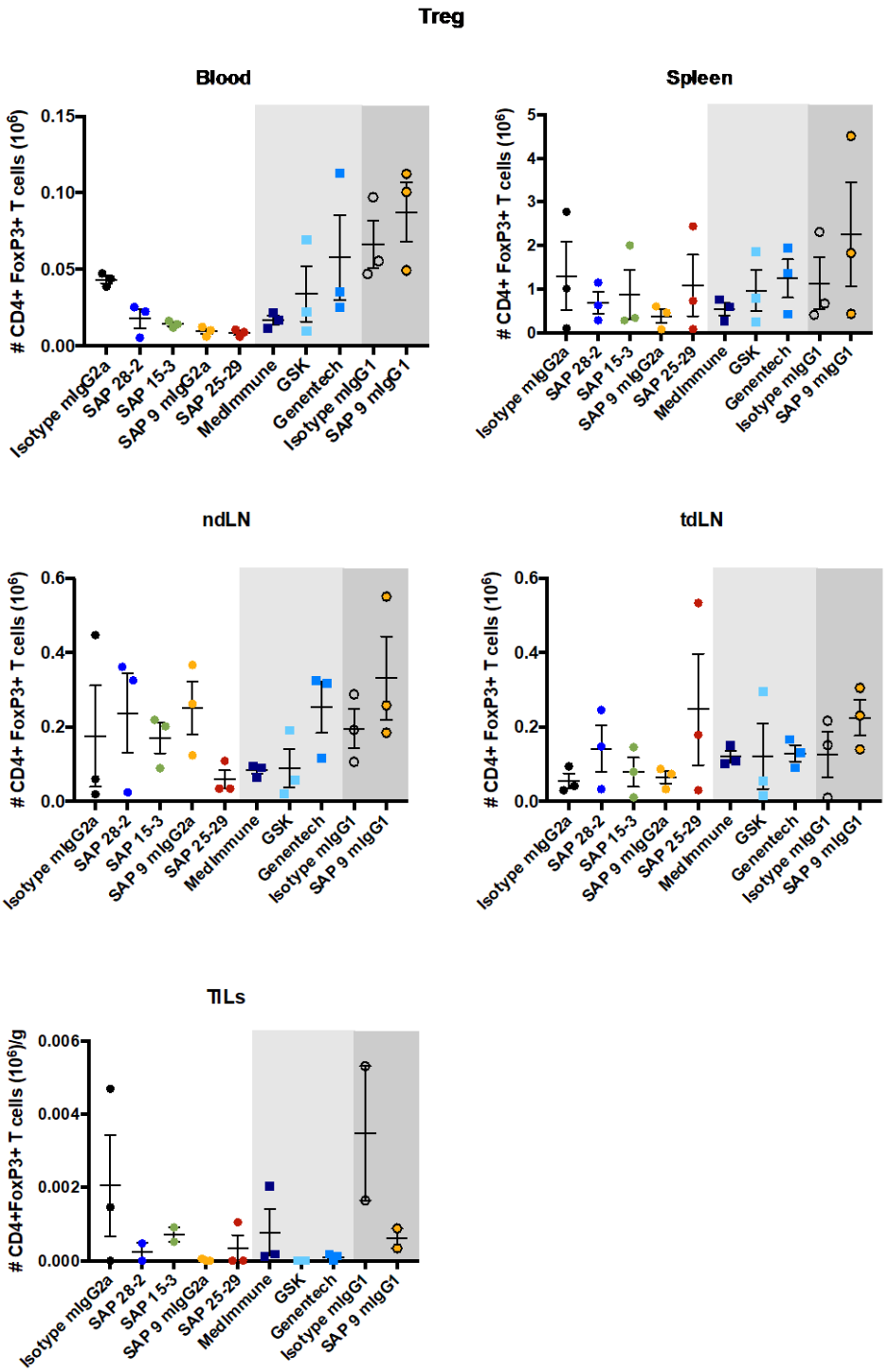

Figure 6.29 Numeration of Tregs within multiple organs from E.G7-Ova bearing hOX40$^{+/+}$ KI mice after treatment with anti-hOX40 mAb (In-house vs clinically-relevant)

The same experimental set up as described in Figure 6.27 was used. Graphs show the number of Treg cells in blood, spleen, ndLN, tdLN and TILs. The white background on the graphs highlights the in-house anti-hOX40 treated mice, the light grey shaded background the clinically-relevant anti-hOX40 treated mice and the dark grey background SAP 9 mIgG1 treated mice. In-house SAP mAb are ordered on the graph according to domain binding (CRD1-4, respectively). Data is representative of 1 independent experiment with N=2/3 mice per treatment group. Each dot represents an individual mouse. Error bars represent mean±SEM

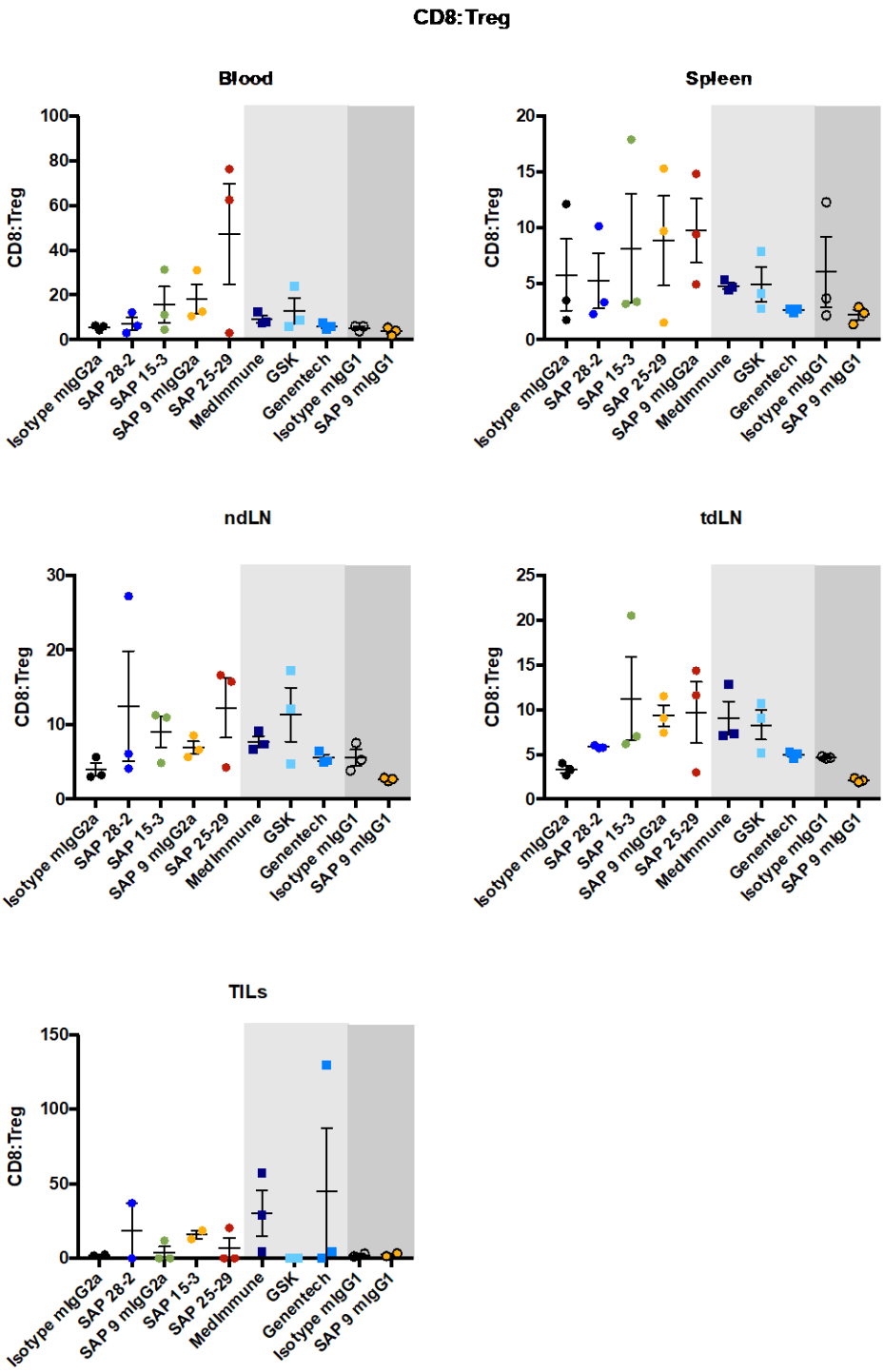

Figure 6.30 CD8:Treg ratio within multiple organs from E.G7-Ova bearing hOX40$^{+/+}$ KI mice after treatment with anti-hOX40 mAb (In-house vs clinically-relevant)

The same experimental set up as described in Figure 6.27 was used. Graphs show the CD8:Treg ratio in blood, spleen, ndLN, tdLN and TILs. The white background on the graphs highlights the in-house anti-hOX40 treated mice, the light grey shaded background the clinically-relevant anti-hOX40 treated mice and the dark grey background SAP 9 mIgG1 treated mice. In-house SAP mAb are ordered on the graph according to domain binding (CRD1-4, respectively). Data is representative of 1 independent experiment with N=2/3 mice per treatment group. Each dot represents an individual mouse. Error bars represent mean±SEM

6.6 Combination of anti-hOX40 with anti-4-1BB

It is well known that combination therapies can provide more efficacious forms of treatment in comparison to monotherapies as discussed in the introduction. As many of the clinically-relevant hOX40 mAb are currently being tested in combination in clinical trials, to further examine our in-house antibodies capacity for therapeutic potential, anti-hOX40 antibodies were combined with anti-4-1BB antibodies. Anti-4-1BB mAb were chosen because they too have emerged as a powerful and effective means of enhancing the anti-tumour immune response in a number of different murine tumour models [198, 355, 356]. Furthermore, they have been shown to synergise *in vivo* resulting in robust CD8 T cell effector function and eradication of established tumours [353]. Of particular interest within this experiment however, was whether combining anti-hOX40 mIgG1 and mIgG2a in the same treatment regime and making use of the two different mechanisms observed in the previous experiments would be more beneficial than targeting two individual receptors as is being done in current clinical trials. To achieve this MC38 tumour cells were injected s.c. into hOX40$^{+/-}$ KI mice. hOX40$^{+/-}$ KI mice were used to mimic an expression pattern of hOX40 which matched more closely that seen in humans (see discussion in Chapter 3). Furthermore, the MC38 tumour model was used as therapy with anti-4-1BB mAb and anti-4-1BB/anti-OX40 combinations had been observed previously within the lab. The treatment regime illustrated in

Figure 6.31 was followed. The total amount of anti-hOX40 mAb per dose given in this experiment was larger than previous experiments for two reasons: 1) due to MC38 tumours being more difficult to treat than E.G7-Ova tumours; 2) to prevent significant numbers of mice being culled prior to mAb treatment completion (due to ulceration) - hence the dosage was increased to shorten the treatment time. Organs were harvested from mice 4 days post final treatment and the number of CD4+, CD8+ and Treg cells determined using flow cytometry.

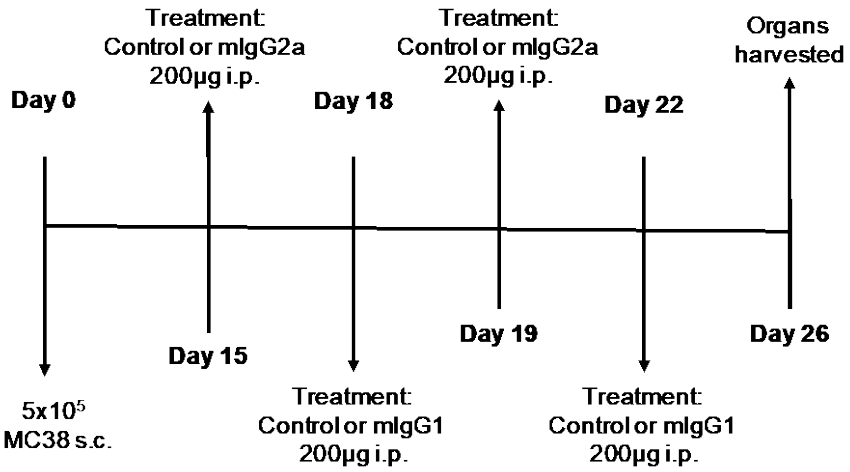

Treatment name	Antibody clone
4-1BB mIgG1	Lob 12.0
4-1BB mIgG2a	Lob 12.0
OX40 mIgG1	SAP 25-29
OX40 mIgG2a	SAP 9

Figure 6.31 Treatment regime and anti-hOX40 mAb used in combination experiment

hOX40$^{+/-}$ KI mice were inoculated with 5x10^5 MC38 tumour cells s.c. 2 weeks post inoculation mice started the treatment regime illustrated above. 4 days post final treatment organs were harvested and T cell subsets numerated using flow cytometry. The table illustrates the antibody clones of anti-4-1BB and anti-OX40 mAb used within this experiment.

The results generated from this experiment, shown in Figure 6.32-Figure 6.35, showed no initial benefit of combination therapy over monotherapy. The data points in this experiment however were very variable as well as some treatment groups only being N=2 due to tumour rupture. It was therefore very difficult to draw any solid conclusions. Furthermore, very small cell numbers were recovered from some organs, again adding to the difficulty of interpreting these results. It would therefore be of benefit to test this combination therapy in a more robust tumour model such as E.G7-Ova to answer the questions about combination discussed above. Performing survival experiments will also enable determination of the ability of the combinations, over monotherapy, to eradicate established tumours; the ultimate aim of any treatment

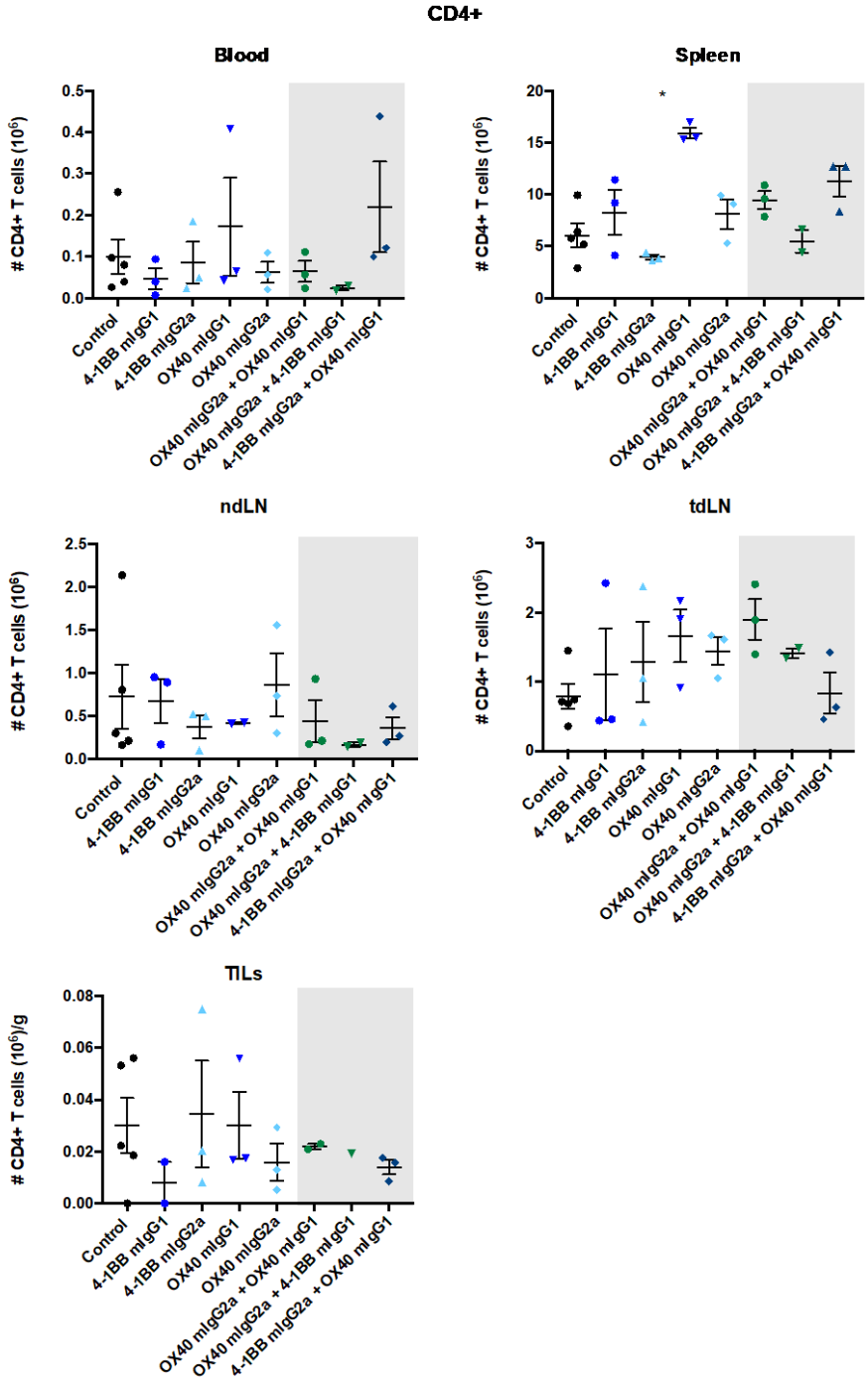

Figure 6.32 Numeration of CD4+ T cells within multiple organs from MC38 bearing hOX40$^{+/-}$ KI mice after combination treatment (anti-hOX40 and anti-m4-1BB)

hOX40$^{+/-}$ KI mice were inoculated with 5x10^5 MC38 tumour cells s.c. Day 15 post tumour innoculation mice were subsequently treated using the regime described in
Figure 6.31. Day 4 post final treatment organs were harvested from mice and T cell subsets numerated using flow cytometry. Graphs show the number of CD4+ T cells in the blood, spleen, ndLN, tdLN and TILs. TIL numbers are normalised to tumour weight (g). The white background on the graphs highlights the monotherapy treatment groups and the grey shaded background combination treatment groups. Data is representative of 1 independent experiment with N=2-5 mice per treatment group. Each dot represents an individual mouse. Error bars represent mean±SEM. Statistical significance was evaluated using a Mann-Whitney test; * P≤ 0.05, ** P≤ 0.01, *** P ≤ 0.001.

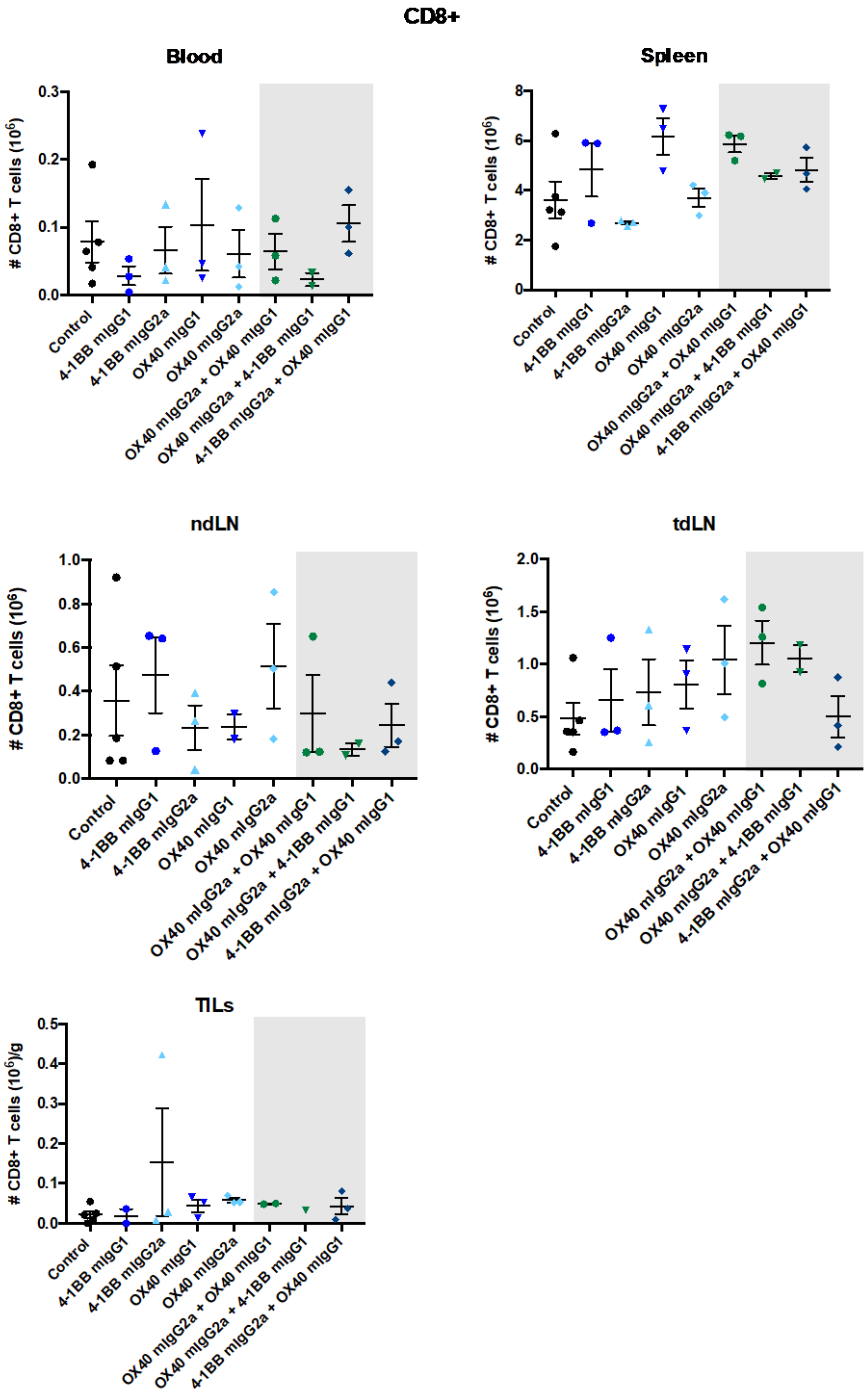

Figure 6.33 Numeration of CD8+ T cells within multiple organs from MC38 bearing hOX40$^{+/-}$ KI mice after combination treatment (anti-hOX40 and anti-m4-1BB)

The same experimental set up as described in Figure 6.32 was used Graphs show the number of CD8+ T cells in the blood, spleen, ndLN, tdLN and TILs. The white background on the graphs highlights the monotherapy treatment groups and the grey shaded background highlights combination treatment groups. Data is representative of 1 independent experiment with N=2-5 mice per treatment group. Each dot represents an individual mouse. Error bars represent mean±SEM. Statistical significance was evaluated using a Mann-Whitney test; * P≤ 0.05, ** P≤ 0.01, *** P ≤ 0.001.

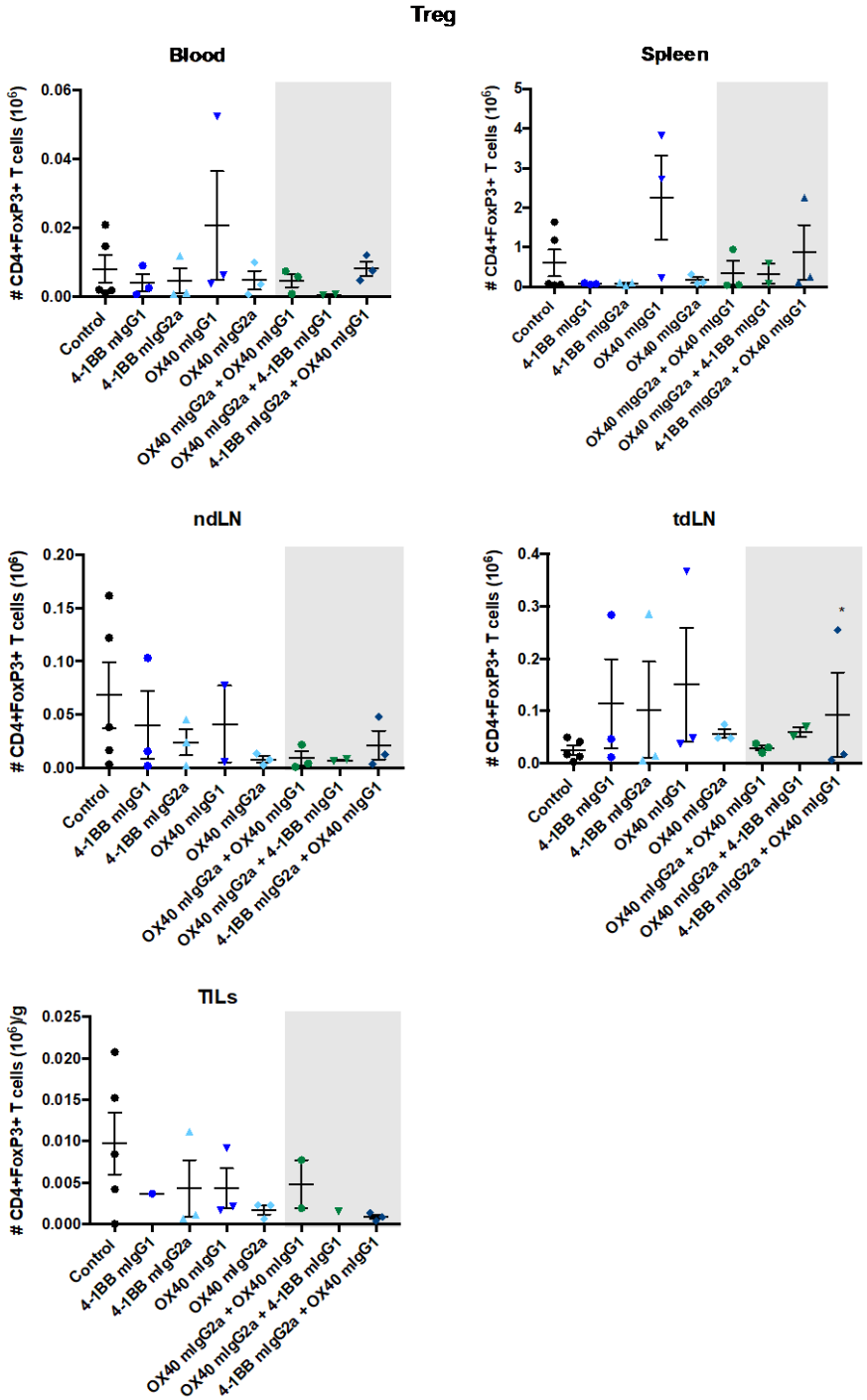

Figure 6.34 Numeration of Tregs within multiple organs from MC38 bearing hOX40$^{+/-}$ KI mice after combination treatment (anti-hOX40 and anti-m4-1BB)

The same experimental set up as described in Figure 6.32 was used Graphs show the number of Tregs in the blood, spleen, ndLN, tdLN and TILs. The white background on the graphs highlights the monotherapy treatment groups and the grey shaded background highlights combination treatment groups. Data is representative of 1 independent experiment with N=2-5 mice per treatment group. Each dot represents an individual mouse. Error bars represent mean±SEM. Statistical significance was evaluated using a Mann-Whitney test; * P≤ 0.05, ** P≤ 0.01, *** P ≤ 0.001.

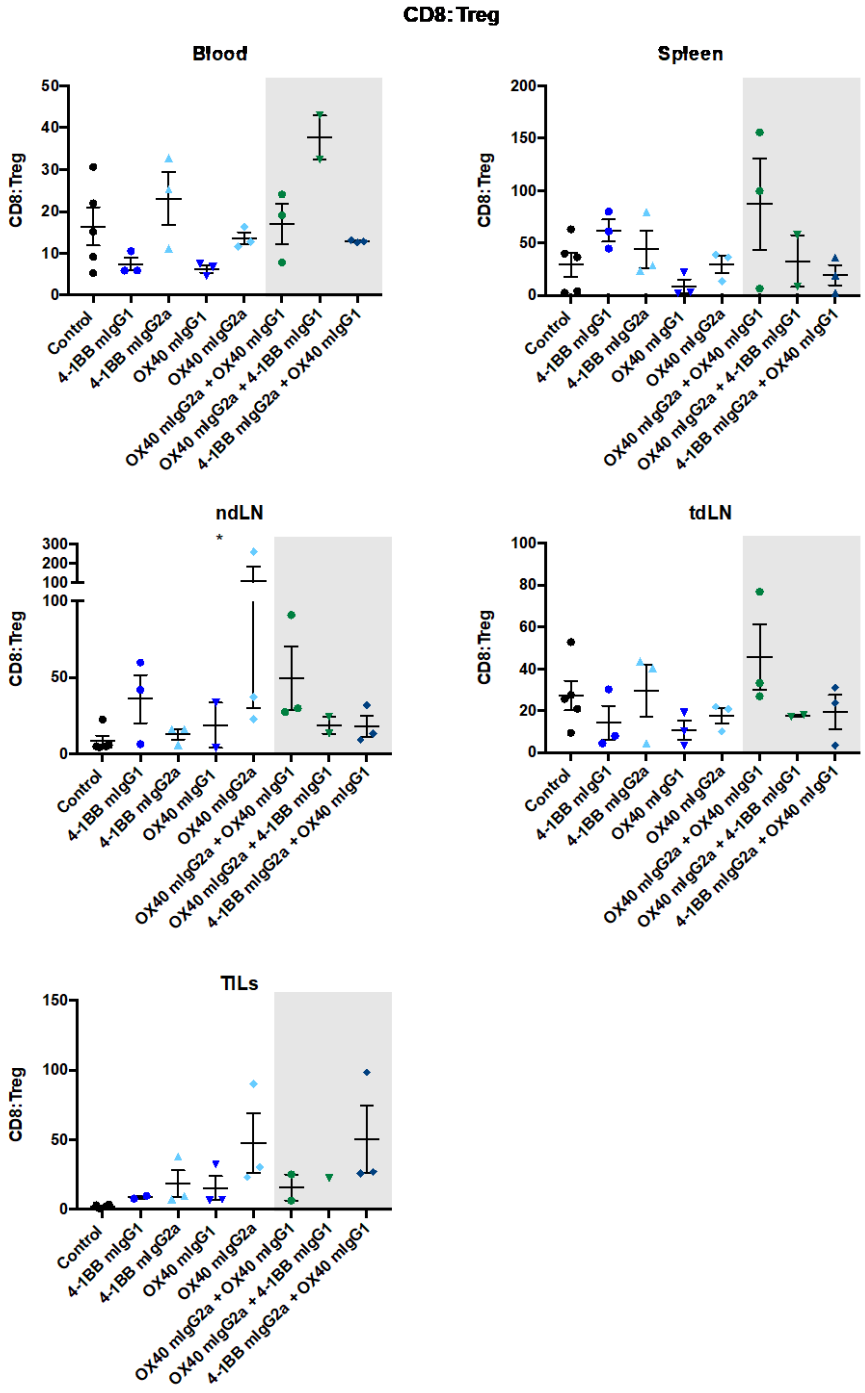

Figure 6.35 CD8:Treg ratio within multiple organs from MC38 bearing hOX40$^{+/-}$ KI mice after combination treatment (anti-hOX40 and anti-m4-1BB)

The same experimental set up as described in Figure 6.32 was used Graphs show the CD8:Treg ratio in the blood, spleen, ndLN, tdLN and TILs. The white background on the graphs highlights the monotherapy treatment groups and the grey shaded background highlights combination treatment groups. Data is representative of 1 independent experiment with N=2-5 mice per treatment group. Each dot represents an individual mouse. Error bars represent mean±SEM. Statistical significance was evaluated using a Mann-Whitney test; * P≤ 0.05, ** P≤ 0.01, *** P ≤ 0.001.

6.7 Discussion

Within this chapter the therapeutic potential of a number of our anti-hOX40 mAb were explored, one that binds each CRD of hOX40, in a number of tumour models. Furthermore, their therapeutic effects were compared to those evoked by clinically-relevant anti-hOX40 mAb.

The results of this chapter have highlighted the already known importance of isotype choice when deciding upon a therapeutic mAb, but also that domain binding needs to be considered when choosing the best therapeutic. Within the E.G7-Ova and MCA-205 tumour models it was demonstrated that dependent on tumour type isotype preference can change. Within the E.G7-Ova model, SAP 25-29 was most active as a mIgG2a, conversely the mIgG1 mAb provided more activity in the MCA-205 model. Rationale behind this includes the amount and nature of immune cell infiltrate that each tumour type elicits; certain tumours are more immunogenic than others which is also true for human cancers. Furthermore, the types of cells and expression of the target will also play a huge role in deciding which isotype will be most beneficial. For example, in terms of the anti-hOX40 mAb as mIgG1 and mIgG2a, if a tumour had a large infiltrate of NK and myeloid cells expressing high levels of activatory FcγR combined with Tregs expressing high levels of hOX40, it is not surprising that a mIgG2a would probably provide better therapy than a mIgG1 mAb in this environment. Currently, data describing the immune infiltrate and expression levels of both hOX40 and FcγR within these two tumours are lacking, preventing us from addressing this hypothesis. That being said, however, all of our mAb were able to cause some level of therapy in the E.G7-Ova tumour model as either isotype. This was perhaps surprising in terms of mIgG1 treated mice as phenotyping of organs from E.G7-Ova bearing mice demonstrated that the mAb were functioning in a similar manner to what was seen in the OT-I model meaning the CD8:Treg ratio was only increased with mIgG2a treated mice.

As eluded to above, the general trends of T cell changes in in the OT-I model were also witnessed in the tumour model; mIgG1 mAb caused expansion of T cell subsets and mIgG2a mAb causing depletion of certain subsets, in particular Treg. This was seen within all organs analysed, however the cell recovery from tumours was poor making it difficult to obtain reliable data. Optimising TIL recovery upon

harvest would therefore be of benefit to these experiments. In addition to manipulation of the enzymatic digestion protocols, an alternative treatment and harvesting strategy could be performed whereby larger groups are initiated and only tumours within very narrow size parameter are treated and harvested. The CD8:Treg ratios were again highest in the mIgG2a treated mice, as had been seen previously in the OT-I model. From the OT-I results it was speculated that the mIgG2a mAb would result in the best therapy due to this increased ratio which has been described in a number of studies as being a good indicator for prolonged survival in both mouse and humans [344]. However, despite the lack of increase in CD8:Treg ratio in the mIgG1 treated mice, they too were able to cause therapy in an E.G7-Ova tumour model. These results highlight that there are multiple factors contributing to a mAb ability to act as a therapeutic and this can vary between different isotypes of the same mAb. Within the phenotyping results assessing T cell numbers within different organs, an element of domain preference was observed, similar to that seen within the OT-I model. mIgG1 anti-hOX40 mAb which bound to CRDs 3+4 tended to be stronger agonists than those binding CRDs 1+2, this however was not seen within all T cell subsets or across all organs assessed. Statistically significant results were witnessed in CD4+, CD8+ and Treg populations but mainly in the lymph nodes over the blood and spleen. Rationale behind his may be the types of immune cells present in the specific organs and therefore FcγR availability. Alternatively, it may be due to the different cytokine milieu. More in depth phenotyping of these organs would enable us to answer these questions. Furthermore, mIgG2a mAb only showed domain binding preference for depletion of cells within the tetramer+ population in the spleen. These results indicate that the organ type and hence environment in a tumour setting influence the tendency of mAb to show a domain preference for strength of functional ability; mIgG1 agonism and mIgG2a depletion.

To dissect further the reasons behind the ability of both isotypes to act therapeutically the T cells were further phenotyped looking at transcription factors T-bet and Eomes as they are known to be key drivers of cytolytic function in both CD8+ and CD4+ T cells. Furthermore, the percentage of cells expressing the effector molecule granzyme B was determined. These results however provided no further understanding/clarity as to why both mIgG1 and mIgG2a anti-hOX40 mAb cause therapy as the levels of double positive cells and granzyme B

expression were similar between both isotype treatments. Interestingly, however, a slight domain trend in terms of the expression of T-bet/Eomes in mIgG1 treated mice was observed but the same was not seen in mIgG2a treated mice. This result highlights the reoccurring theme within this research that domain binding is also an important factor to consider as it seems to influence a number of different functions in an isotype-dependent manner.

The panel of mAb were then compared in anti-tumour efficacy as mIgG2a with several clinically-relevant anti-hOX40 mAb. The in-house mAb provided more efficacious therapy, with the exception of SAP 15-3, when compared to the clinically-relevant mAb in the E.G7-Ova tumour model. Although the phenotyping data was variable, the SAP mAb did increase the CD8:Treg ratio above that of the clinically-relevant mAb. No domain binding preference was seen amongst the clinically relevant mAb as was previously observed with the SAP mAb. However the N numbers within this experiment were small and data points variable, it would be of interest to repeat this experiment as well as test all of the mAb as mIgG1 mAb.

Lastly, mice were assessed for immunotherapy using the OX40 mAb in combination with 4-1BB mAb (again of various isotypes). As discussed in the introduction combinations are usually more effective than monotherapies, it was therefore of interest to determine if this was the case for our anti-hOX40 mAb. These experiments were also designed to assess if a single mAb specificity (OX40) delivered sequentially as two different isotypes (mIgG1 and mIgG2a) was beneficial. In essence, could the separate beneficial functions of the mIgG1 (T cell expansion) and mIgG2a mAb (deletion), be combined to produce a more efficacious form of therapy? Unfortunately, however, the data obtained from phenotyping these mice was very variable which made it difficult to conclude whether this type of combination would be therapeutically beneficial over the monotherapies. It would therefore be of interest to repeat this experiment to allow us to answer the questions proposed above as well as perform survival experiments to determine the ability of the combinations to eradicate established tumours as well as generate memory, as has been seen with the monotherapies.

In summary, the work in this chapter shows that the SAP panel of anti-hOX40 mAb can act therapeutically in a number of tumour models as both mIgG1 and mIgG2a

isotypes, despite obvious mechanistic differences. mAb domain binding preference is also present in certain organs and is therefore another aspect to be considered when choosing a therapeutic mAb. Furthermore, we have shown that our mAb compare favourably with the clinically-relevant mAb and that combination therapy may also be a beneficial route to explore.

Chapter 7 General discussion and future work

Immunomodulatory mAb have shown great potential as novel forms of anti-cancer therapeutics. Agonistic mAb targeting TNFRSF members have shown particular promise in preclinical mouse studies [357]. In this thesis, the T cell co-stimulatory receptor OX40 was assessed. mAb targeting this receptor have been shown to enhance anti-tumour immunity in a number of mouse models, eradicating established tumours and providing memory upon re-challenge [319]. They have also shown limited toxicity both in mouse and in humans probably due to the limited expression of OX40 in normal tissues therefore making OX40 an attractive therapeutic target [234]. However, to date there has been limited therapeutic success when translating these mAb into human patients. The overall aim of this thesis was therefore to assess the therapeutic potential of a panel of anti-hOX40 mAb in a novel hOX40 KI mouse model to better understand how to develop these reagents. In chapter 3, the panel of mAb were characterised in terms of binding domain, binding affinities and functionality *in vitro*, as mIgG2a and mIgG1 isotypes, as well as validating the KI mouse model for studying the agonistic and therapeutic activities of the mAb in a number of model systems. In chapter 4, a hOX40:Fab complex was generated with the intent to crystallise and solve the structure to better understand the structure function relationships of the various mAb. Finally, in chapters 5 and 6, murine models were used to examine the affect of the anti-hOX40 mAb on different T cell subsets, as well as examine their therapeutic benefit in tumour models.

Characterisation of the panel of mAb using SPR classified all mAb as high affinity as both mIgG1 and mIgG2a isotypes (KD values $<10^{-9}$) (Figure 3.12/Table 3.3). Likewise, confirmation of binding to hOX40 was done using SPR as well as using transiently transfected 293F cells and splenocytes from hOX40 KI mice (Figure 3.19). This data also showed that the anti-hOX40 mAb did not cross react with mOX40 (Figure 3.14), allowing confident interpretation of results from hOX40 KI heterozygous mice treated with anti-hOX40 mAb (being solely a result of hOX40 stimulation and not a combination of human and mouse OX40 stimulation). Characterisation of the hOX40 KI mouse model revealed that the kinetics of expression of hOX40 after CD3 stimulation matched that seen on human PBMCs, however expression levels of the human chimeric OX40 receptor appeared higher

in the mouse than what is seen in humans. Furthermore, its constitutive expression on Tregs was more comparable to mouse receptor expression than human (as discussed in Chapter 3). Although this aspects represent possible caveats for interpretation and the translation of the findings into humans, it proved to be a useful tool for the further analysis of hOX40 mAb. Furthermore, it should be noted that the expression level of hOX40 in heterozygous KI mice was fairly equivalent to human expression levels and so although KI homozygote mice were used initially for proof of concept experiments, the findings were confirmed in KI heterozygotes.

Antibody binding experiments revealed that collectively the panel of mAb bound across all 4 CRDs of hOX40, however only those binding to CRD4 could bind in the presence of the natural ligand, hOX40L, as determined by SPR (Figure 3.20). This seems reasonable as it is known from the existing crystal structure of hOX40 in complex with hOX40L (PDB:2HEV) that the ligand contacts CRDs 1-3 (Figure 7.1). This is also true for mOX40L and its interaction with the human receptor (PDB:2HEY). Despite their low sequence homology and structural similarities, mOX40L also spans CRDs 1-3 of human OX40 just like the human ligand [16]. The contact residues however, are distinct between the species and only 11/44 that are involved in the humam:human interaction are identical with the mouse. Previous mutational analysis revealed the importance of two particular amino acids, F180 and N166, which are conserved between murine and human OX40L and make similar contributions to receptor binding [16]. This means that interactions of the mouse ligand with the human receptor should be taken into account when interpreting results from the hOX40 KI mouse model.

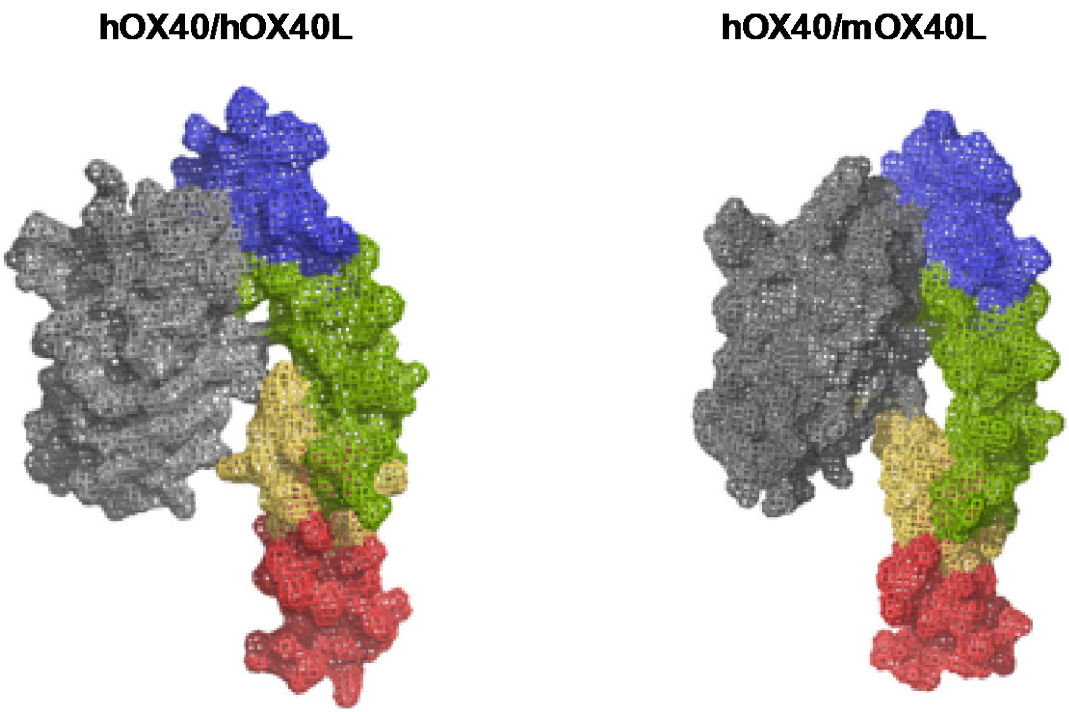

Figure 7.1 Structural comparison of hOX40/hOX40L and hOX40/mOX40L interactions

The crystal structure of the hOX40/hOX40L (2HEV) and hOX40/mOX40L (2HEY) were downloaded from the PDB and adapted using Pymol. The monomer is orientated so that the ligand expressing membrane would be at the top of the image and the receptor expressing membrane at the bottom. Furthermore, it is at an angle which highlights the receptor-ligand interactions. CRDs 1-4 are coloured blue, green, yellow and red, respectively. OX40L is coloured grey. Left hand side = hOX40/hOX40L and right hand side = hOX40/mOX40L.

In chapter 5 a correlation between domain binding and strength of agonism or deletion was observed with the mIgG1 and mIgG2a mAb, respectively. Those mAb which bound to membrane proximal domains (CRDs 3+4) were both stronger agonists and stronger depleters in comparison to mAb binding membrane distal domains (CRD 1+2). Furthermore, the domain bias trend seen in splenocytes isolated from the OT-I model, in relation to effector function, was also observed when phenotyping the OT-I cells in the periphery of $hOX40^{+/+}$ KI mice within the primary response after Ova and mAb administration. Both mIgG1 and mIgG2a treated mice again showed a preference for mAb binding CRDs 3+4 in relation to the production of effector molecule granzyme B. Likewise, mIgG2a treated mice also showed this preference for membrane proximal binding mAb in terms of the percentage of cells produced with an effector phenotype ($KLRG1^{hi}CD127^{lo}$).

In light of the knowledge that mOX40L binds hOX40, it is possible that the differences in strength of effector function of the various mAb are related to ligand binding. For the TNFRSF member CD40, Yu et al. demonstrated that the most agonistic anti-hCD40 mAb all bound to the most membrane distal domain (CRD1) which was the only domain not engaged by CD40L [267]. Theoretically the CRD1 mAb could bind alongside the ligand to achieve more effective receptor clustering. In contrast, those anti-CD40 mAb which interfered with ligand binding, correlated with antagonistic function; inhibiting B cell activation and proliferation mediated by CD40L [267]. The results demonstrated here with anti-hOX40 mAb demonstrated that all mAb, irrespective of domain binding region, possessed functional ability *in vivo* (agonism/depetion and granzyme B production), indicating that blockade of mOX40L binding *in vivo* was not a definitive issue in this system. There are a number of alternative explanations, however, as to why difference in strength of effector function may relate to ligand presence.

First, ligand binding may alter the structure of the receptor in a manner which causes steric hindrance and reduction in the ability of the mAb to bind. Furthermore, in the OT-I model we transferred cells into a hOX40$^{+/+}$ KI mouse which at resting state showed hOX40 expression. However, the resting level and kinetics of mOX40L expression in the system was not determined. We know from the literature that OX40L is up-regulated 1-3 days after an APC encounters antigen [211]. This infers that there would be no mOX40L expression for at least for 24 hours post Ova and mAb administration. This period would allow anti-hOX40 mAb to bind OX40 in the absence of the ligand, hence why some level of effector function was demonstrated with them all. However, once the ligand is up-regulated, further mAb binding may be blocked or have limited binding ability, dependent upon the specific binding epitopes, resulting in the differences in strength of effector function which correlates with binding domain. It would be interesting to determine the potential impact of changing the vaccination scheme used in the OT-I model; what would be the outcome if we gave Ova initially followed by the mAb 48 hours later? Would the mAb show less effector activity because the ligand has had time to be up-regulated and therefore bind the receptor? It would also be important to determine the affinity of the mouse ligand for the human receptor; and compare it to the affinity for the mAb? This could be a contributing factor which negates the preference for mAb or ligand binding.

Furthermore, from the SPR data it is known that anti-hOX40 mAb which bind CRD4 have the ability to bind hOX40 alongside the ligand (Figure 3.20). Whether this is true *in vivo* is undetermined, there may be a preference for mAb over ligand or vice versa. Nevertheless, it is possible that both are able to bind concurrently, in which case the question would be whether the effector function elicited would be superior to ligand/mAb alone as is seen with the CD40 mAb? [267].

Determining the exact binding epitope within the CRDs of hOX40 for each mAb would aid in answering all the questions stated above. This was the aim of work carried out in chapter 4 in which hOX40 ECD:Fab complexes were generated. Unfortunately, none of the material generated crystals sufficient for x-ray crystallography within the available time-frame. However, this would not be an impossible task and would be extremely useful in helping to answer the questions surrounding ligand binding and blocking as discussed above. These results discussed above demonstrate the importance of considering domain binding when choosing an anti-hOX40 mAb. In particular, mAb binding membrane proximal domains elicited more effector like cells in comparison to those binding membrane distal domains, which may be beneficial when it comes to their use in a therapeutic setting.

To date there is no reported evidence suggesting domain binding preference in relation to anti-hOX40 mAb. One paper however has reported a link between domain binding and effector function for the related TNFRSF member 4-1BB. Cleary et al. documented that anti-4-1BB mAb favour certain domains in relation to their ability to carry out ADCC and ADCP effector functions [329]. This was discussed in detail in Chapter 5, however it may be that TNFRSF members, due to their similarities in ECD structure, abide by similar rules and therefore it can be speculated that for mIgG2a function (i.e. deletion) bringing the effector cell close to the target cell allowing for more efficient killing is a general rule. The rationale for why the mIgG1 mAb display a similar domain preference to drive receptor agonism is less clear. Perhaps, targeting mAb binding domains closer to the membrane supports more efficient clustering in some way, thereby driving stronger signalling. Alternatively, as discussed above, with the CRD 4 binding mAb, both the ligand and mAb may be able to bind at the same time causing increased agonism in comparison to mAb which are blocked or hindered by ligand. To explore this further, ADCC and ADCP assays could be performed using the

panel of anti-hOX40 mAb; not only would this confirm that mAb binding certain domains have stronger effector function but it would also help elucidate as to what effector function the mAb are using to cause the depletion of target cells.

Another aspect which could be influencing the differences witnessed in effector function (agonism vs depletion) of the mAb both *in vitro* and *in vivo* is the strength of signalling each mAb is able to elicit. Nf-κB is one of the main signalling axes downstream of TNFRSF members [358] therefore it was reasonable to propose that the magnitude or duration of Nf-κB signalling was correlated to strength of effector function. An Nf-κB reporter cell line was therefore investigated in chapter 3 to assess the signalling strength of each mAb. The results demonstrated that the differences in effector functions observed did not appear to be linked to Nf-κB signalling. It should be noted however that these experiments were performed using a hOX40 construct with a CD40 intracellular region which may not replicate the correct physiological OX40 signalling within the cell. It would therefore be beneficial to repeat these experiments with a fully hOX40 construct to determine with more confidence if Nf-κB signalling plays a role in determining the strength of effector functions elicited by the mAb. No affect of isotype was demonstrated in the signalling assays, which is perhaps to be expected as the reporter cells lacked FcγR.

Throughout this thesis differences in effector function between mAb of differing isotype were demonstrated. Whilst the data obtained regarding mIgG1 mAb was consistent with published data, showing it to be an agonistic isotype akin to results with other TNFRSF members [157], the data from the mIgG2a was perhaps unexpected. mIgG2a mAb to other TNFR targets have been shown not to be agonistic *in vivo* [332] and furthermore the *in vitro* proliferation data failed to show expansion of either CD4+ or CD8+ with the mIgG2a antibody. However, *in vivo,* both mIgG1 and mIgG2a versions of the mAb were able to cause expansion of CD8+ OT-I cells in the periphery of the hOX40$^{+/+}$ KI mice. Although both isotype of mAb were able to elicit expansion of OT-I cells the mechanisms underpinning this were different. The clearest evidence for this was suggested by the results produced when purified CD8+ OT-I/hOX40$^{+/-}$ cells were transferred into WT mice. The sustained ability of the mIgG1 mAb to expand OT-I cells in the WT mice to a similar level as that seen in the hOX40$^{+/+}$ KI mice suggests that these mAb can directly agonise OT-I cells, most probably, as literature suggests, by binding to the

inhibitory FcγR causing enhanced receptor clustering triggering more potent downstream signalling pathways [157]. On the other hand, mIgG2a mAb lost their ability to expand OT-I cells in the periphery suggesting that they cannot directly act upon these cells but instead rely upon the effects they elicit on the non-CD8/supporting cells. Upon numerating the T cell subsets within the spleens of OT-I mice it became apparent that mIgG2a mAb caused depletion of T cells, specifically Tregs, whereas mIgG1 mAb caused expansion of all T cell subsets. It is documented in the literature that mIgG2a mAb cause depletion via interaction with the activatory FcγRs on the surface of macrophages and NK cells [147]. It is likely therefore that the mIgG2a mAb are able to cause CD8+ OT-I T cell expansion in the hOX40 KI mice in part via the depletion of the suppressive Treg population through the mechanism described above.

Considering how to explore further the mechanism behind mIgG2a mAb generated agonism, purified hOX40$^{+/+}$ KI CD4+ cells could be co-transferred with purified hOX40$^{+/-}$/OT-I cells into WT mice. We are already aware from the previous experiments that the mIgG2a mAb cannot act directly on the transferred OT-I cells; therefore, we could begin to answer from this experiment if the effects that the mIgG2a mAb have on the non-CD8/surrounding T cells, which we believe to be depletion, would result in OT-I expansion. Furthermore, more complicated settings whereby Tregs are depleted in WT mice prior to OT-I transfer with and without hOX40$^{+/+}$ CD4+ effectors would allow us to begin to dissect the importance of Treg depletion on the effects. Further examination of the mechanism of action of both isotypes could involve the use of FcγR KO mice. mAb-mediated depletion of target cells has previously been shown to require Fc common gamma chain, thus experiments in these mice would show whether the activity of the mIgG2a is solely dependent on depletion or whether there is some other intrinsic activity. Furthermore, FcγR KO mice could also determine if the mIgG1 requires FcγRII specifically or even if it can agonise without FcγR interaction at all (in an FcγR null mouse) which has been observed with some other mAb targeting TNFRs [267, 331].

One major difference seen between the two mAb isotypes was the strength of the memory response in the OT-I model after rechallenge, with the mIgG1 demonstrating far greater memory. Phenotypic analysis of the OT-I cells at the different stages in the response (primary, resting memory and memory)

highlighted differences between the two isotypes. mIgG2a mAb produced more effector cells (KLRG1^{hi}CD127^{lo}) and granzyme B in the primary response in comparison to mIgG1 mAb, however the converse was true for the percentage of MPECs (KLRG1^{lo}CD127^{hi}) produced by the two isotypes. This was interestingly most significant between mIgG1 and mIgG2a versions of SAP 28-2 and SAP 25-29, mAb binding opposite ends of hOX40, indicating that domain bias is not present when studying expression of these specific markers. These results may explain as to why the mIgG2a memory response was much weaker than the mIgG1 response after rechallenge of mice with SIINFEKL peptide (Figure 5.2) If more memory like progenitor cells are produced in the primary response with mIgG1 mAb, it seems rational to conclude that this may be one of the reasons as to why there is greater expansion of OT-I cells during the memory response in comparison to mIgG2a treated mice. To investigate this further, the markers CXCR3 and CD43 were examined, both of which have been used previously in an infection model to delineate three types of memory cells [119]. The results showed that mice treated with a mIgG1 anti-hOX40 mAb, in comparison to those treated with a mIgG2a mAb, produced a higher percentage of OT-I cells in the memory response with a phenotype associated with highly proliferative cells (CXCR3^{hi}CD43^{lo} and CXCR3^{hi}CD43^{hi}), and a lower percentage of OT-I cells with a phenotype associated with effector-like memory cells (CXCR3^{lo}CD43^{lo}). This ratio of phenotypes was skewed in the opposite direction when comparing mIgG2a treated mice to mIgG1 treated mice, i.e. a lower percentage of highly proliferative OT-I cells and a higher percentage of effector-like memory cells. These findings strengthen the conclusions drawn from phenotyping the cells in the primary response. Thus it appears mIgG1 mAb generate a larger percentage of MPECs in the primary response as well as producing more highly proliferative cells in the resting memory and subsequent rechallenge response in comparison to mIgG2a mAb. This could help to explain the difference in the percentage of OT-I cells produced in the memory response. These results also highlighted that the mIgG2a mAb were capable of producing a higher percentage of effector-like memory cells, preceded by more short lived effector cells and a higher amount of granzyme B producing OT-I cells compared to mIgG1 mAb. Whether this skew towards a more effector like population of cells in both the primary and memory response would be more beneficial over being able to generate a larger number of memory cells in a tumour setting was unknown. We therefore went on to test the therapeutic ability

of these mAb in a number of tumour models as both mIgG1 and mIgG2a isotypes. In the E.G7-Ova model anti-OX40 mAb of both mIgG1 and mIgG2a isotypes were able to elicit tumour control and generate memory sufficient to prevent rechallenge with tumour. This suggests that despite the marked difference in the memory response seen in the OT-I model (mIgG1>>mIgG2a), other factors must be operational to account for the ability of both mAb isotypes to generate protective memory responses. From the OT-I phenotyping data combined with the E.G7-Ova data, it would suggest that it is not just the amount of cells present that is important but also the type of cells present i.e. highly proliferative vs. strong effector function. In addition to the results already generated it would be of interest to test the functionality of the OT-I cells at the different stages in the response to determine if it matches the phenotype observed. For example, carrying out *ex vivo* killing assays as well as exploring the types of cytokines each cell sub-population is expressing would provide more insight into the functional ability of these cells. Furthermore, the lab is currently repeating the memory cell phenotyping experiments above to increase the N numbers and therefore reliability of the conclusions drawn from this data.

In Chapter 5 and 6 the importance of CD8:Treg ratio was explored. Current literature reports the importance of generating a high CD8:Treg ratio, especially within the tumour, in order to produce effective therapy [346], yet others report that in human tumours the presence of a high number of FoxP3+ Tregs is beneficial [348]. Both the OT-I data and E.G7-Ova tumour data demonstrate that mIgG2a mAb increased this ratio in a favourable manner, however the mIgG1 mAb decreased it or showed little change in comparison to isotype control treated mice. mIgG1 mAb, however, were still able to generate effective therapy. Reasons behind this are currently unclear, but may indicate that a simple increase in CD8 effectors is sufficient in some instances (irrespective of concurrent increases in Treg). Regardless, it highlights the complexity of the immune system and the multitude of factors that combine together resulting in effective anti-cancer immunity. As a result it is clear that not only one factor, such as CD8:Treg ratio, needs to be considered but a plethora of other aspects need to be explored before the choice of mAb isotype for therapeutic use is made.

On the basis of the results described above and from documentation of mIgG2a being therapeutic in previous anti-OX40 tumour studies [165] it was somewhat

surprising to witness both isotypes of anti-hOX40 mAb providing effective therapy in both an E.G7-Ova and MCA-205 tumour model. Interestingly though, between the two tumour models a difference in isotype preference in terms of most effective therapy was observed. In the E.G7-Ova model SAP 25-29 mIgG2a provided the most efficient therapy compared to the mIgG1 isotype whereas the converse was true in the MCA-205 tumour model. Furthermore, within the E.G7-Ova model, different mAb showed preference for a certain isotype when observing the overall percent survival of mice (SAP 28-2 and SAP 9 favoured mIgG1 and SAP 15-3 and SAP 25-29 favoured mIgG2a). Why both isotypes are able to act therapeutically within the same model when they show clear differences in mechanism and why different isotypes of the same mAb have different relative therapeutic capacity in distinct models remains unclear. It likely reflects the relative propensity of each mAb to elicit the different effector functions, coupled to the differences in the tumour microenvironments (TME). The latter is known to have profound effects on therapeutic efficacy [359]. For example, if a tumour has a high infiltrate of cells expressing activatory FcγR such as NK cells and macrophages, mIgG2a mAb and depletion of target cells may be favoured over the activity of a mIgG1 mAb. Conversely if a high number of inhibitory FcγRs are present agonism via a mIgG1 mAb may be more prominent. It may therefore be of interest to phenotype tumours and understand the environment more thoroughly to allow the most effective mAb isotype to be administered. As well as addressing the tumour infiltrate, other lymphoid organs were also examined in the E.G7-Ova model. This revealed a difference in strength of effect of the mAb amongst the different organs assessed. Expansion and depletion of cells was most strongly observed within the spleen, then the blood, followed tdLN and lastly ndLN. The reasons behind this and whether it ultimately influences the effects seen in the tumour are still currently unknown. Observing these changes in cell numbers within certain organs and not in others however, may be due to the size of the respective organs and hence the number of cells recovered after processing. Additionally, the variability of data points in some cases could hide the trend being observed in other organs. It would therefore be of interest to determine the amounts of other immune cell types and the presence of FcγRs in the multiple organs as well as the tumour to begin to understand more fully the isotype preference between different tumour models as well as the influence of effect in organs other than the tumour.

Although clear domain trends relating to effector activity were seen in the OT-I model, these were less clear within the tumour model. Within the E.G7-Ova phenotyping experiments the same domain trend of mAb binding related to activity was seen for mIgG1 treated mice but was not consistent across all organs and was not seen in the mIgG2a treated mice. The reason for this is unclear however it correlated with the lack of domain preference observed in the survival experiments. Again the microenvironment present within the tumour may play a role and is potentially more relevant for observing a domain preference when the mIgG2a isotype is used. These results reiterate the need to phenotype these organs more thoroughly as described above.

One possible reason as to why both isotypes were capable of having therapeutic benefit in the EG7 model was that whilst mIgG2a would be good at depleting Tregs, the mIgG1 as well as expanding cell numbers may also drive greater cytotoxicity capacity within the CD4+ and CD8+ T cell populations. This was addressed by phenotyping these cells for the expression of T-bet, Eomes and Granzyme B. The CD8+ population of T cells between mIgG1 and mIgG2a treated mice showed no significant differences between the levels of T-bet/Eomes and granzyme B expression, with the exception of cells in the tdLN of SAP 28-2 treated mice.. On the other hand, the CD4+ population showed preference for a mIgG1 mAb in terms of T-bet/Eomes expression, albeit slight and with limited significance between the isotypes. Conversely, there was no significant difference between mIgG1 and mIgG2a treated mice in terms of granzyme B expression across all organs. Due to the subtle differences observed in this experiment it is difficult to draw solid conclusions, it would therefore be beneficial to repeat the experiment but also to look at other effector markers and cytokines to get a broader understanding of the types of effector cells produced by both mIgG1 and mIgG2a isotypes of anti-hOX40 mAb to see if this furthers our understanding of their mechanisms of action in the tumour setting.

The preliminary results generated from the in-house versus commercial anti-hOX40 mAb and the anti-hOX40/anti-m4-1BB combination experiments were variable and each had small N numbers making it difficult to draw solid conclusions from the data. That being said, however, it highlighted some exciting data which will be pursued further. The in-house anti-hOX40 mAb seemed to produce stronger effector functions and resulted in more efficient therapy in

comparison to the current clinically-relevant anti-hOX40 mAb suggesting that they may be strong contenders in the clinic. Likewise, when comparing the different combination treatments, data was variable and N numbers small. Therefore, to explore this further repeats of the experiment should be carried out followed by survival experiments to assess the ultimate outcome, survival. Current monotherapies using anti-OX40 and anti-4-1BB are having limited efficacy in the clinic therefore it is of interest to explore combination therapies further as they have shown promise in pre-clinical models [200, 278]. All current combinations being trialled in the clinic however are targeting two separate receptors and not looking at the potential of targeting the same receptor but with two different isotypes, it is therefore of interest to pursue this further to determine if this method possesses any therapeutic benefit over the conventional types of combination.

In summary, the research presented in this thesis identified an unexpected theme of domain preference relating to effector function, on two different isotypes of mAb, highlighting that it is not as simple as choosing one isotype of mAb over another but that considerations of multiple aspects, such as epitope and isotype together, need to be considered. Furthermore, the data has demonstrated that both mIgG1 and mIgG2a anti-hOX40 mAb are able to cause therapy in a number of tumour models, albeit via different mechanisms. Mechanism however, is ultimately not the only deciding factor in therapeutic outcome and it is most likely that multiple factors control why one isotype is favoured over another in certain tumour types, particularly aspects of the TME. Taking these considerations forward to the clinic would require gaining more information about immune cell infiltrate and the phenotypes of cells present within human tumours so that more informed decisions about therapeutic mAb isotype can be made in the hope of providing more efficacious treatments. As demonstrated in Table 1.4 the current mAb used in the clinic are typically a hIgG1 isotype. These mAb would be expected to have a depleting function due to their high affinity for the activatory FcγRs, similar to mIgG2a. Pre-clinical studies of anti-hOX40 mAb however, have shown that hIgG1 anti-hOX40 mAb are capable of expanding CD4+ effector cells [271], which was shown to rely on cross linking. This may mean that dependent on the context, a hIgG1 mAb can have dual functions which may or may not be beneficial in a therapeutic setting. To obtain purely agonistic effects a hIgG2 isotype may be used. White et al. have shown that anti-CD40 mAb of a hIgG2 isotype are able to

act agonistically in an FcγR-independent manner due to unique arrangement of hinge disulphides [162]. It may therefore be of interest to explore hIgG2 anti-hOX40 mAb which may be able to provide better agonism than a hIgG1 without the need to rely upon FcγR availability. The possibility of using the mAb as a $F(ab')_2$ or Fc-inert mAb could also rule out the possibility of any depletion to occur, but may mean reduced agonism if FcγR are required for optimal cross-linking and agonism.

The majority of literature supports that a low CD8:Treg ratio within tumour tissue in patients is associated with worse prognosis, this has been seen across a number of cancers including ovarian cancer [360], lung cancer [361], NHL [362], melanoma and other malignancies [363]. This suggests that a Treg depleting mAb may be useful as an effective form of therapy i.e. hIgG1. However, it would have to be in the correct context – high myeloid infiltrate into tumour expressing high levels of activatory FcγR. This highlights the points discussed above about gaining more information on the TME within human cancer.

Hopefully, with further translational end-points and knowledge of the TME in human cancer patients, these decisions relating to choice of isotype and desired effector function will become clearer and lead to more efficacious treatments for patients in the future.

.

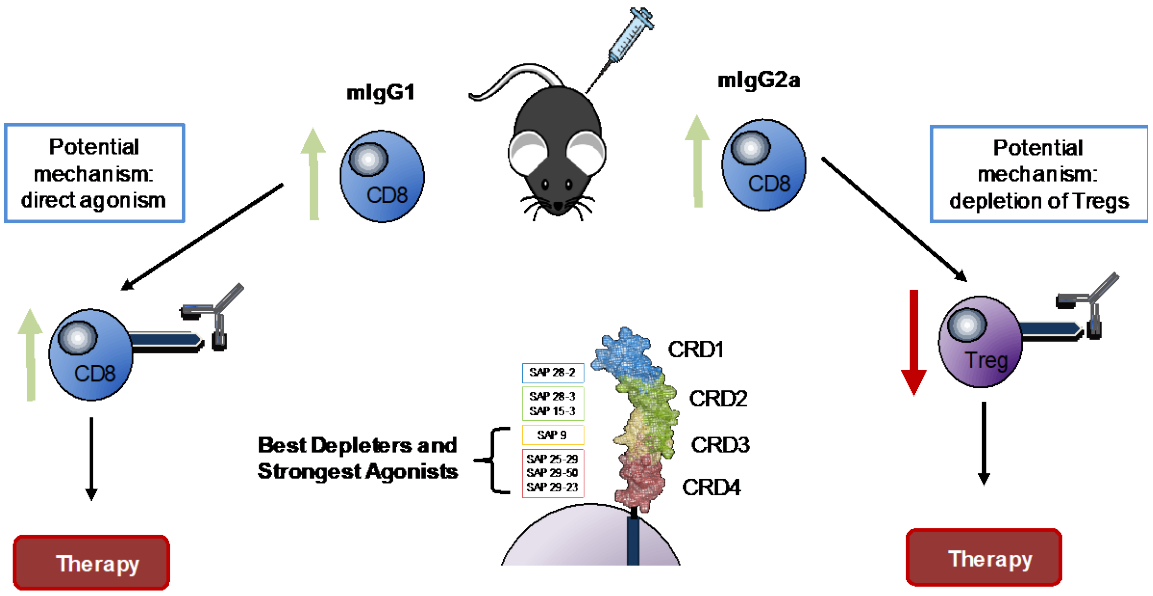

Figure 7.2 Graphical summary of project findings

A schematic demonstrating the ability of both mIgG1 and mIgG2a anti-hOX40 mAb to cause an increase in the number of CD8+ T cells in a hOX40$^{+/+}$ KI mouse model. The proposed mechanisms for each mAb are that mIgG1 are able to act directly on these cells resulting in agonism whereas the mIgG2a mAb rely upon effects elicited on the non-CD8/surrounding cells such as Treg depletion. Both isotype of mAb however are able to provide efficient therapy in mouse tumour models. A domain preference was also observed within this research; mAb binding CRD 3+4 were stronger agonists as a mIgG1 and the best depleters as a mIgG2a in comparison to mAb binding CRD 1+2.

List of References

1. Ahmad, A.S., N. Ormiston-Smith, and P.D. Sasieni, *Trends in the lifetime risk of developing cancer in Great Britain: comparison of risk for those born from 1930 to 1960.* Br J Cancer, 2015. **112**(5): p. 943-7.

2. Hanahan, D. and R.A. Weinberg, *Hallmarks of cancer: the next generation.* Cell, 2011. **144**(5): p. 646-74.

3. Hanahan, D. and R.A. Weinberg, *The hallmarks of cancer.* Cell, 2000. **100**(1): p. 57-70.

4. Dela Cruz, C.S., L.T. Tanoue, and R.A. Matthay, *Lung cancer: epidemiology, etiology, and prevention.* Clin Chest Med, 2011. **32**(4): p. 605-44.

5. De Pergola, G. and F. Silvestris, *Obesity as a major risk factor for cancer.* J Obes, 2013. **2013**: p. 291546.

6. Erdei, E. and S.M. Torres, *A new understanding in the epidemiology of melanoma.* Expert Rev Anticancer Ther, 2010. **10**(11): p. 1811-23.

7. Burd, E.M., *Human papillomavirus and cervical cancer.* Clin Microbiol Rev, 2003. **16**(1): p. 1-17.

8. Campeau, P.M., W.D. Foulkes, and M.D. Tischkowitz, *Hereditary breast cancer: new genetic developments, new therapeutic avenues.* Hum Genet, 2008. **124**(1): p. 31-42.

9. Pal, T., et al., *BRCA1 and BRCA2 mutations account for a large proportion of ovarian carcinoma cases.* Cancer, 2005. **104**(12): p. 2807-16.

10. Vinay, D.S., et al., *Immune evasion in cancer: Mechanistic basis and therapeutic strategies.* Semin Cancer Biol, 2015. **35 Suppl**: p. S185-S198.

11. Ohm, J.E. and D.P. Carbone, *Immune dysfunction in cancer patients.* Oncology (Williston Park), 2002. **16**(1 Suppl 1): p. 11-8.

12. Sudhakar, A., *History of Cancer, Ancient and Modern Treatment Methods.* J Cancer Sci Ther, 2009. **1**(2): p. 1-4.

13. Saltzstein, H.C., P. Levin, and J. Sharp, *The possibilities and limitations of surgery in cancer; a follow-up of 572 personally treated patients.* Am J Surg, 1957. **93**(3): p. 338-55.

14. *Radiotherapy Side Effects* [cited 2018 Available from: https://www.cancerresearchuk.org/about-cancer/cancer-in-general/treatment/radiotherapy/side-effects.

15. Rodriguez, D. *Advantages & Disadvantages of Radiation Therapy*. 2014 14/12/16]; Available from: http://www.livestrong.com/article/513783-advantages-disadvantages-of-radiation-therapy/.

16. Compaan, D.M. and S.G. Hymowitz, *The crystal structure of the costimulatory OX40-OX40L complex.* Structure, 2006. **14**(8): p. 1321-30.

17. Wiemann, B. and C.O. Starnes, *Coley's toxins, tumor necrosis factor and cancer research: a historical perspective.* Pharmacol Ther, 1994. **64**(3): p. 529-64.

18. Mittal, D., et al., *New insights into cancer immunoediting and its three component phases--elimination, equilibrium and escape.* Curr Opin Immunol, 2014. **27**: p. 16-25.

19. Marincola, F.M., et al., *Escape of human solid tumors from T-cell recognition: molecular mechanisms and functional significance.* Adv Immunol, 2000. **74**: p. 181-273.

20. Bubenik, J., *MHC class I down-regulation: tumour escape from immune surveillance? (review).* Int J Oncol, 2004. **25**(2): p. 487-91.

21. Wang, S. and L. Chen, *Co-signaling molecules of the B7-CD28 family in positive and negative regulation of T lymphocyte responses.* Microbes Infect, 2004. **6**(8): p. 759-66.

22. O'Connell, J., et al., *The Fas counterattack: cancer as a site of immune privilege.* Immunology Today, 1999. **20**(1): p. 46-52.

23. Owen, A.J., Punt, J, Stranford, A. S, *Kuby Immunology* Vol. 7th Edition 2013: W.H. Freeman and Company

24. Akashi, K., et al., *A clonogenic common myeloid progenitor that gives rise to all myeloid lineages.* Nature, 2000. **404**(6774): p. 193-7.

25. Manz, M.G., et al., *Dendritic cell potentials of early lymphoid and myeloid progenitors.* Blood, 2001. **97**(11): p. 3333-41.

26. Geissmann, F., et al., *Development of monocytes, macrophages, and dendritic cells.* Science, 2010. **327**(5966): p. 656-61.

27. Sinder, B.P., A.R. Pettit, and L.K. McCauley, *Macrophages: Their Emerging Roles in Bone.* J Bone Miner Res, 2015. **30**(12): p. 2140-9.

28. Austyn, J.M. and S. Gordon, *F4/80, a monoclonal antibody directed specifically against the mouse macrophage.* Eur J Immunol, 1981. **11**(10): p. 805-15.

29. Merad, M., et al., *The dendritic cell lineage: ontogeny and function of dendritic cells and their subsets in the steady state and the inflamed setting.* Annu Rev Immunol, 2013. **31**: p. 563-604.

30. *Dendritic Cell Subsets and Lineage-specific Markers*. [cited 2018 16th September]; Available from: https://www.rndsystems.com/research-area/dendritic-cell-subsets-and-lineage--specific-markers.

31. Mayadas, T.N., X. Cullere, and C.A. Lowell, *The multifaceted functions of neutrophils.* Annu Rev Pathol, 2014. **9**: p. 181-218.

32. *Essential Markers for phenotyping* [cited 2018 16th September]; Available from: https://www.biolegend.com/essential_markers.

33. Karasuyama, H., et al., *Newly discovered roles for basophils: a neglected minority gains new respect.* Nat Rev Immunol, 2009. **9**(1): p. 9-13.

34. Jacobsen, E.A., et al., *The expanding role(s) of eosinophils in health and disease.* Blood, 2012. **120**(19): p. 3882-3890.

35. LeBien, T.W. and T.F. Tedder, *B lymphocytes: how they develop and function.* Blood, 2008. **112**(5): p. 1570-1580.

36. Pelanda, R. and R.M. Torres, *Central B-cell tolerance: where selection begins.* Cold Spring Harb Perspect Biol, 2012. **4**(4): p. a007146.

37. Janeway CA Jr, T.P., Walport M, et al. , *Antigen receptor structure and signaling pathways*, in *mmunobiology: The Immune System in Health and Disease.* . 2001, New York: Garland Science.

38. Janeway CA Jr, T.P., Walport M, et al., *The generation of diversity in immunoglobulins* in *Immunobiology: The Immune System in Health and Disease*. 2001: New York: Garland Science.

39. Fugmann, S.D., et al., *The RAG proteins and V(D)J recombination: complexes, ends, and transposition.* Annu Rev Immunol, 2000. **18**: p. 495-527.

40. Sadofsky, M.J., *The RAG proteins in V(D)J recombination: more than just a nuclease.* Nucleic Acids Res, 2001. **29**(7): p. 1399-409.

41. Maul, R.W. and P.J. Gearhart, *AID and somatic hypermutation.* Adv Immunol, 2010. **105**: p. 159-91.

42. Stavnezer, J., J.E. Guikema, and C.E. Schrader, *Mechanism and regulation of class switch recombination.* Annu Rev Immunol, 2008. **26**: p. 261-92.

43. Liu, M. and D.G. Schatz, *Balancing AID and DNA repair during somatic hypermutation.* Trends Immunol, 2009. **30**(4): p. 173-81.

44. Jacobs, H. and L. Bross, *Towards an understanding of somatic hypermutation.* Curr Opin Immunol, 2001. **13**(2): p. 208-18.

45. Chua, K.F., F.W. Alt, and J.P. Manis, *The function of AID in somatic mutation and class switch recombination: upstream or downstream of DNA breaks.* J Exp Med, 2002. **195**(9): p. F37-41.

46. Manis, J.P., M. Tian, and F.W. Alt, *Mechanism and control of class-switch recombination.* Trends Immunol, 2002. **23**(1): p. 31-9.

47. Nonoyama, S., et al., *B cell activation via CD40 is required for specific antibody production by antigen-stimulated human B cells.* J Exp Med, 1993. **178**(3): p. 1097-102.

48. Durandy, A. and S. Kracker, *Immunoglobulin class-switch recombination deficiencies.* Arthritis Res Ther, 2012. **14**(4): p. 218.

49. Victora, G.D., et al., *Germinal center dynamics revealed by multiphoton microscopy with a photoactivatable fluorescent reporter.* Cell, 2010. **143**(4): p. 592-605.

50. Tangye, S.G. and D.M. Tarlinton, *Memory B cells: effectors of long-lived immune responses.* Eur J Immunol, 2009. **39**(8): p. 2065-75.

51. Treanor, B., *B-cell receptor: from resting state to activate.* Immunology, 2012. **136**(1): p. 21-7.

52. Johansen, F.E., R. Braathen, and P. Brandtzaeg, *Role of J chain in secretory immunoglobulin formation.* Scand J Immunol, 2000. **52**(3): p. 240-8.

53. Chen, K. and A. Cerutti, *The function and regulation of immunoglobulin D.* Curr Opin Immunol, 2011. **23**(3): p. 345-52.

54. Schroeder, H.W., Jr. and L. Cavacini, *Structure and function of immunoglobulins.* J Allergy Clin Immunol, 2010. **125**(2 Suppl 2): p. S41-52.

55. Woof, J.M. and M.A. Kerr, *The function of immunoglobulin A in immunity.* J Pathol, 2006. **208**(2): p. 270-82.

56. Stone, K.D., C. Prussin, and D.D. Metcalfe, *IgE, mast cells, basophils, and eosinophils.* J Allergy Clin Immunol, 2010. **125**(2 Suppl 2): p. S73-80.

57. Ghetie, V., E.S. Ward, and E.S. Vitetta, *Pharmacokinetics of Antibodies and Immunotoxins in Mice and Humans*, in *Handbook of Anticancer Pharmacokinetics and Pharmacodynamics*, W.D. Figg and H.L. McLeod, Editors. 2004, Humana Press: Totowa, NJ. p. 475-498.

58. Janeway CA Jr, T.P., Walport M, et al. , *The structure of a typical antibody molecule*. Vol. 5th edition. 2001.

59. Higel, F., et al., *N-glycosylation heterogeneity and the influence on structure, function and pharmacokinetics of monoclonal antibodies and Fc fusion proteins.* Eur J Pharm Biopharm, 2016. **100**: p. 94-100.

60. Vidarsson, G., G. Dekkers, and T. Rispens, *IgG subclasses and allotypes: from structure to effector functions.* Front Immunol, 2014. **5**: p. 520.

61. Stapleton, N.M., et al., *The multiple facets of FcRn in immunity.* Immunol Rev, 2015. **268**(1): p. 253-68.

62. Roux, K.H., L. Strelets, and T.E. Michaelsen, *Flexibility of human IgG subclasses.* J Immunol, 1997. **159**(7): p. 3372-82.

63. Hayday, A.C., *Gammadelta T cells and the lymphoid stress-surveillance response.* Immunity, 2009. **31**(2): p. 184-96.

64. Carpenter, A.C. and R. Bosselut, *Decision checkpoints in the thymus.* Nat Immunol, 2010. **11**(8): p. 666-73.

65. Starr, T.K., S.C. Jameson, and K.A. Hogquist, *Positive and Negative Selection of T Cells.* Annual Review of Immunology, 2003. **21**(1): p. 139-176.

66. Stritesky, G.L., S.C. Jameson, and K.A. Hogquist, *Selection of self-reactive T cells in the thymus.* Annu Rev Immunol, 2012. **30**: p. 95-114.

67. van Parijs, L., V.L. Perez, and A.K. Abbas, *Mechanisms of peripheral T cell tolerance.* Novartis Found Symp, 1998. **215**: p. 5-14; discussion 14-20, 33-40.

68. Sleckman, B.P., *Lymphocyte antigen receptor gene assembly: multiple layers of regulation.* Immunol Res, 2005. **32**(1-3): p. 253-8.

69. Curtsinger, J.M. and M.F. Mescher, *Inflammatory cytokines as a third signal for T cell activation.* Curr Opin Immunol, 2010. **22**(3): p. 333-40.

70. Birnbaum, M.E., et al., *Molecular architecture of the alphabeta T cell receptor-CD3 complex.* Proc Natl Acad Sci U S A, 2014. **111**(49): p. 17576-81.

71. Brownlie, R.J. and R. Zamoyska, *T cell receptor signalling networks: branched, diversified and bounded.* Nat Rev Immunol, 2013. **13**(4): p. 257-69.

72. Chakraborty, A.K. and A. Weiss, *Insights into the initiation of TCR signaling.* Nature Immunology, 2014. **15**(9): p. 798-807.

73. Brownlie, R. and R. Zamoyska, *LAT polices T cell activation.* Immunity, 2009. **31**(2): p. 174-6.

74. Nakayama, T. and M. Yamashita, *The TCR-mediated signaling pathways that control the direction of helper T cell differentiation.* Semin Immunol, 2010. **22**(5): p. 303-9.

75. Roncagalli, R., et al., *Quantitative proteomics analysis of signalosome dynamics in primary T cells identifies the surface receptor CD6 as a Lat adaptor-independent TCR signaling hub.* Nat Immunol, 2014. **15**(4): p. 384-92.

76. Schwartz, R.H., *T cell anergy.* Annu Rev Immunol, 2003. **21**: p. 305-34.

77. Mescher, M.F., et al., *Activation-induced non-responsiveness (anergy) limits CD8 T cell responses to tumors.* Semin Cancer Biol, 2007. **17**(4): p. 299-308.

78. Hombach, A., et al., *T-cell activation by recombinant receptors: CD28 costimulation is required for interleukin 2 secretion and receptor-mediated T-cell proliferation but does not affect receptor-mediated target cell lysis.* Cancer Res, 2001. **61**(5): p. 1976-82.

79. Gimmi, C.D., et al., *B-cell surface antigen B7 provides a costimulatory signal that induces T cells to proliferate and secrete interleukin 2.* Proc Natl Acad Sci U S A, 1991. **88**(15): p. 6575-9.

80. Thompson, C.B., et al., *CD28 activation pathway regulates the production of multiple T-cell-derived lymphokines/cytokines.* Proc Natl Acad Sci U S A, 1989. **86**(4): p. 1333-7.

81. Cerdan, C., et al., *CD28 costimulation up-regulates long-term IL-2R beta expression in human T cells through combined transcriptional and post-transcriptional regulation.* J Immunol, 1995. **154**(3): p. 1007-13.

82. Boise, L.H., et al., *CD28 costimulation can promote T cell survival by enhancing the expression of Bcl-XL.* Immunity, 1995. **3**(1): p. 87-98.

83. Walunas, T.L., C.Y. Bakker, and J.A. Bluestone, *CTLA-4 ligation blocks CD28-dependent T cell activation.* J Exp Med, 1996. **183**(6): p. 2541-50.

84. Ben-Sasson, S.Z., et al., *IL-1 acts directly on CD4 T cells to enhance their antigen-driven expansion and differentiation.* Proc Natl Acad Sci U S A, 2009. **106**(17): p. 7119-24.

85. Norment, A.M., et al., *Cell-cell adhesion mediated by CD8 and MHC class I molecules.* Nature, 1988. **336**(6194): p. 79-81.

86. Williams, M.A. and M.J. Bevan, *Effector and memory CTL differentiation.* Annu Rev Immunol, 2007. **25**: p. 171-92.

87. Mescher, M.F., et al., *Signals required for programming effector and memory development by CD8+ T cells.* Immunol Rev, 2006. **211**: p. 81-92.

88. Kaech, S.M. and W. Cui, *Transcriptional control of effector and memory CD8+ T cell differentiation.* Nat Rev Immunol, 2012. **12**(11): p. 749-61.

89. Joshi, N.S., et al., *Inflammation directs memory precursor and short-lived effector CD8(+) T cell fates via the graded expression of T-bet transcription factor.* Immunity, 2007. **27**(2): p. 281-95.

90. Joshi, N.S., et al., *Increased numbers of preexisting memory CD8 T cells and decreased T-bet expression can restrain terminal differentiation of secondary effector and memory CD8 T cells.* J Immunol, 2011. **187**(8): p. 4068-76.

91. McLane, L.M., et al., *Differential localization of T-bet and Eomes in CD8 T cell memory populations.* J Immunol, 2013. **190**(7): p. 3207-15.

92. Banerjee, A., et al., *Cutting edge: The transcription factor eomesodermin enables CD8+ T cells to compete for the memory cell niche.* J Immunol, 2010. **185**(9): p. 4988-92.

93. Groscurth, P. and L. Filgueira, *Killing Mechanisms of Cytotoxic T Lymphocytes.* News Physiol Sci, 1998. **13**: p. 17-21.

94. Voskoboinik, I., J.C. Whisstock, and J.A. Trapani, *Perforin and granzymes: function, dysfunction and human pathology.* Nat Rev Immunol, 2015. **15**(6): p. 388-400.

95. Ramaswamy, M., et al., *Many checkpoints on the road to cell death: regulation of Fas-FasL interactions and Fas signaling in peripheral immune responses.* Results Probl Cell Differ, 2009. **49**: p. 17-47.

96. Chinnaiyan, A.M., et al., *FADD, a novel death domain-containing protein, interacts with the death domain of Fas and initiates apoptosis.* Cell, 1995. **81**(4): p. 505-12.

97. Ashkenazi, A. and V.M. Dixit, *Death receptors: signaling and modulation.* Science, 1998. **281**(5381): p. 1305-8.

98. Tau, G. and P. Rothman, *Biologic functions of the IFN-gamma receptors.* Allergy, 1999. **54**(12): p. 1233-51.

99. Pfeffer, K., *Biological functions of tumor necrosis factor cytokines and their receptors.* Cytokine Growth Factor Rev, 2003. **14**(3-4): p. 185-91.

100. Hildeman, D.A., et al., *Activated T cell death in vivo mediated by proapoptotic bcl-2 family member bim.* Immunity, 2002. **16**(6): p. 759-67.

101. Mueller, S.N., et al., *Memory T cell subsets, migration patterns, and tissue residence.* Annu Rev Immunol, 2013. **31**: p. 137-61.

102. Doyle, C. and J.L. Strominger, *Interaction between CD4 and class II MHC molecules mediates cell adhesion.* Nature, 1987. **330**(6145): p. 256-9.

103. Lupar, E., et al., *Eomesodermin Expression in CD4+ T Cells Restricts Peripheral Foxp3 Induction.* J Immunol, 2015. **195**(10): p. 4742-52.

104. Sakaguchi, S., et al., *Regulatory T cells and immune tolerance.* Cell, 2008. **133**(5): p. 775-87.

105. Larkin, J., 3rd, et al., *CD4+CD25+ regulatory T cell repertoire formation shaped by differential presentation of peptides from a self-antigen.* J Immunol, 2008. **180**(4): p. 2149-57.

106. Curotto de Lafaille, M.A. and J.J. Lafaille, *Natural and adaptive foxp3+ regulatory T cells: more of the same or a division of labor?* Immunity, 2009. **30**(5): p. 626-35.

107. Murai, M., et al., *Interleukin 10 acts on regulatory T cells to maintain expression of the transcription factor Foxp3 and suppressive function in mice with colitis.* Nat Immunol, 2009. **10**(11): p. 1178-84.

108. Shevach, E.M., *Mechanisms of foxp3+ T regulatory cell-mediated suppression.* Immunity, 2009. **30**(5): p. 636-45.

109. Vignali, D.A.A., L.W. Collison, and C.J. Workman, *How regulatory T cells work.* Nature Reviews Immunology, 2008. **8**(7): p. 523-532.

110. Banchereau, J., V. Pascual, and A. O'Garra, *From IL-2 to IL-37: the expanding spectrum of anti-inflammatory cytokines.* Nat Immunol, 2012. **13**(10): p. 925-31.

111. Bopp, T., et al., *Cyclic adenosine monophosphate is a key component of regulatory T cell mediated suppression.* Journal of Experimental Medicine, 2007. **204**(6): p. 1303-1310.

112. Wang, K. and A.T. Vella, *Regulatory T Cells and Cancer: A Two-Sided Story.* Immunol Invest, 2016. **45**(8): p. 797-812.

113. Pennock, N.D., et al., *T cell responses: naive to memory and everything in between.* Adv Physiol Educ, 2013. **37**(4): p. 273-83.

114. Laidlaw, B.J., J.E. Craft, and S.M. Kaech, *The multifaceted role of CD4(+) T cells in CD8(+) T cell memory.* Nat Rev Immunol, 2016. **16**(2): p. 102-11.

115. Schenkel, J.M. and D. Masopust, *Tissue-resident memory T cells.* Immunity, 2014. **41**(6): p. 886-97.

116. Casey, K.A., et al., *Antigen-independent differentiation and maintenance of effector-like resident memory T cells in tissues.* J Immunol, 2012. **188**(10): p. 4866-75.

117. Jiang, X., et al., *Skin infection generates non-migratory memory CD8+ T(RM) cells providing global skin immunity.* Nature, 2012. **483**(7388): p. 227-31.

118. Topham, D.J. and E.C. Reilly, *Tissue-Resident Memory CD8(+) T Cells: From Phenotype to Function.* Front Immunol, 2018. **9**: p. 515.

119. Hikono, H., et al., *Activation phenotype, rather than central- or effector-memory phenotype, predicts the recall efficacy of memory CD8+ T cells.* J Exp Med, 2007. **204**(7): p. 1625-36.

120. Leong, J.W. and T.A. Fehniger, *Human NK cells: SET to kill.* Blood, 2011. **117**(8): p. 2297-8.

121. Jurisic, V., et al., *[The role of cytokine in regulation of the natural killer cell activity].* Srp Arh Celok Lek, 2008. **136**(7-8): p. 423-9.

122. Pegram, H.J., et al., *Activating and inhibitory receptors of natural killer cells.* Immunol Cell Biol, 2011. **89**(2): p. 216-24.

123. Zafirova, B., et al., *Regulation of immune cell function and differentiation by the NKG2D receptor.* Cell Mol Life Sci, 2011. **68**(21): p. 3519-29.

124. Bhatnagar, N., et al., *FcgammaRIII (CD16)-mediated ADCC by NK cells is regulated by monocytes and FcgammaRII (CD32).* Eur J Immunol, 2014. **44**(11): p. 3368-79.

125. Bendelac, A., P.B. Savage, and L. Teyton, *The biology of NKT cells.* Annu Rev Immunol, 2007. **25**: p. 297-336.

126. Ortaldo, J.R., et al., *Comparative studies of CD3- and CD3+ CD56+ cells: examination of morphology, functions, T cell receptor rearrangement, and pore-forming protein expression.* Cell Immunol, 1991. **136**(2): p. 486-95.

127. Brennan, P.J., M. Brigl, and M.B. Brenner, *Invariant natural killer T cells: an innate activation scheme linked to diverse effector functions.* Nat Rev Immunol, 2013. **13**(2): p. 101-17.

128. Seino, K. and M. Taniguchi, *Functionally distinct NKT cell subsets and subtypes.* J Exp Med, 2005. **202**(12): p. 1623-6.

129. Dhodapkar, M.V. and V. Kumar, *Type II NKT Cells and Their Emerging Role in Health and Disease.* Journal of Immunology, 2017. **198**(3): p. 1015-1021.

130. Lee, H., et al., *The presence of CD8+ invariant NKT cells in mice.* Exp Mol Med, 2009. **41**(12): p. 866-72.

131. Kohler, G. and C. Milstein, *Continuous cultures of fused cells secreting antibody of predefined specificity.* Nature, 1975. **256**(5517): p. 495-7.

132. Kipps, T.J., et al., *Importance of immunoglobulin isotype in human antibody-dependent, cell-mediated cytotoxicity directed by murine monoclonal antibodies.* J Exp Med, 1985. **161**(1): p. 1-17.

133. Shawler, D.L., et al., *Human immune response to multiple injections of murine monoclonal IgG.* J Immunol, 1985. **135**(2): p. 1530-5.

134. Ober, R.J., et al., *Differences in promiscuity for antibody-FcRn interactions across species: implications for therapeutic antibodies.* Int Immunol, 2001. **13**(12): p. 1551-9.

135. Hudson, P.J. and C. Souriau, *Engineered antibodies.* Nat Med, 2003. **9**(1): p. 129-34.

136. McCafferty, J., et al., *Phage antibodies: filamentous phage displaying antibody variable domains.* Nature, 1990. **348**(6301): p. 552-4.

137. Lonberg, N., *Human antibodies from transgenic animals.* Nat Biotechnol, 2005. **23**(9): p. 1117-25.

138. Scott, A.M., J.P. Allison, and J.D. Wolchok, *Monoclonal antibodies in cancer therapy.* Cancer Immun, 2012. **12**: p. 14.

139. Daeron, M., *Fc receptor biology.* Annu Rev Immunol, 1997. **15**: p. 203-34.

140. Warmerdam, P.A., et al., *Polymorphism of the human Fc gamma receptor II (CD32): molecular basis and functional aspects.* Immunobiology, 1992. **185**(2-4): p. 175-82.

141. Ravetch, J.V. and B. Perussia, *Alternative membrane forms of Fc gamma RIII(CD16) on human natural killer cells and neutrophils. Cell type-specific expression of two genes that differ in single nucleotide substitutions.* J Exp Med, 1989. **170**(2): p. 481-97.

142. Cartron, G., et al., *Therapeutic activity of humanized anti-CD20 monoclonal antibody and polymorphism in IgG Fc receptor FcgammaRIIIa gene.* Blood, 2002. **99**(3): p. 754-8.

143. Weng, W.K. and R. Levy, *Two immunoglobulin G fragment C receptor polymorphisms independently predict response to rituximab in patients with follicular lymphoma.* J Clin Oncol, 2003. **21**(21): p. 3940-7.

144. Bruhns, P., et al., *Specificity and affinity of human Fcgamma receptors and their polymorphic variants for human IgG subclasses.* Blood, 2009. **113**(16): p. 3716-25.

145. Veri, M.C., et al., *Monoclonal antibodies capable of discriminating the human inhibitory Fcgamma-receptor IIB (CD32B) from the activating Fcgamma-receptor IIA (CD32A): biochemical, biological and functional characterization.* Immunology, 2007. **121**(3): p. 392-404.

146. Metes, D., et al., *Expression of functional CD32 molecules on human NK cells is determined by an allelic polymorphism of the FcgammaRIIC gene.* Blood, 1998. **91**(7): p. 2369-80.

147. Hogarth, P.M. and G.A. Pietersz, *Fc receptor-targeted therapies for the treatment of inflammation, cancer and beyond.* Nat Rev Drug Discov, 2012. **11**(4): p. 311-31.

148. Ra, C., et al., *A macrophage Fc gamma receptor and the mast cell receptor for IgE share an identical subunit.* Nature, 1989. **341**(6244): p. 752-4.

149. Tan, P.S., et al., *Unique monoclonal antibodies define expression of Fc gamma RI on macrophages and mast cell lines and demonstrate heterogeneity among subcutaneous and other dendritic cells.* Journal of Immunology, 2003. **170**(5): p. 2549-2556.

150. Kim, H.Y., S. Kim, and D.H. Chung, *FcgammaRIII engagement provides activating signals to NKT cells in antibody-induced joint inflammation.* J Clin Invest, 2006. **116**(9): p. 2484-92.

151. Nimmerjahn, F. and J.V. Ravetch, *Fcgamma receptors: old friends and new family members.* Immunity, 2006. **24**(1): p. 19-28.

152. Wang, W., et al., *NK Cell-Mediated Antibody-Dependent Cellular Cytotoxicity in Cancer Immunotherapy.* Front Immunol, 2015. **6**: p. 368.

153. Gul, N. and M. van Egmond, *Antibody-Dependent Phagocytosis of Tumor Cells by Macrophages: A Potent Effector Mechanism of Monoclonal Antibody Therapy of Cancer.* Cancer Res, 2015. **75**(23): p. 5008-13.

154. Minard-Colin, V., et al., *Lymphoma depletion during CD20 immunotherapy in mice is mediated by macrophage FcgammaRI, FcgammaRIII, and FcgammaRIV.* Blood, 2008. **112**(4): p. 1205-13.

155. Bulliard, Y., et al., *Activating Fc gamma receptors contribute to the antitumor activities of immunoregulatory receptor-targeting antibodies.* J Exp Med, 2013. **210**(9): p. 1685-93.

156. Romano, E., et al., *Ipilimumab-dependent cell-mediated cytotoxicity of regulatory T cells ex vivo by nonclassical monocytes in melanoma patients.* Proc Natl Acad Sci U S A, 2015. **112**(19): p. 6140-5.

157. Beers, S.A., M.J. Glennie, and A.L. White, *Influence of immunoglobulin isotype on therapeutic antibody function.* Blood, 2016. **127**(9): p. 1097-101.

158. Li, F. and J.V. Ravetch, *Inhibitory Fcgamma receptor engagement drives adjuvant and anti-tumor activities of agonistic CD40 antibodies.* Science, 2011. **333**(6045): p. 1030-4.

159. DiLillo, D.J. and J.V. Ravetch, *Fc-Receptor Interactions Regulate Both Cytotoxic and Immunomodulatory Therapeutic Antibody Effector Functions.* Cancer Immunol Res, 2015. **3**(7): p. 704-13.

160. Li, F. and J.V. Ravetch, *Antitumor activities of agonistic anti-TNFR antibodies require differential FcgammaRIIB coengagement in vivo.* Proc Natl Acad Sci U S A, 2013. **110**(48): p. 19501-6.

161. Li, F. and J.V. Ravetch, *A general requirement for FcgammaRIIB co-engagement of agonistic anti-TNFR antibodies.* Cell Cycle, 2012. **11**(18): p. 3343-4.

162. White, A.L., et al., *Conformation of the human immunoglobulin G2 hinge imparts superagonistic properties to immunostimulatory anticancer antibodies.* Cancer Cell, 2015. **27**(1): p. 138-48.

163. Xu, Y., et al., *Fc gamma Rs modulate cytotoxicity of anti-Fas antibodies: implications for agonistic antibody-based therapeutics.* J Immunol, 2003. **171**(2): p. 562-8.

164. Li, F. and J.V. Ravetch, *Apoptotic and antitumor activity of death receptor antibodies require inhibitory Fcgamma receptor engagement.* Proc Natl Acad Sci U S A, 2012. **109**(27): p. 10966-71.

165. Bulliard, Y., et al., *OX40 engagement depletes intratumoral Tregs via activating FcgammaRs, leading to antitumor efficacy.* Immunol Cell Biol, 2014. **92**(6): p. 475-80.

166. Coe, D., et al., *Depletion of regulatory T cells by anti-GITR mAb as a novel mechanism for cancer immunotherapy.* Cancer Immunol Immunother, 2010. **59**(9): p. 1367-77.

167. Selby, M.J., et al., *Anti-CTLA-4 antibodies of IgG2a isotype enhance antitumor activity through reduction of intratumoral regulatory T cells.* Cancer Immunol Res, 2013. **1**(1): p. 32-42.

168. Clynes, R.A., et al., *Inhibitory Fc receptors modulate in vivo cytotoxicity against tumor targets.* Nat Med, 2000. **6**(4): p. 443-6.

169. Marabelle, A., et al., *Depleting tumor-specific Tregs at a single site eradicates disseminated tumors.* J Clin Invest, 2013. **123**(6): p. 2447-63.

170. Marabelle, A., et al., *Intratumoral immunotherapy: using the tumor as the remedy.* Ann Oncol, 2017. **28**(suppl_12): p. xii33-xii43.

171. Guo, C., et al., *Therapeutic cancer vaccines: past, present, and future.* Adv Cancer Res, 2013. **119**: p. 421-75.

172. Fukuhara, H., Y. Ino, and T. Todo, *Oncolytic virus therapy: A new era of cancer treatment at dawn.* Cancer Sci, 2016. **107**(10): p. 1373-1379.

173. Ardolino, M., J. Hsu, and D.H. Raulet, *Cytokine treatment in cancer immunotherapy.* Oncotarget, 2015. **6**(23): p. 19346-7.

174. Perica, K., et al., *Adoptive T cell immunotherapy for cancer.* Rambam Maimonides Med J, 2015. **6**(1): p. e0004.

175. Weiner, L.M., J.C. Murray, and C.W. Shuptrine, *Antibody-based immunotherapy of cancer.* Cell, 2012. **148**(6): p. 1081-4.

176. Grillo-Lopez, A.J., et al., *Rituximab: the first monoclonal antibody approved for the treatment of lymphoma.* Curr Pharm Biotechnol, 2000. **1**(1): p. 1-9.

177. Topalian, S.L., G.J. Weiner, and D.M. Pardoll, *Cancer immunotherapy comes of age.* J Clin Oncol, 2011. **29**(36): p. 4828-36.

178. Jago, C.B., et al., *Differential expression of CTLA-4 among T cell subsets.* Clin Exp Immunol, 2004. **136**(3): p. 463-71.

179. Schwartz, R.H., *Costimulation of T lymphocytes: the role of CD28, CTLA-4, and B7/BB1 in interleukin-2 production and immunotherapy.* Cell, 1992. **71**(7): p. 1065-8.

180. Khattri, R., et al., *Lymphoproliferative disorder in CTLA-4 knockout mice is characterized by CD28-regulated activation of Th2 responses.* J Immunol, 1999. **162**(10): p. 5784-91.

181. Parry, R.V., et al., *CTLA-4 and PD-1 receptors inhibit T-cell activation by distinct mechanisms.* Mol Cell Biol, 2005. **25**(21): p. 9543-53.

182. Nishimura, H., et al., *Development of lupus-like autoimmune diseases by disruption of the PD-1 gene encoding an ITIM motif-carrying immunoreceptor.* Immunity, 1999. **11**(2): p. 141-51.

183. Wang, J., et al., *Establishment of NOD-Pdcd1-/- mice as an efficient animal model of type I diabetes.* Proc Natl Acad Sci U S A, 2005. **102**(33): p. 11823-8.

184. Francisco, L.M., et al., *PD-L1 regulates the development, maintenance, and function of induced regulatory T cells.* J Exp Med, 2009. **206**(13): p. 3015-29.

185. Sharpe, A.H. and K.E. Pauken, *The diverse functions of the PD1 inhibitory pathway.* Nat Rev Immunol, 2018. **18**(3): p. 153-167.

186. Dine, J., et al., *Immune Checkpoint Inhibitors: An Innovation in Immunotherapy for the Treatment and Management of Patients with Cancer.* Asia Pac J Oncol Nurs, 2017. **4**(2): p. 127-135.

187. Sharma, P. and J.P. Allison, *Immune checkpoint targeting in cancer therapy: toward combination strategies with curative potential.* Cell, 2015. **161**(2): p. 205-14.

188. Seidel, J.A., A. Otsuka, and K. Kabashima, *Anti-PD-1 and Anti-CTLA-4 Therapies in Cancer: Mechanisms of Action, Efficacy, and Limitations.* Front Oncol, 2018. **8**: p. 86.

189. Topalian, S.L., C.G. Drake, and D.M. Pardoll, *Immune checkpoint blockade: a common denominator approach to cancer therapy.* Cancer Cell, 2015. **27**(4): p. 450-61.

190. Wing, K., et al., *CTLA-4 control over Foxp3+ regulatory T cell function.* Science, 2008. **322**(5899): p. 271-5.

191. Phan, G.Q., et al., *Cancer regression and autoimmunity induced by cytotoxic T lymphocyte-associated antigen 4 blockade in patients with metastatic melanoma.* Proc Natl Acad Sci U S A, 2003. **100**(14): p. 8372-7.

192. Ahmadzadeh, M., et al., *Tumor antigen-specific CD8 T cells infiltrating the tumor express high levels of PD-1 and are functionally impaired.* Blood, 2009. **114**(8): p. 1537-44.

193. Keir, M.E., et al., *PD-1 and its ligands in tolerance and immunity.* Annu Rev Immunol, 2008. **26**: p. 677-704.

194. Barber, D.L., et al., *Restoring function in exhausted CD8 T cells during chronic viral infection.* Nature, 2006. **439**(7077): p. 682-7.

195. Freeman-Keller, M., et al., *Nivolumab in Resected and Unresectable Metastatic Melanoma: Characteristics of Immune-Related Adverse Events and Association with Outcomes.* Clin Cancer Res, 2016. **22**(4): p. 886-94.

196. Croft, M., *The role of TNF superfamily members in T-cell function and diseases.* Nat Rev Immunol, 2009. **9**(4): p. 271-85.

197. Vonderheide, R.H., et al., *Clinical activity and immune modulation in cancer patients treated with CP-870,893, a novel CD40 agonist monoclonal antibody.* J Clin Oncol, 2007. **25**(7): p. 876-83.

198. Melero, I., et al., *Monoclonal antibodies against the 4-1BB T-cell activation molecule eradicate established tumors.* Nat Med, 1997. **3**(6): p. 682-5.

199. Curti, B.D., et al., *OX40 is a potent immune-stimulating target in late-stage cancer patients.* Cancer Res, 2013. **73**(24): p. 7189-98.

200. Moran, A.E., M. Kovacsovics-Bankowski, and A.D. Weinberg, *The TNFRs OX40, 4-1BB, and CD40 as targets for cancer immunotherapy.* Curr Opin Immunol, 2013. **25**(2): p. 230-7.

201. Bremer, E., *Targeting of the tumor necrosis factor receptor superfamily for cancer immunotherapy.* ISRN Oncol, 2013. **2013**: p. 371854.

202. van Kooten, C. and J. Banchereau, *Functions of CD40 on B cells, dendritic cells and other cells.* Curr Opin Immunol, 1997. **9**(3): p. 330-7.

203. Khong, A., et al., *The use of agonistic anti-CD40 therapy in treatments for cancer.* Int Rev Immunol, 2012. **31**(4): p. 246-66.

204. Todryk, S.M., et al., *CD40 ligation for immunotherapy of solid tumours.* J Immunol Methods, 2001. **248**(1-2): p. 139-47.

205. Medina-Echeverz, J., et al., *Systemic Agonistic Anti-CD40 Treatment of Tumor-Bearing Mice Modulates Hepatic Myeloid-Suppressive Cells and Causes Immune-Mediated Liver Damage.* Cancer Immunol Res, 2015. **3**(5): p. 557-66.

206. Snell, L.M., et al., *T-cell intrinsic effects of GITR and 4-1BB during viral infection and cancer immunotherapy.* Immunol Rev, 2011. **244**(1): p. 197-217.

207. Cannons, J.L., et al., *4-1BB ligand induces cell division, sustains survival, and enhances effector function of CD4 and CD8 T cells with similar efficacy.* J Immunol, 2001. **167**(3): p. 1313-24.

208. Murillo, O., et al., *Therapeutic antitumor efficacy of anti-CD137 agonistic monoclonal antibody in mouse models of myeloma.* Clin Cancer Res, 2008. **14**(21): p. 6895-906.

209. Chester, C., et al., *Immunotherapy targeting 4-1BB: mechanistic rationale, clinical results, and future strategies.* Blood, 2018. **131**(1): p. 49-57.

210. Niu, L., et al., *Cytokine-mediated disruption of lymphocyte trafficking, hemopoiesis, and induction of lymphopenia, anemia, and thrombocytopenia in anti-CD137-treated mice.* J Immunol, 2007. **178**(7): p. 4194-213.

211. Croft, M., *Control of immunity by the TNFR-related molecule OX40 (CD134).* Annu Rev Immunol, 2010. **28**: p. 57-78.

212. Paterson, D.J., et al., *Antigens of activated rat T lymphocytes including a molecule of 50,000 Mr detected only on CD4 positive T blasts.* Mol Immunol, 1987. **24**(12): p. 1281-90.

213. Redmond, W.L., C.E. Ruby, and A.D. Weinberg, *The role of OX40-mediated co-stimulation in T-cell activation and survival.* Crit Rev Immunol, 2009. **29**(3): p. 187-201.

214. Jensen, S.M., et al., *Signaling through OX40 enhances antitumor immunity.* Semin Oncol, 2010. **37**(5): p. 524-32.

215. Baumann, R., et al., *Functional expression of CD134 by neutrophils.* Eur J Immunol, 2004. **34**(8): p. 2268-75.

216. Zaini, J., et al., *OX40 ligand expressed by DCs costimulates NKT and CD4+ Th cell antitumor immunity in mice.* J Clin Invest, 2007. **117**(11): p. 3330-8.

217. Liu, C., et al., *Plasmacytoid dendritic cells induce NK cell-dependent, tumor antigen-specific T cell cross-priming and tumor regression in mice.* J Clin Invest, 2008. **118**(3): p. 1165-75.

218. Gramaglia, I., et al., *The OX40 costimulatory receptor determines the development of CD4 memory by regulating primary clonal expansion.* J Immunol, 2000. **165**(6): p. 3043-50.

219. Gramaglia, I., et al., *Ox-40 ligand: a potent costimulatory molecule for sustaining primary CD4 T cell responses.* J Immunol, 1998. **161**(12): p. 6510-7.

220. Rogers, P.R., et al., *OX40 promotes Bcl-xL and Bcl-2 expression and is essential for long-term survival of CD4 T cells.* Immunity, 2001. **15**(3): p. 445-55.

221. Bansal-Pakala, P., et al., *Costimulation of CD8 T cell responses by OX40.* J Immunol, 2004. **172**(8): p. 4821-5.

222. Dubey, C., M. Croft, and S.L. Swain, *Naive and effector CD4 T cells differ in their requirements for T cell receptor versus costimulatory signals.* J Immunol, 1996. **157**(8): p. 3280-9.

223. Willoughby, J., et al., *OX40: Structure and function - What questions remain?* Mol Immunol, 2017. **83**: p. 13-22.

224. Ito, T., et al., *TSLP-activated dendritic cells induce an inflammatory T helper type 2 cell response through OX40 ligand.* J Exp Med, 2005. **202**(9): p. 1213-23.

225. Murata, K., et al., *Impairment of antigen-presenting cell function in mice lacking expression of OX40 ligand.* J Exp Med, 2000. **191**(2): p. 365-74.

226. Croft, M., *Costimulation of T cells by OX40, 4-1BB, and CD27.* Cytokine Growth Factor Rev, 2003. **14**(3-4): p. 265-73.

227. Stuber, E., et al., *Cross-linking of OX40 ligand, a member of the TNF/NGF cytokine family, induces proliferation and differentiation in murine splenic B cells.* Immunity, 1995. **2**(5): p. 507-21.

228. Ohshima, Y., et al., *Expression and function of OX40 ligand on human dendritic cells.* J Immunol, 1997. **159**(8): p. 3838-48.

229. Weinberg, A.D., et al., *Blocking OX-40/OX-40 ligand interaction in vitro and in vivo leads to decreased T cell function and amelioration of experimental allergic encephalomyelitis.* J Immunol, 1999. **162**(3): p. 1818-26.

230. Kashiwakura, J., et al., *T cell proliferation by direct cross-talk between OX40 ligand on human mast cells and OX40 on human T cells: comparison of gene expression profiles between human tonsillar and lung-cultured mast cells.* J Immunol, 2004. **173**(8): p. 5247-57.

231. Zingoni, A., et al., *Cross-talk between activated human NK cells and CD4+ T cells via OX40-OX40 ligand interactions.* J Immunol, 2004. **173**(6): p. 3716-24.

232. Burgess, J.K., et al., *Detection and characterization of OX40 ligand expression in human airway smooth muscle cells: a possible role in asthma?* J Allergy Clin Immunol, 2004. **113**(4): p. 683-9.

233. Imura, A., et al., *The human OX40/gp34 system directly mediates adhesion of activated T cells to vascular endothelial cells.* J Exp Med, 1996. **183**(5): p. 2185-95.

234. Croft, M., et al., *The significance of OX40 and OX40L to T-cell biology and immune disease.* Immunol Rev, 2009. **229**(1): p. 173-91.

235. Watts, T.H., *TNF/TNFR family members in costimulation of T cell responses.* Annu Rev Immunol, 2005. **23**: p. 23-68.

236. Arch, R.H. and C.B. Thompson, *4-1BB and Ox40 are members of a tumor necrosis factor (TNF)-nerve growth factor receptor subfamily that bind TNF receptor-associated factors and activate nuclear factor kappaB.* Mol Cell Biol, 1998. **18**(1): p. 558-65.

237. Kawamata, S., et al., *Activation of OX40 signal transduction pathways leads to tumor necrosis factor receptor-associated factor (TRAF) 2- and TRAF5-mediated NF-kappaB activation.* J Biol Chem, 1998. **273**(10): p. 5808-14.

238. Song, J., T. So, and M. Croft, *Activation of NF-kappaB1 by OX40 contributes to antigen-driven T cell expansion and survival.* J Immunol, 2008. **180**(11): p. 7240-8.

239. Song, J., et al., *The costimulation-regulated duration of PKB activation controls T cell longevity.* Nat Immunol, 2004. **5**(2): p. 150-8.

240. Song, J., et al., *Sustained survivin expression from OX40 costimulatory signals drives T cell clonal expansion.* Immunity, 2005. **22**(5): p. 621-31.

241. Song, J., et al., *The kinases aurora B and mTOR regulate the G1-S cell cycle progression of T lymphocytes.* Nat Immunol, 2007. **8**(1): p. 64-73.

242. Baum, P.R., et al., *Molecular characterization of murine and human OX40/OX40 ligand systems: identification of a human OX40 ligand as the HTLV-1-regulated protein gp34.* EMBO J, 1994. **13**(17): p. 3992-4001.

243. Godfrey, W.R., et al., *Identification of a human OX-40 ligand, a costimulator of CD4+ T cells with homology to tumor necrosis factor.* J Exp Med, 1994. **180**(2): p. 757-62.

244. Maxwell, J.R., et al., *Danger and OX40 receptor signaling synergize to enhance memory T cell survival by inhibiting peripheral deletion.* J Immunol, 2000. **164**(1): p. 107-12.

245. Salek-Ardakani, S., et al., *OX40 (CD134) controls memory T helper 2 cells that drive lung inflammation.* J Exp Med, 2003. **198**(2): p. 315-24.

246. Kopf, M., et al., *OX40-deficient mice are defective in Th cell proliferation but are competent in generating B cell and CTL Responses after virus infection.* Immunity, 1999. **11**(6): p. 699-708.

247. Zhang, Z., et al., *Activation of OX40 augments Th17 cytokine expression and antigen-specific uveitis.* Am J Pathol, 2010. **177**(6): p. 2912-20.

248. Xiao, X., et al., *The Costimulatory Receptor OX40 Inhibits Interleukin-17 Expression through Activation of Repressive Chromatin Remodeling Pathways.* Immunity, 2016.

249. So, T., et al., *Signals from OX40 regulate nuclear factor of activated T cells c1 and T cell helper 2 lineage commitment.* Proc Natl Acad Sci U S A, 2006. **103**(10): p. 3740-5.

250. Flynn, S., et al., *CD4 T cell cytokine differentiation: the B cell activation molecule, OX40 ligand, instructs CD4 T cells to express interleukin 4 and upregulates expression of the chemokine receptor, Blr-1.* J Exp Med, 1998. **188**(2): p. 297-304.

251. Rogers, P.R. and M. Croft, *CD28, Ox-40, LFA-1, and CD4 modulation of Th1/Th2 differentiation is directly dependent on the dose of antigen.* J Immunol, 2000. **164**(6): p. 2955-63.

252. Ito, T., et al., *Plasmacytoid dendritic cells regulate Th cell responses through OX40 ligand and type I IFNs.* J Immunol, 2004. **172**(7): p. 4253-9.

253. Jember, A.G., et al., *Development of allergic inflammation in a murine model of asthma is dependent on the costimulatory receptor OX40.* J Exp Med, 2001. **193**(3): p. 387-92.

254. Hoshino, A., et al., *Critical role for OX40 ligand in the development of pathogenic Th2 cells in a murine model of asthma.* Eur J Immunol, 2003. **33**(4): p. 861-9.

255. Kim, M.Y., et al., *OX40 signals during priming on dendritic cells inhibit CD4 T cell proliferation: IL-4 switches off OX40 signals enabling rapid proliferation of Th2 effectors.* J Immunol, 2005. **174**(3): p. 1433-7.

256. Nakae, S., et al., *IL-17 production from activated T cells is required for the spontaneous development of destructive arthritis in mice deficient in IL-1 receptor antagonist.* Proc Natl Acad Sci U S A, 2003. **100**(10): p. 5986-90.

257. Li, J., et al., *Negative regulation of IL-17 production by OX40/OX40L interaction.* Cell Immunol, 2008. **253**(1-2): p. 31-7.

258. Dawicki, W., et al., *4-1BB and OX40 act independently to facilitate robust CD8 and CD4 recall responses.* J Immunol, 2004. **173**(10): p. 5944-51.

259. Lee, S.W., et al., *Functional dichotomy between OX40 and 4-1BB in modulating effector CD8 T cell responses.* J Immunol, 2006. **177**(7): p. 4464-72.

260. Fujita, T., et al., *Functional characterization of OX40 expressed on human CD8+ T cells.* Immunol Lett, 2006. **106**(1): p. 27-33.

261. Piconese, S., B. Valzasina, and M.P. Colombo, *OX40 triggering blocks suppression by regulatory T cells and facilitates tumor rejection.* J Exp Med, 2008. **205**(4): p. 825-39.

262. Piconese, S., et al., *A non-redundant role for OX40 in the competitive fitness of Treg in response to IL-2.* Eur J Immunol, 2010. **40**(10): p. 2902-13.

263. Takeda, I., et al., *Distinct roles for the OX40-OX40 ligand interaction in regulatory and nonregulatory T cells.* J Immunol, 2004. **172**(6): p. 3580-9.

264. Vu, M.D., et al., *OX40 costimulation turns off Foxp3+ Tregs.* Blood, 2007. **110**(7): p. 2501-10.

265. Griseri, T., et al., *OX40 is required for regulatory T cell-mediated control of colitis.* J Exp Med, 2010. **207**(4): p. 699-709.

266. So, T. and M. Croft, *Cutting edge: OX40 inhibits TGF-beta- and antigen-driven conversion of naive CD4 T cells into CD25+Foxp3+ T cells.* J Immunol, 2007. **179**(3): p. 1427-30.

267. Yu, X., et al., *Complex Interplay between Epitope Specificity and Isotype Dictates the Biological Activity of Anti-human CD40 Antibodies.* Cancer Cell, 2018. **33**(4): p. 664-675 e4.

268. Xiao, X., et al., *OX40/OX40L costimulation affects induction of Foxp3+ regulatory T cells in part by expanding memory T cells in vivo.* J Immunol, 2008. **181**(5): p. 3193-201.

269. Ito, T., et al., *OX40 ligand shuts down IL-10-producing regulatory T cells.* Proc Natl Acad Sci U S A, 2006. **103**(35): p. 13138-43.

270. Ruby, C.E., et al., *Cutting Edge: OX40 agonists can drive regulatory T cell expansion if the cytokine milieu is right.* J Immunol, 2009. **183**(8): p. 4853-7.

271. Voo, K.S., et al., *Antibodies targeting human OX40 expand effector T cells and block inducible and natural regulatory T cell function.* J Immunol, 2013. **191**(7): p. 3641-50.

272. Gri, G., et al., *CD4+CD25+ regulatory T cells suppress mast cell degranulation and allergic responses through OX40-OX40L interaction.* Immunity, 2008. **29**(5): p. 771-81.

273. Valzasina, B., et al., *Triggering of OX40 (CD134) on CD4(+)CD25+ T cells blocks their inhibitory activity: a novel regulatory role for OX40 and its comparison with GITR.* Blood, 2005. **105**(7): p. 2845-51.

274. Hirschhorn-Cymerman, D., et al., *OX40 engagement and chemotherapy combination provides potent antitumor immunity with concomitant regulatory T cell apoptosis.* J Exp Med, 2009. **206**(5): p. 1103-16.

275. Ali, S.A., et al., *Anti-tumour therapeutic efficacy of OX40L in murine tumour model.* Vaccine, 2004. **22**(27-28): p. 3585-94.

276. Gough, M.J., et al., *Adjuvant therapy with agonistic antibodies to CD134 (OX40) increases local control after surgical or radiation therapy of cancer in mice.* J Immunother, 2010. **33**(8): p. 798-809.

277. Morris, A., et al., *Induction of anti-mammary cancer immunity by engaging the OX-40 receptor in vivo.* Breast Cancer Res Treat, 2001. **67**(1): p. 71-80.

278. Linch, S.N., M.J. McNamara, and W.L. Redmond, *OX40 Agonists and Combination Immunotherapy: Putting the Pedal to the Metal.* Front Oncol, 2015. **5**: p. 34.

279. Sugamura, K., N. Ishii, and A.D. Weinberg, *Therapeutic targeting of the effector T-cell co-stimulatory molecule OX40.* Nat Rev Immunol, 2004. **4**(6): p. 420-31.

280. Weinberg, A.D., et al., *Science gone translational: the OX40 agonist story.* Immunol Rev, 2011. **244**(1): p. 218-31.

281. Song, A., et al., *Cooperation between CD4 and CD8 T cells for anti-tumor activity is enhanced by OX40 signals.* Eur J Immunol, 2007. **37**(5): p. 1224-32.

282. Redmond, W.L., S.N. Linch, and M.J. Kasiewicz, *Combined targeting of costimulatory (OX40) and coinhibitory (CTLA-4) pathways elicits potent effector T cells capable of driving robust antitumor immunity.* Cancer Immunol Res, 2014. **2**(2): p. 142-53.

283. Guo, Z., et al., *PD-1 blockade and OX40 triggering synergistically protects against tumor growth in a murine model of ovarian cancer.* PLoS One, 2014. **9**(2): p. e89350.

284. Redmond, W.L., et al., *Dual anti-OX40/IL-2 therapy augments tumor immunotherapy via IL-2R-mediated regulation of OX40 expression.* PLoS One, 2012. **7**(4): p. e34467.

285. Joshi, R.N., et al., *Phosphoproteomics Reveals Regulatory T Cell-Mediated DEF6 Dephosphorylation That Affects Cytokine Expression in Human Conventional T Cells.* Front Immunol, 2017. **8**: p. 1163.

286. Ohno, Y., et al., *Association of epigenetic alterations in the human C7orf24 gene with the aberrant gene expression in malignant cells.* J Biochem, 2013. **154**(4): p. 355-62.

287. Montufar-Solis, D., et al., *Hematopoietic not systemic impairment of Roquin expression accounts for intestinal inflammation in Roquin-deficient mice.* Sci Rep, 2014. **4**: p. 4920.

288. Soto-Feliciano, Y.M., et al., *PHF6 regulates phenotypic plasticity through chromatin organization within lineage-specific genes.* Genes Dev, 2017. **31**(10): p. 973-989.

289. Pappalardo, J.S., et al., *In vitro transfection of bone marrow-derived dendritic cells with TATp-liposomes.* Int J Nanomedicine, 2014. **9**: p. 963-73.

290. Gloviczki, M.L., et al., *TGF expression and macrophage accumulation in atherosclerotic renal artery stenosis.* Clin J Am Soc Nephrol, 2013. **8**(4): p. 546-53.

291. al-Shamkhani, A., et al., *OX40 is differentially expressed on activated rat and mouse T cells and is the sole receptor for the OX40 ligand.* Eur J Immunol, 1996. **26**(8): p. 1695-9.

292. Ch'en, I.L., et al., *Mechanisms of necroptosis in T cells.* J Exp Med, 2011. **208**(4): p. 633-41.

293. Rasmussen, J.W., et al., *Mac-1+ cells are the predominant subset in the early hepatic lesions of mice infected with Francisella tularensis.* Infect Immun, 2006. **74**(12): p. 6590-8.

294. Zenaro, E., M. Donini, and S. Dusi, *Induction of Th1/Th17 immune response by Mycobacterium tuberculosis: role of dectin-1, Mannose Receptor, and DC-SIGN.* J Leukoc Biol, 2009. **86**(6): p. 1393-401.

295. Parlane, N.A., et al., *Novel particulate vaccines utilizing polyester nanoparticles (bio-beads) for protection against Mycobacterium bovis infection - a review.* Vet Immunol Immunopathol, 2014. **158**(1-2): p. 8-13.

296. Yoshino, N., et al., *Upgrading of flow cytometric analysis for absolute counts, cytokines and other antigenic molecules of cynomolgus monkeys (Macaca fascicularis) by using anti-human cross-reactive antibodies.* Exp Anim, 2000. **49**(2): p. 97-110.

297. Sido, J.M., P.S. Nagarkatti, and M. Nagarkatti, *Delta(9)-Tetrahydrocannabinol attenuates allogeneic host-versus-graft response and delays skin graft rejection through activation of cannabinoid receptor 1 and induction of myeloid-derived suppressor cells.* J Leukoc Biol, 2015. **98**(3): p. 435-47.

298. Laidlaw, B.J., et al., *Production of IL-10 by CD4(+) regulatory T cells during the resolution of infection promotes the maturation of memory CD8(+) T cells.* Nat Immunol, 2015. **16**(8): p. 871-9.

299. Kitaichi, N., et al., *Diminution of experimental autoimmune uveoretinitis (EAU) in mice depleted of NK cells.* J Leukoc Biol, 2002. **72**(6): p. 1117-21.

300. Aswad, F., H. Kawamura, and G. Dennert, *High sensitivity of CD4+CD25+ regulatory T cells to extracellular metabolites nicotinamide adenine dinucleotide and ATP: a role for P2X7 receptors.* J Immunol, 2005. **175**(5): p. 3075-83.

301. Gibson, H., et al., *Immunotherapeutic intervention with oncolytic adenovirus in mouse mammary tumors.* Oncoimmunology, 2015. **4**(1): p. e984523.

302. Maiti, A., G. Maki, and P. Johnson, *TNF-alpha induction of CD44-mediated leukocyte adhesion by sulfation.* Science, 1998. **282**(5390): p. 941-3.

303. Siegelman, M.H., et al., *The mouse lymph node homing receptor is identical with the lymphocyte cell surface marker Ly-22: role of the EGF domain in endothelial binding.* Cell, 1990. **61**(4): p. 611-22.

304. Menendez, C.M., J.K. Jinkins, and D.J. Carr, *Resident T Cells Are Unable To Control Herpes Simplex Virus-1 Activity in the Brain Ependymal Region during Latency.* J Immunol, 2016. **197**(4): p. 1262-75.

305. Keil, M., et al., *General control non-derepressible 2 (GCN2) in T cells controls disease progression of autoimmune neuroinflammation.* J Neuroimmunol, 2016. **297**: p. 117-26.

306. Salmond, R.J., et al., *The tyrosine phosphatase PTPN22 discriminates weak self peptides from strong agonist TCR signals.* Nat Immunol, 2014. **15**(9): p. 875-883.

307. Kim, D.H., et al., *Regulation of chitinase-3-like-1 in T cell elicits Th1 and cytotoxic responses to inhibit lung metastasis.* Nat Commun, 2018. **9**(1): p. 503.

308. Wang, H., et al., *IL-12 Influence mTOR to Modulate CD8(+) T Cells Differentiation through T-bet and Eomesodermin in Response to Invasive Pulmonary Aspergillosis.* Int J Med Sci, 2017. **14**(10): p. 977-983.

309. Hsieh, W.C., et al., *IL-6 receptor blockade corrects defects of XIAP-deficient regulatory T cells.* Nat Commun, 2018. **9**(1): p. 463.

310. Wong, T.W., et al., *Eosinophils regulate peripheral B cell numbers in both mice and humans.* J Immunol, 2014. **192**(8): p. 3548-58.

311. Rogel, A., et al., *Akt signaling is critical for memory CD8(+) T-cell development and tumor immune surveillance.* Proc Natl Acad Sci U S A, 2017. **114**(7): p. E1178-E1187.

312. Kvanta, A., et al., *Stimulation of T-cells with OKT3 antibodies increases forskolin binding and cyclic AMP accumulation.* Cell Signal, 1990. **2**(5): p. 461-70.

313. Ferran, C., et al., *Inter-mouse strain differences in the in vivo anti-CD3 induced cytokine release.* Clin Exp Immunol, 1991. **86**(3): p. 537-43.

314. Luhder, F., et al., *Topological requirements and signaling properties of T cell-activating, anti-CD28 antibody superagonists.* J Exp Med, 2003. **197**(8): p. 955-66.

315. Araujo-Jorge, T., et al., *An Fc gamma RII-, Fc gamma RIII-specific monoclonal antibody (2.4G2) decreases acute Trypanosoma cruzi infection in mice.* Infect Immun, 1993. **61**(11): p. 4925-8.

316. Clarke, S.R., et al., *Characterization of the ovalbumin-specific TCR transgenic line OT-I: MHC elements for positive and negative selection.* Immunol Cell Biol, 2000. **78**(2): p. 110-7.

317. Bartkowiak, T. and M.A. Curran, *4-1BB Agonists: Multi-Potent Potentiators of Tumor Immunity.* Front Oncol, 2015. **5**: p. 117.

318. Schaer, D.A., J.T. Murphy, and J.D. Wolchok, *Modulation of GITR for cancer immunotherapy.* Curr Opin Immunol, 2012. **24**(2): p. 217-24.

319. Aspeslagh, S., et al., *Rationale for anti-OX40 cancer immunotherapy.* Eur J Cancer, 2016. **52**: p. 50-66.

320. Park, J.J., et al., *Expression of anti-HVEM single-chain antibody on tumor cells induces tumor-specific immunity with long-term memory.* Cancer Immunol Immunother, 2012. **61**(2): p. 203-214.

321. He, L.Z., et al., *Development of a Human Anti-CD27 Antibody with Efficacy in Lymphoma and Leukemia Models by Two Distinct Mechanisms.* Blood, 2011. **118**(21): p. 1234-1234.

322. Weinberg, A.D., et al., *Engagement of the OX-40 receptor in vivo enhances antitumor immunity.* J Immunol, 2000. **164**(4): p. 2160-9.

323. Montler, R., et al., *OX40, PD-1 and CTLA-4 are selectively expressed on tumor-infiltrating T cells in head and neck cancer.* Clin Transl Immunology, 2016. **5**(4): p. e70.

324. Lai, C., et al., *OX40+ Regulatory T Cells in Cutaneous Squamous Cell Carcinoma Suppress Effector T-Cell Responses and Associate with Metastatic Potential.* Clin Cancer Res, 2016. **22**(16): p. 4236-48.

325. Timperi, E., et al., *Regulatory T cells with multiple suppressive and potentially pro-tumor activities accumulate in human colorectal cancer.* Oncoimmunology, 2016. **5**(7): p. e1175800.

326. Mallett, S., S. Fossum, and A.N. Barclay, *Characterization of the MRC OX40 antigen of activated CD4 positive T lymphocytes--a molecule related to nerve growth factor receptor.* EMBO J, 1990. **9**(4): p. 1063-8.

327. McHugh, R.S., et al., *CD4(+)CD25(+) immunoregulatory T cells: gene expression analysis reveals a functional role for the glucocorticoid-induced TNF receptor.* Immunity, 2002. **16**(2): p. 311-23.

328. Barr, T.A. and A.W. Heath, *Functional activity of CD40 antibodies correlates to the position of binding relative to CD154.* Immunology, 2001. **102**(1): p. 39-43.

329. Cleary, K.L.S., et al., *Antibody Distance from the Cell Membrane Regulates Antibody Effector Mechanisms.* J Immunol, 2017. **198**(10): p. 3999-4011.

330. Casadevall, A. and A. Janda, *Immunoglobulin isotype influences affinity and specificity.* Proc Natl Acad Sci U S A, 2012. **109**(31): p. 12272-3.

331. White, A.L., S.A. Beers, and M.S. Cragg, *FcgammaRIIB as a key determinant of agonistic antibody efficacy.* Curr Top Microbiol Immunol, 2014. **382**: p. 355-72.

332. White, A.L., et al., *FcgammaRIotaIotaB controls the potency of agonistic anti-TNFR mAbs.* Cancer Immunol Immunother, 2013. **62**(5): p. 941-8.

333. Klein, C., et al., *Epitope interactions of monoclonal antibodies targeting CD20 and their relationship to functional properties.* MAbs, 2013. **5**(1): p. 22-33.

334. Shim, H., *One target, different effects: a comparison of distinct therapeutic antibodies against the same targets.* Exp Mol Med, 2011. **43**(10): p. 539-49.

335. Teeling, J.L., et al., *The biological activity of human CD20 monoclonal antibodies is linked to unique epitopes on CD20.* J Immunol, 2006. **177**(1): p. 362-71.

336. Cragg, M.S. and M.J. Glennie, *Antibody specificity controls in vivo effector mechanisms of anti-CD20 reagents.* Blood, 2004. **103**(7): p. 2738-43.

337. Niederfellner, G., et al., *Epitope characterization and crystal structure of GA101 provide insights into the molecular basis for type I/II distinction of CD20 antibodies.* Blood, 2011. **118**(2): p. 358-67.

338. Scientific, T.F. *Zero Blunt TOPO PCR Cloning Kit* Accessed November 2016 Available from: https://www.thermofisher.com/order/catalog/product/K280002.

339. Altman, J.D., et al., *Phenotypic analysis of antigen-specific T lymphocytes.* Science, 1996. **274**(5284): p. 94-6.

340. Plumlee, C.R., et al., *Early Effector CD8 T Cells Display Plasticity in Populating the Short-Lived Effector and Memory-Precursor Pools Following Bacterial or Viral Infection.* Sci Rep, 2015. **5**: p. 12264.

341. Sallusto, F., et al., *Two subsets of memory T lymphocytes with distinct homing potentials and effector functions.* Nature, 1999. **401**(6754): p. 708-12.

342. Myers, L., et al., *Effector CD8 T cells possess suppressor function after 4-1BB and Toll-like receptor triggering.* Proceedings of the National Academy of Sciences of the United States of America, 2003. **100**(9): p. 5348-5353.

343. Stewart, R., Hammond, S.A., Oberst, M. et al. , *The role of Fc gamma receptors in the activity of immunomodulatory antibodies for cancer.* j. immunotherapy cancer (2014).

344. Facciabene, A., G.T. Motz, and G. Coukos, *T-regulatory cells: key players in tumor immune escape and angiogenesis.* Cancer Res, 2012. **72**(9): p. 2162-71.

345. Yu, P., et al., *Intratumor depletion of CD4+ cells unmasks tumor immunogenicity leading to the rejection of late-stage tumors.* J Exp Med, 2005. **201**(5): p. 779-91.

346. Sato, E., et al., *Intraepithelial CD8+ tumor-infiltrating lymphocytes and a high CD8+/regulatory T cell ratio are associated with favorable prognosis in ovarian cancer.* Proc Natl Acad Sci U S A, 2005. **102**(51): p. 18538-43.

347. Shimizu, J., S. Yamazaki, and S. Sakaguchi, *Induction of tumor immunity by removing CD25+CD4+ T cells: a common basis between tumor immunity and autoimmunity.* J Immunol, 1999. **163**(10): p. 5211-8.

348. Shang, B., et al., *Prognostic value of tumor-infiltrating FoxP3+ regulatory T cells in cancers: a systematic review and meta-analysis.* Sci Rep, 2015. **5**: p. 15179.

349. Kjaergaard, J., et al., *Therapeutic efficacy of OX-40 receptor antibody depends on tumor immunogenicity and anatomic site of tumor growth.* Cancer Res, 2000. **60**(19): p. 5514-21.

350. Yokouchi, H., et al., *Anti-OX40 monoclonal antibody therapy in combination with radiotherapy results in therapeutic antitumor immunity to murine lung cancer.* Cancer Sci, 2008. **99**(2): p. 361-7.

351. Kitamura, N., et al., *OX40 costimulation can abrogate Foxp3+ regulatory T cell-mediated suppression of antitumor immunity.* Int J Cancer, 2009. **125**(3): p. 630-8.

352. Redmond, W.L., et al., *Defects in the acquisition of CD8 T cell effector function after priming with tumor or soluble antigen can be overcome by the addition of an OX40 agonist.* J Immunol, 2007. **179**(11): p. 7244-53.

353. Lee, S.J., et al., *4-1BB and OX40 dual costimulation synergistically stimulate primary specific CD8 T cells for robust effector function.* J Immunol, 2004. **173**(5): p. 3002-12.

354. Boissonnas, A., et al., *In vivo imaging of cytotoxic T cell infiltration and elimination of a solid tumor.* J Exp Med, 2007. **204**(2): p. 345-56.

355. Melero, I., et al., *NK1.1 cells express 4-1BB (CDw137) costimulatory molecule and are required for tumor immunity elicited by anti-4-1BB monoclonal antibodies.* Cell Immunol, 1998. **190**(2): p. 167-72.

356. Taraban, V.Y., et al., *Expression and costimulatory effects of the TNF receptor superfamily members CD134 (OX40) and CD137 (4-1BB), and their role in the generation of anti-tumor immune responses.* Eur J Immunol, 2002. **32**(12): p. 3617-27.

357. Schaer, D.A., D. Hirschhorn-Cymerman, and J.D. Wolchok, *Targeting tumor-necrosis factor receptor pathways for tumor immunotherapy.* J Immunother Cancer, 2014. **2**: p. 7.

358. Ward-Kavanagh, L.K., et al., *The TNF Receptor Superfamily in Co-stimulating and Co-inhibitory Responses.* Immunity, 2016. **44**(5): p. 1005-19.

359. Klemm, F. and J.A. Joyce, *Microenvironmental regulation of therapeutic response in cancer.* Trends Cell Biol, 2015. **25**(4): p. 198-213.

360. Curiel, T.J., et al., *Specific recruitment of regulatory T cells in ovarian carcinoma fosters immune privilege and predicts reduced survival.* Nat Med, 2004. **10**(9): p. 942-9.

361. Tao, H., et al., *Prognostic potential of FOXP3 expression in non-small cell lung cancer cells combined with tumor-infiltrating regulatory T cells.* Lung Cancer, 2012. **75**(1): p. 95-101.

362. Yang, Z.Z., et al., *Intratumoral CD4+CD25+ regulatory T-cell-mediated suppression of infiltrating CD4+ T cells in B-cell non-Hodgkin lymphoma.* Blood, 2006. **107**(9): p. 3639-46.

363. deLeeuw, R.J., et al., *The prognostic value of FoxP3+ tumor-infiltrating lymphocytes in cancer: a critical review of the literature.* Clin Cancer Res, 2012. **18**(11): p. 3022-9.